Computational Simulation of Atmospheric Flows Over Mountainous Regions Using the Commercial CFD Software Star-CCM+®

Vitor Manuel Martins Gonçalves da Costa Gomes

Final Project Report

Supervisor: Prof. José Manuel Laginha Mestre da Palma

Co-supervisor: Dr. Carlos Miguel Pereira da Silva Santos

Faculdade de Engenharia da Universidade do Porto

Mestrado Integrado em Engenharia Mecânica

July 2009

I would like to dedicate this to my parents, for their constant care and for giving me their unrelenting support.

Computational Simulation of Atmospheric Flows Over Mountainous Regions Using the Commercial CFD Software Star-CCM+®

Abstract

This project focuses on the study of wind when flowing over a mountainous region in mainland Portugal where a wind farm with 13 wind turbines is to be installed. The main aim is that of reviewing wind conditions for safe wind turbine deployment on that site. To this end CFD simulation software was used, more specifically Star-CCM+®.

After producing some preliminary studies with course meshes where one grew accustomed to the simulation software and to wind flow simulation particularities, more detailed studies followed, using a fine mesh and more accurately defined physics models. These were applied to the predominant wind direction sectors in the area, within which 12 directions were selected based on analyzed wind data measured on-site: 105º, 112.5º, 120º, 127.5º, 135º and 142.5º on the SE sector of the wind rose and 285º, 292.5º, 300º, 307.5º, 315º and 322.5º on the NW sector. Numerical results were compared to measured data in an attempt to evaluate result quality and to calibrate the used physics model. Relative differences of ±15% were found on both horizontal speed and turbulent intensity and absolute errors of ±5º direction-wise. The conclusions of this study were fed into the final result analysis.

Results were reviewed keeping in mind wind parameter (turbulence intensity, shear factor and flow pitch) ranges considered safe for wind turbine operation. Severe wind conditions were found on wind turbines WT 01, WT 02, WT 06, WT 07 and WT 08, where shear factor and/or flow pitch reached excessive levels. Wind turbines WT 09 and WT 10 also presented, to a lesser scale, worrying levels of shear factor.

Further study of wind conditions on the referred wind turbines respective locations is advisable, to clarify wind turbine safety and if necessary improve the suggested wind farm layout.

Simulação Computacional de Escoamentos Atmosféricos Sobre Regiões Montanhosas Usando o Software de CFD Comercial Star-CCM+®

Resumo

Este projecto está focado no estudo do vento quando este escoa sobre uma região montanhosa de Portugal continental onde está projectada a instalação de um parque eólico com 13 aerogeradores, com o intuito de avaliar as condições de vento seguras para instalação dos mesmos nesse local. Para este fim uma aplicação de simulação CFD foi utilizada, mais especificamente o Star-CCM+®.

Após produzir alguns estudos preliminares com malhas grosseiras, par melhor habituação ao software e às particularidades de simulação numérica de ventos, seguiram-se estudos mais detalhados, já utilizando malhas finas e modelos físicos caracterizados em maior detalhe. Estes foram aplicados aos sectores de direcção do vento predominantes na região, dentro dos quais foram escolhidas 12 direcções baseado na análise de dados de vento medidos no local: 105º, 112,5º, 120º, 127,5º, 135º e 142,5º no sector SE da rosa-dos-ventos e 285º, 292,5º, 300º, 307,5º, 315º e 322,5º no sector NW. Os resultados numéricos foram comparados com dados das medições na tentativa de avaliar a qualidade dos mesmos e de calibrar o modelo de física utilizado. Foram encontradas diferenças relativas de ±15% para a velocidade horizontal e intensidade de turbulência, e erros absolutos de ±5º ao nível da direcção do vento. As conclusões retiradas desde estudo foram utilizadas na análise final de resultados.

Os resultados numéricos foram analisados tendo em mente as gamas dentro das quais os parâmetros de vento (intensidade de turbulência, *shear factor* e inclinação do escoamento) são considerados seguros para o funcionamento de turbinas eólicas. Condições de vento severas foram encontradas nas turbinas WT 01, WT 02, WT 06, WT 07 e WT 08, onde o *shear factor* e/ou a inclinação do escoamento atingiram níveis excessivos. As turbinas WT 09 e WT 10 também apresentaram, numa escala mais reduzida, níveis preocupantes de *shear factor*.

Um estudo mais aprofundado das condições de vento nos locais das máquinas referidas é aconselhável, de forma a clarificar a segurança operacional das mesmas e se necessário melhorar a disposição proposta para o parque eólico.

Acknowledgments

I would like to express my gratitude to my supervisor, Prof. José Manuel Laginha Mestre da Palma and my co-supervisor, Dr. Carlos Miguel Pereira da Silva Santos, for their invaluable guidance, encouragement and useful suggestions regarding both the studied subject and good working methods, helping to overcome many doubts throughout the of this project.

I am thankful for the support given by Mr. João Correia Lopes, professor at the Department of Informatics Engineering at FEUP, for all the time put at my disposal whenever help was required regarding expert programming techniques, which were beyond my capabilities. I would also like to give my sincere thanks to Mr. Alberto Pinzello, CD-adapco® account manager, for his support throughout the project and valuable suggestions regarding modeling detail. My regards also to Lucia Game at CD-adapco® for the help at handling software licensing issues and Alice Silva, Carlos Maia and Jorge Cunha at CICA, for all the support at installing those licenses on campus servers.

I would also like to give my thanks and best wishes to António Oliveira, Rui Moura and Dário Fonseca, my colleagues for all their suggestions, ideas and shared knowledge.

Conteúdo

List of Tables

List of Figures

1. Introduction

The use of CFD in engineering is getting more and more common, and with it grows the number and quality of the options available in the CFD software market able to perform a certain task. This study seeks to review the performance of a software package in a context where the tool is used do study atmospheric flows over mountains and evaluate wind conditions in a given region.

Simulating flow over mountainous regions is essential in the study of wind farm allocations, when the installation of these involves investments in the level of millions of Euros, when every parameter of a wind farm (number, position and type of wind generator) depends on the evaluation of the wind conditions that result from the study, and high levels of correlation with measured data and confidence in the quality of data generated are required.

1.1 Project description

The proposed problem is the study of an area where a wind farm is planned to be installed. It was presented as a comparative study of the adequacy to the task and quality of results obtained from various commercial CFD software packages. The packages that are part of this study can be divided in two categories:

- General CFD applications, which allow simulation of mass/heat transfer, combustion, fusion/solidification or chemical reactions. These are extremely powerful and versatile, but may have steep learning curves and demand extensive knowledge of the numerical nuances related to CFD software, in order to use them to their full potential;
- CFD applications specific to analysis of wind flows, specially developed to study problems such as wind resource distribution, pollutant spread or fire hazard prediction. These being restricted to a specific type of problem are somewhat "pre-configured" with numerical tools and options best adapted to that purpose. These are potentially friendlier to use and more efficient at that task.

Involved in the project are 4 CFD tools: Fluent®, Star-CCM+® (these belonging to the general type), Meteodyn® and WindSim® (wind flow simulation specific). This report details the use of the Star-CCM+® software package, developed by CD-adapco®.

Wind measurement data was supplied, sourced from 3 weather stations installed in the area subjected to study. From that data (after its filtering, statistical and graphical treatment), 4 directions were selected to focus the study upon. Those 4 main directions were further divided in 3 subdirections each, to fully characterize those segments of the wind rose. Simulations were run in each of those 12 directions. After numerical results were produced, correlation was seeked between that data and the weather station data supplied in order to validate the models created. This was done using by analyzing differences in horizontal wind speed, direction, turbulence intensity and shear factor.

Once confidence in the quality of the simulation data was achieved, relevant data was collected from the several data maps created:

- 2D contour maps of horizontal speed, turbulence intensity, flow pitch at *nacelle* height and at the heights of the extremes of the area swept by the rotor;
- Velocity vectors to demonstrate the trajectory followed by the air masses;
- Point values of horizontal speed, turbulence intensity, flow pitch and shear factor at *nacelle* height and at the heights of the extremes of the area swept by the rotor;
- Vertical profiles of horizontal speed, flow pitch, turbulence intensity and shear factor at wind turbine location.

This data permitted an evaluation of the presented wind turbine layout, the main objective being to study and if possible validate safe operating conditions for all installed machines. Locations where wind turbine integrity may be compromised are discouraged, by reviewing those locations under the light of some parameters tied to wind turbine integrity when in service:

- Turbulence intensity > 0.18;
- Shear factor < 0 or > 0.2;
- Flow pitch < -8º or >8º;

To ensure that results from different software packages were comparable, parameters were standardized for the various CFD packages (where possible, depending on software characteristics and the validity of numerical results):

- Domain dimensions;
- Number and distribution of elements in the domain;
- Turbulence model configurations;
- Wind speed and turbulence profiles at the domain entry

1.2 Report Structure

This document's structure loosely follows the chronological order in which the various steps where executed. Section 2 describes the necessary period of adaptation to CFD techniques, to gain the "feel" for the needed manipulation of the numerical processes involved, and to understand "cause-effect" relations between model and solver characteristics and the extraction of reasonable results, as well as the computational power and time required to achieve those. Descriptions of the software used, the tools it supplies the user and the training process underwent are also included in this section.

Section 3 handles the modeling and simulation method, detailing the options taken and the relevant difficulties encountered during the process. The following stages are included:

- Terrain geometry importing method into the modeling software;
- Domain modeling and mesh construction

- Mesh handling, solver and boundary condition setup;
- Numerical data extraction.

Numerical results analysis is depicted in section 5. In it are included numerical data/measured data correlation analysis, a study of the global data contours as result of domain geometry and the wind farm layout review.

Final conclusions relating to the subjects handled in sections 3 and 4 and an evaluation of the software package performance for the task at hand is laid out in section 5.

In Annex A analysis of supplied wind data is presented. Annex B contains the extensive numerical data produced during the study in graphical or table format. All user created code employed during modeling is displayed on Annex C.

2 The Star-CCM+® simulation software and preliminary simulations

CD-adapco® is one of worldwide leading companies in the supply of CFD applications and CFD and FEA (Finite Element Analysis) services in the CAE (Computer Assisted Engineering) field. They possess an extensive client base, to whom they give support through 21 offices spread out over the globe. Their business focuses in the marketing of Star-CD® and Star-CCM+® tools, software packages dedicated to CFD simulation.

Star-CD® was developed in the 80s based on FORTRAN programming language. In 1999 CD-adapco® decided to develop a new software package, more modern, flexible and with added ease of use, based on C++ programming language. Launched in 2004, it was called Star-CCM+® and is now the headline product in the CD-adapco® lineup. It nowadays represents most of the company's business, with Star-CD® still being marketed only for certain specific applications. It can be complemented with other CD-adapco® products, such as Star-Design©, Star-View® or Star-Cast®, and through the Star-CAD® package can be easily integrated in the environment of some of more prominent CAD tools used in the industry, such as CATIA V5®, Pro/ENGINEER® or SolidWorks®.

CD-adapco® competes in the CFD software market through its Star-CCM+® with other software packages: the market is dominated by Star-CCM+® and Fluent®, the latter belonging to ANSYS®, a market leader in CAE analysis tools. In the field which concerns this project, that of simulation of atmospheric flow over mountainous regions, these packages compete with software developed specifically with this type of studies in mind. Of these, WAsP®, WindSim® or Meteodyn® can be referred. These are based on the same physical (Navier-Stokes equations) and numerical principles (finite volume method theory), but are adapted numerically, physically and graphically to the task, having the potential to produce high quality results, allied to an easy and fast user interface.

2.1 CFD

CFD stands for computational fluid dynamics and is used as an acronym to refer to the area of computer technology applied to solving fluid dynamics problems, in particular those not easily solved analytically.

2.1.1 RANS equations

Fluid flow can be described by the Navier-Stokes equations. To solve turbulent flows they are often converted into the Reynolds Averaged Navier-Stokes (RANS) equations. These are obtained by an averaging operation called Reynolds decomposition, by which a flow variable may be separated into the mean component (a time averaged component) and the fluctuating

component. The additional terms that appear from this separation are called Reynolds stresses. In order to provide closure to the equation set, the Reynolds stresses are expressed in terms of the averaged variables using a turbulence model.

A commonly used turbulence transport model is the two equation *k*-ϵ model (Launder and Spalding, 1972, 1974). One equation models turbulent kinetic energy, *k*, which expresses the turbulence energy content; the second equation models turbulent dissipation rate, ϵ, a variable which determines turbulence scale.

In standard notation, the full set of steady state incompressible RANS equations set [3] is made up of the continuity (1) and momentum (2) equations, as follows:

$$\frac{\partial U_i}{\partial x_i} = 0 \tag{1}$$

$$U_j \frac{\partial U_i}{\partial x_j} = -\frac{1}{\rho}\frac{\partial P}{\partial x_i} + \frac{\partial}{\partial x_j}\left(\upsilon\left(\frac{\partial U_i}{\partial x_j} + \frac{\partial U_j}{\partial x_i}\right) - \left(\overline{u_i u_j}\right)\right) \tag{2}$$

where the turbulent Reynolds stresses - $\overline{u_i u_j}$ - are related to the mean velocity variables through the turbulent viscosity υ_T (3);

$$\overline{u_i u_j} = -\upsilon_T\left(\frac{\partial U_i}{\partial x_j} + \frac{\partial U_j}{\partial x_i}\right) + \frac{2}{3}\delta_{ij}k \tag{3}$$

The *k*- ϵ model then relates (4) turbulent viscosity to turbulent kinetic energy (5) and turbulent dissipation rate (6),

$$\upsilon_T = c_\mu \frac{k^2}{\epsilon} \tag{4}$$

$$\frac{\partial}{\partial x_i}(U_i k) = \frac{\partial}{\partial x_i}\left(\frac{\upsilon_T}{\sigma_k}\frac{\partial k}{\partial x_i}\right) + P_k - \epsilon \tag{5}$$

$$\frac{\partial}{\partial x_i}(U_i \epsilon) = \frac{\partial}{\partial x_i}\left(\frac{\upsilon_T}{\sigma_\epsilon}\frac{\partial \epsilon}{\partial x_i}\right) + c_{\epsilon 1}\frac{\epsilon}{k}P_k - c_{\epsilon 2}\frac{\epsilon^2}{k} \tag{6}$$

where c_μ, σ_ϵ, $c_{\epsilon 1}$ and $c_{\epsilon 2}$ are *k*- ϵ model constants and the turbulent production term P_k (7) is

$$P_k = \upsilon_T\left(\frac{\partial U_i}{\partial x_j} + \frac{\partial U_j}{\partial x_i}\right)\frac{\partial U_i}{\partial x_j} \tag{7}$$

2.1.2 Discretization techniques

The finite volume method (FVM) is a method for solving partial differential equations by converting them into algebraic equations, calculating the relevant variables at discrete places on a meshed geometry. "Finite volume" refers to the small volume surrounding each node point on a mesh. This is the "classical" or standard approach used most often in commercial software and research codes. The governing equations, as in any fluid dynamics problems, are solved in a control volume, albeit a discretized one. FVM recasts the RANS equations in discretized form to each control volume, calculating boundary fluxes on each volume to connect and reconstruct the whole domain. By guaranteeing the conservation of fluxes through each control volume, it ensures that conservation is maintained for the whole domain.

2.2 Star-CCM+® software package description

CD-adapco® supplied a software package which included Star-CCM+®, Star-Design® and Star-View+®, which became available on 23/04/09. Of the three, Star-CCM+® is the main simulation and data analysis tool. It possesses advanced meshing tools, but is limited in geometry creation and manipulation. As such, other tools would have to be used to the task of creating the domains.

Star-Design® is mainly a geometry creation tool. It is able to create 2D and 3D figures and execute algebraic operations with them. It has automatic meshing tools, but user control over dimensional parameter is limited. It is also able to run CFD simulations upon created geometry, but once again user control over the solver and physics models is reduced.

Star-View+® is a simple portable visualization tool for results produced within Star-CCM+®. Its utility is to display 3D data plots in a light package, without requiring a connection to the software license files. Since the numerical results did not need to be exported to another computer for visual analysis, it has little relevance to this project.

The package hence is composed of two simulation programs, each with a range of capabilities and different complexity levels: Star-Design® is practical and accessible, being capable of quickly producing results, at the expense of precision; to execute tight control over physics models selection and configuration, numerical solver control and having powerful visualization tools, one must necessarily use Star-CCM+®.

2.3 Familiarization with the tool

To gain familiarity with the software, an initiation tutorial was followed, which is described in detail in the software User Guide [1]. In it are detailed the essential steps in the process of simulating a simple flow problem:

1. Mesh importation;
2. Domain boundary manipulation;
3. Geometry and mesh visualization setup;
4. Physics models selection and configuration;
5. Defining initial values and boundary conditions;
6. Convergence criteria and other solver parameters setup;
7. Simulation progress monitoring;
8. 3D solution data visualization;
9. 2D solution data plotting;

This tutorial revealed to be vital, as the user interface is not intuitive for the first time user: all simulation objects and functions are condensed into a lateral tree structure, and their location is not obvious at first sight. The tutorial is sufficient to transform user experience into an easy and light task, just a few mouse "clicks" being needed to access almost every useful function.

2.4 Preliminary simulations using Star-CCM+®

2.4.1 Topography manipulation

Having the knowledge of how to use Star-CCM+®'s main functions, simple wind flow simulations were carried out. Topographical maps of the area were supplied – a 55×55 km map centered on the wind farm location – as well as UTM coordinates of the 3 weather stations installed on site. Figure 1 displays these, as well as the contour of the area covered by the projected wind farm.

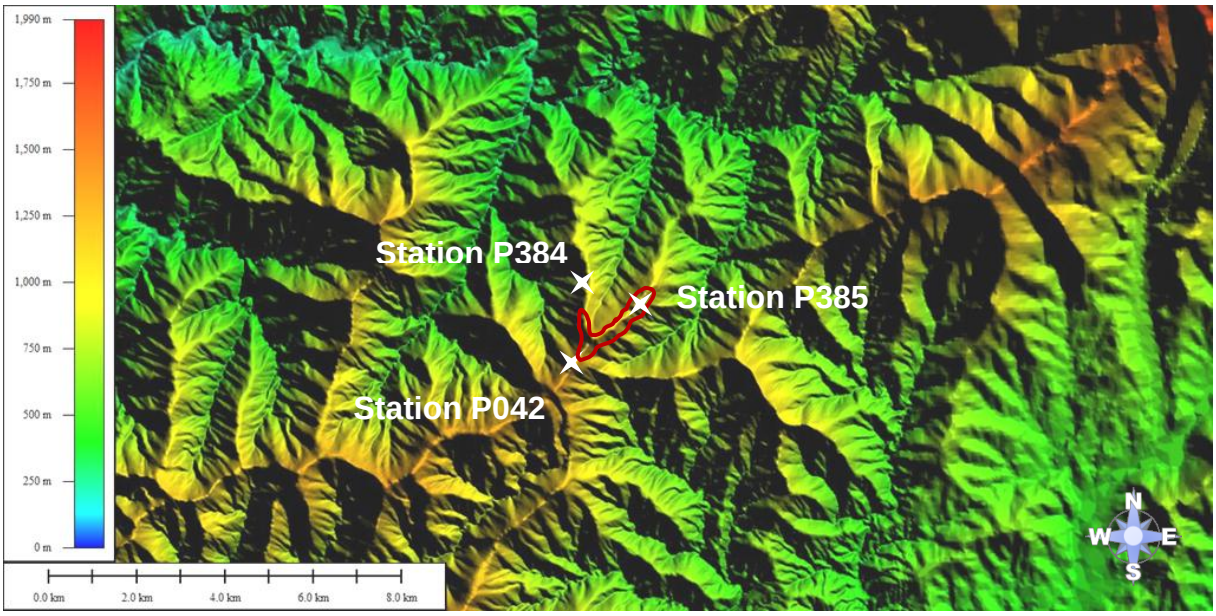

Figure 1 - Local topography; marked are the locations 3 the weather stations and the projected wind farm area

Since an area of 55×55 km was not only unnecessary but also computationally "heavy", a 20x20km section was trimmed centered on the wind farm location. This trimmed section was transformed into `.xyz` file format, the points triangulated and finally exported to `.stl` format. This map was then imported into GAMBIT®, where the domain and mesh was to be created. This program was selected for this task since a certain level of confidence in its use and knowledge of its capabilities and limitations had already been gained, and because it was known as a fact that it would give the control in fine detailing needed in mesh creation. It allowed a vital issue to be bypassed: learning how to use the Star-CCM+® mesher, which while highly capable, being fully automated, would likely make harder the creation of a mesh complying to specific dimensions. Additionally, difficulties in importing geometry into Star-CCM+® were expected, and as it was known that Star-CCM+® was fully compatible with GAMBIT®s `.msh` mesh format, it would be one less problem to solve. It would also allow the comparison with FLUENT® to be more balanced by using the same tool for mesh creation, since it is the simulation and not meshing capabilities of the software that were under evaluation.

Having the square ground surface imported into GAMBIT®, a box with "virtual" geometry was created with the ground as a bottom and a ceiling of 5.8 km (absolute). Operations were done in virtual geometry since the surface, as imported, was a virtual face and its transformation to real geometry would provoke program instability. The particularity of virtual geometry is that it cannot be exported in any format, only serving as reference and support geometry for real operations. This wouldn't be a problem, since the only element needed outside GAMBIT® was the mesh itself, which a virtual volume can house. Figure 2 shows the created virtual volume.

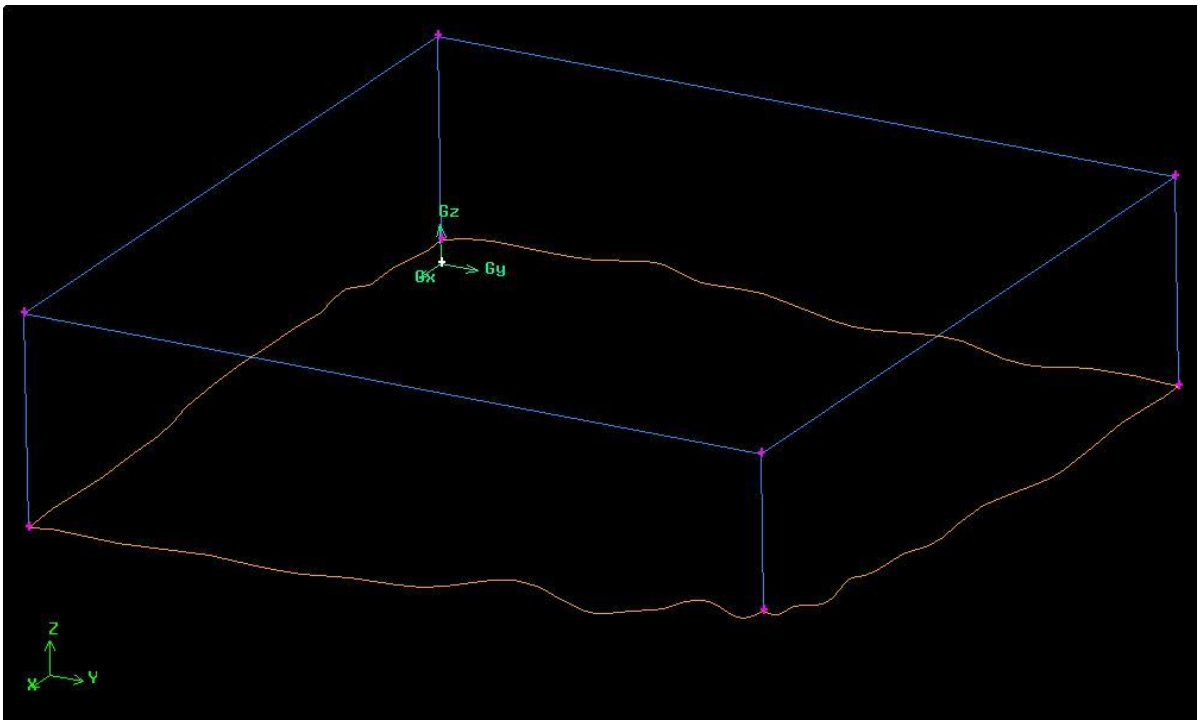

Figure 2- 20*20*5.8 km domain created in GAMBIT

A course structured mesh was created with hexahedral elements, each being 1000 m sided squares (on the XY plane), and using a vertical resolution of 10 elements. Some concentration on the surface was used, having the first 5 elements condensed in the first 500 m. Immediately it was obvious all resolution present in the ground surface was lost, with elements of such dimensions not being remotely able to convey even the biggest geometrical details. Since this was to be a simple simulation to try out Star-CCM+® in modeling wind flows, learning methodologies and beginning to find and solve small problems that would appear during the course of the finer simulations to be done, that lack of resolution was dismissed as non-problematic.

2.4.2 Simulating simplified models

To explore the capabilities of a dual core modern processor, a simulation running 2 parallel processes was created in Star-CCM+®, and into it was imported the `.msh` format mesh created in GAMBIT®. Boundary conditions defined in GAMBIT® (such as symmetry, wall, velocity inlet, etc.) were not recognized by Star-CCM+®, and so had to be defined in it. All 6 surfaces were recognized as one, and as such had to be separated by angle criteria into 6 independent surfaces, which could then be characterized:

- Top, East and West faces: *symmetry* boundary, to simulate continuity of the domain in those directions (translucid blue, in figure 3);
- Ground face: *wall* boundary, imposing no-slip conditions and forcing a boundary layer (solid grey, in figure 3);

- North face: *velocity input* boundary, through which the flow enters the domain (translucid pink, in figure 3);
- South face: *pressure outlet* boundary, through which the flow exits the domain (translucid yellow, in figure 3);

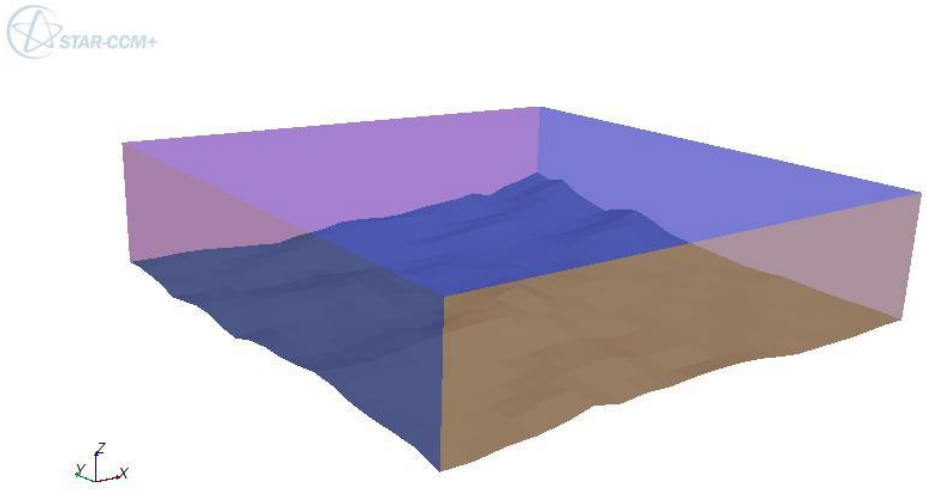

Figure 3 - Geometry displayed in Star-CCM+®, with color coded boundary types

Building the physical model in Star-CCM+® is done in a modular fashion. One window condenses the selection of any models available in the software, the selection of one model opening a branch of related options (figure 4 shows the branches opened by steady, gas and coupled flow model selections) and automatically selecting indispensable models, until all models necessary to run a simulation are selected. Aside from this process are optional models, not strictly necessary to run a simulation.

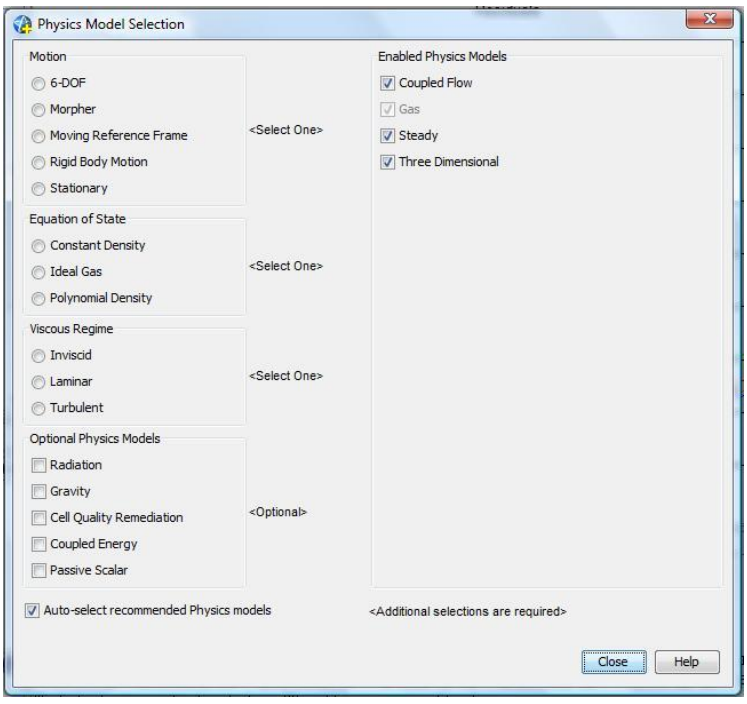

Figure 4 - Physics model selection screen

Default solver and physics models options were not altered: only a constant velocity profile was added at the inlet boundary, of 7 m/s absolute value and the ground defined as a rough wall type boundary, again maintaining default parameters.

In this process, the first problem tackled was that of the density model: initially the ideal gas density model was selected. It implied using the energy equation as well, unnecessary as no heat transfer phenomena existed in the domain. Its substitution for a constant density model allowed greater computational efficiency, by reducing convergence time from ~7 min to 4 min, with no visible alteration in final results.

While attempting to visualize final results another problem surfaced: how to plot data at a plane parallel to the ground, at a given height. Several solutions were tried, such as importing a plane topographically equal to the ground, moved upward to the desired height, or using a *cell surface*, which allowed only to display the first layer of cell adjacent to a given boundary (providing no control over plane height from the ground), all to no avail. Finally, a function called *Wall Distance* was found in the extensive list of user functions included in the software, which combined with an *Iso Surface* allowed to create a surface of constant wall distance, referencing the only wall boundary in the domain, the ground.

The next step would be to optimize the studies by orienting the domain to a given direction, thereby maintaining a structured hexahedral mesh (numerically the most efficient and precise type of mesh for these flow problems, and still capable of accurately representing the ground geometry) and flow oriented mesh.

2.4.3 Optimizing the domain position

The domain would go from a square to a rectangle (when viewed from above), and its faces would no longer be orientated with the North-South and East-West directions, but it would be orientated along the studied direction. The wind farm location would no longer be centered in the domain: the domain would extend from 10 km upstream of a pivot point (centered on the wind farm) to 6 km downstream of it, and be 10 km wide transversally to the flow. That way one was able to reduce the computational demands by drastically reducing the domain size; simultaneously, sufficient map would be maintained upstream - to ensure the wind profile was one influenced by the upstream topography – and both downstream and sideways - to allow the measurements at the wind farm location not to be affected by the nearby presence of the outflow and symmetry boundaries. The case described ahead was one with the domain oriented at 315º.

In order to create the orientated ground surfaces, first attempts experiments with cutting a big enough section of map (in the orthogonal North-South and East-West directions), one able to fit a 16×10 km box orientated in the wanted direction, going from z = 0 m to 5000 m, and through algebraic operations on GAMBIT® use the imported ground surface to separate the box in two, leaving only the needed geometry. GAMBIT® exhibited a lot of difficulties in this

process, being somewhat unreliable. Hence another method was used[1], consisting of rotating the map in `.xyz` format in the wanted direction and "zeroing" all points exterior to the wanted area. After conversion into `.stl` format, the surface was imported into GAMBIT® and the 16×10×5 km domain was created using a slow process of sectioning every edge in the ground and top faces into smaller 500 m sections, forming small faces in the lateral boundaries of the domain with each top/ground edge pair, and finally reuniting all the faces to form the domain's 4 lateral faces. This was the method found which later on would enable the creation of a valid mesh – other methods would result in elements with negative volumes, unacceptable from both a logical and a numerical point of view.

A course mesh was used once again, this still being a simplistic approach to the problem, purely for "debugging" and learning purposes: 32 elements longitudinally by 20 transversally to the flow resulted in square elements with 500 m sides, and vertically 20 elements were used, with some concentration near the ground. The solver and physics model configuration was kept from the first simulation. The results (see figure 5) were able to show local flow acceleration at high altitude points, including in the relevant area, as well as stagnation points downstream of major elevations. What they also revealed was the lack of a developed wind profile at most of the domain, visible by the difference in speed range at the start of the domain (6-8 m/s) and near the outflow boundary (1-3 m/s). Figure 6 highlights this by showing vertical slices of wind speed at inflow boundary, near the wind farm location and at outflow boundary. Starting with a constant speed profile of 7 m/s, when reaching the wind farm near ground minimum speeds were down to 3-4 m/s and by the outflow boundary had reduced further to 1.5 m/s.

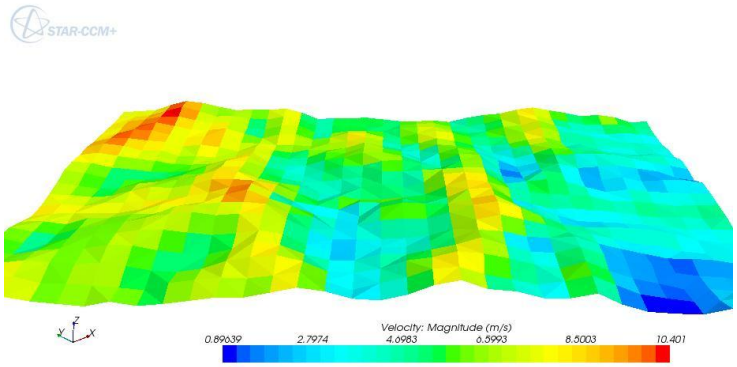

Figure 5 - Wind speed for course mesh simulation @ 85m from the ground, oriented at 315º (flow from left to right)

[1] Devised by Rui Moura using Matlab®

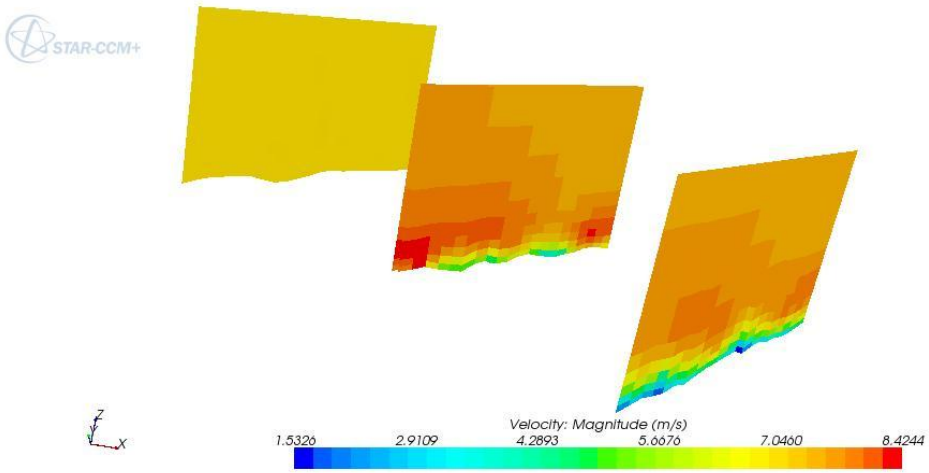

Figure 6 - Vertical slices of wind speed fields for a course mesh simulation, oriented at 315º, at domain inflow, wind farm location and at domain outflow

Extracting reasonable results would mean implementing a logarithmic wind speed profile. It would be defined by

$$u(z) = (u^*/K)\log((z + z_0)/z_0) \quad for\ z \leq \Delta z$$

$$u(z) = (u^*/K)\log((\Delta z + z_0)/z_0) \quad for\ z \geq \Delta z$$

$$v(z) = w(z) = 0.$$

with $\Delta z = 1500$ m being the boundary layer height,

u being the longitudinal speed perpendicular to the inflow boundary,

u^* being the ground friction speed,

$K = 0.4$ being the von Kármán constant,

z_0 being ground roughness length in meters.

First attempts to implement the profile were made through a `.dll` user function library. This required C++ programming to compile the `.dll` library file and hence was presenting a lot of difficulties. Support was gathered[2], but ultimately this approach was dropped in favor of a simpler route[3]: custom user functions can be created within the Star-CCM+® environment, through the field function list. With simple programming and ability to reference other field functions (both default and user-created), using the Star-CCM+® user guide, the logarithmic profile was easily created. This capability revealed to be essential throughout the program's usage, in defining various inflow profiles and custom data plotting functions. The coded functions created can be looked up in Annex C.

[2] Support was given by Mr. João Correia Lopes, professor at the Department of Informatics Engineering at FEUP, who proved extremely helpful in debugging the C++ compiler

[3] Revealed by Mr. Alberto Pinzello, CD-adapco® account manager

3 Modeling the case study

Once sufficient background knowledge had been acquired, more detailed simulations were performed. To this purpose, new, more detailed topography was supplied, along with comprehensive specifications for the turbulence model employed and mesh dimensions and concentration parameters.

Studying the graphic results of the wind data analysis (presented on Annex A), particularly the wind energy roses (the value of greatest interest to this project, since it represents average available wind power), the dominant sectors are southeast and northwest. The values graphed there were clear: for the P042 station data, for which an excellent time spread of data (11 full years) was available, the SE, NW and the NNW sectors together summed up over 75% of the local wind power distribution; for the P384 station, the E, ESE, SE and NW sectors were dominant, at both 30 m and 60 m height cup anemometers; for the P385 station, at 30 m and 60 m height sensors, the SE, NW and NNW again racked up about 75% of total wind power distribution. From these results, it was decided that the 4 main directions to be simulated would be ESE, SE, NW and NNW (112.5º, 135º, 292.5º and 315º in angle format). These 4 sectors were then further divided into 3 each, resulting in 12 directions to be studied, 6 in the southeastern quadrant and other six in the northwestern quadrant, as placed on table 1.

NW	285º	**292.5º**	300º	307,5º	**315º**	322.5º
SE	105º	**112.5º**	120º	127.5º	**135º**	142.5º

Table 1 - Directions simulated, separated by NW and SE quadrants, main directions in bold

3.1 Topography

The new topography was supplied in `.xyz` format. Appended was also a surface roughness map in `.xyr` format - important in defining the boundary layer wall function - and projected wind turbine coordinates. The full map measured roughly 34×35 km. Below (figure 7) is shown an area of about 20 km wide centered on the wind farm, with markings for both the wind turbine and weather station locations, the former in white dots and the latter in black.

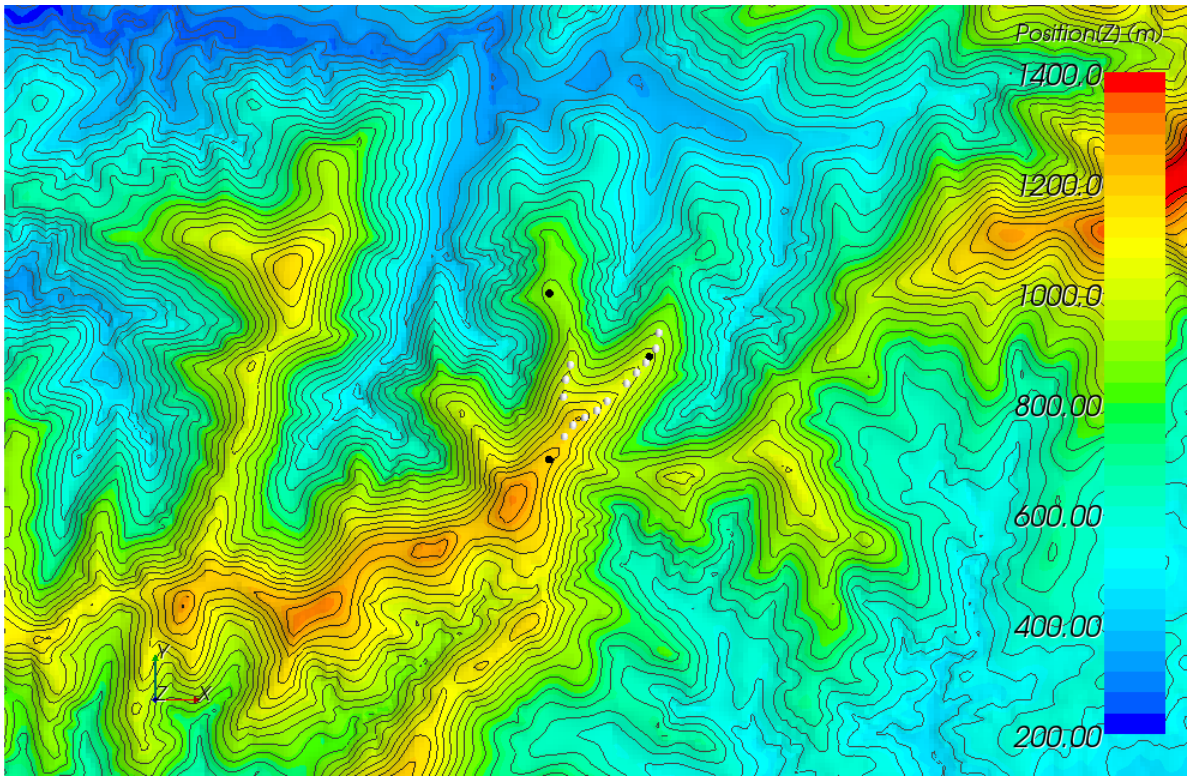

Figure 7 - Wind farm sorrouding topography, with marked weather stations(white dots) and wind turbines(black dots). Y axis oriented North

The location forms a "V" shape roughly oriented NNE, surrounded by considerable elevations on the WSW and ENE directions. The 13 wind turbines are to be placed on both ridges of the mountain range, and the weather stations are located on the vertices of the 'triangle' formed by the shape of the mountains.

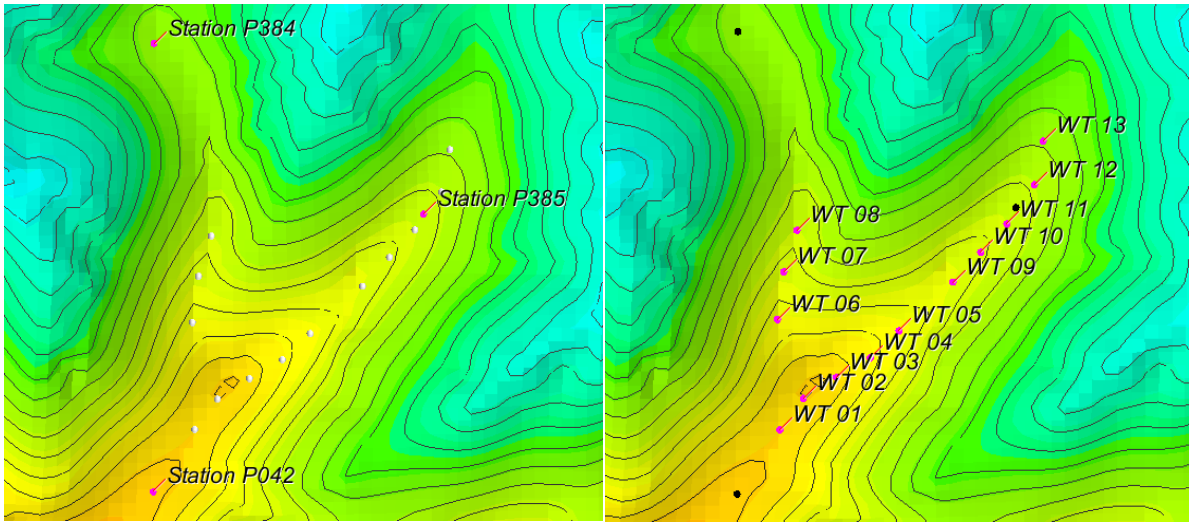

Figure 8 – Weather Station (left) and wind turbine (right) position and names

Being the highest point in the wind farm, the base of the "V", near P042 station (see figure 8), is likely to have generally higher wind speed than near the ends of the mountain range "arms". Most frequently coming from the SE and the NW, the incoming wind is generally calm, as no extreme elevations are present upstream in those general directions; however, some influence is to be expected from the wake provoked by the nearby mountains in the same directions,

particularly when simulating for the ESE and WNW directions: flow recirculation can happen in the valley formed between those mountains. Also, given the orientation of the mountain geometry, when simulating flows from the southeastern quadrant, low speeds may occur on the western branch of the wind farm as it would sit in the wake of the eastern branch. The inverse also applies for simulation of flows from the northwestern quadrant, if in a smaller scale, since the western ridge of the wind farm does not rise as high as the eastern one.

3.2 Domain modeling

As described in section 2, the wanted area was trimmed from the map using a MATLAB function, and re-coded in `.xyz` format. When triangulated and exported to `.stl` format, the ground surface could then be imported into GAMBIT. The domain was modeled using the same slow method of sectioning edges into 500 m segments to create small lateral faces and reunite them in the domain side faces. The dimensions are as used in the last studies of chapter 2: the domain extends 10 km aft to 6 km fore of the pivot point, in the flow direction, 5km each side transversally to the flow and up to a height of 5000m above sea level. A sufficiently fine mesh had to be used to allow reasonable detail in the wind farm location and near the ground, but without being excessively heavy in computer terms. Total mesh size was decided to be of 130 nodes longitudinally, 85 nodes transversally and 50 nodes vertically. In order to accurately portrait the flow field near the wind farm mesh concentration was applied, by having element size progress from a minimum of 30m on the pivot point and increasing towards the boundaries, both in the longitudinal and the transversal direction. The mesh in the xy plane is as shown in figure 9.

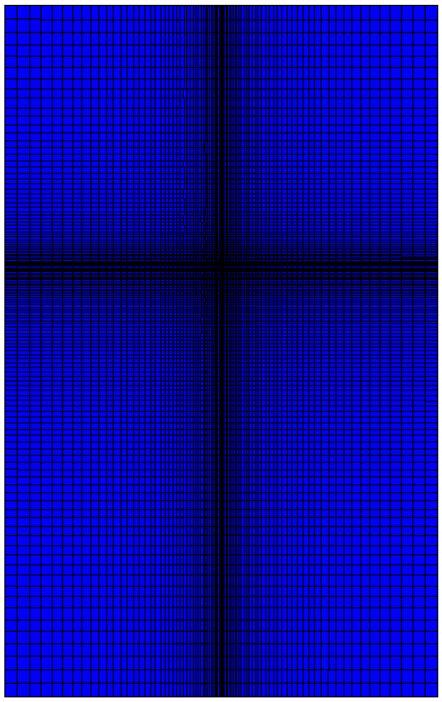

Figure 9 - Mesh concentration in the XY plane

In the vertical direction, an element expansion ratio was used so that the first element near the ground measured 2m (figure 10), spacing the remaining 49 elements accordingly. This level of near-ground mesh refinement is necessary in order that the wall roughness function (as explained further in section 3.3) is correctly described numerically.

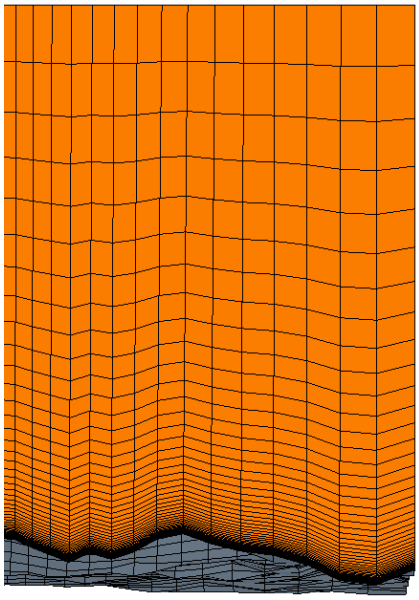

Figure 10 - Domain vertical mesh distribution

3.3 Solver configuration

An obvious model choice was that of a steady gas flow. The chosen density model was one of constant density, since it was a good approximation to the expected gas behavior: relatively low speeds occur in this type of problems (flow compressibility is important at high Mach speeds) and no heat transfer was to happen, as the domain was to be thermally homogeneous.

In initial simulations, a coupled solver for the pressure/momentum equations was used, but this proved to be of both slow convergence and high final residuals when using finer meshes. In theory, a coupled solver uses more memory but is of faster convergence, for it solves both momentum and pressure equations simultaneously as an equation system, unlike the segregated solver, which solves them separately by feeding the latest results of one into the other. However this was not the case, as the coupled solver took, for a similar test case, up to 8h of solver time to stabilize at residuals in the order of 10^{-3}, while the segregated solver completed the same task in less than 2h. From that moment on, the segregated solver was maintained, with good results. Fully implicit formulation is the default solver setup for all equations and was maintained from the start, for the enhanced stability it brings to the solution. As for the discretization method, Star-CCM+® allows the user to choose solely, for the previously enumerated models, between 1st and 2nd order upwind discretizations. If the 1st order upwind method showed to have faster convergence and lower residuals, the solution

quality that was being lost was too high a price to pay for computational efficiency, so the 2nd order upwind method was used for all equations.

In order to solve the Reynolds Averaged Navier-Stokes equations, the k-ε turbulence model was chosen. The values of the constants in the model set by default in Star-CCM+® were changed to those given in table 2, similar values to those presented in [3].

C_μ	$C_{\varepsilon 1}$	$C_{\varepsilon 2}$	σ_k	σ_ε
0.033	1.44	1.92	1.0	1.835

Table 2 – Turbulence model constants used in simulation

Wall treatment is paramount in realistic simulation of the boundary layer flow. To the effect of the no-slip condition (provoking the typical near wall logarithmic speed profile) is added that of ground roughness. It further decelerates the flow throughout the ABL, and promotes turbulence near the ground, thus greatly affecting wind turbine performance. For a large period of the project time-spread, a flawed version of Star-CCM+® (v4.02.007) was used, in which a bug existed in the wall roughness definition: the blended wall and roughness function configuration nodes would appear as normal, but the vital roughness height definition node would not. This was solved when a more recent version of the software package became available (v4.02.011), for which that bug had been removed.

The roughness map supplied suggested a nearly constant roughness length (z_0) of 0.03 m, so the simplification of considering constant surface roughness was applied. The problem of roughness parameter resurfaced when it was realized that Star-CCM+® requires the specification not of the roughness length, but of the sand-grain equivalent roughness height - K_s [1]. Using the conversion formula from X. Zhang [2] $K_s = \frac{E.z_0}{C_s}$, with 0.5 for C_s and 9.793 for E (blended wall function parameter), K_s results in 0,5878 m. This roughness parameter modifies the blended wall function (representing the blending of the viscous sublayer and the logarithmic region) by means of a roughness function *f*, within it defining whether the wall is considered smooth, fully rough or belonging in a transitional roughness regime. The Star-CCM+® User Guide [1] quotes "It should be noted that it is not physically meaningful for $y^+ < R^+$, so the user should take care that the distance from each wall-adjacent cell centroid to the wall is larger than the wall roughness height. Should this condition be violated, STAR-CCM+ will locally limit the roughness height such that $R^+ = y^+$". Being R^+ the adimensionalized roughness parameter and y^+ the adimensionalized wall-adjacent centroid height, it means that the roughness parameter should not be higher than half the wall-adjacent height: K_s being 0.5878 m, a first cell height of 2m (as specified in section 3.2) is sufficient condition to fulfill this. The von Kármán constant used for the blended wall function (as well as for domain entry velocity and turbulence profiles) was 0.4.

As viewed in section 2.4.3, domain entry variable profiles can greatly affect the final result. Perfect velocity and turbulence entry profiles are impossible to define, but good approximations can and should be used, to minimize profile adaptation in the initial part of the domain. The velocity profile used was the same referred in section 2.4.3:

$$u(z) = (u^*/K)\log((z + z_0)/z_0) \;\; for\; z \le \Delta z$$

$$u(z) = (u^*/K)\log((\Delta z + z_0)/z_0) \;\; for\; z \ge \Delta z$$

$$v(z) = w(z) = 0$$

with $\Delta z = 1500$ m being the boundary layer height,

u being the longitudinal speed perpendicular to the inflow boundary,

$u^* = 0.283$ m/s being the ground friction speed (calibrated to produce a main flow speed of aprox. 7.65 m/s),

$K = 0.4$ being the von Kármán constant,

z_0 being ground roughness length in meters.

Non constant turbulence (turbulent dissipation rate ε, and turbulent kinetic energy k) profiles were specified as well. Initially turbulence profiles were sourced from [3], until later on better adapted profiles were supplied, defined by the equations:

$$k(z) = \frac{u^{*2}}{\sqrt{C_\mu}}\left(1 - \frac{z}{\Delta z}\right)^2, \qquad if\; z \le 0{,}99.\Delta z$$

$$k(z) = \frac{u^{*2}}{\sqrt{C_\mu}}(1 - 0{,}99)^2, \qquad if\; z > 0{,}99.\Delta z$$

$$\varepsilon(z) = \frac{{C_\mu}^{3/4}.k^{3/2}}{K}\left(\frac{1}{z + z_0}\right), \qquad if\; z \le 0{,}95.\Delta z$$

$$\varepsilon(z) = \frac{{C_\mu}^{3/4}.k^{3/2}}{K}\left(\frac{1}{0{,}95.\Delta z + z_0}\right), \qquad if\; z > 0{,}95.\Delta z$$

with C_μ being a $k - \varepsilon$ turbulence model parameter.

These newer profiles did not alter significantly the flow map, but in critical areas (pits, valleys and other flow stagnation areas) turbulence was drastically increased. All entry profiles were defined as user created Field Functions. Their Star-CCM+® field function codes are defined in detail in annex C.

Star-CCM+® being a general purpose CFD tool, fine-tuning of the solution convergence characteristics is allowed. The default setup of the various equations solver is as presented on table 3.

Segregated Flow solver					
Velocity			Pressure		
Under Relaxation Factor	AMG Linear Solver Cycle	AMG Linear Solver Convergence Tolerance	Under Relaxation Factor	AMG Linear Solver Cycle	AMG Linear Solver Convergence Tolerance
0.7	Flex Cycle	0.1	0.3	Fixed Cycle	-

$k-\varepsilon$ Turbulence solver		
Under Relaxation Factor	AMG Linear Solver Cycle	AMG Linear Solver Convergence Tolerance
0.8	Flex Cycle	0.1

$k-\varepsilon$ Turbulent Viscosity Solver
Maximum Ratio
100000

Table 3 - Default solver configuration

Under relaxation factors are numerical parameters that allow tuning of the convergence rate of the solution. As the result of an updated solution to the equations emerges, instead of fully using the new solution as entry values to the next iteration, the solver adds the difference between the previous and the most recent solution to the older set, multiplied by a factor α, called under relaxation factor or URF. These can assume any value greater then 0, but are usually maintained below 1 (if they are greater than 1 they are usually called over relaxation factors). This is because URFs greater than 1 (and many times even URFs lower than 1, as will be shown next) usually provoke instability in the solution, hence causing divergence. Optimum URF setup is usually problem specific, so as no standard setup was available for use one would have to be found through testing. Internally, various iterations of a specific equation are executed, to ensure that the slow convergence of an equation does not affect the remaining equations. This is done using the AMG Linear solver, which can employ 2 strategies: a "Flex Cycle", that does the necessary number of internal iterations to reach a certain minimum residual (called convergence tolerance) or a "Fixed Cycle", in which are defined precisely the number of passes done on the given equation. Further information on the specifities of each cycle type are defined in the application's User Guide [1].

The default setup lead to solutions with high residuals, without the quality required by the problem. An extensive program of testing with different parameters was carried out, by increasing the URFs in search of the solver stability limits and testing both AMG Linear solver cycles searching for the fastest possible convergence. High URFs during the initial iterations can cause strong divergence, so the default values were kept at least for the first 200 iterations. A $k-\varepsilon$ turbulence solver URF of 1 provoked severe instabilities in the solution, so a compromise was found at 0,95. Pressure and velocity URFs of 0.5 and 0.9, respectively, lead to the same behavior, so a rise to 0.8 in pressure and 0.4 in velocity URFs accelerated convergence without destabilizing the solver. The turbulence viscosity ratio (ratio between local turbulent viscosity and laminar viscosity) was limited at default value of 100000, which resulted in constant warnings by the solver of internal limiting of the parameter. This automatic limiting is done to prevent occurrence of solver instability in some situations. This occurred particularly when using the initial turbulence profiles, improving (if not completely) once the newer profiles were adopted. In [2] it is said to be a common occurrence when simulating ABL flows, where much higher numbers are expected. As such, a maximum ratio

of 2,0E7 was adopted. Final solver parameters, used in all final simulations, are specified in table 4.

Segregated Flow solver					
Velocity			Pressure		
Under Relaxation Factor	AMG Linear Solver Cycle	AMG Linear Solver Convergence Tolerance	Under Relaxation Factor	AMG Linear Solver Cycle	AMG Linear Solver Convergence Tolerance
0.7 rising to 0.8 on iterations 200 till 250	Flex Cycle	0.1	0.3 rising to 0.4 on iterations 200 till 250	Flex Cycle	0.1

$k-\varepsilon$ Turbulence solver		
Under Relaxation Factor	AMG Linear Solver Cycle	AMG Linear Solver Convergence Tolerance
0.8 rising to 0.95 on iterations 250 till 300	Flex Cycle	0.01

$k-\varepsilon$ Turbulent Viscosity Solver
Maximum Ratio
20000000

Table 4 - Final solver configuration

The solver stopping criteria were setup so that a final solution was reached as soon as continuity, x, y and z momentum, k and ε equation residuals reached a minimum of 5,0E-5. Higher precision would not necessarily yield better results and would consume valuable computer time (at low residual levels convergence can be slow, exponentially increasing this factor). Also, the horizontal speed profile on wind turbine WT01 was monitored to ensure that solution data had stabilized.

3.4 Result extraction

The format in which numerical data is extracted from each simulation is important in that the data processing method may require some alteration to correctly use the data. Two main result formats were extracted from the program: direct printouts of the 2D turbulent intensity, horizontal velocity and flow pitch contours at various heights and raw point data at weather station and wind turbine locations.

The 2D contour printouts were done without major difficulties. Care was taken to ensure that the same map scale and pivot point was used in all maps. This scale and pivot point were chosen so that the whole wind farm and some surrounding area (in particular in the upwind and downwind directions, where relevant flow detail may appear) were shown, while still allowing to clearly distinguish wind turbine position in relation to the different color contours. The different color scales were also adapted so that, for the turbulent intensity and flow pitch contour maps, the "default" acceptance limit values were discretized. On the horizontal velocity maps flow vectors were also plotted, in order to show the path taken by the wind, highlighting refluxes and major flow deviations. A bug was found in the turbulent intensity plots, where the coloring is plotted correctly only up until values of 0.12. Values higher than those are plotted one color higher than they actually are (ex: points in the 0.12 to 0.15 range

are plotted as belonging to the 0.15-0.18 range and so forth). Various attempts at resolving this defect were tried, such as different color ranges and scale partitioning, all to no avail. As the reader may be mislead by the falsely plotted values, this fact should be kept in mind when consulting the annexed turbulent intensity contour maps.

The point data revealed to be more problematic in its processing. In order to construct vertical profiles of several variables, measurements at various heights were done. To accomplish this, vertical lines were placed on the relevant locations, starting roughly below the ground surface and measuring about 250 m, sufficient to ensure that measurements were captured to profile any variable from ground height up to at least 150 m. On those lines 50 measurements were made, ranging from ground height to the highest point in the line. This resulted in a minimum theoretical height resolution of 5 m (a part of the 250 m of line were outside the domain, on most locations the real resolution is of 4-4.5 m). A higher resolution was not used as it would create an excessive amount of information, making the data processing slower and more tiresome. Ideally, measurements would be made at a series of chosen ground heights (capturing the exact heights of 30, 60, 44, 85 and 126 m), but no easy method to do so was found. As such, the measurement method lead to "random" height values, not precisely on the needed points but reasonably near. The choice of using interpolation to capture the referred heights was pondered, but as it would further difficultate data processing with negligible precision gains, it was chosen to take the nearest extracted measurement as the point value for the point data tables presented in annex B. On the vertical profiles presented the same section, plotting on heights below 10 m were avoided, as rarely would the lowest extracted value be near enough to 0 m to capture the near ground no-slip profile behavior, falsely leading the reader to think this condition was not included in the model.

Added to tabulating and plotting the point data extracted directly from Star-CCM+®, one other parameter was used in evaluating the flow field and wind conditions. This was the shear factor. It is a way of expressing the velocity profile incline: how steeply velocity varies with the *z* coordinate. The expression used to calculate shear factor is

$$SF = \log\frac{v_2}{v_1} \Big/ \log\frac{z_2}{z_1}$$

with the 2 index referencing point higher then point 1, and v being horizontal velocity.

Some necessary flow characteristics were not defined within the default Star-CCM+® field function library. Their mathematical definition is presented ahead, with the equivalent Star-CCM+®'s field function code presented on annex C.

Horizontal velocity:

$$v_h = \sqrt{{v_x}^2 + {v_y}^2}$$

Turbulent intensity:

$$TI = \frac{\sqrt{\frac{2}{3}k}}{v_h}$$

Flow pitch:

$$Flow\ Pitch = \tan^{-1}(v_z/V)$$

Flow yaw:

$$Flow\ Yaw = \pi + \cos^{-1}\frac{v_x}{v_h}\ , \quad for\ NW\ sector\ directions$$

$$Flow\ Yaw = \pi - \cos^{-1}\frac{v_x}{v_h}\ , \quad for\ SE\ sector\ directions$$

4 Result analysis

Site assessment studies with CFD serve the need to describe in both quantity and quality the wind resource of an area. Analyzing a site, wind turbine locations are chosen by successively applying filters which progressively restrict the valid areas. In that sequence, maximizing wind resource exploration through optimum layout follows the elimination of areas where wind turbine integrity cannot be assured, perspective through which this study intends to follow.

The first step in analyzing a numerical flow field is to ensure the validity of the physical/numerical model employed. This is done through a comparison of the produced numerical results and real field measurement data of various points. This seeks not so much to find total precision of numerical results, but moreso to ensure the model portraits the general flow behavior throughout the majority of the considered area – how the flow pitches, yaws and accelerates, where it stalls and where it is most disturbed by the topography – in a form as similar as possible to the actual on-site flow.

Following model validation, a thorough review of the flow field can be done, in this case study taking into consideration the planned wind farm layout. Weather station measurements are put aside, and wind turbine point values, vertical profiles and 2D map contours are taken on to question wind turbine placement (according to previously referred parameters) and generally describe the flow field according to the topography.

4.1 Solution Convergence

On the computational side of the results, care was taken to guarantee total convergence on all simulations, independently of number of iterations and solver time taken to accomplish the task. On occasions the solver tended to diverge strongly deep into the simulation, greatly increasing number of iterations and solver time taken to reach the desired residual levels. These numbers are presented on table 5.

Simulation	Solver Time (min)	Nº Iterations	Residuals					
			Continuity	X momentum	Y momentum	Z momentum	TDR	TKE
105º	173	820	1.62E-6	4.48E-5	3.35E-5	4.16E-6	4.98E-5	8.48E-6
112.5º	105	698	2.90E-6	4.99E-5	2.93E-5	4.32E-6	9.34E-6	8.31E-6
120º	212	1100	1.83E-6	4.99E-5	3.24E-5	3.78E-6	3.07E-5	5.40E-6
127.5º	561	2529	4.49E-6	4.27E-5	3.29E-5	3.78E-6	4.99E-5	5.32E-6
135º	160	883	2.26E-6	4.98E-5	4.40E-5	6.04E-6	3.99E-5	3.64E-6
142.5º	83	304	6.47E-6	4.99E-5	4.73E-5	5.23E-6	3.14E-6	3.81E-6
285º	136	739	1.94E-6	4.99E-5	3.44E-5	4.32E-6	1.93E-5	8.18E-6
292.5º	151	873	2.87E-6	4.98E-5	4.42E-5	5.08E-6	3.56E-5	7.88E-6
300º	216	1152	9.23E-7	2.80E-5	1.93E-5	2.39E-6	4.99E-5	7.67E-6
307.5º	120	617	1.78E-6	4.87E-5	4.97E-5	4.11E-6	2.76E-6	8.97E-6
315	199	599	1.59E-6	4.97E-5	4.38E-5	3.29E-6	2.41E-5	7.88E-6
322º	97	559	2.81E-6	4.99E-5	4.93E-5	3.95E-6	1.59E-5	6.11E-6

Table 5 - Star-CCM+ solver convergence data

All simulations were run on an ASUS FV8 series notebook, equipped with an Intel Core 2 Duo P8400 processor and 3.0 Gb of RAM memory.

4.2 Model Validation and correlation study

A model validation study is no straightforward comparison of local values: data comparison only makes sense when one is comparing produced numerical results with data measured when the wind had roughly similar characteristics, situation in which quantifying the differences between both is meaningful. As such, this is done taking a reference location for which the model is calibrated: when the wind (measured and simulated) has similar properties on the reference location, a good model should guarantee that equally similar properties are seen on other points of the map.

The first step in this method is to list synchronized measurements for all 5 measurement points. This is done by appending all simultaneous registers to the same timestamp, being then possible to filter all data according to any selected measurement. P384 and P385 weather station data were easily synchronized (both had the same measurement period), P042 requiring truncating in order to select the same time period as the two other stations (March 2007 to September 2008).

For this correlation study, P384 weather station's measurements at 30 m height were used as calibration reference. Velocity and flow direction values were selected as calibration parameters, meaning that registers possessing similar velocity and direction values to the numerical results (of a given simulation) were selected from the whole time frame. The numerical data for the remaining cup anemometer locations are then compared with the average of the simultaneous measurements (post filtering).

Naturally, a comparison between measured and numerical velocities and directions for the calibration reference is not significant, as the studied registers were precisely those that had approximately the same value, resulting in very low relative error percentages. Turbulent intensity, on the other hand, was not a calibration parameter and as such the same comparison is in this case valid. The numerical shear factors presented in tables 5 and 6 are not extracted from those plotted on figures 41 through 46 of annex B, but are calculated using solely the velocity at 30 and 60 m height, so as to be comparable with the measured shear factor.

The reason why turbulent intensity was not used as a calibration parameter is of a practical nature: selecting data with relatively fine filters on 2 parameters easily causes low sample sizes; adding a third parameter would greatly reduce an already small sample size, jeopardizing the statistical validity of this analysis. Adding to that factor, turbulence modeling is still, to date, one of the most troubling areas in CFD and proves in many cases difficult to describe accurately, so higher discrepancy between numerical and measured data may be significantly higher than on other variables, restricting sample size even further. Filter tolerances were of ±0.5 m/s on velocity and of ± 3º on direction.

4.2.1 Correlation error analysis

Depending on the considered direction, sample sizes are above 100 registers on all but the 322.5º direction, on which only 55 registers remained following filtering. Even so, when comparing relative errors for that simulation with those from other simulations (some with much higher sample dimensions) no notable differences are seen, relieving concern over using such a small sample.

In a quick view over the error values presented on tables 5 and 6, one notices a general tendency for relatively low error levels, most under 15%. This is a positive initial pointer, but further study is advisable. It should also be highlighted that the shear factor errors can rise at times to extremely high numbers, but those errors should be viewed with care, for reasons explained further ahead in this section. Highlight also to the relative importance of the errors for the different variables: errors in velocity predictions can be of much greater importance than TI, for example, since in terms of wind energy, an overestimation of 15% in the velocity equates to overestimating wind energy by over 50%.

The P042 station revealed to be the one most diverged from measured data. If the direction was always reasonably accurate, usually overestimating by about 10º (except for the three directions nearest to E, where the numerical direction was slightly under the expected level), velocity and TI showed much higher differences, reaching at a velocity error of 57.3% for the 142.5º direction and a TI error of 64.6% on the 300º direction. For SE inbound winds, velocities were usually overestimated and TI underestimated, while the opposite occurred for NW inbound winds.

These discrepancies on velocity and turbulence values on the P042 station may be due to several facts:

- it is the most distant to the reference station;
- P042 is placed at a greater height than the P384, in a location where the flow is strongly accelerated and model errors can be amplified by it;
- it is placed only 30 m above ground level, in an area of extreme flow acceleration, where wind conditions (particularly speed) can vary steeply with height.

		Numerical Data				Measured Data				Error Analysis			
		Dir. (º)	Hor. Vel. (m/s)	TI	SF	Dir.(º)	Hor. Vel. (m/s)	TI	SF	δ_{dir} (º)	ε_{vel} (%)	ε_{TI} (%)	δ_{SF}
		105º (sample size: 100)											
P042	30 m	115.6	8.43	0.094	-	125.6	8.01	0.100	-	-10.1	5.1%	-6.1%	-
P384	30 m	97.9	6.77	0.128	0.05	98.2	6.70	0.163	0.05	-0.2	1.1%	-21.3%	0.005
	60 m	98.6	7.03	0.131		112.2	6.93	0.159		-13.6	1.4%	-17.5%	
P385	30 m	114.8	8.53	0.124	-0.03	135.6	7.66	0.112	-0.01	-20.8	11.4%	10.8%	-0.018
	60 m	113.5	8.35	0.127		137.0	7.60	0.115		-23.5	10.0%	9.6%	
		112.5º (sample size: 140)											
P042	30 m	121.5	9.57	0.093	-	123.8	8.09	0.116	-	-2.3	18.3%	-19.7%	-
P384	30 m	105.9	7.21	0.128	0.04	106.2	7.22	0.151	0.05	-0.3	-0.2%	-15.5%	-0.004
	60 m	106.2	7.42	0.131		105.7	7.46	0.147		0.5	-0.5%	-10.7%	
P385	30 m	118.3	8.56	0.128	0.00	134.4	7.59	0.119	-0.01	-16.1	12.8%	7.9%	0.014
	60 m	118.5	8.58	0.128		133.7	7.54	0.124		-15.3	13.9%	3.1%	
		120º (sample size: 117)											
P042	30 m	123.8	10.11	0.082	-	125.6	7.34	0.124	-	-1.7	37.7%	-34.3%	-
P384	30 m	114.4	5.53	0.156	0.06	113.7	5.66	0.169	0.08	0.7	-2.2%	-7.5%	-0.020
	60 m	114.1	5.78	0.162		111.6	5.99	0.157		2.5	-3.5%	3.1%	
P385	30 m	130.4	6.18	0.124	0.00	137.9	6.50	0.131	0.00	-7.5	-4.9%	-5.3%	0.005
	60 m	129.1	6.19	0.134		137.7	6.48	0.136		-8.6	-4.5%	-1.1%	
		127.5º (sample size: 126)											
P042	30 m	129.5	9.42	0.092	-	126.4	7.23	0.120	-	3.0	30.3%	-23.1%	-
P384	30 m	116.1	5.37	0.165	0.06	116.2	5.36	0.171	0.10	-0.1	0.1%	-3.4%	-0.036
	60 m	117.2	5.60	0.174		113.7	5.73	0.159		3.5	-2.3%	9.0%	
P385	30 m	130.5	8.31	0.115	-0.02	137.5	6.41	0.130	0.00	-7.0	29.7%	-11.4%	-0.023
	60 m	130.9	8.18	0.120		137.7	6.41	0.132		-6.7	27.7%	-9.0%	
		135º (sample size: 200)											
P042	30 m	141.0	7.55	0.118	-	128.3	7.05	0.112	-	12.7	7.1%	5.4%	-
P384	30 m	127.2	5.85	0.154	0.05	126.9	5.84	0.148	0.09	0.3	0.1%	4.0%	-0.032
	60 m	127.7	6.07	0.161		121.0	6.20	0.136		6.7	-2.1%	18.2%	
P385	30 m	135.9	7.42	0.109	0.02	145.1	6.65	0.121	-0.03	-9.2	11.5%	-9.2%	0.051
	60 m	136.5	7.54	0.116		145.2	6.53	0.124		-8.7	15.5%	-6.1%	
		142.5º (sample size: 206)											
P042	30 m	137.0	10.05	0.094	-	130.1	6.39	0.114	-	6.9	57.3%	-16.9%	-
P384	30 m	133.6	4.87	0.167	0.05	134.0	4.84	0.190	0.09	-0.4	0.8%	-12.4%	-0.039
	60 m	133.6	5.05	0.178		128.5	5.15	0.179		5.1	-1.9%	-0.7%	
P385	30 m	136.9	6.53	0.141	0.08	144.5	6.35	0.127	-0.04	-7.6	2.7%	10.4%	0.122
	60 m	138.5	6.89	0.145		144.7	6.17	0.127		-6.2	11.8%	14.5%	

Table 6 - Weather station point data and correlation error for SE sector simulations

Numerical velocity and direction were very close to those measured at the P384 60 m cup anemometer, particularly for the NW sector winds, with an average absolute error of about ±2º for the direction and ±2% for the velocity. On the SE front, absolute direction errors were only marginally higher (±4º average), except to the direction on the 105º direction, were a 13.6º underestimation was registered. This level of errors was to be expected, measuring locations being separated by just 30 m. TI values were not as close to those measured, with errors ranging from -28.5% to 18.2%. This demonstrates how hard phenomena turbulence is to model, when other flow characteristics are so accurately predicted.

As with the P384 60 m cup anemometer, flow direction errors at the P385 weather station revolved around ±2º on the NW sector and were slightly higher on the SE sector (±6º), 105º and 112.5º directions excepted, where underestimations of over 15 to 20º were found. This tendency for greater accuracy in direction values when simulating winds of the NW sector can be explained by the presence of sizeable elevation upstream of winds incoming from SE,

which may be deflecting the flow prior to the P385 station more extremely than the simulations suggest.

		Numerical Data				Measured Data				Error Analysis			
		Dir. (º)	Hor. Vel. (m/s)	TI	SF	Dir. (º)	Hor. Vel. (m/s)	TI	SF	δ_{dir} (º)	ε_{vel} (%)	ε_{TI} (%)	δ_{SF}
		285º (sample size: 185)											
P042	30 m	302.4	8.96	0.117	-	291.2	9.47	0.115	-	11.2	-5.4%	1.8%	-
P384	30 m	277.9	6.35	0.112	0.02	278.2	6.37	0.149	0.03	-0.4	-0.2%	-25.3%	-0.013
	60 m	278.9	6.42	0.123		276.1	6.50	0.147		2.8	-1.2%	-16.4%	
P385	30 m	295.2	7.22	0.134	0.01	297.6	8.07	0.126	-0.06	-2.5	-10.5%	6.9%	0.068
	60 m	294.2	7.28	0.140		294.5	7.75	0.129		-0.3	-6.1%	8.5%	
		292.5º (sample size: 263)											
P042	30 m	301.2	8.98	0.119	-	293.3	11.08	0.095	-	7.9	-18.9%	26.2%	-
P384	30 m	288.4	7.73	0.109	0.00	288.2	7.72	0.127	0.03	0.2	0.1%	-14.3%	-0.030
	60 m	288.7	7.73	0.115		286.6	7.88	0.118		2.1	-1.9%	-2.8%	
P385	30 m	300.7	8.09	0.120	0.01	300.7	10.04	0.101	-0.04	0.0	-19.5%	19.5%	0.047
	60 m	299.8	8.13	0.127		298.6	9.78	0.105		1.2	-16.8%	21.4%	
		300º (sample size: 285)											
P042	30 m	309.6	11.00	0.144	-	296.2	11.57	0.087	-	13.4	-4.9%	64.6%	-
P384	30 m	293.1	7.65	0.111	0.03	292.8	7.63	0.132	0.04	0.4	0.3%	-15.9%	-0.008
	60 m	293.9	7.83	0.119		291.5	7.85	0.124		2.4	-0.3%	-4.4%	
P385	30 m	305.2	8.76	0.120	0.01	303.6	10.85	0.091	-0.05	1.6	-19.3%	32.3%	0.056
	60 m	304.6	8.81	0.127		301.4	10.50	0.096		3.2	-16.1%	32.7%	
		307.5º (sample size: 313)											
P042	30 m	309.5	10.30	0.091	-	298.0	10.65	0.092	-	11.5	-3.2%	-1.4%	-
P384	30 m	296.3	6.62	0.126	0.04	295.6	6.60	0.146	0.05	0.7	0.2%	-13.7%	-0.011
	60 m	297.8	6.81	0.132		295.0	6.85	0.133		2.8	-0.5%	-1.2%	
P385	30 m	307.8	8.33	0.126	-0.02	305.8	9.98	0.096	-0.06	1.9	-16.5%	31.2%	0.046
	60 m	307.4	8.23	0.130		303.7	9.54	0.100		3.7	-13.8%	29.1%	
		315º (sample size: 232)											
P042	30 m	314.2	11.50	0.079	-	300.8	10.75	0.092	-	13.3	7.0%	-13.7%	-
P384	30 m	307.4	6.44	0.131	0.03	306.6	6.42	0.159	0.07	0.8	0.3%	-17.6%	-0.032
	60 m	308.3	6.60	0.134		303.9	6.73	0.146		4.4	-1.9%	-8.0%	
P385	30 m	314.6	9.20	0.099	-0.06	312.0	10.52	0.095	-0.09	2.6	-12.6%	4.9%	0.028
	60 m	314.6	8.83	0.105		310.8	9.90	0.099		3.8	-10.9%	5.4%	
		322.5º (sample size: 55)											
P042	30 m	317.5	9.75	0.092	-	306.5	11.41	0.084	-	11.0	-14.5%	10.3%	-
P384	30 m	316.7	6.92	0.113	0.04	316.5	6.96	0.175	0.09	0.3	-0.5%	-35.4%	-0.054
	60 m	317.2	7.11	0.116		318.9	7.41	0.162		-1.7	-4.1%	-28.5%	
P385	30 m	318.1	7.87	0.088	0.06	315.9	11.53	0.093	-0.08	2.3	-31.7%	-5.0%	0.141
	60 m	318.7	8.21	0.094		315.5	10.91	0.095		3.2	-24.7%	-1.7%	

Table 7 - Weather station point data and correlation error for NW sector simulations

Wind velocity results were not as similar to measured data as flow direction values for the P385 station. For the SE sector, errors were generally around +10% and peaked at almost 30% for the 127.5º direction. The NW sector simulations revealed a considerable tendency to underestimate wind velocity, frequently closing on -20% and peaking at -31.7% for the 322.5º direction. For this sector velocity was always more severely underestimated at 30 m.

Turbulent intensity at the P385 location was generally overestimated (except for the 120º, 127.5º, 135º and 322.5º, where it was slightly underestimated), particularly in the 300º and 307.5º direction, where errors of over 30% occurred.

Shear factor is a difficult characteristic to accurately capture in ABL flows, if the ground is other than a nearly flat surface. Aggressive topography combined with a rough wall can lead to wildly variable vertical wind profiles, as can be seen on the velocity vertical profiles shown in annex B. Given the logarithmical nature of the shear factor function, velocity variations are greatly amplified in the shear factor values. The very slight differences expected between velocities at different heights of the same location added to the approximate nature of CFD analysis can lead to naturally different measured and numerical shear factors, maybe even switching from a positive to negative SF or vice versa. For this reason, shear factor correlation should not be too valued, so as to not give the wrong impression about the model quality. Some improvement could be attained by studying in finer detail the applied wall treatment and near-wall mesh fineness.

P384 shows the best shear factor correlation results of all. Both numerical and measured SF are always positive, errors showing some undervaluing by the numerical model, with absolute errors being kept below 0.02. This tendency is increased with the proximity to the north/south axis, where peak errors of over 0.03 occur.

A grimmer scenery appears on the P385 weather station: measured data shows negative shear factors throughout the field, whereas numerical data frequently show positive shear factors. In some cases (142.5º and 322.5º directions) absolute error reaches levels above 0.1, where measured and numerical SF have highly opposed figures.

The conclusions presented in this section should be taken into account in the following flow field study. Tendencies to over or underestimate parameters in certain locations or wind sectors should be input into the analysis of those same parameters, where the executed calibration can make a difference in considering a location appropriate or not for wind turbine deployment.

4.3 Flow Field analysis

Two sets of studies were executed on the flow field result produced on Star-CCM+®. Firstly, the local contour maps were reviewed to learn how the topography affects the relevant variables in the wind farm area and respective surroundings: areas of high flow acceleration, stagnation and recirculation, excessively disturbed wind and extreme surface incline effect on flow pitch are identified, and the global wind farm layout is viewed in relation to these parameters.

Following this global approach to wind condition study on the wind farm, a more profound analysis is executed, in which individual wind turbine variable plots are taken into account and particularly problematic locations are highlighted, in light of the relevant wind condition parameters (turbulent intensity, flow pitch, shear factor) that restrict safe wind turbine behavior. The used “standard” limits for those parameters are those laid out on section 1, and are repeated here for the reader’s convenience:

- Turbulent intensity > 0.18;
- Shear factor < 0 or > 0.2;
- Flow pitch < -8º or >8º.

These limits are only reference values, they do not need to be followed too strictly. Some overstepping of these boundaries is allowed without the need for alarm. Only if more than one of the parameters is at or slightly over the referred limits, or when one of the variables majorly exceeds them, should special care be taken and possible alternative locations for that specific wind turbine sought.

4.3.1 Flow field map review according to topography

Turbulent flow over a flat smooth surface is one easily characterized, for which empirically derived profiles exist for many years now. However, atmospheric flows over irregular geometry such as mountains is a wholelly different problem, with highly unpredictable flow patterns whose characterization implies the use of tools and techniques such as those described in this report.

Possessing an idea of the topography of the area, one can predict some tendencies (though not in extreme detail) of flow behavior, as done in section 3.1, or inversely search for explanations in the topography for phenomena encountered.

All contour maps presented within this section are but cropped sections of the full contour maps presented on annex B (figures 56 through 91).

4.3.1.1 Velocity field

Wind flow accelerates over topography in a relatively straightforward fashion, flow speed up increasing with the elevation, and falling abruptly downstream of big elevations. However, the relative position of the elevations when viewed from the inflow direction leads to effects harder to predict, with the mountain inclines deviating the flow in a highly varying manner and wake position and dimension changing considerably. Velocity contour maps are presented on figures 56 through 67 on annex B. Supporting those figures on this analysis are the individual wind turbine point data tables 8 through 20 of annex B, for discrete values at the various heights studied.

When viewing the contour map at various heights (figure 11), flow acceleration effects on the wind farm site smoothen as height increases. Also, as one steps away from the ground irregularities, effects as flow recirculation, wind stagnation and flow deviation soften.

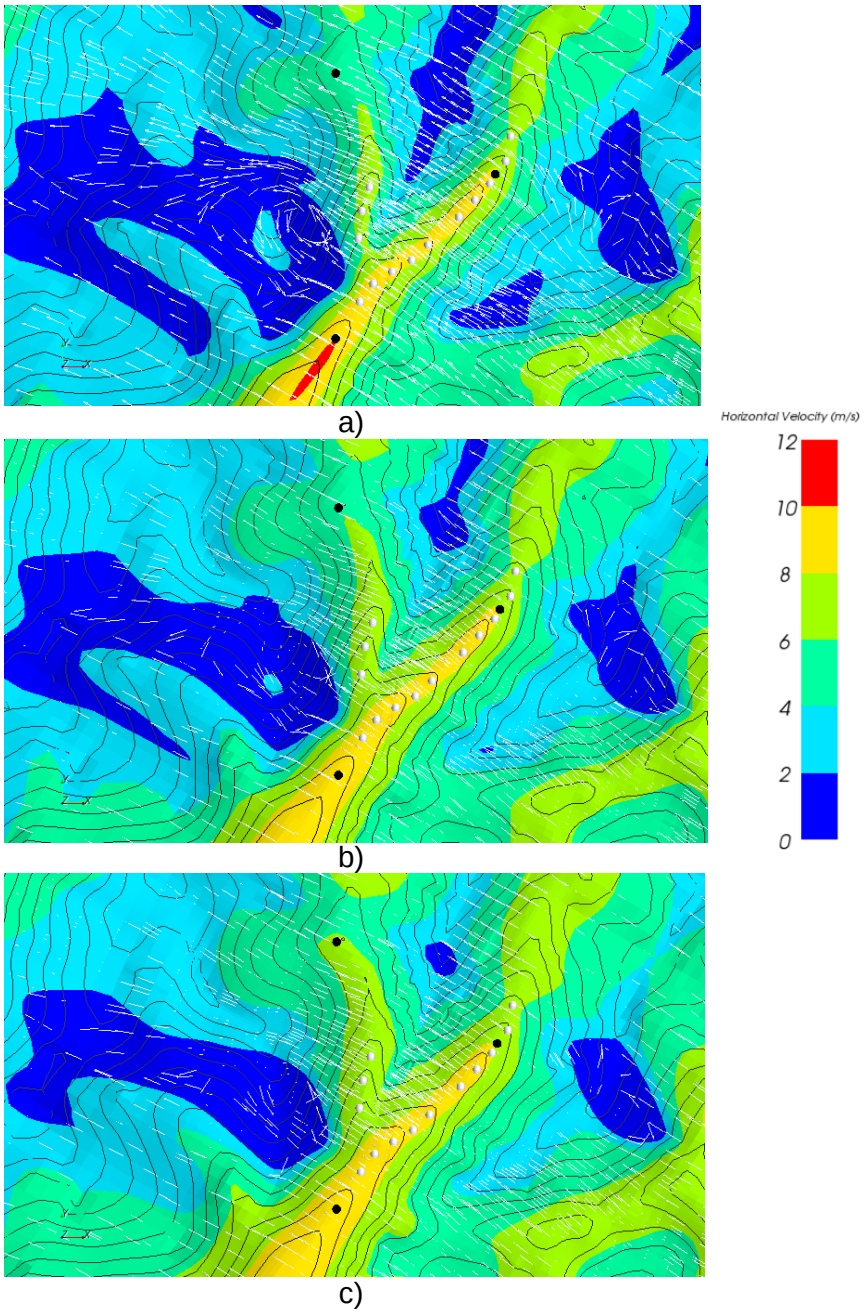

Figure 11 – Local horizontal speed plots at 44 (a), 85 (b) and 126 (c) m a.g.l., for the 120º direction

On the SE sector simulations, at 44 m a.g.l., the flow accelerates mainly near the mountain range peak (near P042) up to nearly 10 m/s and to about 8-9 m/s on the eastern ridge. The western ridge tends to fall in the wake of that speed up zone, falling to 6 to 7 m/s. A major stagnation and recirculation point appears immediately downwind of the mountain range (affecting peak speeds in the southern part of the wind farm on directions 127.5º and 135º, as seen in figure 12); flow stagnates also in between eastern and western ridges and just upwind of the eastern ridge, caused by the elevation that precede those zones.

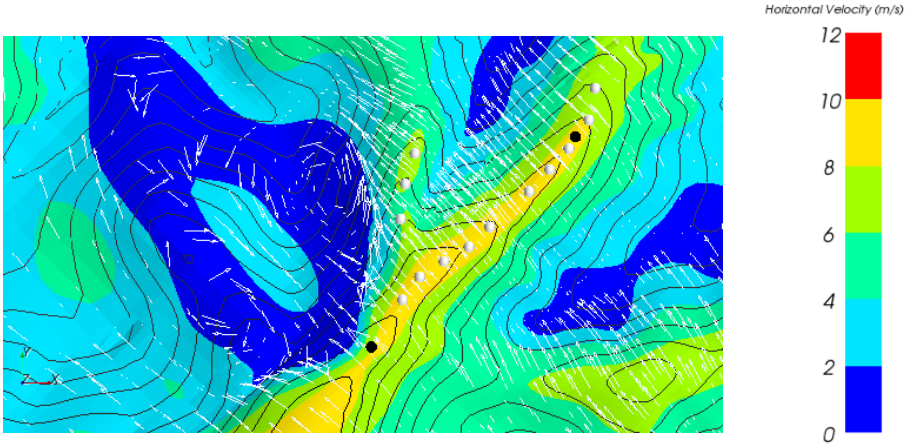

Figure 12 - Stagnation zone downstream of the main elevation afecting peak velocities at the southern branch of the wind farm, on the 135º direction @ 85m a.g.l.

As the incoming wind direction progresses from SE sector to more South oriented, speeds at the western ridge tend to diminish. This may be a consequence of that area beginning to fall under the wake of the main southern elevation (where WT 01 is located) and the flow beginning to deviate north amid the two wind farm ridges (see directions 127.5º through 142.5º).

At 85 m a.g.l., the scenery does not change drastically. The two smaller stagnation points described above nearly disappear, as does the flow deviation between the eastern and western ridge. Speed generally decreases, except for the western ridge, where a slight increase is verified. At the level of 126 m a.g.l., this tendency further progresses, and wind stays generally undisturbed direction-wise, as it passes over the mountain range, practically only the stagnation downwind of the mountain range remaining.

For NW sector winds, the velocity distribution on the wind farm area is not as uniform as for SW sector winds. Velocities at the highest point of the wind farm (WT 01, WT 02 and WT 03) now reach levels higher than 10 m/s and at the western ridge they are a bit higher than for the SW winds (at 7-8 m/s). Curiously speeds near turbines WT 05 and WT 09 are lower than at the extreme of the eastern ridge or the southern part of the wind farm, as figure 13 shows.

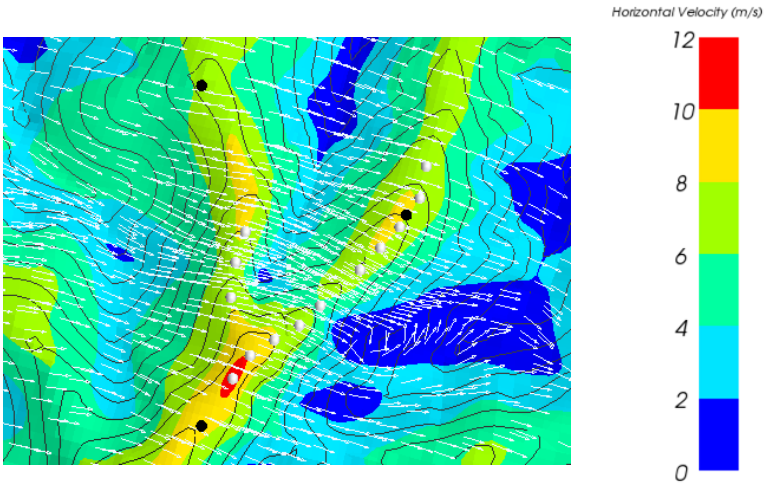

Figure 13 - Particularly low speeds occur near turbines WT 05 and WT 09, for NW sector winds (pictured is the contour map for the 285º direction @ 44m a.g.l.)

A major stagnation point occurs immediately downwind of the range, with major recirculations for the 285º, 292.5 and 300º directions. When the incoming flow direction approaches NW, the flow tends to deviate strongly at that point, turning south sharply while passing between the wind farm area and the elevation east of it. At the same time, speeds at the western ridge tend to decrease, the opposite happening at the eastern ridge.

As one progresses from ground heights of 44 m a.g.l. to higher numbers, unlike expected, stagnation points do not seem to diminish. Flow deviation amid the wind farm and the mountains to the east of it also seems to maintain. Only at 126 m a.g.l. on the 285º, 292.5º and 300º directions do stagnated flow areas seem to decrease (figure 14).

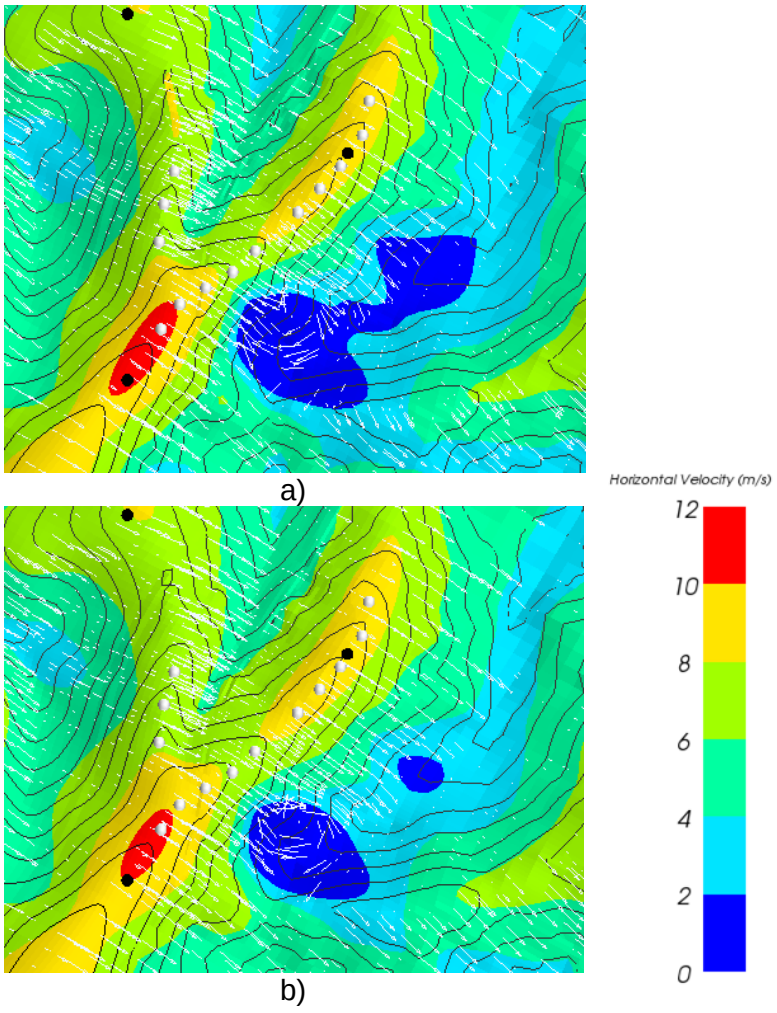

Figure 14 - Stagnated flow areas diminish between 85 (a) 126 (b) m a.g.l for the 300º direction

4.3.1.2 Flow pitch field

The flow pitch contours plot all values above 8º or under -8º as dark red or dark blue, hence the area moderate pitch (-8º to 8º) is reduced, and discretizing between different values in

that range can be hard. However, this allows easy identification of wind turbines under excessive flow inclinations.

Flow pitch has a generally predictable behavior, as it mainly follows the incline of the surface it is flowing over. Hence, in flat areas it takes near 0º values. As expected, on the wind farm ridge flow pitch is generally moderate, since on it the surface has practically 0º incline. Because of this, the following analysis mainly serves to identify locations of the wind farm where this does not comply. The contour maps for flow pitch are present on figures 68 through 79 of annex B.

When wind enters the domain from the SE sector, the southern and eastern ridges turbines are within the 4-8º range, with a tendency to progress to a more moderate pitch as the flow starts to hit the wind farm mountain range more transversally to it, as figure 15 shows. The western range of the wind farm is affected by a moderately negative pitch, except for WT 06 where it seems to be on (and at times overcome) the -8º limit. The flow pitch numbers seem to become less aggressive as distance from the ground increases, with only WT 06 remaining critical.

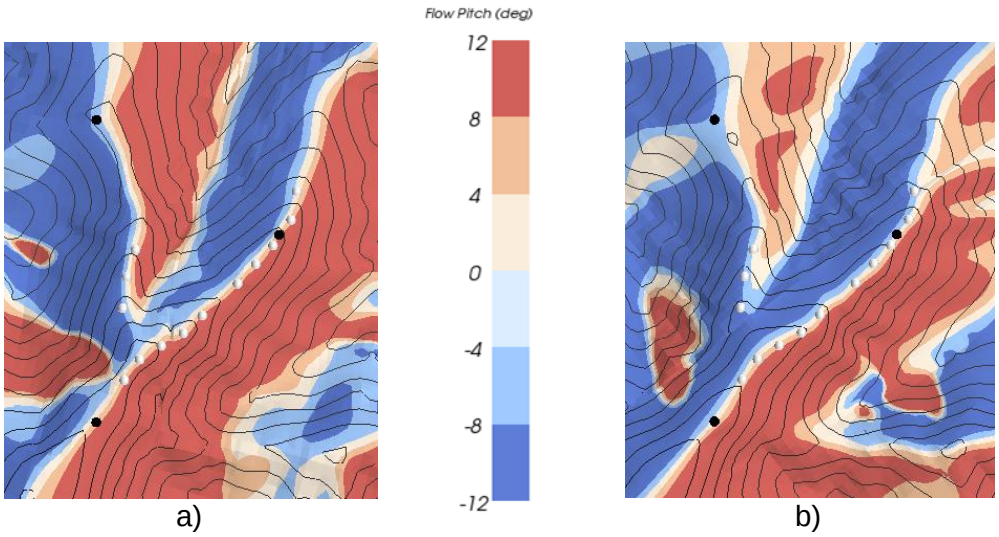

Figure 15 - Flow pitch on the wind farm neutralizes as incoming wind direction shifts from 105º (a) to 142.5º (b) (44m a.g.l. contours pictured)

As for the NW sector simulations, all the way from 44 m a.g.l. to 126 m a.g.l. the southern and eastern ridges change from a moderately negative pitch to a moderately positive pitch number as the incoming flow direction changes from W to NW, generally going from -4º to +4º. The single significant change with ground height is that of the widening of the referred moderate pitch area on the southern and eastern ridges. Opposite to the SE sector simulations, the western ridge is now under positive pitch numbers, with problematic numbers for turbines WT 06 and WT 07.

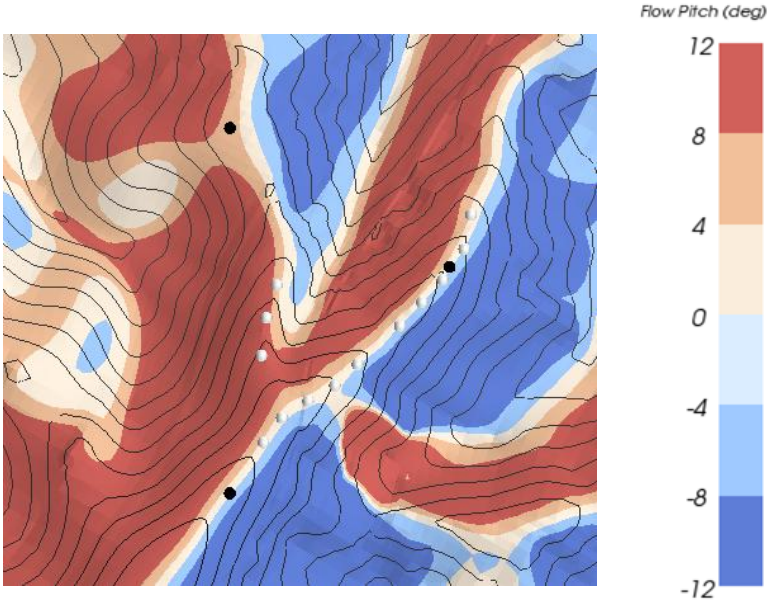

Figure 16 – Near zero flow pitch values on the southern and eastern ridges and strong positive values on the western ridge for NW inbound winds (pictured is the contour map for the 300º direction @ 85m a.g.l.)

4.3.1.3 Turbulence Intensity field

Sharp variations in the ground incline are the main promoters for turbulence. When wind flows over a crest where it is accelerated and ground surface falls quickly, the flow detaches from the surface and chaotic variations in wind speed and direction (turbulence itself, which turbulence intensity measures) increase. With the scale of the topography studied in this report, this turbulent wake can extend for multiple kilometers and reach high levels.

The TI contours presented in figures 80 through 91 of annex B use a color scale limited to 0.24, but this level can easily be exceeded within the plotted areas, but when that does happen, it does so at places where one would expect it and in areas of no interest to this study, which focuses on the ridge of the wind farm mountain range.

When the wind enters the domain from the SE sector, turbulence shoots up downstream of the wind farm, after flowing over its peak and descending into the valley that follows, the wake extending far into the limit of the depicted area (see figure 17). High turbulence regions are also present in the valleys between the E and W ridges of the mountain range and at the valley formed between the E ridge and the elevation upstream of it.

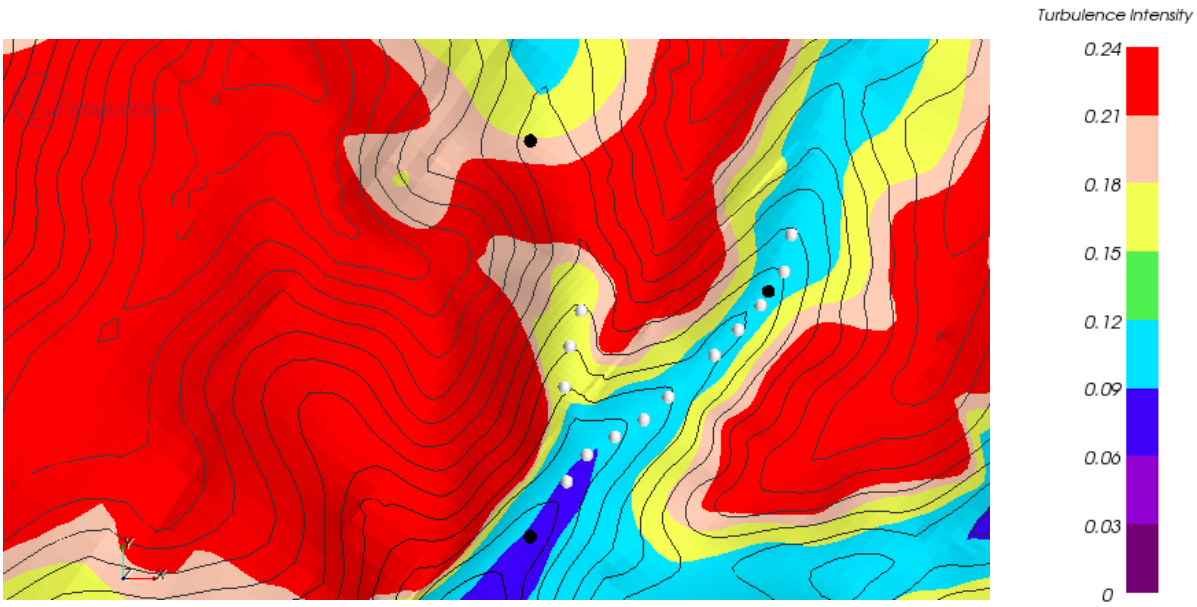

Figure 17 - Extensive turbulent wake forms downstream of the wind farm for SE sector winds (contour map for the 127.5º direction @ 85m a.g.l. pictured)

The southern ridge of the wind farm always possesses low turbulence intensity (in the 0.06 to 0.09 range), as the wind enters it generally undisturbed. The western and eastern ridges suffer from higher TI's (particularly the western ridge), being located in the wake of the turbulent zones described above, but these never enter dangerous levels. TI tends to increase on the western and eastern ridges as the wind direction progresses form 105º to 142.5º, as the flow begins to detach over the southern ridge and a wake is formed in a position increasingly north of it. Global turbulence levels fall off at higher heights, with practically the whole wind farm falling in the 0.06 to 0.12 range at 126 m a.g.l.

The flow enters the wind farm mountain range less disturbed for NW sector winds than with SE sector winds: a large TI area exists upstream of the wind farm, but TI levels dissipate as the flow approaches the wind farm. Just as with the SE sector winds, a large wake is formed downstream of the mountain range, being the biggest elevation in the zone. TI levels at the western ridge are lower than for SE sector winds, where they were affected by the wake from the E ridge, now rarely going over 0.12.

As the wind direction shifts from 285º over to 322.5º, TI levels at the eastern ridge drop, since the flow hits the western ridge less directly, reducing the turbulence zone amid the eastern and western ridges, TI level dropping down to about 0.09 for the 322.5º direction.

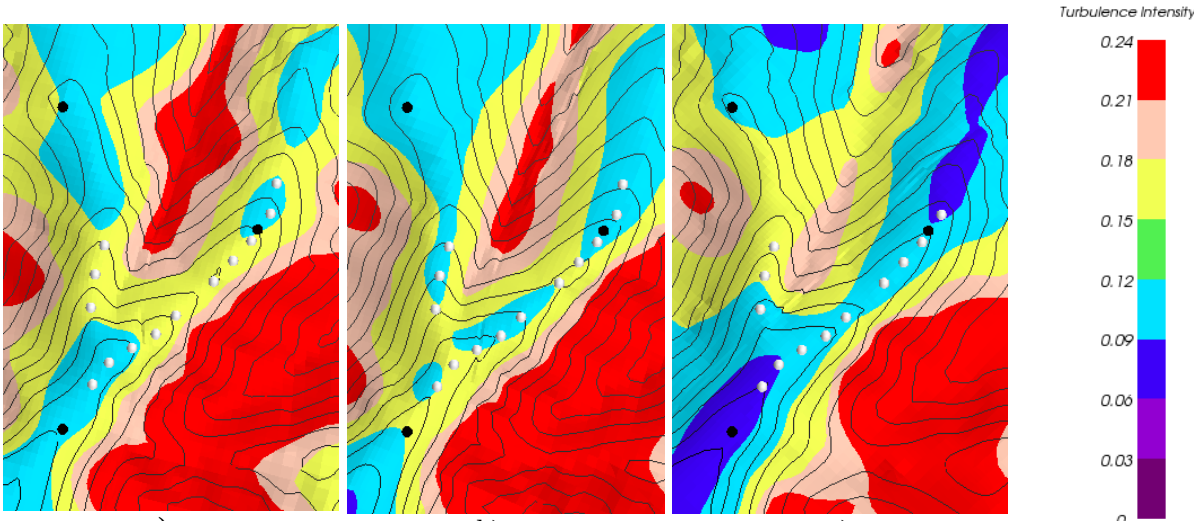

a) b) c)

Figure 18 - High turbulence levels remain in the 285º (a), 292.5º (b) and 315º (c) directions at 126 m a.g.l.

TI levels gradually drop down to levels below 0.12 throughout the wind farm, maintaining levels above that only on the 285º, 292.5º and 315º directions.

4.3.2 Wind turbine location assessment

Some troubling areas of the wind farm have already been identified in the previous flow field analysis. Now wind turbines will be individually reviewed in search of wind parameters on levels endangering safe wind turbine operation.

The western ridge has been seen to be under effect of high levels of flow pitch, so special care will be taken in its study. The southern and eastern ridge also presented some possibly dangerous levels of flow pitch, so this analysis will serve to decide whether one should show concern over the turbines placed on them in concrete terms. Added to the variables used before, shear factor will too take an important part in the inspection executed hereon.

All velocity (figures 33 through 36), shear factor (figures 37 through 40), turbulent intensity (figures 47 through 50) and flow pitch (figures 52 through 55) vertical plots are located within annex B. When relevant, copies of individual plots will be presented in this section for the reader's convenience.

4.3.2.1 Wind Turbine WT 01

WT 01 shows average speed levels on the SE sector in the 7-10 m/s range, rising as high as 11 m/s for the NW sector. The major difficulty with the NW sector speed plots are their

considerable incline, which result in significant negative shear factors (between 0.05 and 0.09), particularly for the 292.5º direction, for which it alarmingly falls below -0.1 for most of the wind turbine rotor span (figure 19). Flow pitch rises near the reference values on the 112.5º and 292.5º directions but never overcoming them.

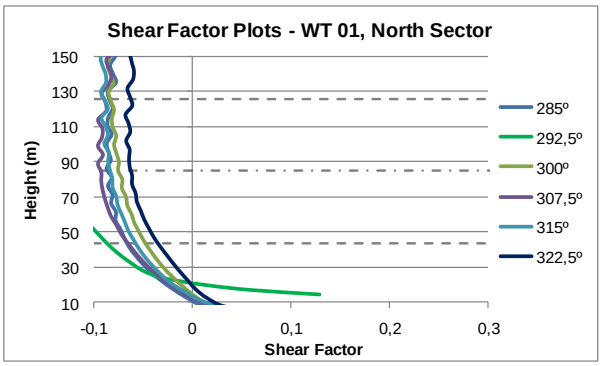

Figure 19 - WT 01 showing strong negative shear factors for NW sector winds

4.3.2.2 Wind Turbine WT 02

Velocity levels are similar to those seen on WT 01, with speed profile steepness diminishing throughout the range. Still, NW sector winds lead to strongly negative SF levels, 292.5º direction being once again of particular concern as shear factor steps under -0.1 for the top end of the rotor span (figure 20). Flow pitch is on the 8º limit near ground level for the 105º and 112.5º directions, but it falls to more neutral levels by 44 m a.g.l.

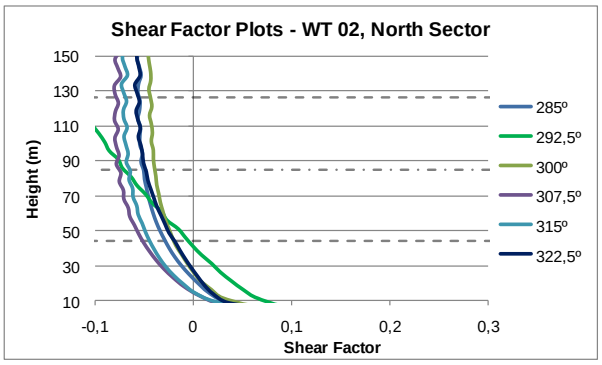

Figure 20 - WT 02, as WT 01 presenting aggressive negative shear factors on the NW sectors, particularly on the 292.5º direction

4.3.2.3 Wind Turbine WT 03

Velocity plots present some negative slope of levels more moderate than on WT 01 and WT 02, with peak velocity on the NW sector lowering to slightly over 10 m/s. Shear factor plots reveal this softer tendency, with shear factors globally above -0.05 on all but the 292.5º and 307.5º directions, where they slowly progress to -0.06 near 126 m a.g.l.

At ground level flow pitch takes values of nearly 10º for the SE sectors and -10º for the NW sectors, but these levels rapidly decrease to acceptable numbers (particularly for the NW sector simulations, where they almost reach 0º by 150 m a.g.l.), falling inside the permissible range in wind turbine rotor span area.

4.3.2.4 Wind Turbines WT 04 and WT 05

Being very homogeneous on most simulations, WT 04 wind velocities show a steep profile on the 300º direction, leading to a strong positive shear factor, nearing the 0.2 limit (but never overstepping that boundary) amid 44 m and 85 m a.g.l., to then drop to about 0.1 at greater heights. Direction 135º on the other hand presents a negative shear profile deserving of notice, reaching -0.07 at about 85 m a.g.l. As such, the situation occurring at a single simulation, the situation does not show much cause for preoccupation.

On WT 05 velocity profiles present average velocity levels, with generally moderate negative shear factors. As with turbine WT 04, shear factor reaches -0.07 on the 135º direction. No other results worthy of notice lead to the dismissal of this number as an isolated effect of little potential real consequence.

4.3.2.5 Wind Turbine WT 06

This is one of the few wind turbines presenting distinctly positive shear factors, if only for the SE sector directions. Upon seeing the velocity plots for the sector this is expected, amounting to shear factors above 0.2 on directions 127.5º through 142.5º (figure 21), particularly under 44 m a.g.l., but still exceeding that reference on the lower part of the rotor span. This SF number may in reality be further exaggerated, since one verified on section 4.1 that shear factors near the P384 weather station tend to be under measured levels. This worrying trend adds to high flow pitch levels (figure 22), particularly for the NW sector simulations where levels as high as 11º are reached on various directions, and TI levels nearing 0.18 at 44 m a.g.l. to form a hash case for this location.

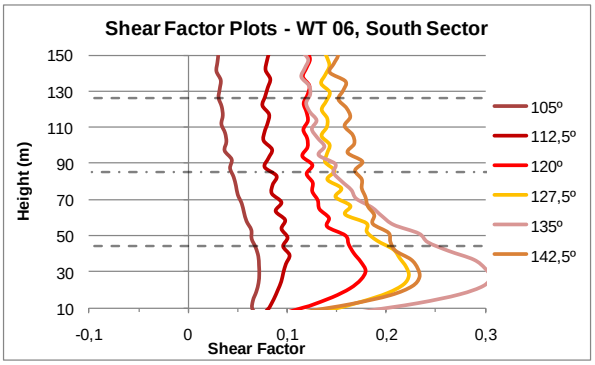

Figure 21 - Strong positive shear factors on WT 06 for the SE sector simulations

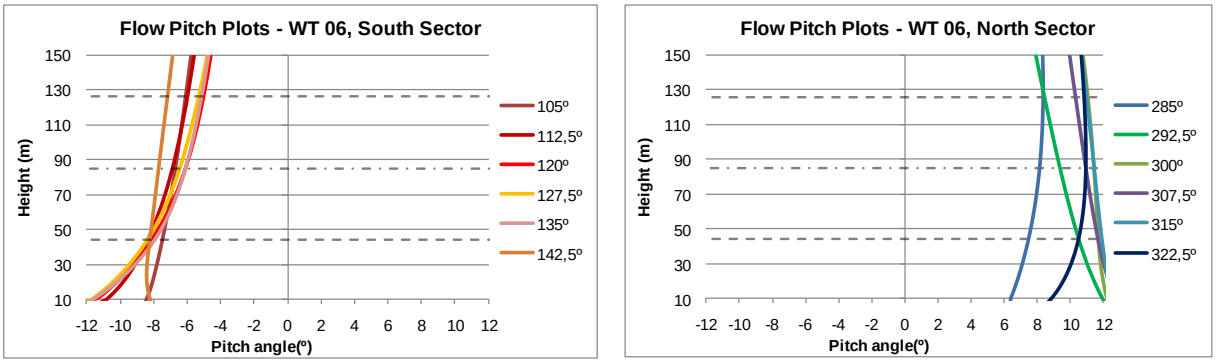

Figure 22 - Elevated flow pitch numbers at turbine WT 06

4.3.2.6 Wind Turbine WT 07

A similar scenario to wind turbine WT 06, if not as drastic, is presented on WT 07. On the SE sector simulations, the 142.5º direction resulted in nearly 0.2 shear factor on the whole rotor span (figure 23) with TI levels bordering on 0.18 at 44 m a.g.l and borderline negative flow pitch levels on multiple directions. As before (on WT 06), these shear factor levels may be higher in actual conditions, considering the model calibration showed that real measurements seem to present greater numbers.

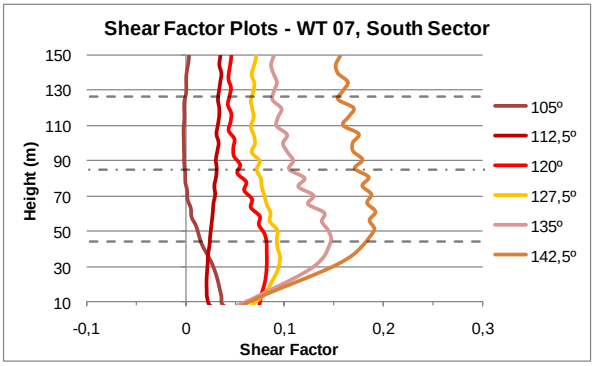

Figure 23 - Elevated shear factors on WT 07 turbine may be intensified in actual conditions

NW sector winds reveal far more worrying, with strong negative shear factors on the lower half of the rotor span (figure 24) for directions 285º and 300º combined with flow pitch

numbers above 8º on multiple simulations (figure 25). Model calibration tells us that shear factors in this area, for NW sector winds, tend to be underestimated, so these values may in the real world be more reasonable. Still, numerical results suggest dealing with WT 07's location with care.

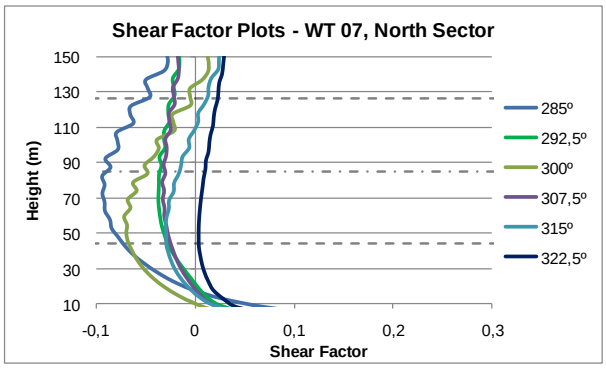

Figure 24 - Strong negative shear factors on turbine WT 07 on directions 285º and 300º

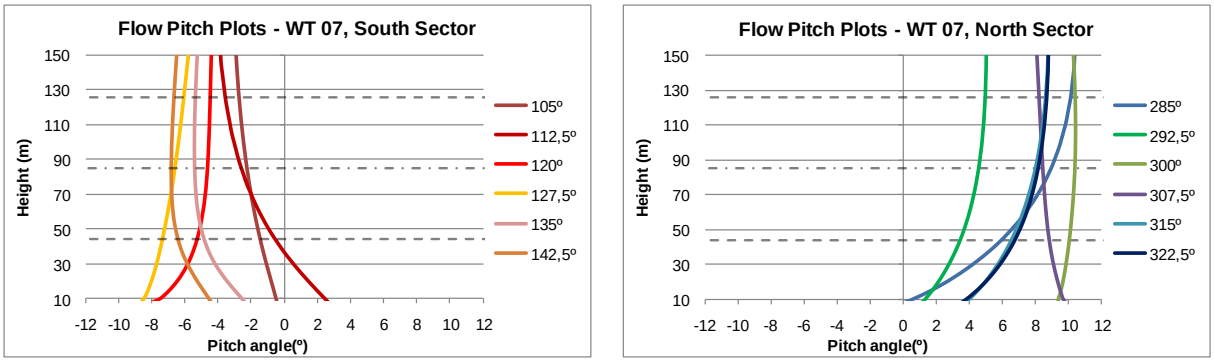

a) b)

Figure 25 - Steeply inclined flow on several directions of the SE (a) and NW (b) sector at WT 07

4.3.2.7 Wind Turbine WT 08

At WT 08 strong positive shear factors appear once again on all SE sector simulations, if not as meaningful as on WT 06 and WT 07 turbines. TI plots show near limit levels of turbulence near 44 m a.g.l, decreasing along the rotor span. NW sector winds present a calm scenario on TI and flow pitch plots, but the shear factor plots (figure 26) show worryingly high negative shears on direction 285º. If, as seen before, real shear factor numbers may be slightly higher, such an extreme trend should not be taken lightly.

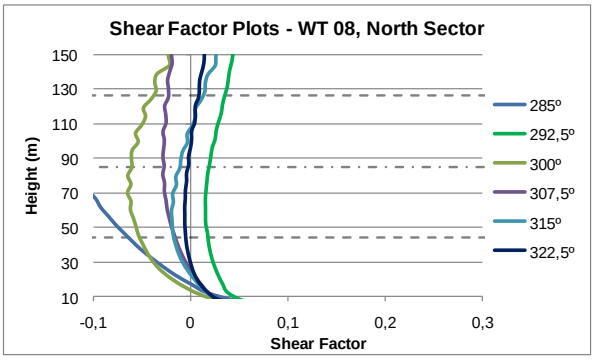

Figure 26 - Strong negative shear factor at WT 08, on the 285º direction

4.3.2.8 Wind Turbines WT 09 and WT 10

Numerical results express moderately negative shear factors (-0.05 at most) on practically all directions of both wind turbines. While numbers for the NW sector winds are further lessened in real terms, judging by the analysis done on model calibration, the 120º and 135º directions are cause for preoccupation: peak levels of shear factor of -0.07 were captured in simulation (figure 27), with a tendency to be further exaggerated on site, as the nearby P385 weather station correlation study revealed a trend of SF overestimating. This represents a valid cause for worry.

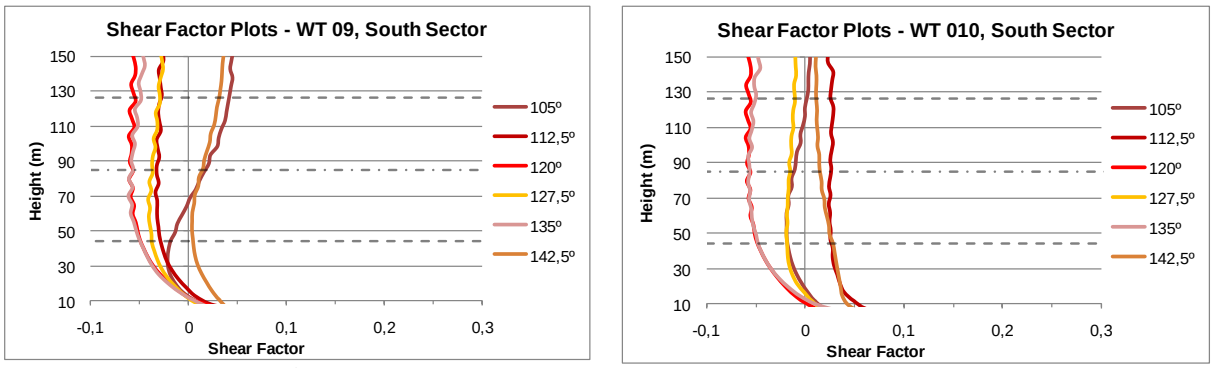

a) b)

Figure 27 - Moderate negative shear factors on turbine WT 09 (a) and WT 10 (b) can be further exagerated in real world conditions

TI levels on both turbines for the 300º direction go near the 0.18 limit at lower heights, but never actually overcome them.

4.3.2.9 Wind Turbines WT 11, WT 12 and WT 13

Shear factor wise, the scenario is similar to turbines WT 09 and WT 10, except for the fading out of the strong values seen on directions 120º and 135º. Turbulence intensity results are also very similar to those seen on those locations, particularly for turbine WT 11.

Neutral pitch flow numbers are observed throughout the map. The single notable exception happens on direction 292.5º at WT 13, where a near constant +8.1º pitch level is maintained on the whole rotor span. The +8º is not exceeded in a remarkable fashion, and it presents itself as an isolated occurrence and so does not prove deserving of much attention.

5 Conclusion

CFD revealed to be an extremely complex subject: profound knowledge of fluid dynamics and numerical methods are required in order to use it legitimately as an engineering tool. The initiating user is presented with an extremely steep learning curve, being asked to show solid foundations on those subjects, strong logical thought process and analytical skills to accurately comprehend the processes at work in its application. Adding to the understanding of the way the RANS equations translate to a numerically solvable problem, the user should also comprehend domain meshing methods, in the form of the implications of mesh size and element shape in producing high quality results. Many hours were spent learning about solver configuration to discover numerical stability limits and ensure full problem convergence. Other skill sets, such as comprehension of the details regarding statistical analysis of wind data, were acquired in the process.

Characterization of atmospheric boundary layer flows in wind condition studies involve various parameters and modeling characteristics specific to this area. Turbulence and velocity profiles are difficult to characterize, and much research has been and still is dedicated to the understanding of their form, how they relate to topography through wall law functions. This study was done under the light of the work developed by many individuals and institutions who dedicated many hours to this cause.

5.1 User experience in using Star-CCM+®

Initially intimidating in the way a lot of information is displayed to the user, Star-CCM+® reveals, as confidence grows, to be of great ease of use, all functions required to fully configure the solver, physical models, domain boundaries and solution visualization being readily available in the user interface. An extremely powerful and flexible visualization tool was found integrated in the software. Tasks such as adding objects, plotting multiple variables in the same scene and 3D view manipulation were executed rapidly and in a stress-free manner, resulting always in high quality plots. These characteristics dominated the handling of the software package.

During specific phases of the study, certain fine points integrated in the program revealed to be extremely helpful, reducing considerably user time expenditure in tasks not meaningful to the purpose of the study. When studying solver configuration, the fact that it could be altered "on the fly" without interrupting the progress of the simulation, shortened a job that, if long, could have taken much longer in completing. In producing the final various simulations, the possibility to open multiple cases simultaneously and transfer objects between them revealed instrumental in avoiding the chore of repeatedly creating the same objects, such as visualization scenes, point data reports, field functions and derived parts.

The single major difficulty found in the usage of Star-CCM+® occurred when extracting discrete local values to construct point data tables and variable profiles: no form of precise placing of the probe points on relevant ground heights (such as 30 and 60 m a.g.l for weather station data and 44, 85 and 126 m a.g.l. for wind turbine data) was found, resorting as such to acquiring approximate height values, incurring in some lack of precision. A solution to this, combining the *Wall Distance* field function with some user programmed function or a certain combination of Derived Parts, might have been possible through further experimentation.

5.2 Wind conditions on the studied wind farm location

During correlation study and model calibration revealed generally low error levels. Direction errors were usually in the ±5º range, while turbulence intensity and velocity results fell on average within ±15% of actual measurement values. Only shear factor prediction proved to be truly difficult, with absolute differences of ±0.04, many times numerical and measured values presenting opposing signals. This may be given to wall law definition: its influence in the results is extensive and affects, to a great extent, the area of interest of this study, the lower part of the boundary layer from 0 to 150 m a.g.l. Further research on the form in which Star-CCM+® models the wall law could be pursued in search of improved results. Investigating the effect of finer mesh resolution at near ground heights might also prove to be worthwhile: cell height was fixed at 2 m at ground level, but references [1] and [2] show that ground level cell centroid height should be no smaller than the sand-grain equivalent roughness height, which was set at 0.5878 m, hence leaving scope to decrease ground level cell height to about 1.2 m. Further studies using other calibration references could have been done to verify or find other trends.

Results show a flow field troubled by the presence of the wind farm mountain range, its surroundings being strongly affected by the flow detachment that occurs downstream of it, promoting turbulence and resulting in areas of strong recirculation and flow stagnations. The elevation east to the wind farm mountain range also proved to affect results on the eastern branch of the wind farm, as the flow detaches passing over it for SE sector winds. Strong flow deviation for both NW and SE sector winds was found amid the eastern branch of the wind farm and that same elevation, particularly when the wind enters the domain on a orientation near the North-South axis.

Depending on whether the flow enters the domain from NW or SE, the eastern or western ridges of the wind farm, respectively, fell in the wake of one another, strongly affecting wind characteristics on them. This effect was most noticeable on the western ridge, the lower of the two, where wind speeds were strongly diminished by that effect, leading as well to a distinctively positive shear factor, not commonly found throughout the whole result map. A similar effect was encountered on more northbound winds, as the flow detached passing over the southern ridge and the wake formed began to invade the rest of the wind farm, primarily the western ridge.

TI contours never raised much concern over any particular areas of the wind farm. Flow pitch, on the other hand, presented a harder case for the western branch, where strong negative flow pitch areas appeared on NW sector simulations. Flow pitch on the eastern and southern areas of the wind farm seemed to progress from near limit positive numbers to more neutral ones, as wind direction shifted from east to southeast oriented.

When finally analyzing wind turbine individual situations, rough wind conditions were found in some of them. Wind Turbines WT 06 and WT 07 accumulate various severe effects, inspiring the most worry. Flow pitch was near or over the -8º to +8º limit on multiple directions of both wind turbines. This fact added to shear factor numbers reaching (and stepping over, at the WT 06 turbine) the +0.2 levels on southeast sector winds, and going very near the -0.1 level, in case of turbine WT 07 on northwest sector winds. The correlation study showed that the model was underestimating shear factor levels near the P384 weather station, which while lessening the latter case (negative shear factors on turbine NW sector winds), tends to show that the situation might be further worsened on the SE sector.

Turbines WT 01 and WT 02 suffer from strong negative shear factors on NW sector simulations, nearly at -0.1 on most cases and on the 292.5º direction even going far below that level. WT 08 also showed shear factor shooting far under the -0.1 number, though in truth it might be lessened by the tendency of the model to more severe values than those actually measured. If such occurred on a single direction for these wind turbines, still it remains deserving of further attention, so as not to place wind turbines on locations with potentially destructive wind conditions.

Not particularly worrying but deserving of notice, turbines WT 09 and WT 10 presented reasonably high levels of shear factor on SE sector simulations, bearing in mind that the model leans to harsher shear factors than actual wind data showed. The remaining wind turbines did not reveal major causes for worry, shear factors usually falling slightly under 0, pitch flow revolving always around neutral levels and TI never going much over 0.12. Velocity fell in the 7-9 m/s range, rarely stepping above or below. The fact remains that severe wind conditions were observed at various wind turbine locations, enticing more profound study of those precise sites or search for improved wind turbine placements, within the designated wind farm area.

Bibliography

[1] Star-CCM+ 4.02.007 User Guide

[2] Xiaodong Zhang, CFD Simulation of neutral ABL Flows, Risø-R-1688(EN), 2009

[3] Arne R. Gravdahl, Meso Scale Modeling with a Reynolds Averaged Navier-Stokes Solver: Assessment of wind resources along the Norwegian coast, 1998

Annex A – Wind Data

Wind data was supplied from 3 measuring stations installed in the area. These were stations P042, P384 and P385. P042 collected data at a height of 30m; P384 and P385 collected at heights of both 30m and 60m. All anemometers were of the cup type, hence only horizontal speeds were measured. The installed data loggers registered, each 10min period, the following fields:

- Average wind direction, in º;
- Average wind speed, in m/s;
- Maximum measured wind gust, in m/s;
- Minimum measured wind speed, in m/s;
- Wind speed standard deviation, in m/s.

Wind data treatment is a simple but long task to do by hand, so a trial version of Windographer was used. It compiled and graphed the data entered directly in raw .dat format, allowing to employ fixed limits to variable values (to eliminate erroneous data produced by malfunctioning sensor or data logger), delete excess data from that necessary to form whole year periods, as well as other convenient functions.

Supplied station data covered the periods:

- P042: 1st September 1997 to the 1st September 2008;
- P384 & P385: 1st March 2007 to the 1st September 2008.

Windographer suffered of the slight hitch of not being able to select a full consecutive year, unless it was a complete year (as in from 1st of January 2008 to 1st of January 2009). In order to commit no time series errors, time stamp data was manipulated for the P384 and P385 stations, by moving all data timestamps backwards 3 months, thus having a full "2007" year, in reality corresponding to a full year from March 2007 to March 2008. All data was used for the P042 station, as it corresponded to a full 11 years of data, irrespective of timestamp starting value.

The following pages present graphed results from all measuring stations, in the form of frequency, average sector speed and energy roses, as well as wind speed histograms, respective Weibull function approximation and mean turbulence intensity vs. wind speed plots.

P042 station @ 30m, data from September 1997 to September 2008

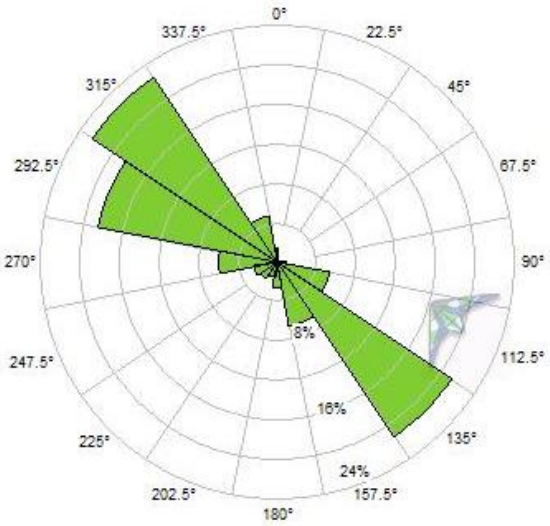

Wind frequency rose

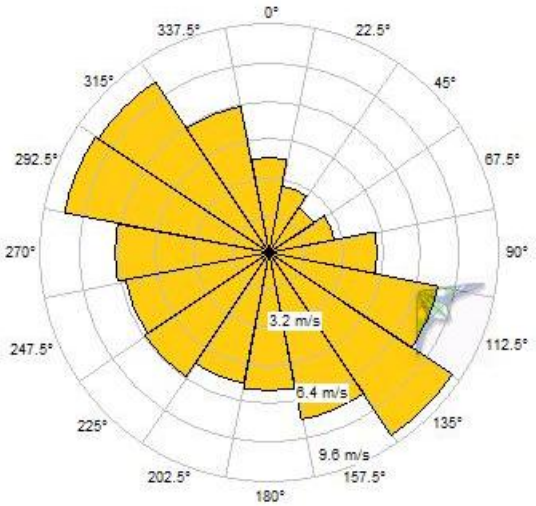

Average sector wind speed rose

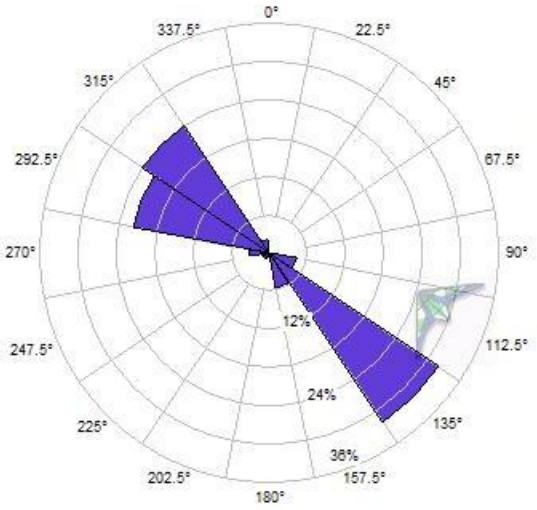

Wind energy rose

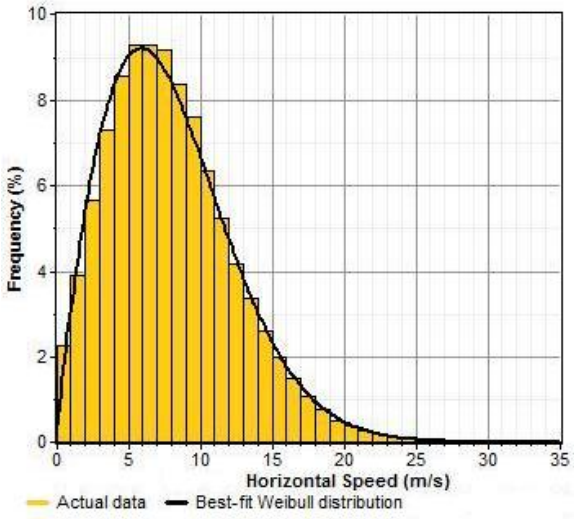

Wind speed histogram, with best-fit Weibull distribution (k=1.86, c=8.93m/s)

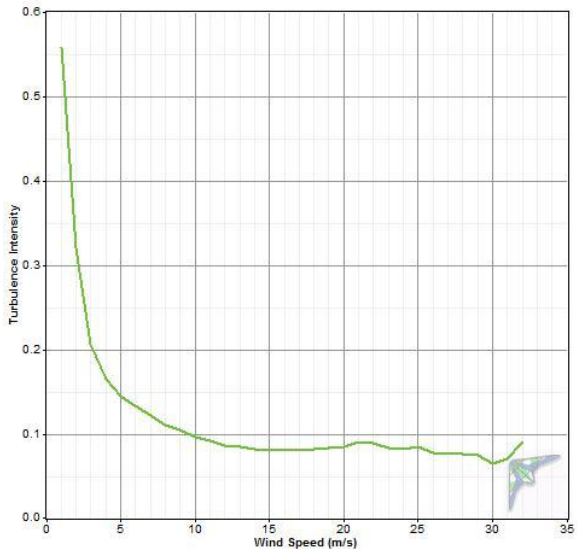

Mean TI vs. wind speed plot

Figure 28 - Wind rose, speed histogram and TI vs. Velocity plots for the P042 weather station @ 30 m

P384 station @ 30m, data from March 2007 to March 2008

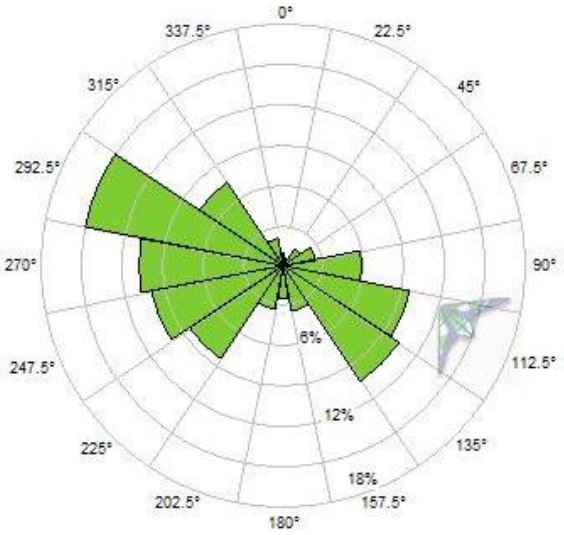

Wind frequency rose

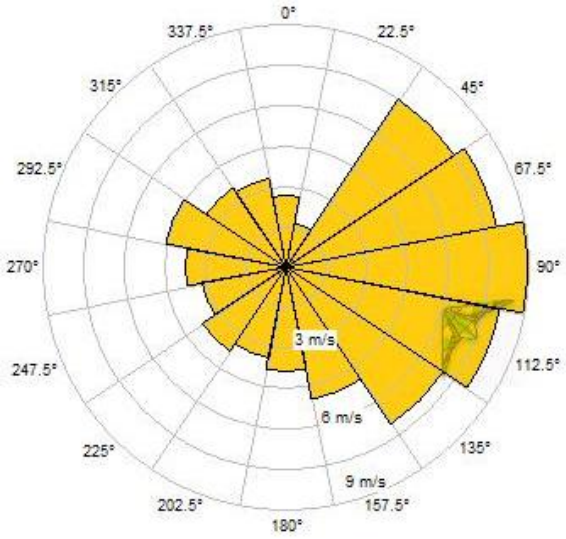

Average sector wind speed rose

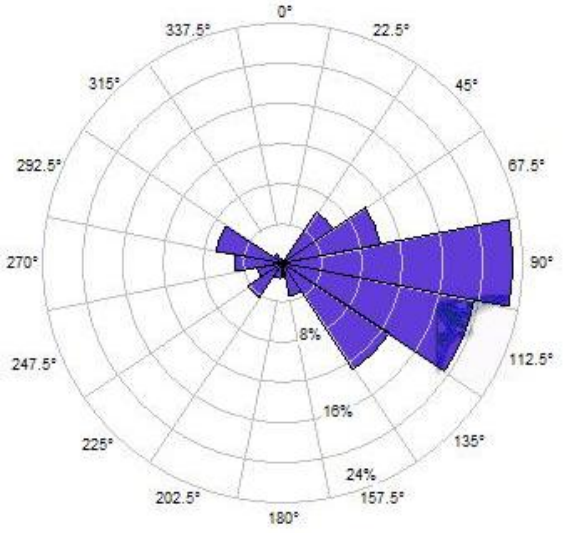

Wind energy rose

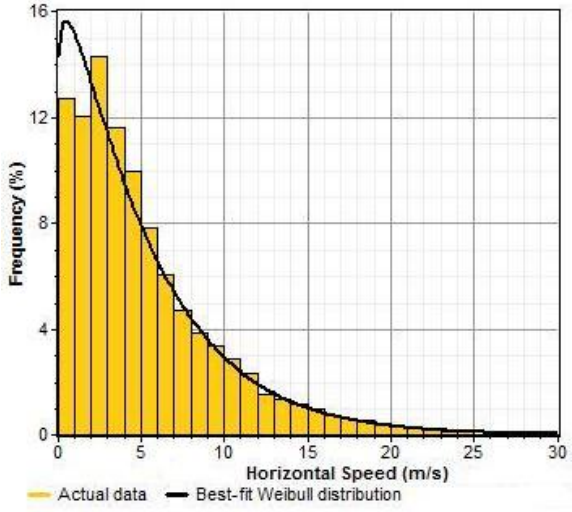

Wind speed histogram, with best-fit Weibull distribution (k=1.08, c=5.27 m/s)

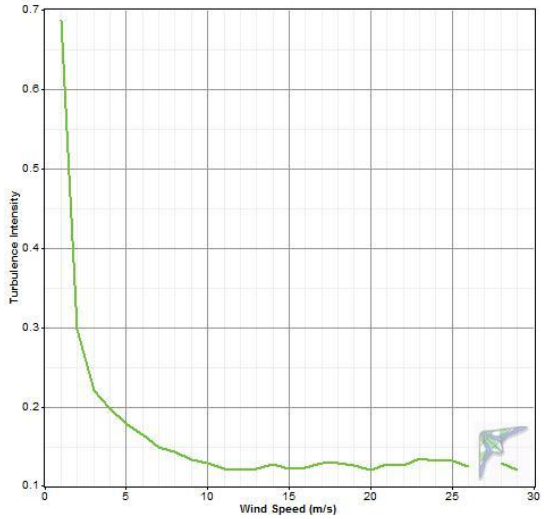

Mean TI vs. wind speed plot

Figure 29 - Wind rose, speed histogram and TI vs. Velocity plots for the P384 weather station @ 30 m

P384 station @ 60m, data from March 2007 to March 2008

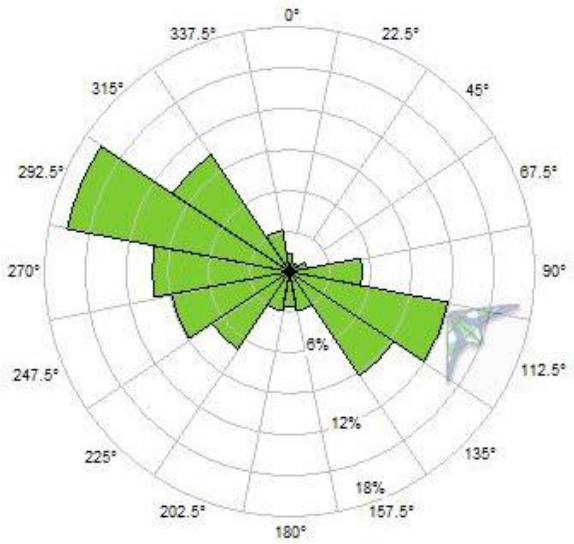

Wind frequency rose

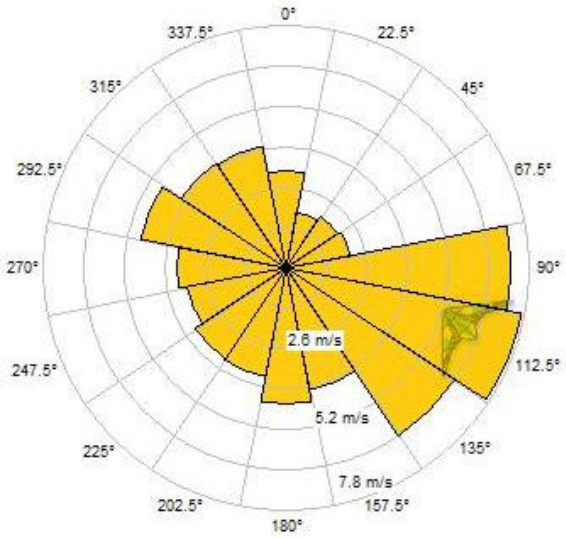

Average sector wind speed rose

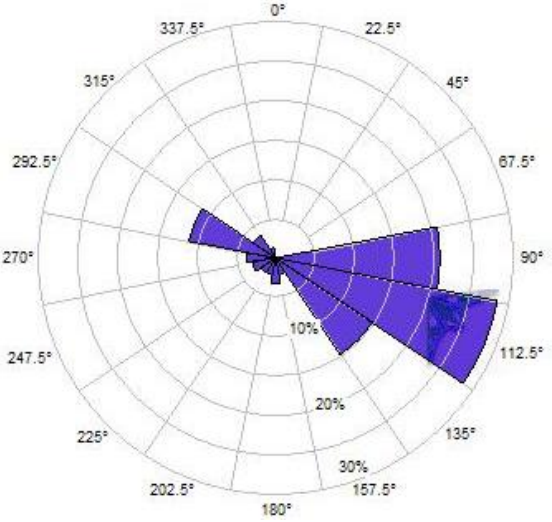

Wind energy rose

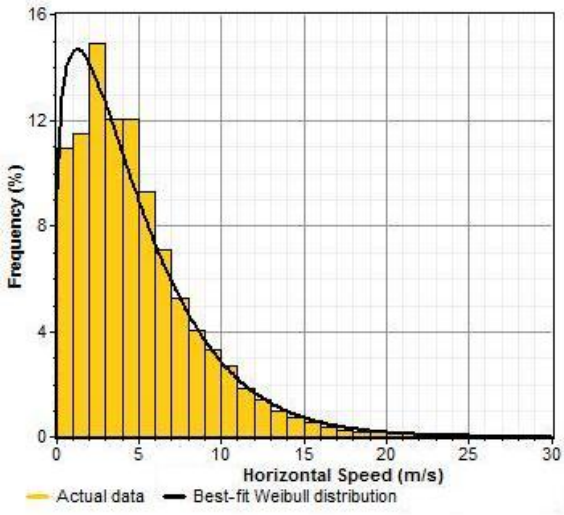

Wind speed histogram, with best-fit Weibull distribution (k=1.22, c=5.09 m/s)

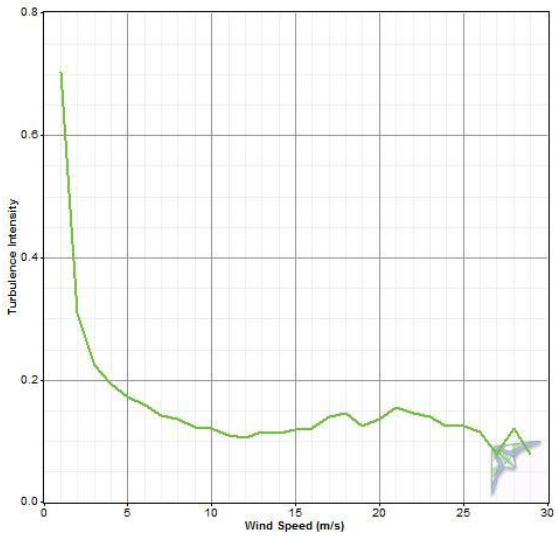

Mean TI vs. wind speed plot

Figure 30 - Wind rose, speed histogram and TI vs. Velocity plots for the P384 weather station @ 60 m

P385 station @ 30m, data from March 2007 to March 2008

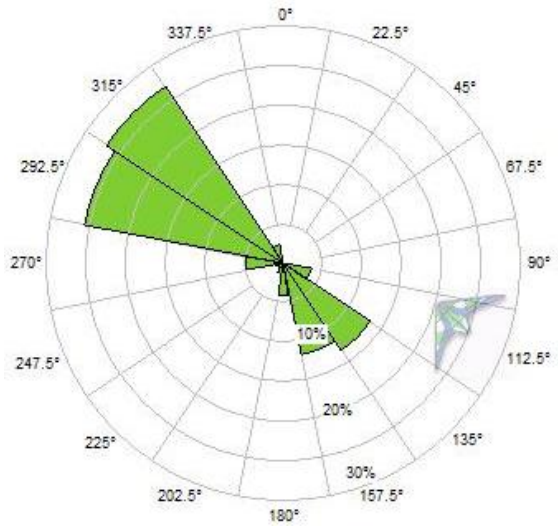

Wind frequency rose

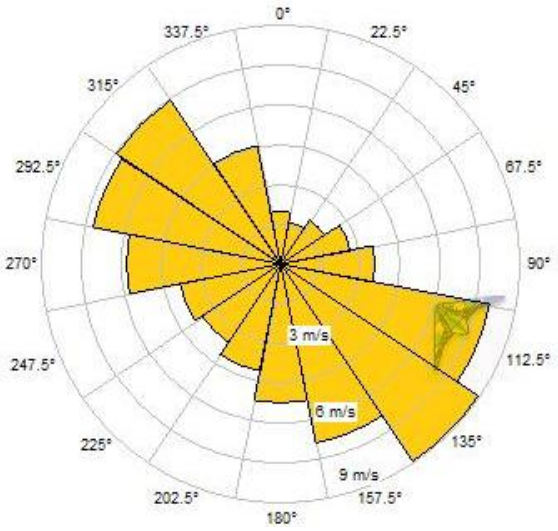

Average sector wind speed rose

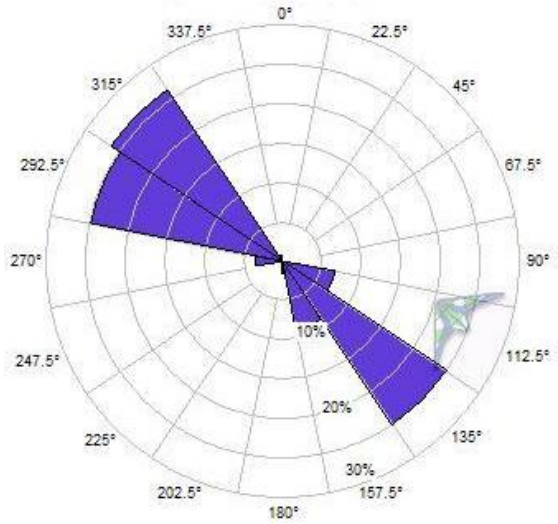

Wind energy rose

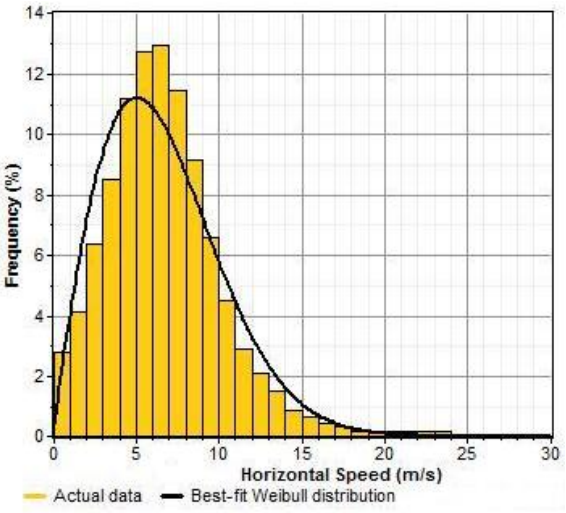

Wind speed histogram, with best-fit Weibull distribution (k=1.91, c=7.44 m/s)

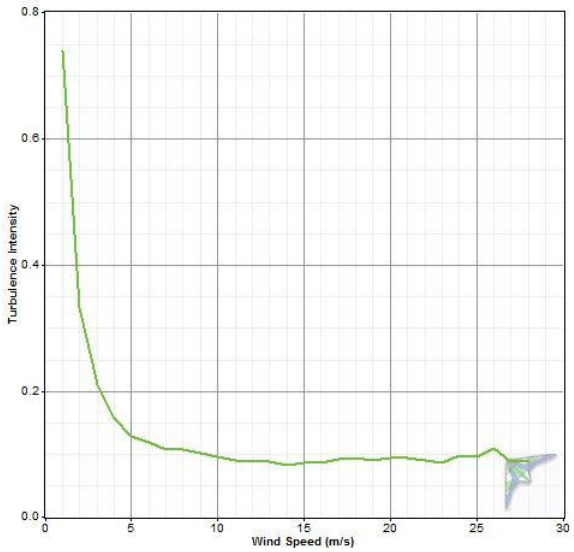

Mean TI vs. wind speed plot

Figure 31 – Wind rose, speed histogram and TI vs. Velocity plots for the P385 weather station @ 60 m

P385 station @ 60m, data from March 2007 to March 2008

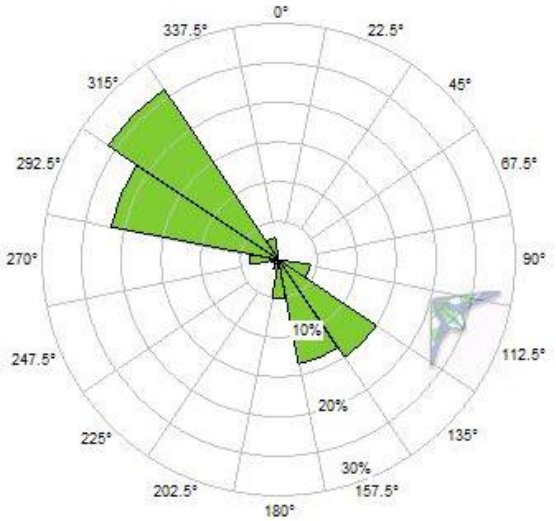

Wind frequency rose

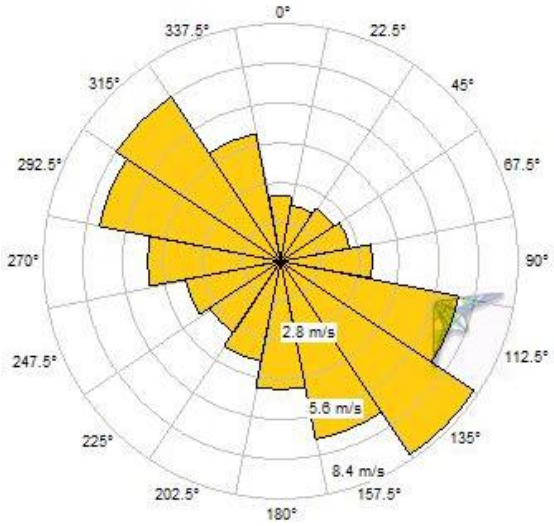

Average sector wind speed rose

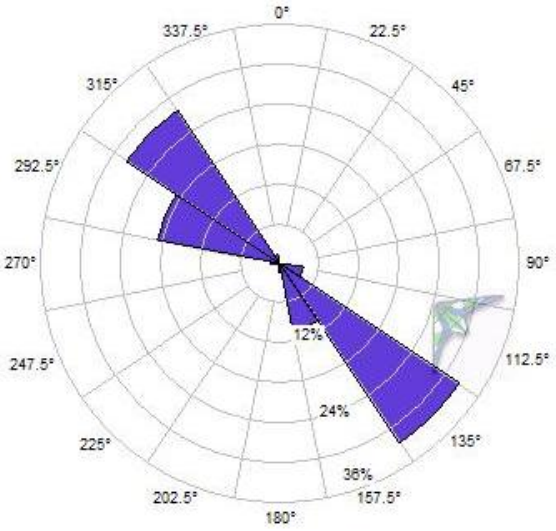

Wind energy rose

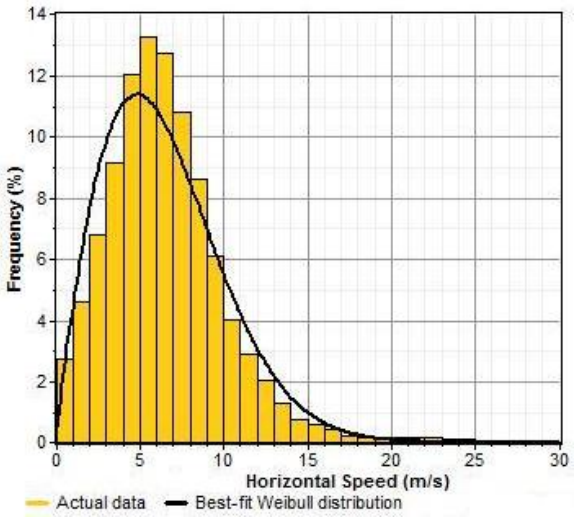

Wind speed histogram, with best-fit Weibull distribution (k=1.88, c=7,25 m/s)

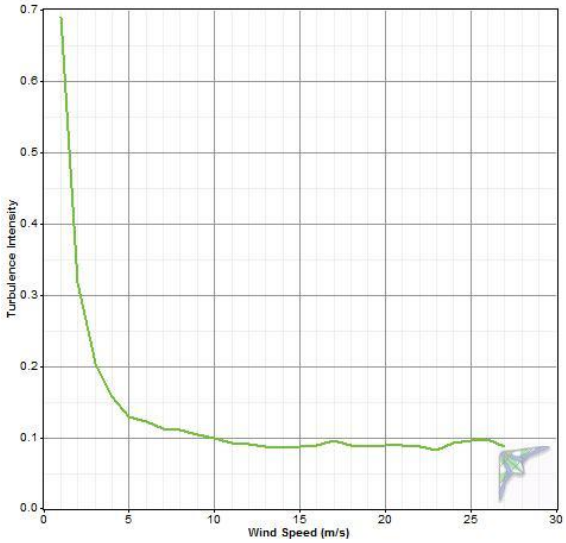

Mean TI vs. wind speed plot

Figure 32 - Wind rose, speed histogram and TI vs. Velocity plots for the P385 weather station @ 60 m

Annex B – Numerical results

Wind turbine point data

	Hor. Vel. (m/s)	Flow Pitch (º)	TI	SF	Hor. Vel. (m/s)	Flow Pitch (º)	TI	SF
	105º				285º			
44 m	8.2	8.2	0.114	0.03	10.5	1.2	0.114	-0.07
85 m	8.3	8.3	0.105	0.00	10.0	1.2	0.119	-0.09
126 m	8.3	8.3	0.101	-0.01	9.6	0.9	0.115	-0.08
	112.5º				292.5º			
44 m	8.6	1.7	0.098	-0.04	9.1	3.2	0.114	-0.09
85 m	8.3	2.8	0.104	-0.05	8.5	4.9	0.127	-0.14
126 m	8.2	3.3	0.107	-0.03	8.0	5.9	0.136	-0.18
	120º				300º			
44 m	9.1	1.1	0.089	0.00	11.1	0.6	0.150	-0.05
85 m	9.0	2.2	0.090	-0.03	10.7	1.0	0.153	-0.08
126 m	8.9	2.8	0.089	-0.04	10.3	1.2	0.145	-0.08
	127.5º				307.5º			
44 m	8.6	3.0	0.094	-0.05	10.8	1.7	0.092	-0.07
85 m	8.4	4.1	0.098	-0.04	10.3	2.0	0.101	-0.09
126 m	8.2	4.6	0.099	-0.03	9.9	2.1	0.104	-0.09
	135º				315º			
44 m	9.2	1.9	0.089	-0.03	11.3	1.8	0.091	-0.06
85 m	8.9	3.2	0.089	-0.05	10.8	2.1	0.096	-0.08
126 m	8.7	3.8	0.086	-0.04	10.4	2.2	0.096	-0.09
	142.5º				322.5º			
44 m	10.1	0.6	0.089	-0.03	9.6	2.5	0.098	-0.03
85 m	9.8	1.0	0.089	-0.04	9.2	2.8	0.108	-0.06
126 m	9.6	1.2	0.086	-0.05	9.0	3.1	0.110	-0.06

Table 8 - WT 01 wind turbine numerical point data

	Hor. Vel. (m/s)	Flow Pitch (º)	TI	SF	Hor. Vel. (m/s)	Flow Pitch (º)	TI	SF
	105º				285º			
44 m	8.8	3.4	0.108	-0.02	9.8	-0.2	0.122	-0.03
85 m	8.7	3.5	0.107	-0.03	9.5	0.2	0.124	-0.05
126 m	8.6	3.5	0.103	-0.03	9.3	0.3	0.119	-0.05
	112.5º				292.5º			
44 m	7.7	5.8	0.113	0.02	8.9	-2.0	0.128	-0.01
85 m	7.8	4.8	0.115	0.01	8.7	-0.1	0.137	-0.07
126 m	7.8	4.4	0.115	0.01	8.4	0.9	0.142	-0.12
	120º				300º			
44 m	9.0	3.0	0.093	-0.02	10.1	-1.2	0.152	-0.02
85 m	8.9	3.3	0.094	-0.04	9.9	0.1	0.155	-0.04
126 m	8.7	3.4	0.093	-0.04	9.7	0.8	0.149	-0.04
	127.5º				307.5º			
44 m	8.6	3.7	0.099	-0.04	10.7	-0.1	0.091	-0.05
85 m	8.4	4.1	0.103	-0.04	10.3	0.5	0.098	-0.07
126 m	8.3	4.2	0.102	-0.02	9.9	0.9	0.100	-0.08
	135º				315º			
44 m	9.2	2.6	0.086	-0.04	10.5	0.2	0.094	-0.04
85 m	9.0	3.1	0.090	-0.05	10.2	0.8	0.101	-0.06
126 m	8.8	3.3	0.088	-0.05	9.9	1.2	0.102	-0.07
	142.5º				322.5º			
44 m	9.8	2.1	0.086	-0.01	9.3	0.3	0.100	-0.02
85 m	9.6	1.9	0.090	-0.03	9.1	1.3	0.106	-0.05
126 m	9.5	1.7	0.088	-0.04	8.9	1.9	0.108	-0.05

Table 9 - WT 02 wind turbine numerical point data

	Hor. Vel. (m/s)	Flow Pitch (º)	TI	SF	Hor. Vel. (m/s)	Flow Pitch (º)	TI	SF
	105º				285º			
44 m	8.6	7.9	0.115	0.00	8.4	-5.9	0.132	0.02
85 m	8.5	6.5	0.111	-0.01	8.4	-4.1	0.135	0.01
126 m	8.5	5.7	0.105	-0.02	8.5	-2.9	0.130	0.01
	112,5º				292.5º			
44 m	7.8	6.2	0.127	0.02	8.9	-2.5	0.132	0.00
85 m	7.8	5.9	0.126	0.00	8.8	-2.4	0.136	-0.04
126 m	7.8	5.3	0.123	0.01	8.6	-2.2	0.137	-0.06
	120º				300º			
44 m	8.5	7.8	0.100	0.00	8.5	-0.9	0.145	0.02
85 m	8.5	6.7	0.103	-0.01	8.6	0.0	0.148	0.01
126 m	8.5	5.9	0.101	-0.01	8.7	0.6	0.146	0.02
	127,5º				307.5º			
44 m	8.7	7.2	0.102	-0.02	10.2	-4.8	0.100	-0.01
85 m	8.6	5.9	0.104	-0.03	10.0	-2.9	0.102	-0.05
126 m	8.5	5.1	0.103	-0.03	9.8	-1.9	0.100	-0.06
	135º				315º			
44 m	9.3	4.4	0.090	-0.03	9.6	-3.3	0.106	-0.02
85 m	9.0	4.2	0.094	-0.05	9.4	-1.6	0.110	-0.04
126 m	8.9	4.0	0.093	-0.06	9.2	-0.7	0.110	-0.05
	142,5º				322.5º			
44 m	9.6	5.0	0.090	0.00	9.1	-2.7	0.103	0.00
85 m	9.5	4.1	0.094	-0.02	9.0	-1.3	0.108	-0.03
126 m	9.4	3.5	0.093	-0.04	8.8	-0.2	0.108	-0.04

Table 10 - WT 03 wind turbine numerical point data

	Hor. Vel. (m/s)	Flow Pitch (º)	TI	SF	Hor. Vel. (m/s)	Flow Pitch (º)	TI	SF
	105º				285º			
44 m	8.5	4.4	0.111	-0.01	7.1	-2.1	0.156	0.05
85 m	8.4	5.0	0.110	-0.02	7.3	-1.8	0.150	0.04
126 m	8.3	5.2	0.105	-0.02	7.5	-1.5	0.145	0.05
	112.5º				292.5º			
44 m	8.3	5.9	0.126	-0.02	9.0	-4.4	0.141	0.00
85 m	8.1	5.4	0.126	-0.02	8.9	-3.7	0.138	-0.03
126 m	8.1	5.0	0.120	-0.02	8.8	-3.3	0.132	-0.04
	120º				300º			
44 m	8.4	7.2	0.107	0.00	6.5	-3.3	0.150	0.17
85 m	8.3	6.4	0.110	-0.01	7.3	-0.6	0.144	0.14
126 m	8.3	5.9	0.107	-0.01	7.7	0.7	0.141	0.10
	127.5º				307.5º			
44 m	9.0	6.8	0.105	-0.03	9.5	-4.8	0.118	0.02
85 m	8.8	5.7	0.107	-0.04	9.5	-3.2	0.114	-0.01
126 m	8.6	5.0	0.104	-0.04	9.5	-2.2	0.108	-0.03
	135º				315º			
44 m	9.4	4.6	0.099	-0.05	8.5	-1.6	0.128	0.01
85 m	9.0	4.5	0.100	-0.07	8.5	-0.6	0.127	0.00
126 m	8.8	4.2	0.098	-0.06	8.5	0.0	0.124	-0.01
	142.5º				322.5º			
44 m	9.3	3.7	0.099	-0.01	9.0	-1.8	0.112	0.00
85 m	9.2	3.6	0.100	-0.03	8.9	-0.8	0.115	-0.03
126 m	9.1	3.5	0.098	-0.03	8.8	-0.2	0.112	-0.03

Table 11 - WT 04 wind turbine numerical point data

	Hor. Vel. (m/s)	Flow Pitch (º)	TI	SF	Hor. Vel. (m/s)	Flow Pitch (º)	TI	SF
	105º				285º			
44 m	8.8	7.4	0.115	-0.04	5.6	-2.7	0.168	0.08
85 m	8.6	6.1	0.112	-0.04	6.1	-0.5	0.159	0.13
126 m	8.4	5.4	0.105	-0.04	6.4	0.7	0.152	0.10
	112.5º				292.5º			
44 m	8.8	6.5	0.124	-0.05	9.1	-3.0	0.133	-0.03
85 m	8.5	5.3	0.122	-0.05	9.0	-2.5	0.133	-0.03
126 m	8.4	4.7	0.115	-0.04	8.8	-2.3	0.127	-0.03
	120º				300º			
44 m	8.8	6.0	0.116	-0.05	7.8	-3.4	0.155	-0.01
85 m	8.6	5.1	0.115	-0.05	7.7	-1.3	0.150	-0.01
126 m	8.4	4.5	0.111	-0.04	7.7	-0.3	0.143	0.01
	127.5º				307.5º			
44 m	9.0	5.9	0.114	-0.04	9.2	-0.6	0.123	0.00
85 m	8.8	4.5	0.114	-0.05	9.2	0.4	0.121	-0.01
126 m	8.6	3.9	0.110	-0.05	9.1	0.9	0.114	-0.02
	135º				315º			
44 m	9.3	1.5	0.108	-0.05	8.2	1.9	0.129	-0.01
85 m	9.0	2.3	0.107	-0.07	8.1	2.1	0.133	-0.01
126 m	8.7	2.5	0.104	-0.07	8.1	2.2	0.131	0.00
	142.5º				322.5º			
44 m	8.9	1.6	0.108	0.00	9.0	2.3	0.106	-0.01
85 m	8.8	2.1	0.107	-0.01	8.9	2.2	0.109	-0.02
126 m	8.8	2.2	0.104	-0.02	8.8	2.1	0.107	-0.03

Table 12 - WT 05 wind turbine numerical point data

	Hor. Vel. (m/s)	Flow Pitch (º)	TI	SF	Hor. Vel. (m/s)	Flow Pitch (º)	TI	SF
	105º				285º			
44 m	7.6	-7.5	0.129	0.07	7.9	7.5	0.134	-0.04
85 m	7.9	-6.7	0.119	0.04	7.7	8.2	0.142	-0.04
126 m	8.0	-6.1	0.113	0.03	7.6	8.4	0.143	-0.01
	112.5º				292.5º			
44 m	6.5	-8.4	0.167	0.10	8.5	10.6	0.137	-0.02
85 m	6.9	-6.9	0.149	0.09	8.3	9.3	0.143	-0.02
126 m	7.2	-6.0	0.136	0.08	8.3	8.4	0.140	-0.02
	120º				300º			
44 m	6.2	-8.0	0.155	0.16	7.9	11.7	0.136	-0.01
85 m	6.8	-6.1	0.133	0.12	7.9	11.4	0.145	0.00
126 m	7.1	-5.0	0.123	0.12	7.9	11.1	0.146	0.03
	127.5º				307.5º			
44 m	5.7	-8.5	0.160	0.21	8.7	11.6	0.113	-0.01
85 m	6.5	-6.4	0.140	0.15	8.6	10.9	0.115	0.00
126 m	6.8	-5.4	0.133	0.14	8.6	10.3	0.112	0.01
	135º				315º			
44 m	6.1	-7.8	0.139	0.24	7.8	11.9	0.124	0.01
85 m	6.8	-6.1	0.123	0.15	7.9	11.4	0.128	0.02
126 m	7.2	-5.1	0.117	0.12	8.0	10.9	0.126	0.03
	142.5º				322.5º			
44 m	6.0	-8.3	0.139	0.21	7.2	10.5	0.129	0.03
85 m	6.9	-7.7	0.123	0.17	7.4	11.0	0.130	0.03
126 m	7.4	-7.2	0.117	0.15	7.5	10.8	0.127	0.05

Table 13 - WT 06 wind turbine numerical point data

	Hor. Vel. (m/s)	Flow Pitch (º)	TI	SF	Hor. Vel. (m/s)	Flow Pitch (º)	TI	SF
	105º				285º			
44 m	8.0	-1.4	0.142	0.02	7.3	5.7	0.111	-0.07
85 m	8.1	-2.2	0.132	0.00	6.9	9.0	0.132	-0.08
126 m	8.1	-2.8	0.121	0.00	6.7	10.1	0.143	-0.05
	112.5º				292.5º			
44 m	7.4	-0.4	0.154	0.02	8.7	3.4	0.138	-0.03
85 m	7.5	-2.6	0.145	0.03	8.5	4.5	0.138	-0.04
126 m	7.6	-3.6	0.135	0.03	8.4	4.9	0.131	-0.02
	120º				300º			
44 m	7.0	-5.3	0.165	0.08	7.8	10.0	0.123	-0.07
85 m	7.3	-4.7	0.144	0.05	7.5	10.3	0.134	-0.05
126 m	7.4	-4.5	0.130	0.04	7.4	10.3	0.139	0.00
	127.5º				307.5º			
44 m	6.6	-7.3	0.157	0.09	8.9	8.8	0.114	-0.03
85 m	7.0	-6.6	0.143	0.07	8.7	8.4	0.118	-0.03
126 m	7.2	-6.1	0.133	0.07	8.6	8.2	0.114	-0.02
	135º				315º			
44 m	6.3	-4.9	0.168	0.15	7.6	6.5	0.135	-0.03
85 m	6.8	-5.4	0.141	0.10	7.5	8.0	0.142	-0.02
126 m	7.1	-5.4	0.129	0.09	7.5	8.6	0.140	0.01
	142.5º				322.5º			
44 m	5.8	-6.5	0.168	0.19	7.3	6.7	0.136	0.00
85 m	6.5	-6.8	0.141	0.17	7.3	8.2	0.137	0.01
126 m	6.9	-6.7	0.129	0.15	7.4	8.7	0.132	0.02

Table 14 - WT 07 wind turbine numerical point data

	Hor. Vel. (m/s)	Flow Pitch (º)	TI	SF	Hor. Vel. (m/s)	Flow Pitch (º)	TI	SF
	105º				285º			
44 m	7.1	2.9	0.154	0.02	8.1	0.5	0.121	-0.06
85 m	7.2	1.4	0.149	0.05	7.6	2.7	0.137	-0.12
126 m	7.4	0.2	0.137	0.07	7.2	3.8	0.142	-0.13
	112.5º				292.5º			
44 m	7.2	1.6	0.157	0.06	7.7	0.7	0.137	0.02
85 m	7.4	-0.3	0.146	0.06	7.8	2.6	0.141	0.02
126 m	7.6	-1.4	0.136	0.04	7.8	3.4	0.136	0.03
	120º				300º			
44 m	7.3	-0.7	0.160	0.02	8.1	3.3	0.135	-0.05
85 m	7.4	-2.2	0.149	0.02	7.8	4.7	0.141	-0.06
126 m	7.5	-3.0	0.136	0.02	7.7	5.4	0.140	-0.04
	127.5º				307.5º			
44 m	6.5	-3.1	0.170	0.07	8.7	3.4	0.115	-0.02
85 m	6.8	-4.0	0.159	0.09	8.5	4.4	0.120	-0.03
126 m	7.0	-4.4	0.145	0.09	8.5	4.9	0.118	-0.02
	135º				315º			
44 m	6.5	-3.5	0.174	0.08	7.1	3.1	0.141	-0.02
85 m	6.9	-4.5	0.155	0.08	7.1	5.0	0.149	-0.01
126 m	7.1	-4.8	0.141	0.07	7.1	6.1	0.148	0.01
	142.5º				322.5º			
44 m	5.5	-2.3	0.174	0.13	7.4	4.4	0.126	0.00
85 m	6.1	-3.9	0.155	0.17	7.4	5.6	0.132	0.00
126 m	6.6	-4.6	0.141	0.16	7.4	6.2	0.129	0.01

Table 15 - WT 08 wind turbine numerical point data

	Hor. Vel. (m/s)	Flow Pitch (º)	TI	SF	Hor. Vel. (m/s)	Flow Pitch (º)	TI	SF
	105º				285º			
44 m	7.8	5.1	0.133	-0.02	7.4	-2.8	0.162	-0.02
85 m	7.7	5.0	0.135	0.02	7.2	-1.3	0.162	-0.04
126 m	7.8	4.7	0.126	0.04	7.1	-0.6	0.157	-0.05
	112.5º				292.5º			
44 m	8.7	2.9	0.124	-0.03	7.7	-0.1	0.143	0.00
85 m	8.5	2.9	0.120	-0.03	7.8	0.6	0.144	0.02
126 m	8.4	2.9	0.112	-0.03	7.9	0.8	0.138	0.05
	120º				300º			
44 m	9.0	5.2	0.110	-0.05	9.1	-4.2	0.172	-0.01
85 m	8.6	4.1	0.113	-0.06	9.0	-2.5	0.168	-0.04
126 m	8.5	3.4	0.110	-0.05	8.8	-1.6	0.157	-0.05
	127.5º				307.5º			
44 m	8.7	6.2	0.116	-0.04	8.6	-1.9	0.133	0.01
85 m	8.5	4.7	0.118	-0.04	8.6	0.6	0.129	0.01
126 m	8.4	3.9	0.113	-0.03	8.6	1.6	0.123	0.00
	135º				315º			
44 m	9.0	1.9	0.123	-0.05	8.6	1.0	0.115	-0.04
85 m	8.7	2.1	0.124	-0.06	8.4	1.5	0.120	-0.05
126 m	8.5	2.0	0.120	-0.05	8.2	1.8	0.120	-0.04
	142.5º				322.5º			
44 m	7.9	1.1	0.123	0.00	9.4	1.6	0.092	-0.02
85 m	8.0	1.4	0.124	0.02	9.3	1.7	0.096	-0.04
126 m	8.0	1.4	0.120	0.03	9.1	1.8	0.096	-0.05

Table 16 - WT 09 wind turbine numerical point data

	Hor. Vel. (m/s)	Flow Pitch (º)	TI	SF	Hor. Vel. (m/s)	Flow Pitch (º)	TI	SF
	105º				285º			
44 m	8.1	4.1	0.126	-0.02	8.0	-3.3	0.154	0.00
85 m	8.0	3.8	0.128	-0.01	7.9	-2.0	0.155	-0.03
126 m	8.0	3.6	0.121	0.00	7.8	-1.5	0.148	-0.04
	112.5º				292.5º			
44 m	7.9	-0.5	0.142	0.03	7.5	5.1	0.141	0.01
85 m	8.0	1.4	0.137	0.03	7.6	3.8	0.143	0.02
126 m	8.1	2.2	0.126	0.03	7.7	3.0	0.138	0.04
	120º				300º			
44 m	8.9	4.7	0.117	-0.05	9.0	-4.2	0.174	0.03
85 m	8.6	3.5	0.117	-0.06	9.1	-1.9	0.170	-0.01
126 m	8.4	2.7	0.111	-0.06	9.1	-1.0	0.158	-0.03
	127.5º				307.5º			
44 m	8.3	6.0	0.124	-0.02	8.8	-2.9	0.134	0.01
85 m	8.2	4.6	0.122	-0.02	8.8	-0.4	0.131	-0.01
126 m	8.2	3.7	0.115	-0.01	8.7	0.8	0.123	-0.03
	135º				315º			
44 m	9.0	1.3	0.122	-0.05	9.2	1.7	0.108	-0.04
85 m	8.7	1.4	0.123	-0.06	8.8	1.5	0.114	-0.07
126 m	8.5	1.3	0.116	-0.05	8.6	1.5	0.114	-0.07
	142.5º				322.5º			
44 m	7.9	-0.9	0.122	0.03	9.4	2.6	0.095	0.00
85 m	8.0	-0.5	0.123	0.02	9.3	2.3	0.097	-0.03
126 m	8.1	-0.2	0.116	0.01	9.2	2.2	0.096	-0.05

Table 17 - WT 10 wind turbine numerical point data

	Hor. Vel. (m/s)	Flow Pitch (º)	TI	SF	Hor. Vel. (m/s)	Flow Pitch (º)	TI	SF
	105º				285º			
44 m	8.5	7.0	0.123	-0.04	8.0	-4.8	0.150	0.03
85 m	8.3	5.2	0.122	-0.04	8.1	-3.3	0.148	0.00
126 m	8.1	4.3	0.115	-0.03	8.1	-2.7	0.141	-0.01
	112.5º				292.5º			
44 m	8.6	1.9	0.129	-0.02	7.9	2.5	0.131	-0.01
85 m	8.4	2.5	0.127	-0.02	7.9	2.5	0.134	0.00
126 m	8.4	2.7	0.118	-0.01	7.9	2.3	0.130	0.01
	120º				300º			
44 m	8.4	5.9	0.123	-0.03	9.1	2.3	0.173	0.02
85 m	8.2	3.9	0.125	-0.04	9.2	1.6	0.168	-0.01
126 m	8.1	2.6	0.119	-0.03	9.1	1.3	0.155	-0.03
	127.5º				307.5º			
44 m	8.1	6.4	0.123	-0.01	8.5	-4.2	0.135	0.02
85 m	8.1	4.7	0.123	0.00	8.6	-1.9	0.132	-0.01
126 m	8.1	3.7	0.115	0.01	8.5	-1.0	0.126	-0.02
	135º				315º			
44 m	8.8	2.7	0.115	-0.04	9.5	0.6	0.104	-0.05
85 m	8.5	1.9	0.118	-0.04	9.1	0.7	0.109	-0.07
126 m	8.4	1.5	0.114	-0.03	8.8	0.8	0.109	-0.07
	142.5º				322.5º			
44 m	7.9	0.7	0.115	-0.01	9.6	1.6	0.092	-0.02
85 m	7.9	0.6	0.118	0.00	9.4	1.5	0.095	-0.05
126 m	7.9	0.4	0.114	0.01	9.2	1.6	0.094	-0.06

Table 18 - WT 11 wind turbine numerical point data

	Hor. Vel. (m/s)	Flow Pitch (º)	TI	SF	Hor. Vel. (m/s)	Flow Pitch (º)	TI	SF
	105º				285º			
44 m	8.4	5.0	0.121	-0.03	7.8	-4.3	0.129	0.02
85 m	8.2	4.4	0.123	-0.04	7.9	-3.4	0.133	0.01
126 m	8.1	3.9	0.117	-0.03	7.9	-2.8	0.131	0.00
	112.5º				292.5º			
44 m	8.6	0.2	0.125	0.06	8.0	4.5	0.119	0.01
85 m	8.7	1.4	0.118	-0.02	8.0	3.3	0.123	0.00
126 m	8.6	1.7	0.109	-0.04	8.0	2.6	0.122	0.00
	120º				300º			
44 m	7.2	5.4	0.152	-0.04	8.9	-4.3	0.154	0.02
85 m	7.0	3.5	0.165	-0.03	9.0	-2.6	0.155	0.00
126 m	6.9	2.6	0.164	0.01	8.9	-1.7	0.149	-0.02
	127.5º				307.5º			
44 m	8.3	4.7	0.111	-0.01	8.4	-3.5	0.123	-0.01
85 m	8.2	3.0	0.112	-0.01	8.3	-1.7	0.126	-0.02
126 m	8.1	2.2	0.106	-0.01	8.3	-0.6	0.124	-0.02
	135º				315º			
44 m	8.1	1.3	0.109	-0.01	9.3	0.3	0.100	-0.02
85 m	8.0	1.1	0.113	-0.01	9.1	0.5	0.102	-0.05
126 m	8.0	1.0	0.109	0.00	8.9	0.6	0.101	-0.06
	142.5º				322.5º			
44 m	7.5	-1.0	0.109	0.01	9.2	3.1	0.095	-0.02
85 m	7.5	-0.4	0.113	0.01	9.0	2.6	0.098	-0.04
126 m	7.6	-0.2	0.109	0.03	8.9	2.3	0.096	-0.04

Table 19 - WT 12 wind turbine numerical point data

	Hor. Vel. (m/s)	Flow Pitch (º)	TI	SF	Hor. Vel. (m/s)	Flow Pitch (º)	TI	SF
	105º				285º			
44 m	8.0	-0.7	0.108	0.00	7.2	-0.4	0.130	0.01
85 m	8.0	0.0	0.112	-0.01	7.3	0.3	0.136	0.01
126 m	7.9	0.4	0.110	-0.02	7.3	0.6	0.135	0.02
	112.5º				292.5º			
44 m	8.6	-3.3	0.107	0.01	8.1	8.1	0.115	0.01
85 m	8.6	-2.1	0.108	-0.01	8.1	8.1	0.120	0.00
126 m	8.5	-1.3	0.104	-0.02	8.1	8.1	0.119	0.00
	120º				300º			
44 m	6.2	0.0	0.159	0.00	8.8	1.8	0.143	0.02
85 m	6.2	1.3	0.174	0.02	8.8	1.7	0.147	0.00
126 m	6.3	1.9	0.177	0.08	8.8	1.5	0.143	-0.02
	127.5º				307.5º			
44 m	8.3	-1.6	0.102	-0.02	8.3	3.1	0.112	-0.01
85 m	8.2	-1.7	0.105	-0.03	8.2	2.8	0.117	-0.03
126 m	8.1	-1.7	0.103	-0.03	8.1	2.7	0.117	-0.03
	135º				315º			
44 m	7.4	-2.3	0.106	0.02	9.2	1.7	0.108	-0.04
85 m	7.5	-2.0	0.109	0.03	8.8	1.5	0.114	-0.07
126 m	7.7	-1.8	0.104	0.04	8.6	1.5	0.114	-0.07
	142.5º				322.5º			
44 m	6.5	-5.1	0.106	0.10	7.9	6.3	0.109	0.07
85 m	6.9	-4.0	0.109	0.07	8.2	5.5	0.106	0.04
126 m	7.1	-3.4	0.104	0.08	8.3	5.1	0.103	0.02

Table 20 - WT 13 wind turbine numerical point data

Wind Turbine horizontal velocity plots

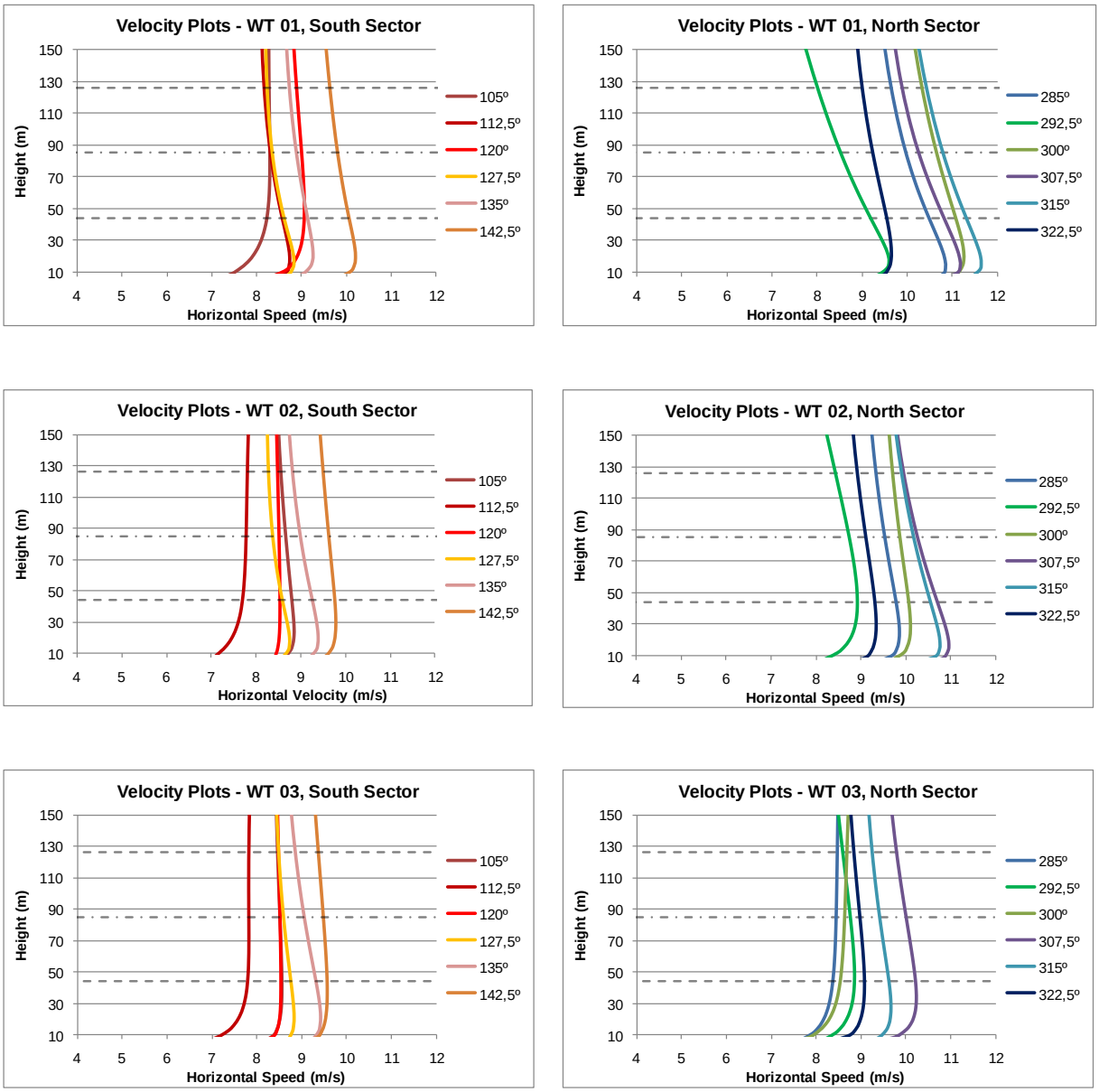

Figure 33 - Velocity vertical plots for wind turbines WT 01, WT 02 and WT 03

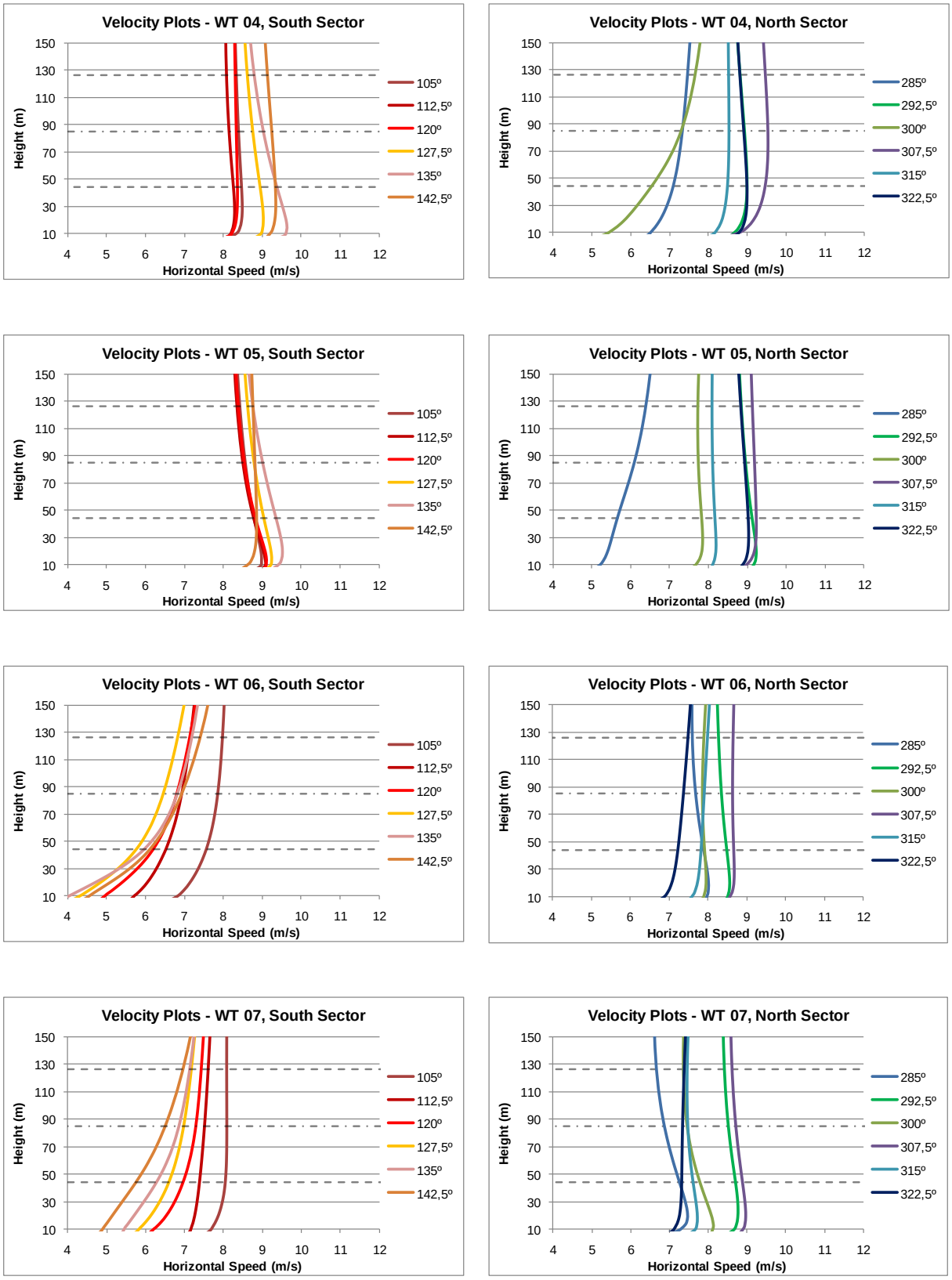

Figure 34 - Velocity vertical plots for wind turbines WT 04, WT 05, WT 06 and WT 07

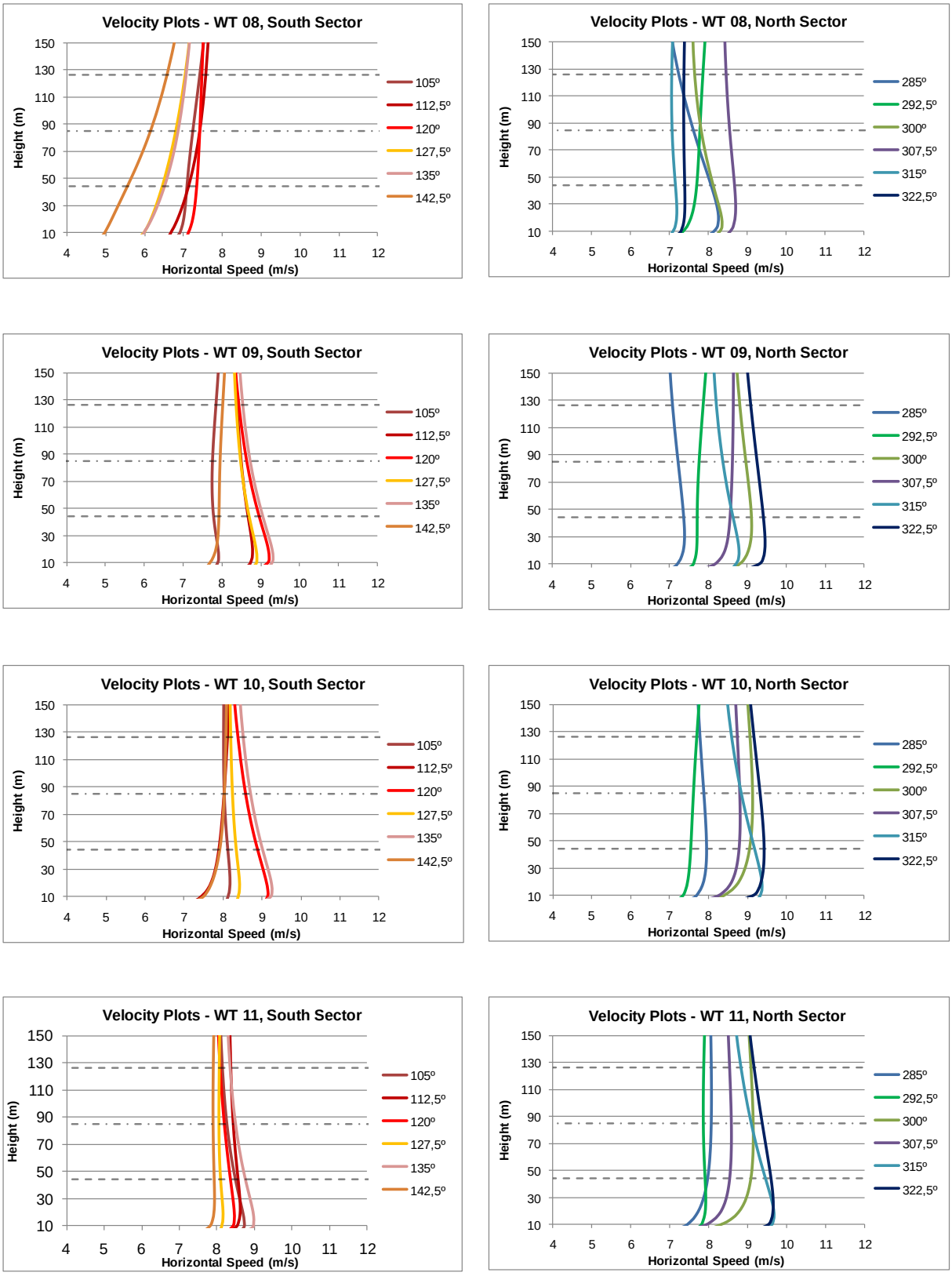

Figure 35 - Velocity vertical plots for wind turbines WT 08, WT 09, WT 10 and WT 11

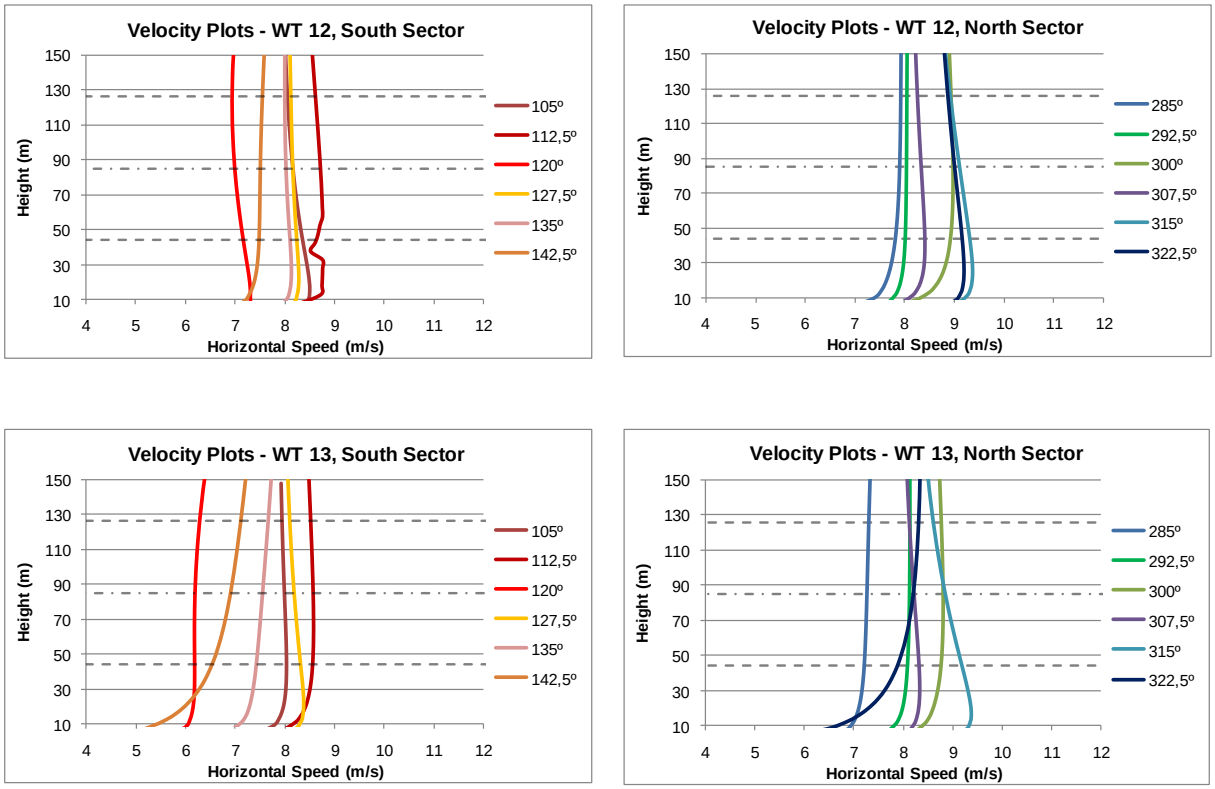

Figure 36 - Velocity vertical plots for wind turbines WT 12 and WT 13

Wind Turbine Shear Factor plots

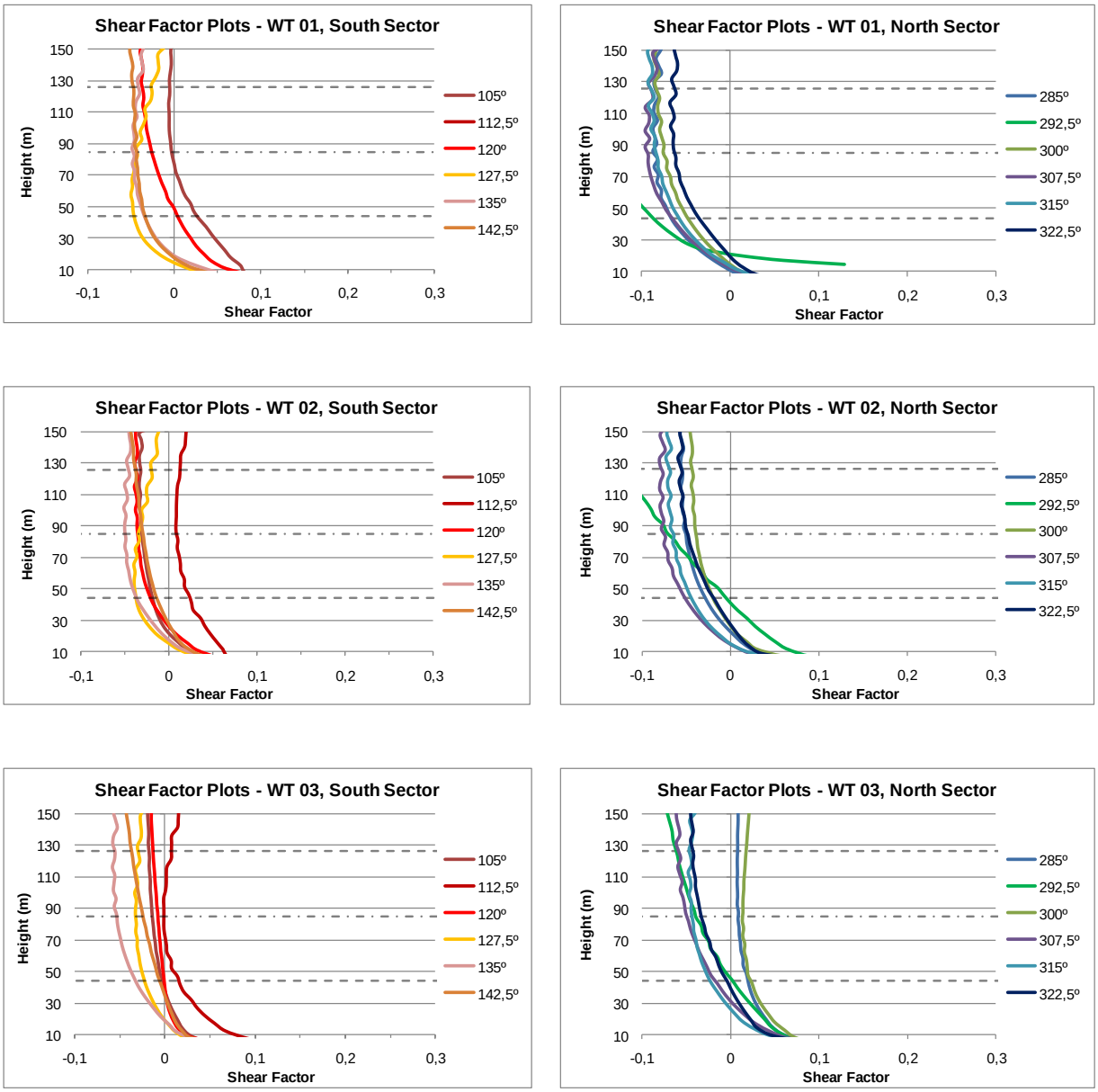

Figure 37 - Shear factor vertical plots for wind turbines WT 01, WT 02 and WT 03

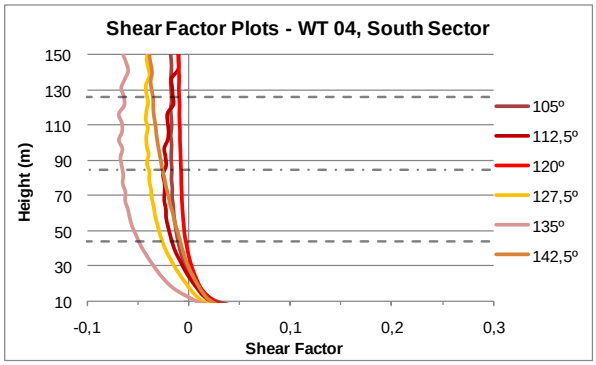

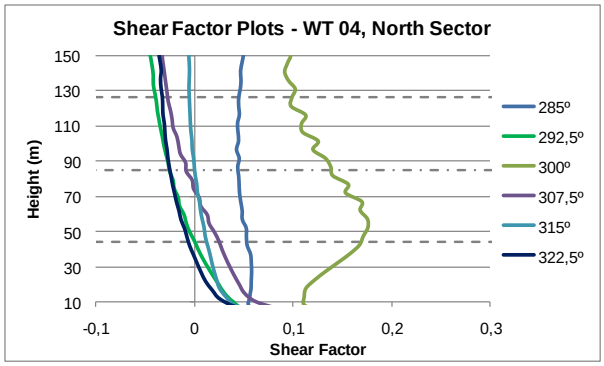

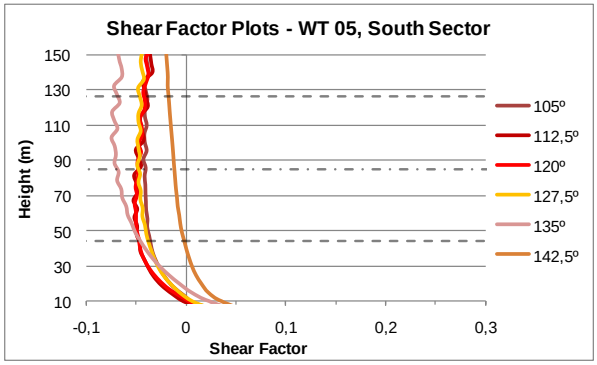

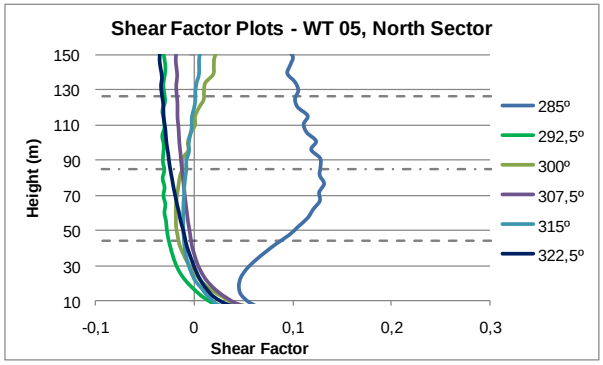

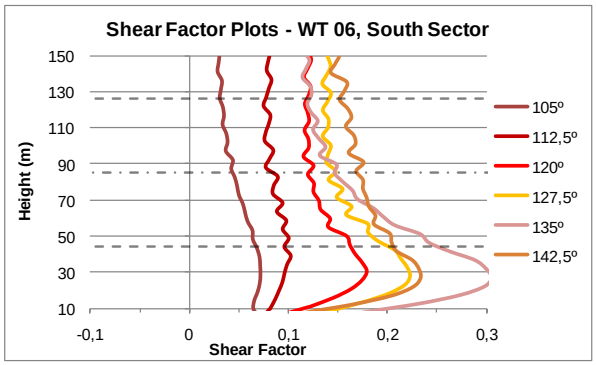

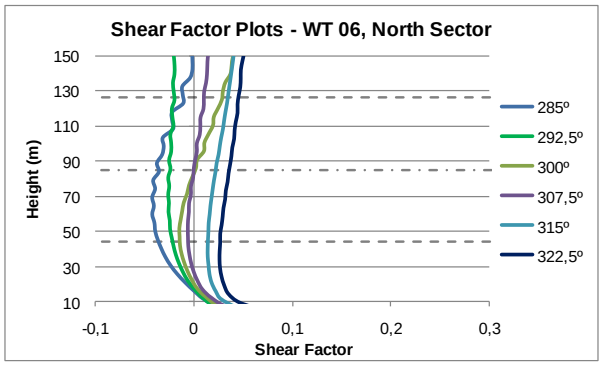

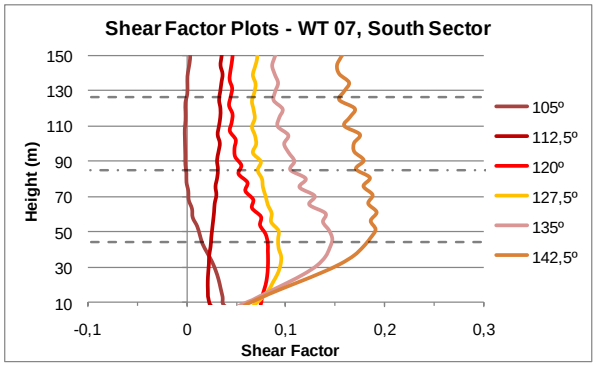

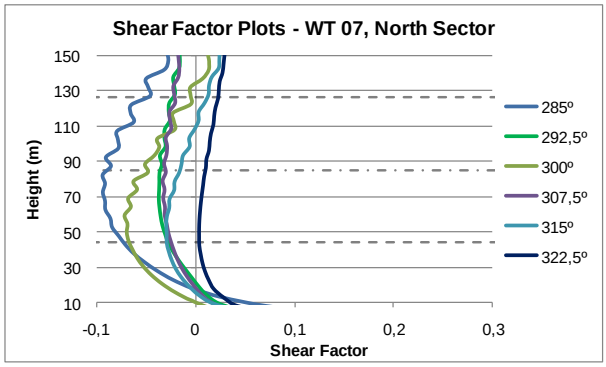

Figure 38 - Shear Factor vertical plots for wind turbines WT 04, WT 05, WT 06 and WT 07

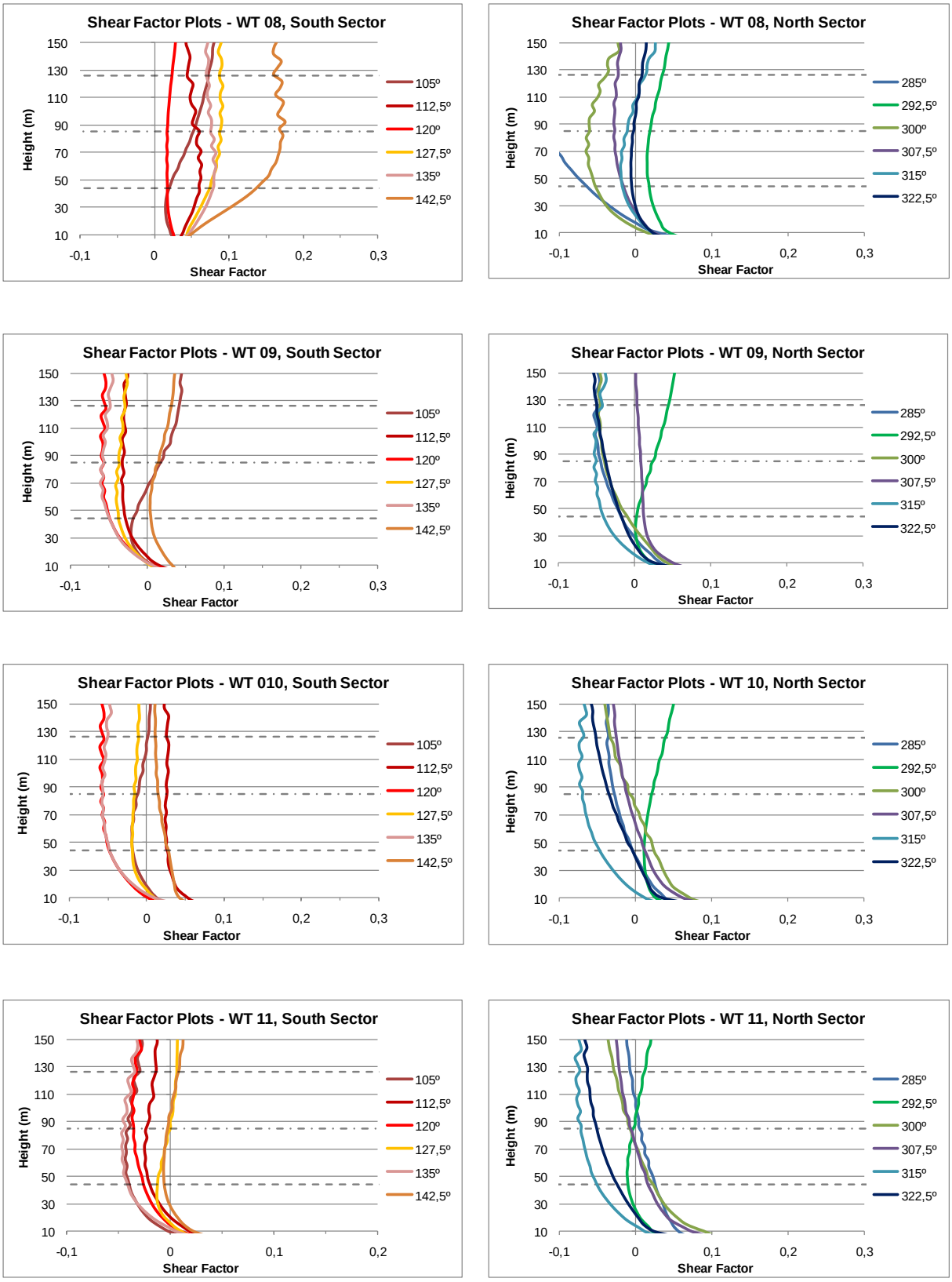

Figure 39 - Shear factor vertical plots for wind turbines WT 08, WT 09, WT 10 and WT 11

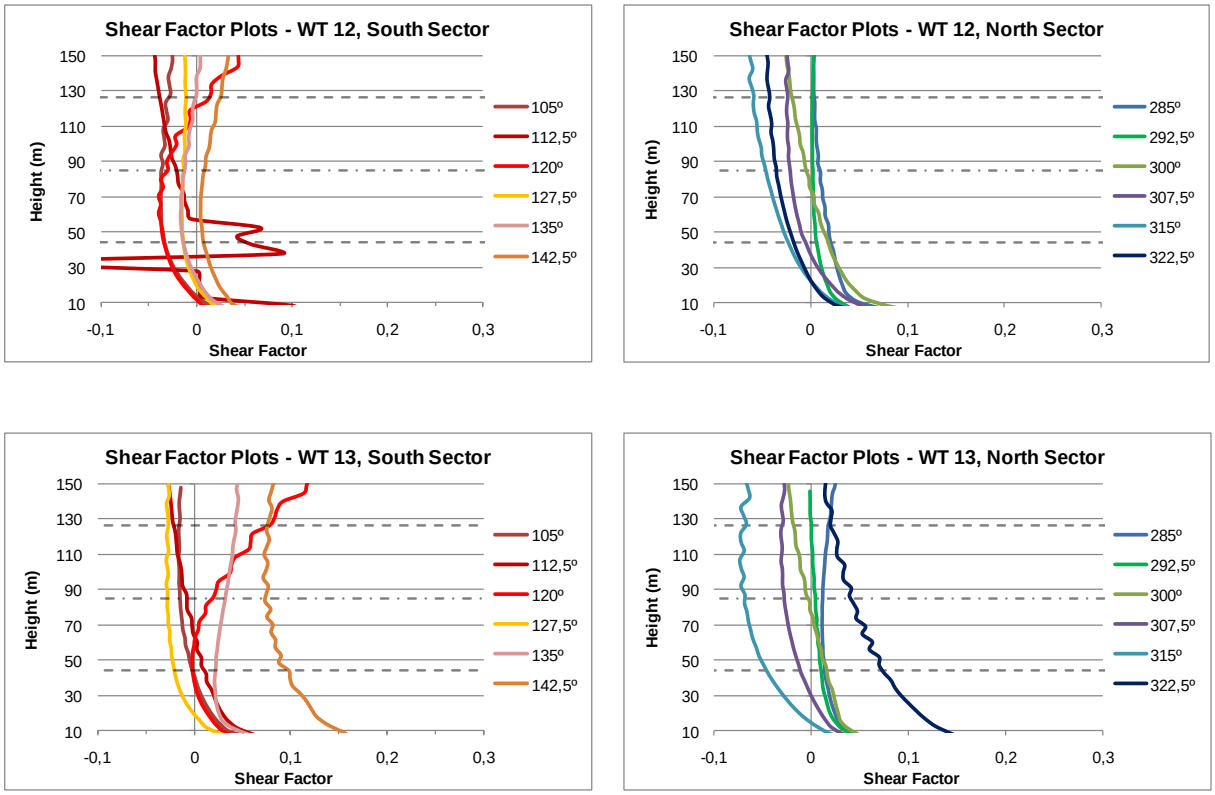

Figure 40 - Shear factor vertical plots for wind turbines WT 12 and WT 13

Weather station numerical horizontal velocity & shear factor plots

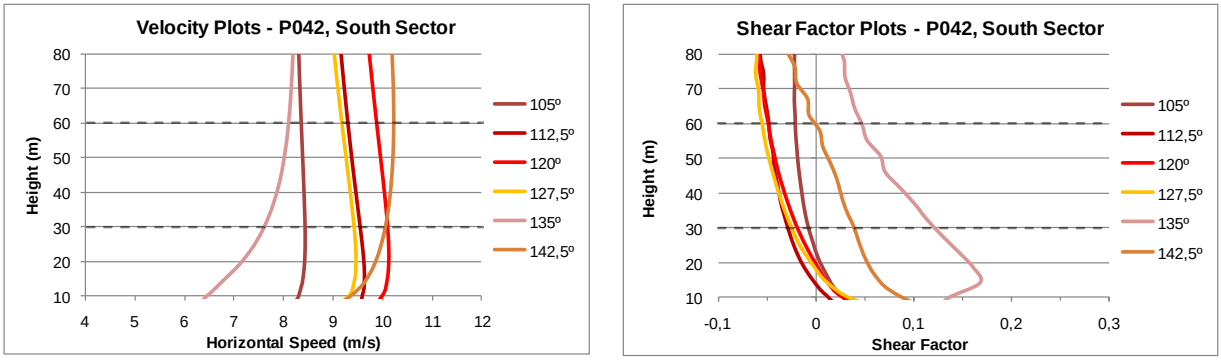

Figure 41 - Velocity and shear factor vertical plots for the P042 weather station, SE sector

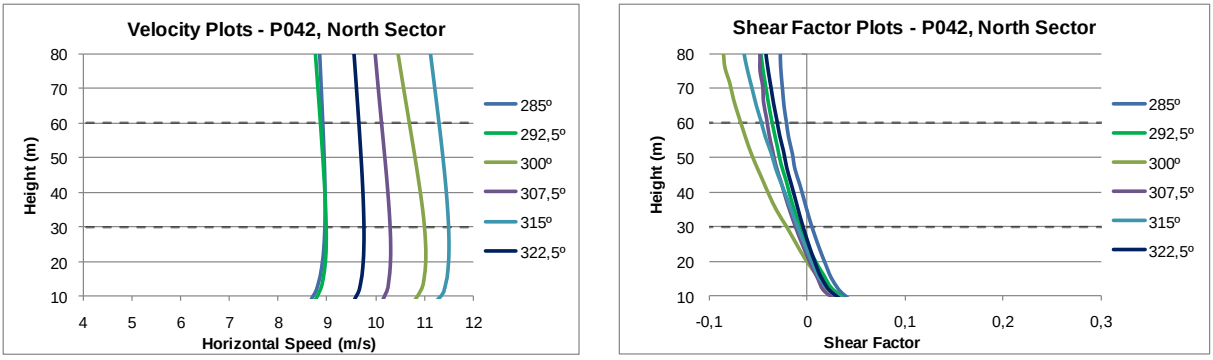

Figure 42 - Velocity and shear factor vertical plots for the P042 weather station, NW sector

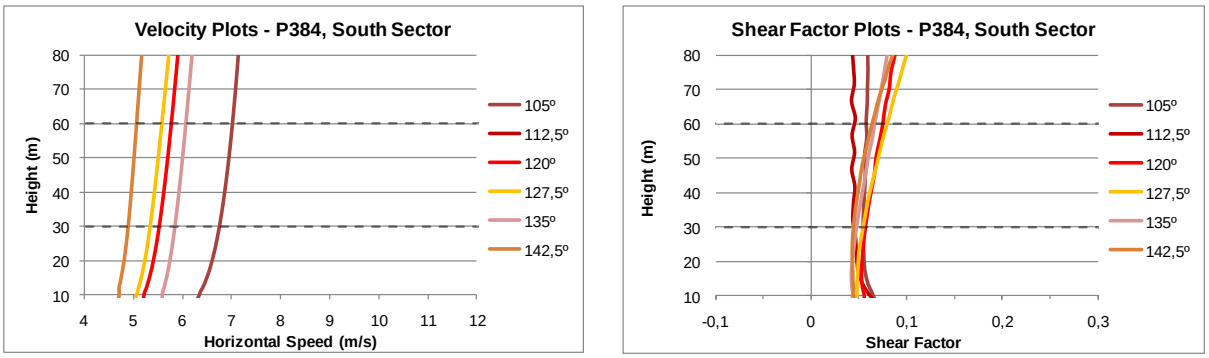

Figure 43 - Velocity and shear factor vertical plots for the P384 weather station, SE sector

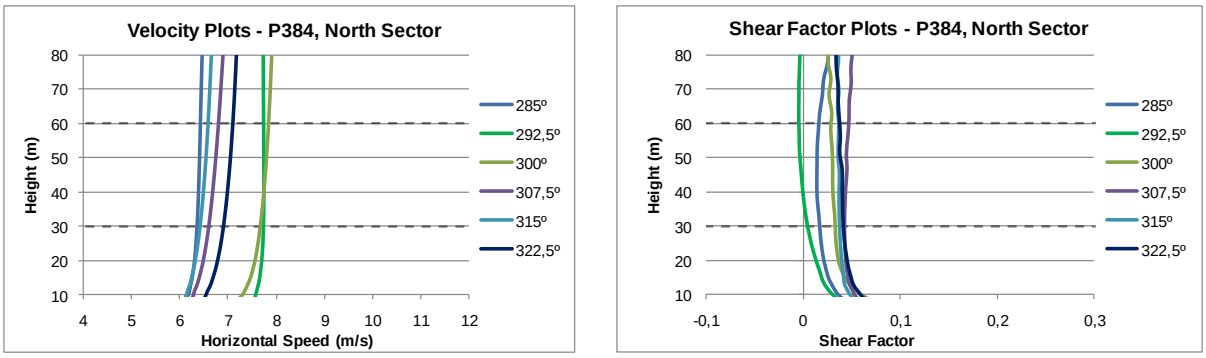

Figure 44 - Velocity and shear factor vertical plots for the P384 weather station, NW sector

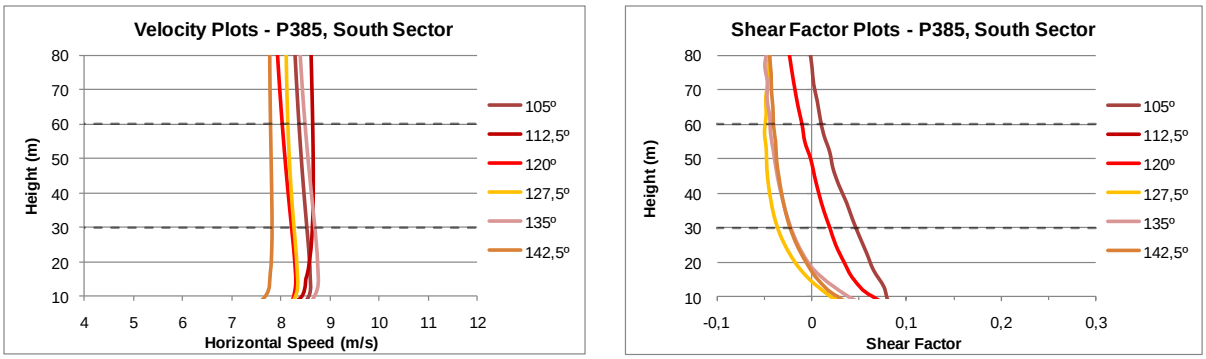

Figure 45 - Velocity and shear factor vertical plots for the P385 weather station, SE sector

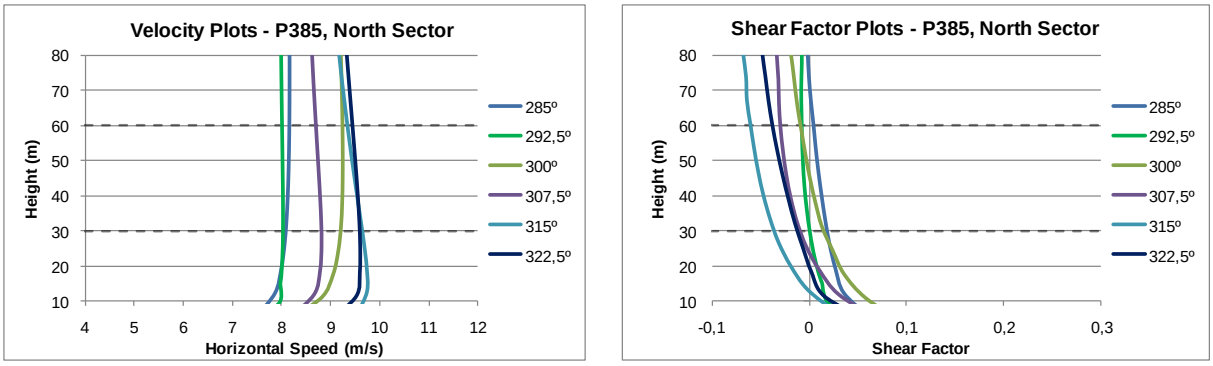

Figure 46 - Velocity and shear factor vertical plots for the P385 weather station , NW sector

Wind Turbine Turbulent Intensity plots

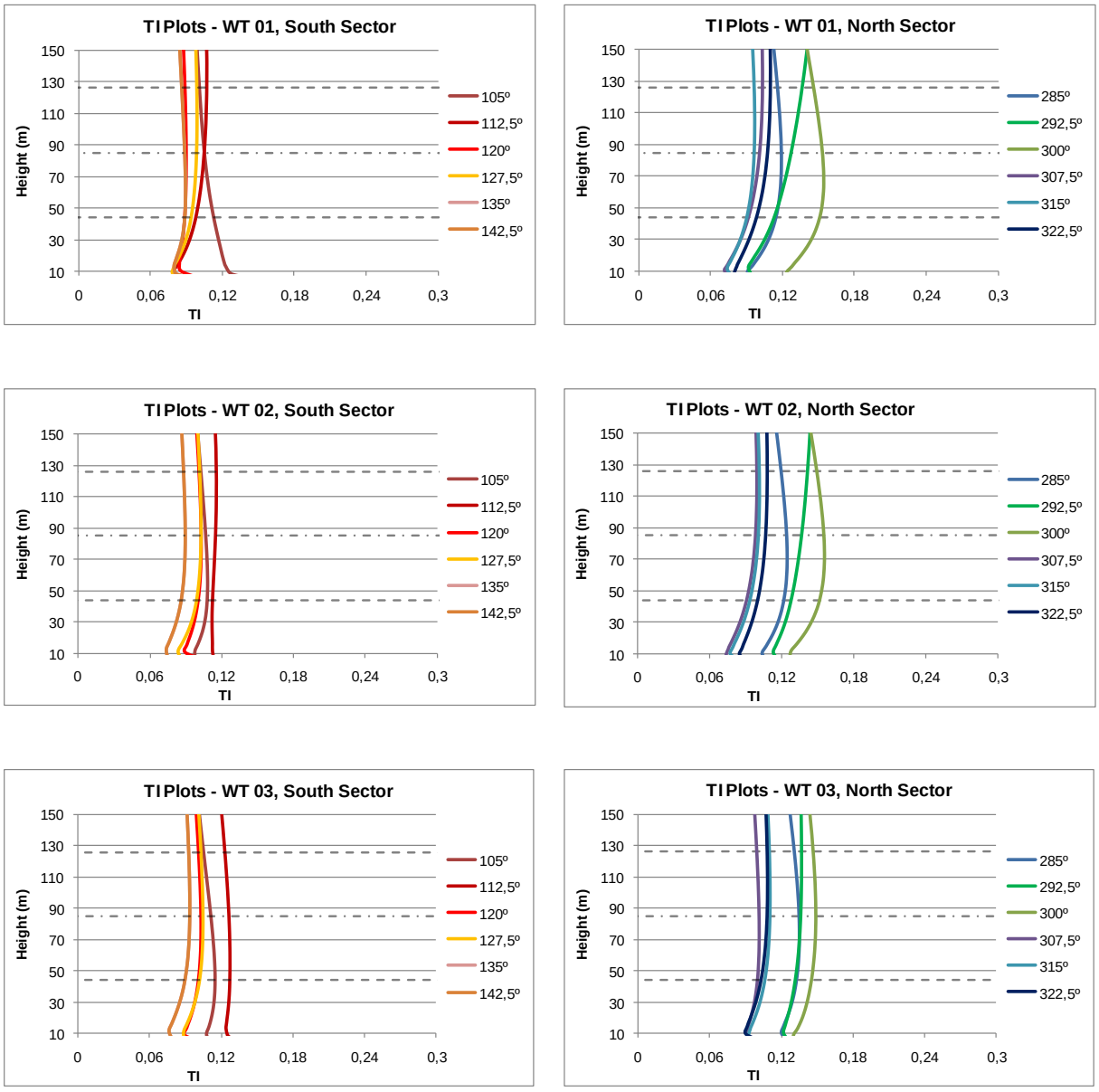

Figure 47 - TI vertical plots for wind turbines WT 01, WT 02 and WT 03

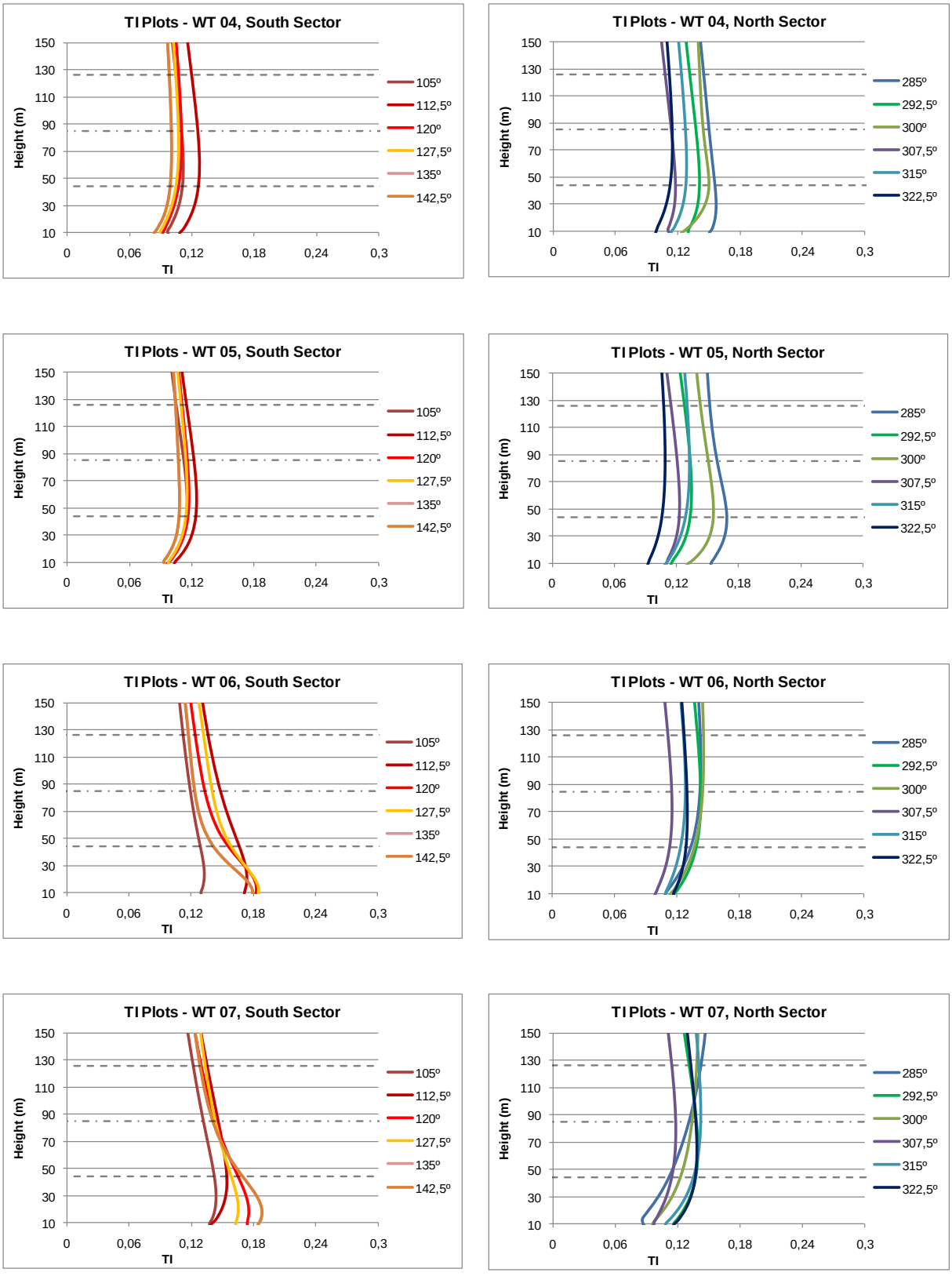

Figure 48 - TI vertical plots for wind turbines WT 04, WT 05, WT 06 and WT 07

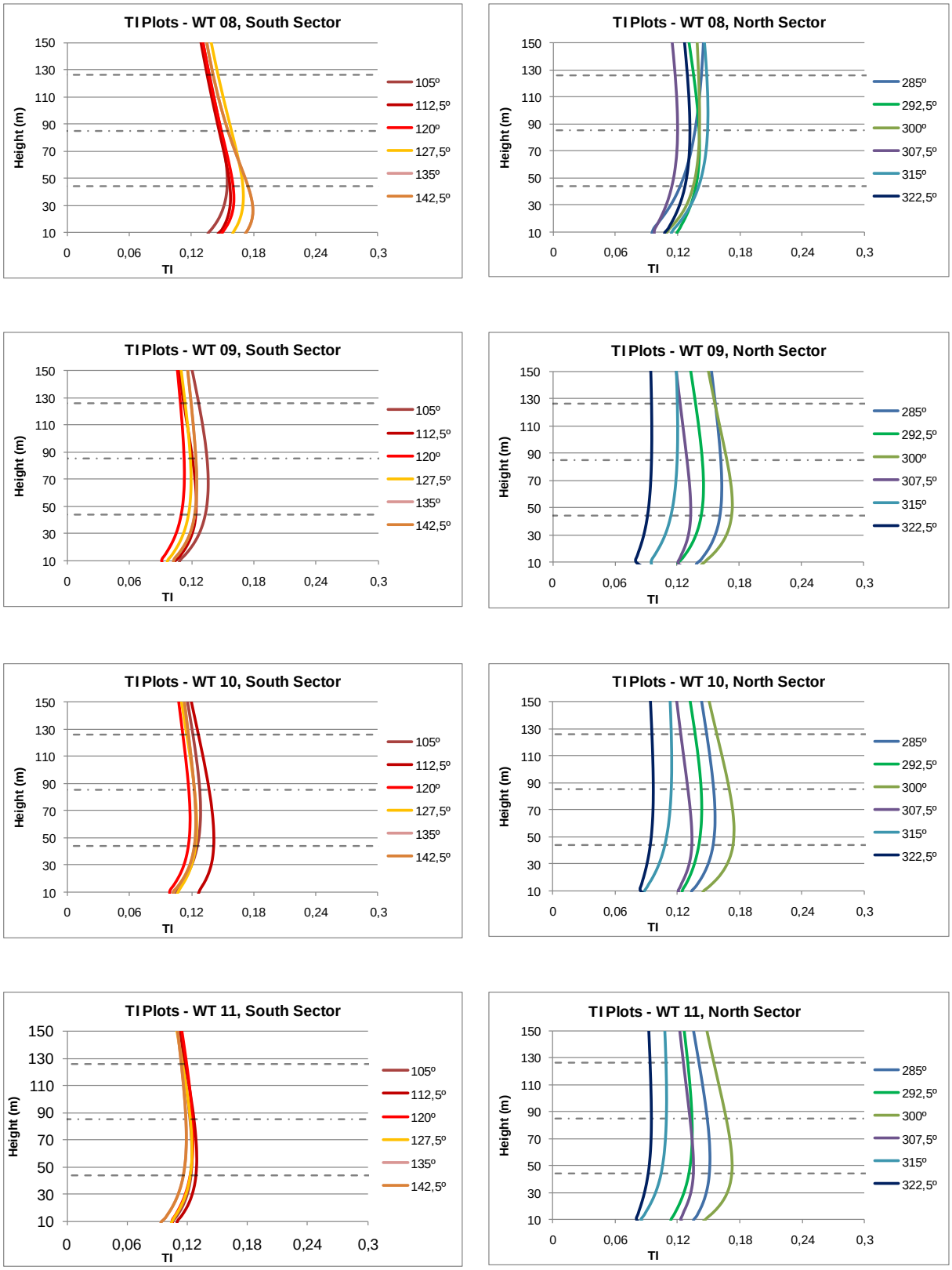

Figure 49 - TI vertical plots for wind turbines WT 08, WT 09, WT 10 and WT 11

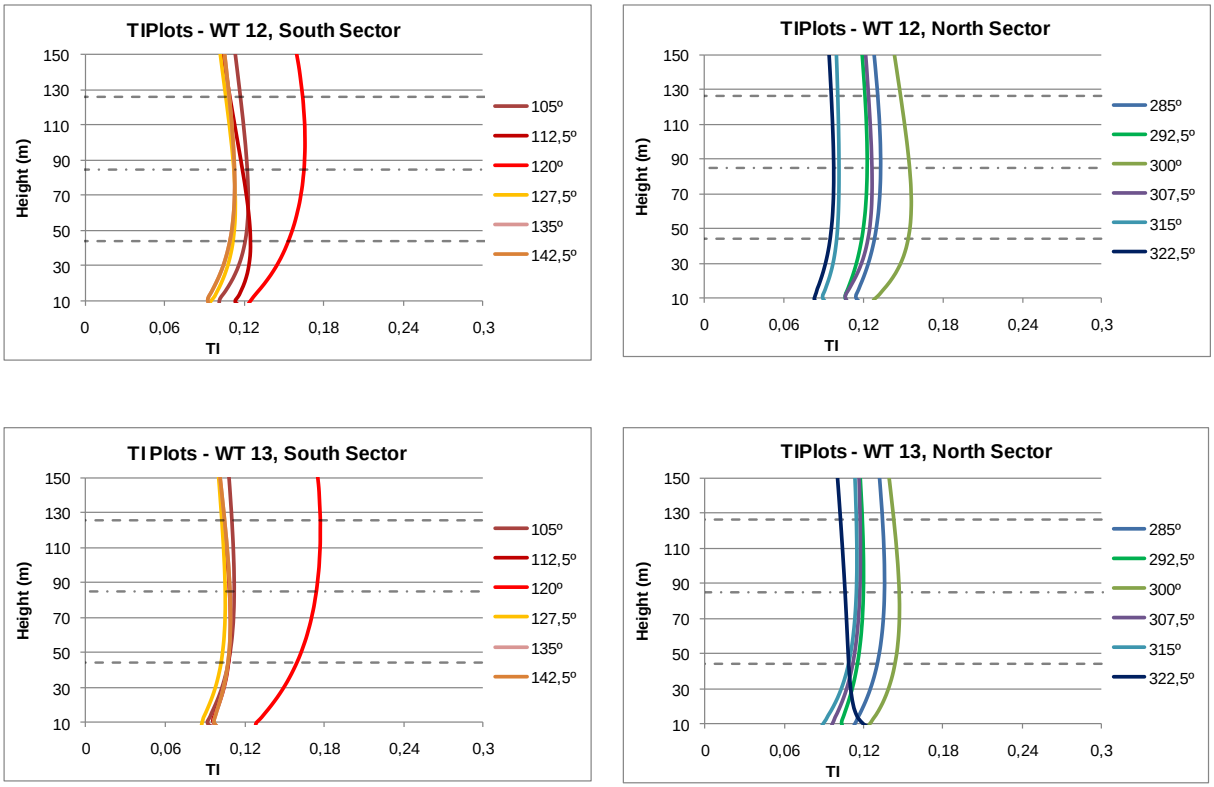

Figure 50 - TI vertical plots for wind turbines WT 12 and WT 13

Weather Station Turbulent Intensity plots

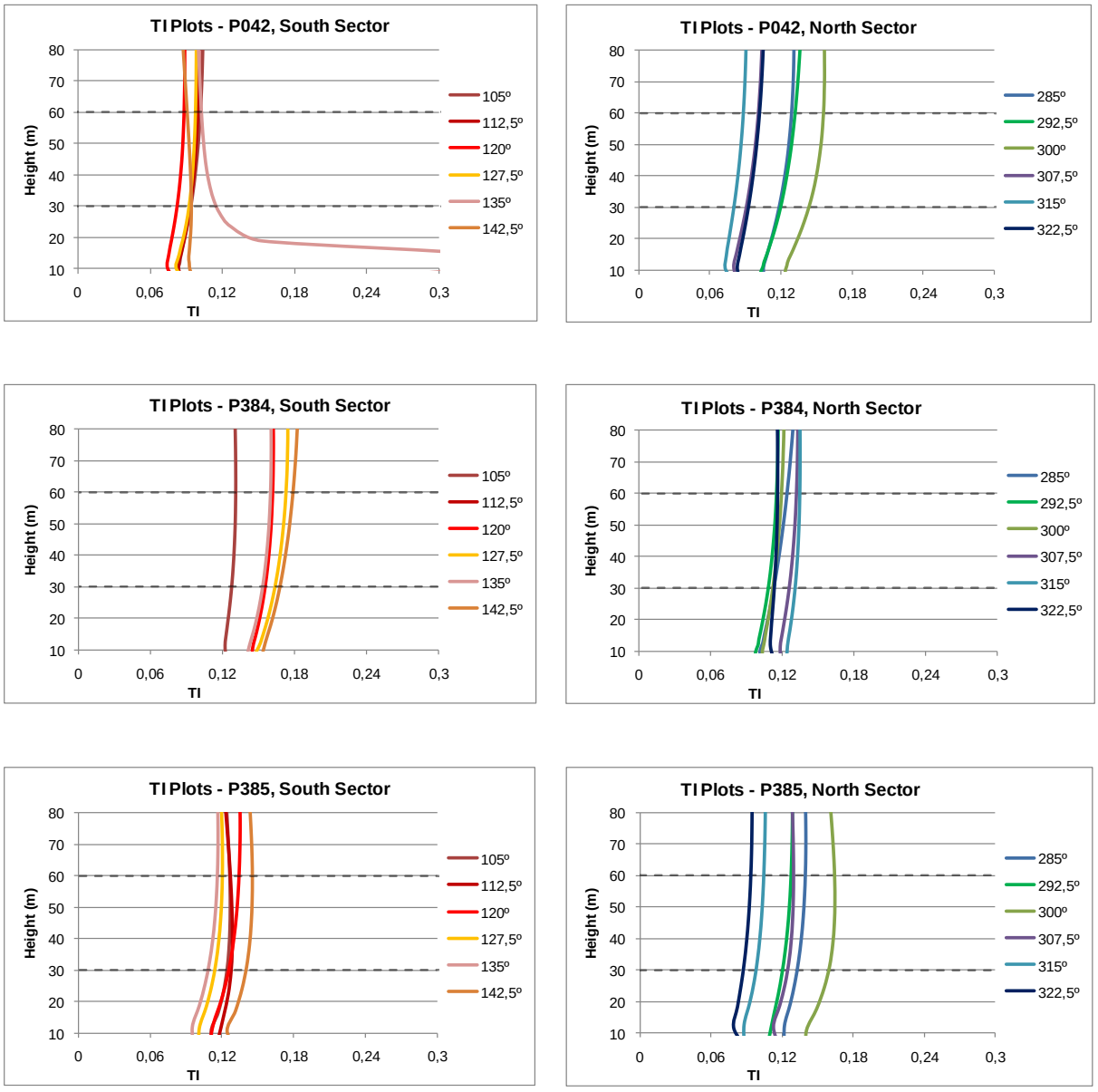

Figure 51 - TI vertical plots for weather stations P042, P384 and P385

Wind Turbine Flow Pitch plots

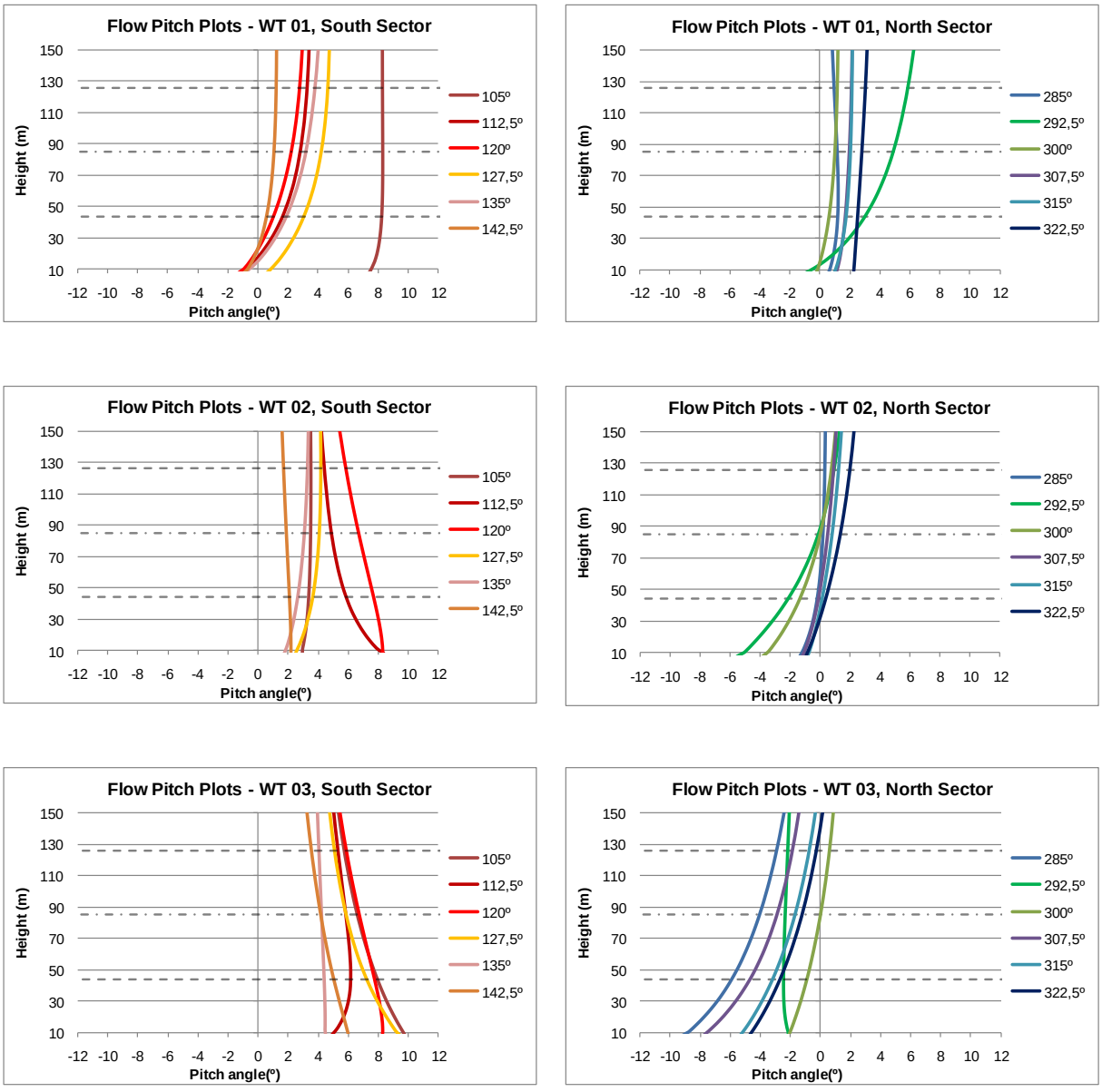

Figure 52 - Flow pitch vertical plots for wind turbines WT 01, WT 02 and WT 03

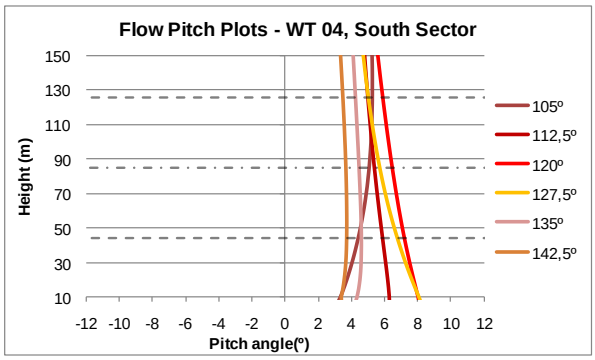

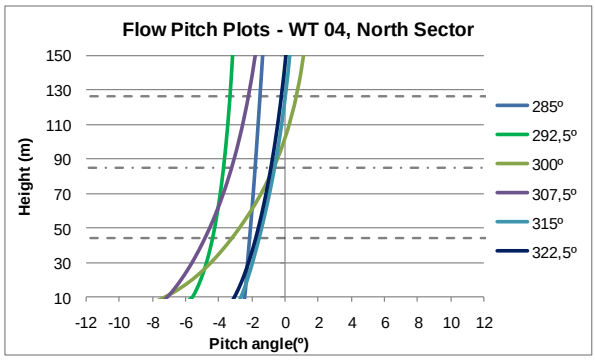

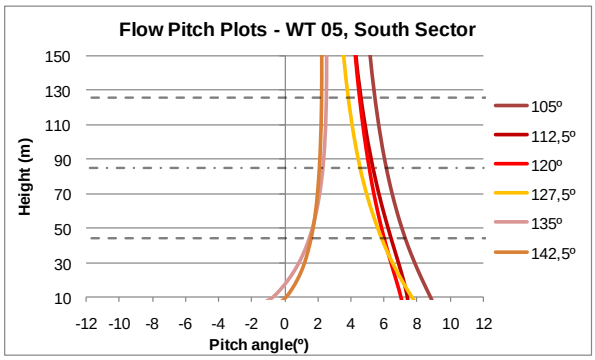

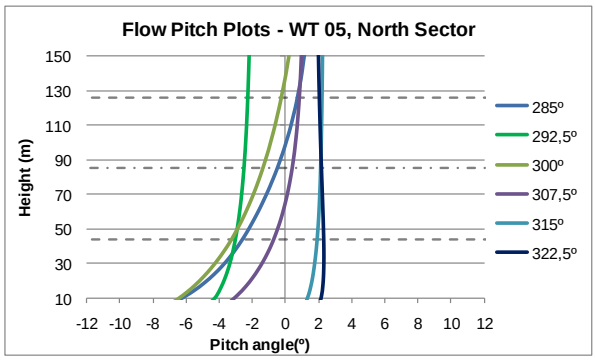

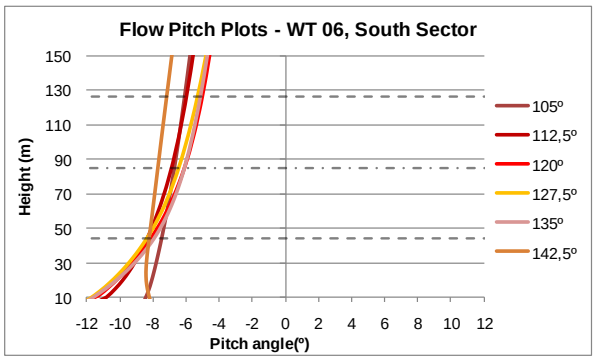

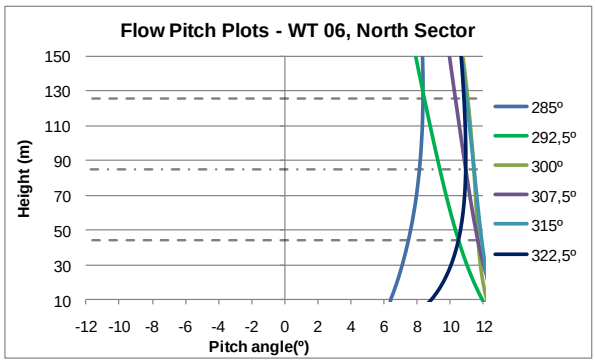

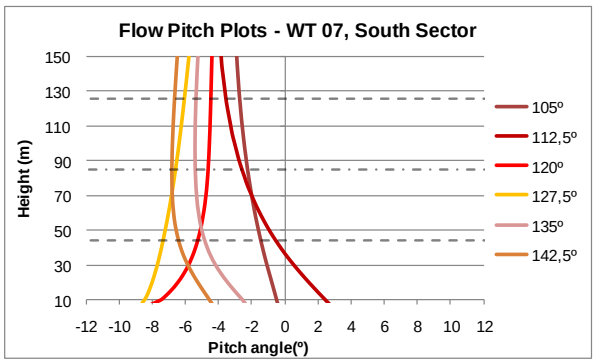

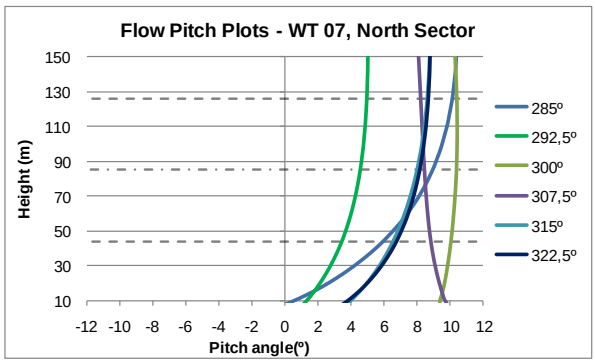

Figure 53 - Flow pitch vertical plots for wind turbines WT 04, WT 05, WT 06 and WT 07

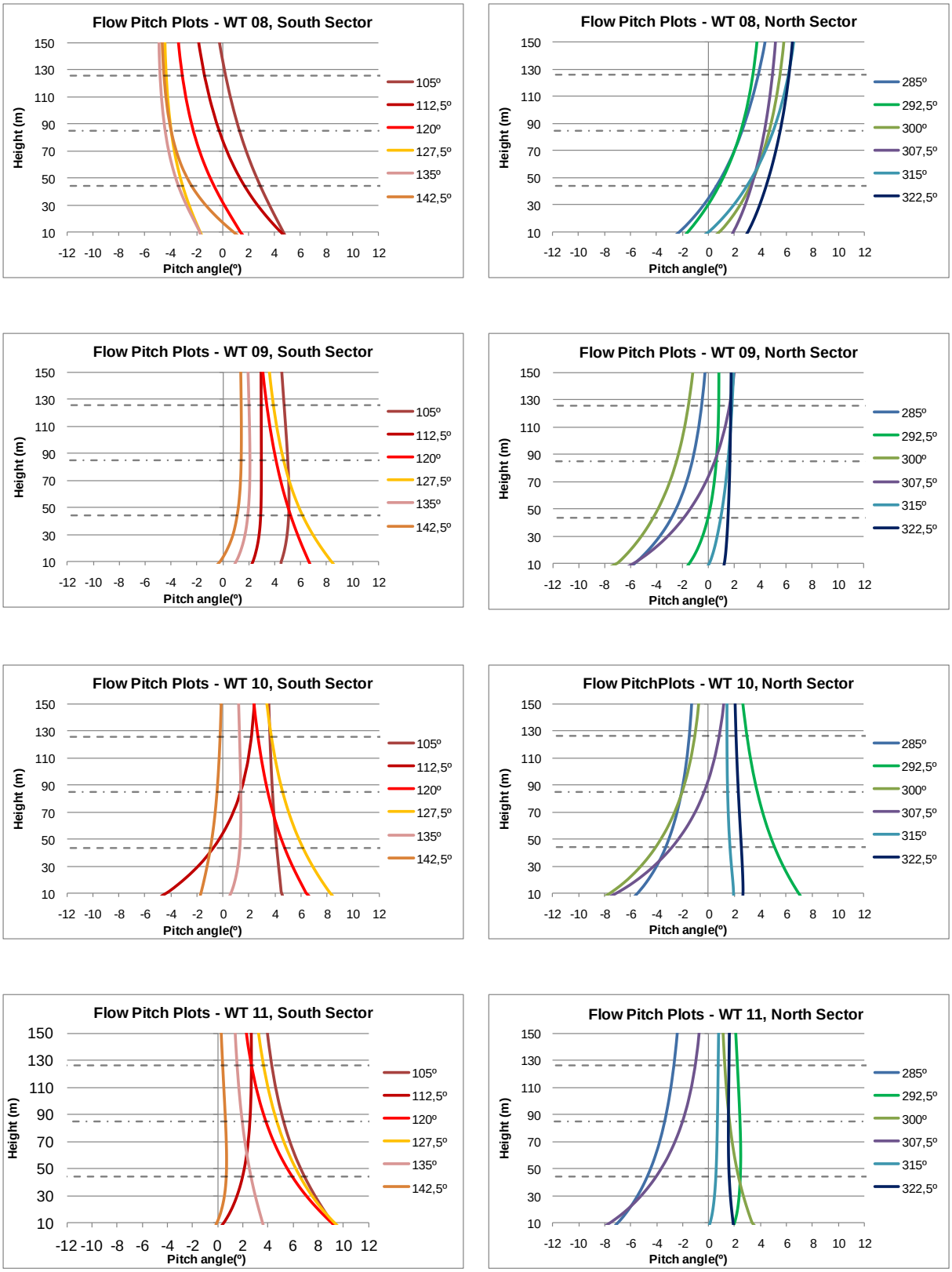

Figure 54 - Flow pitch vertical plots for wind turbines WT 08, WT 09, WT 10 and WT 11

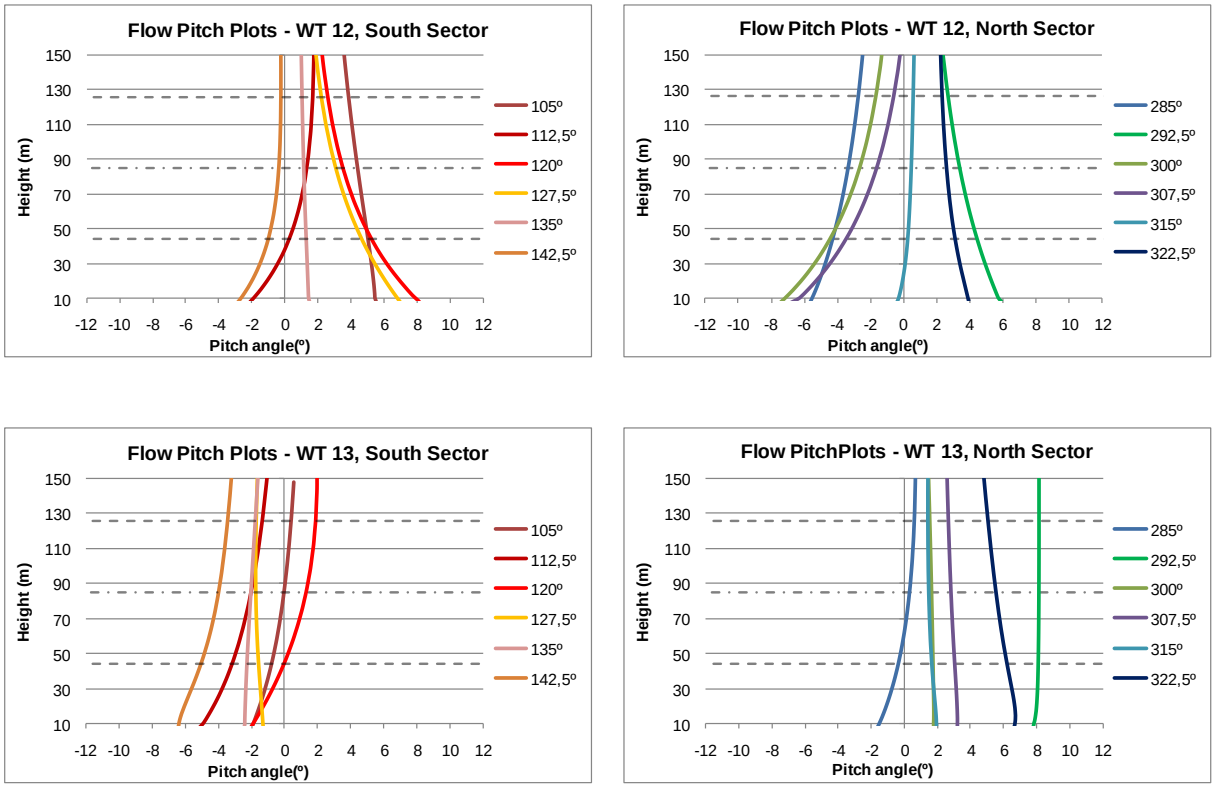

Figure 55 - Flow pitch vertical plots for wind turbines WT 12 and WT 13

Horizontal velocity 2D contours @ 44m a.g.l.

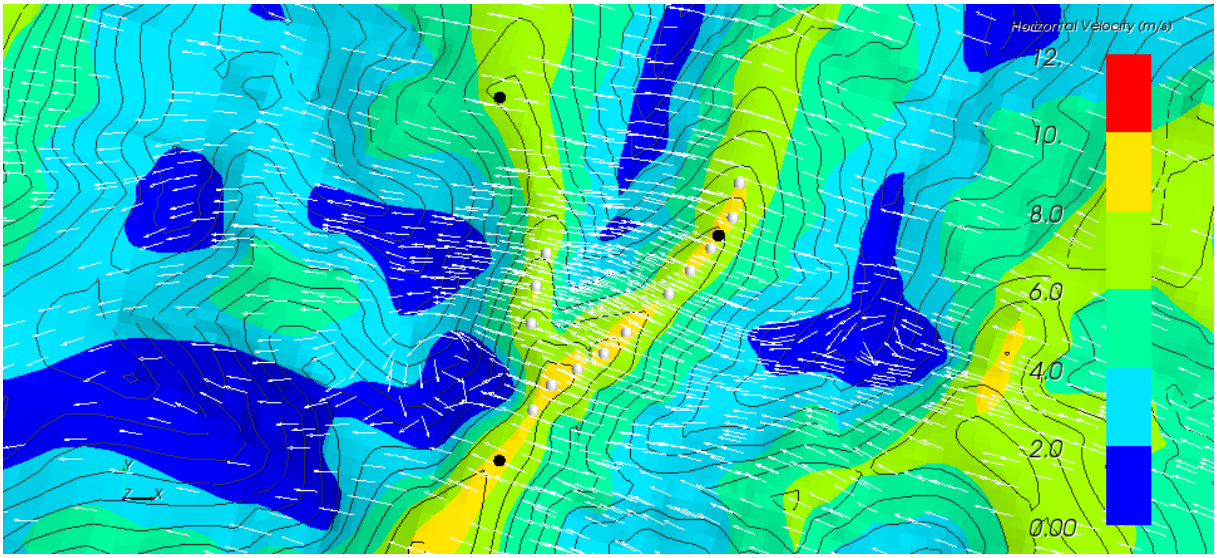

105º Direction

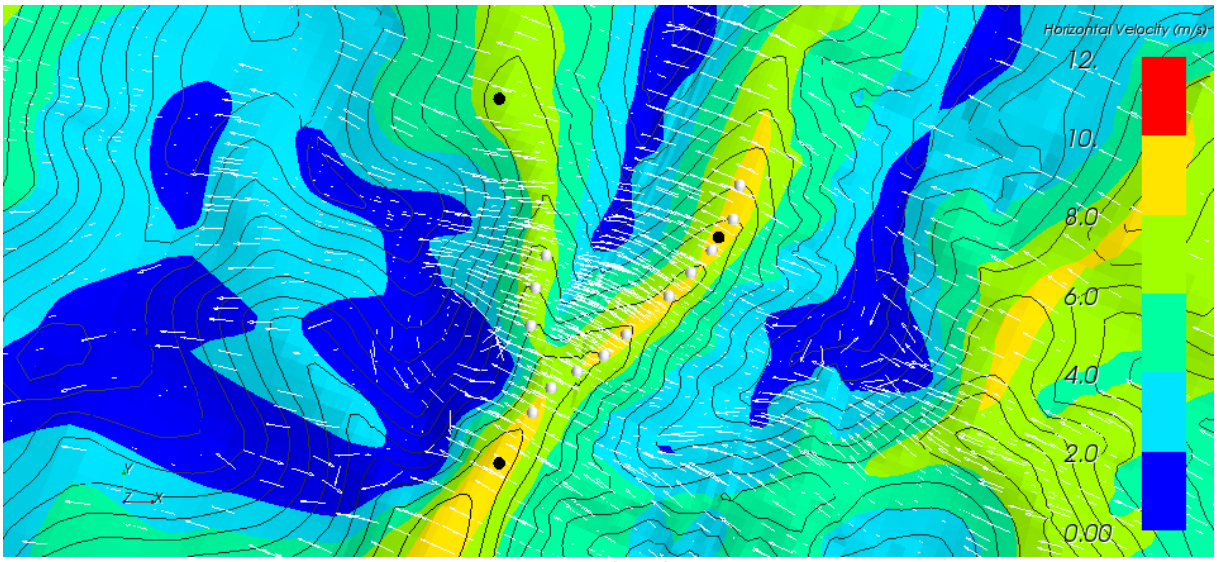

112,5º Direction

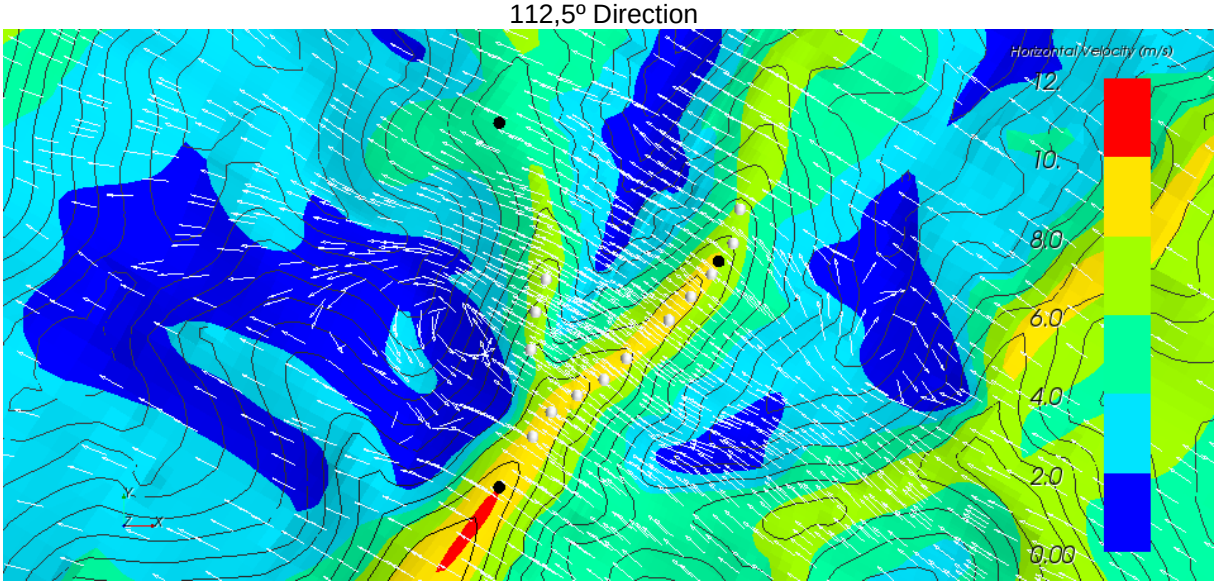

120º Direction

Figure 56 - Horizontal velocity contour maps at 44 m a.g.l., for directions 105º through 120º

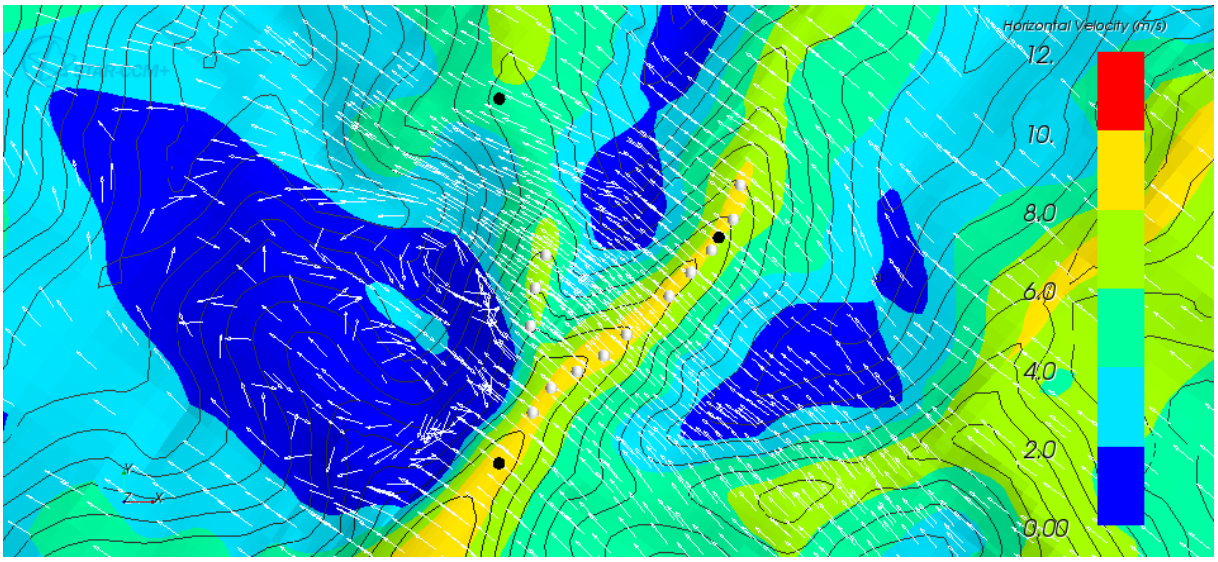

127,5º Direction

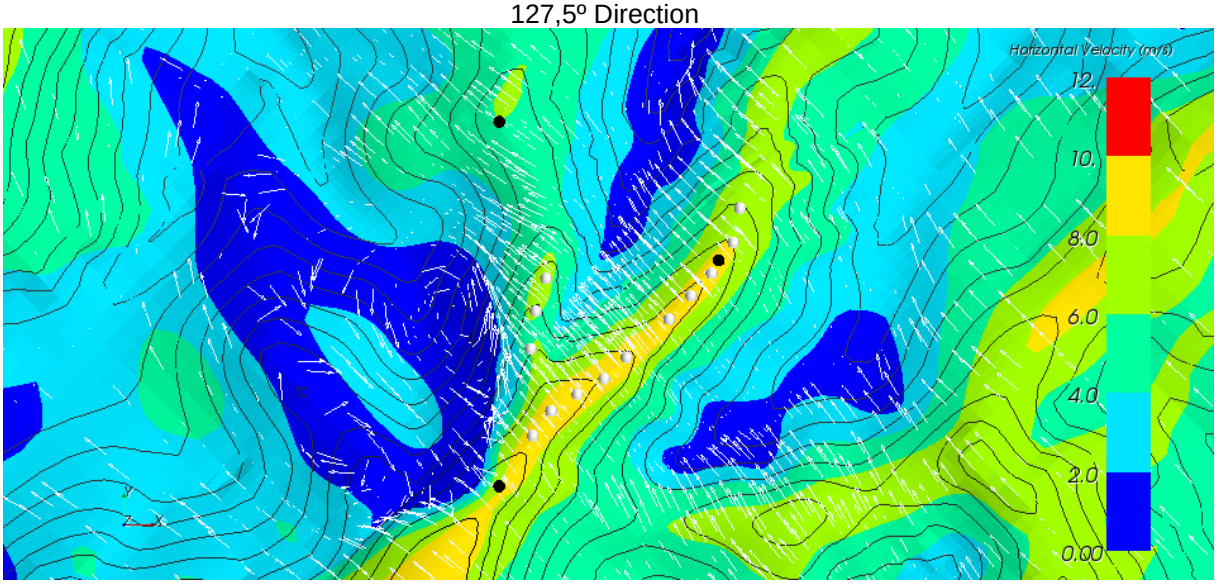

135º Direction

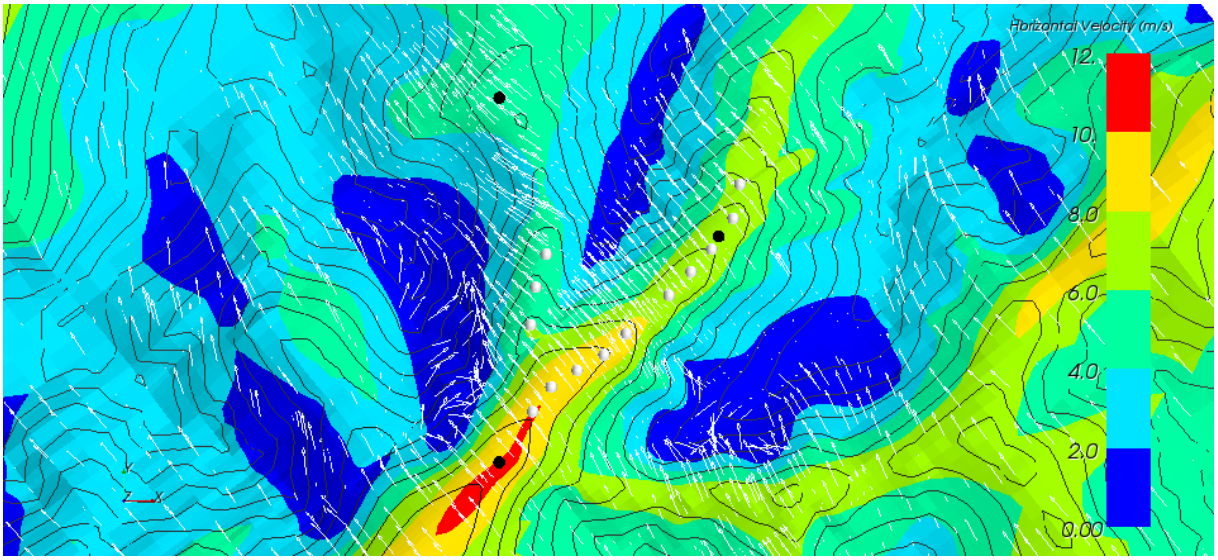

142,5º Direction

Figure 57 - Horizontal velocity contour maps at 44 m a.g.l., for directions 127.5º through 142.5º

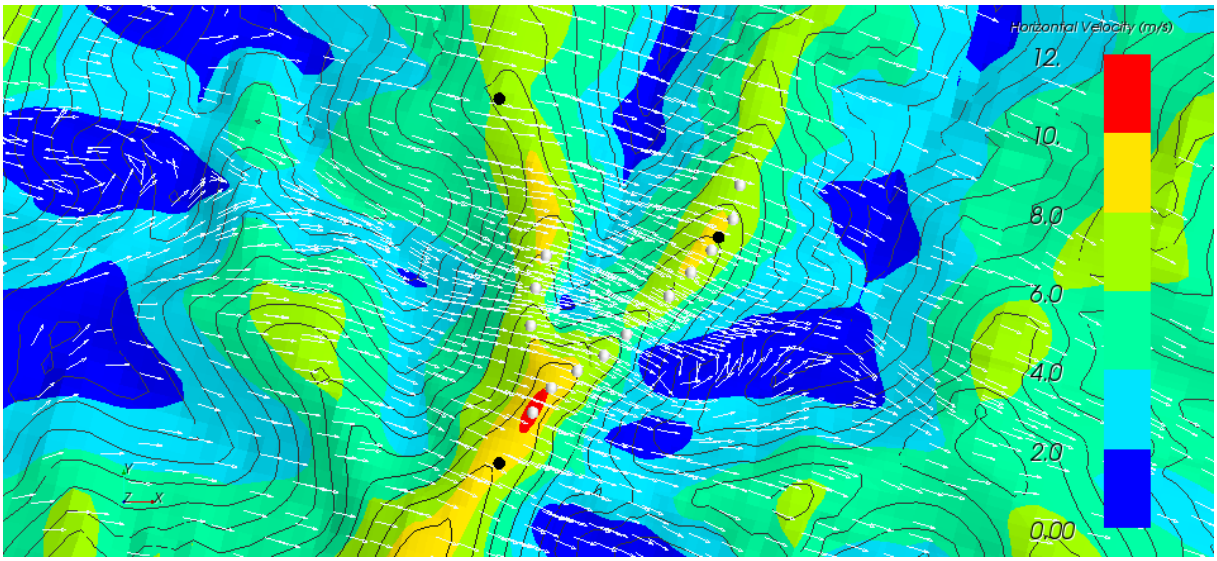

285º Direction

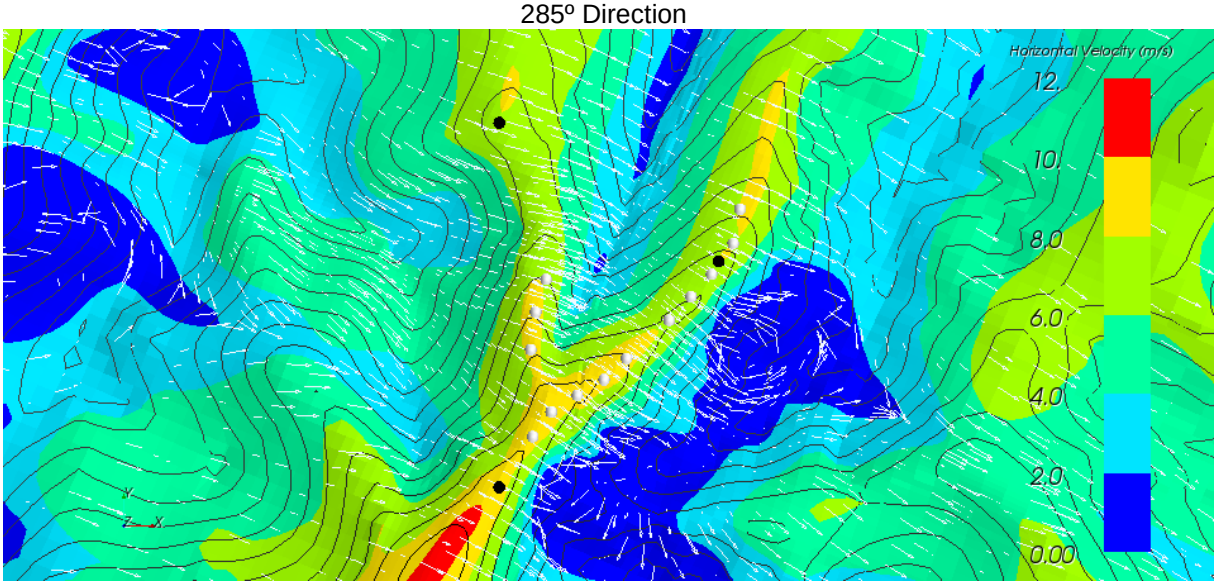

292,5º Direction

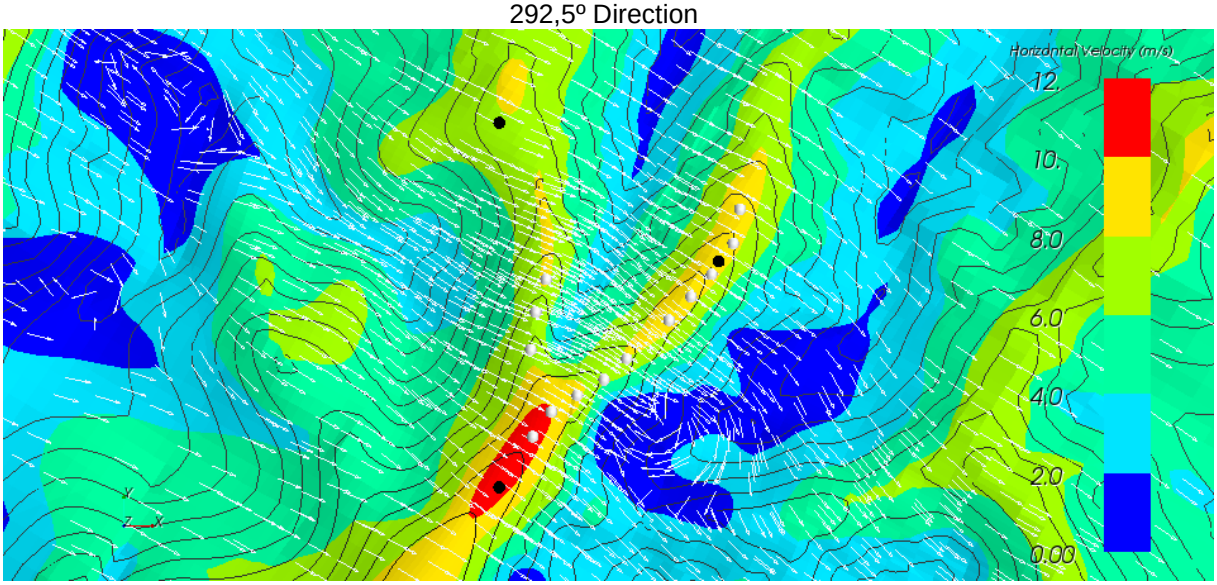

300º Direction

Figure 58 - Horizontal velocity contour maps at 44 m a.g.l., for directions 285º through 300º

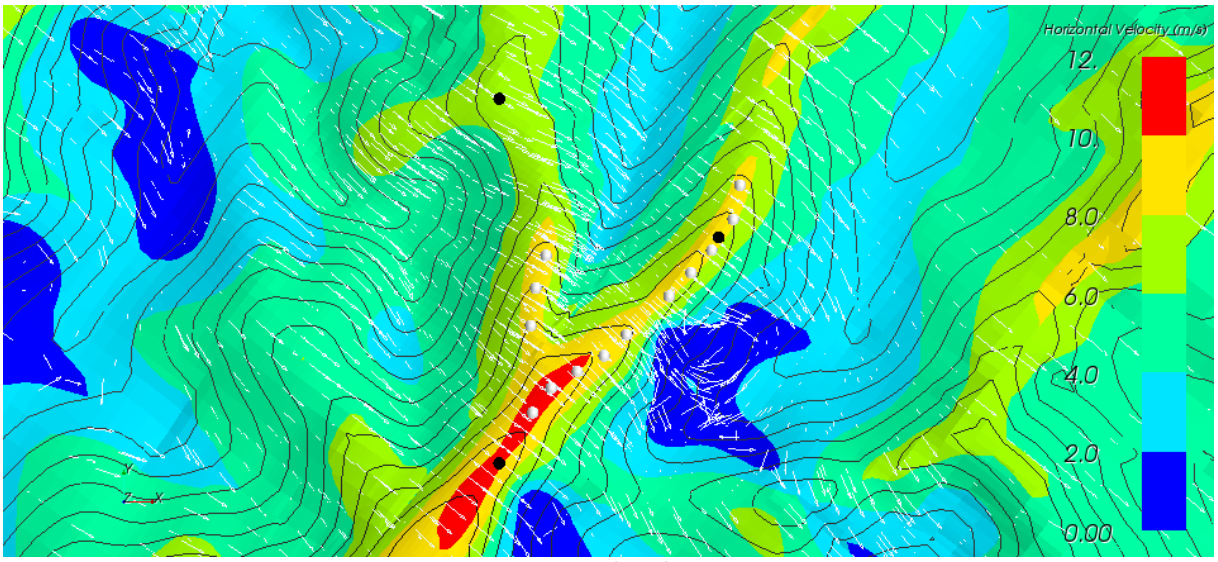

307,5º Direction

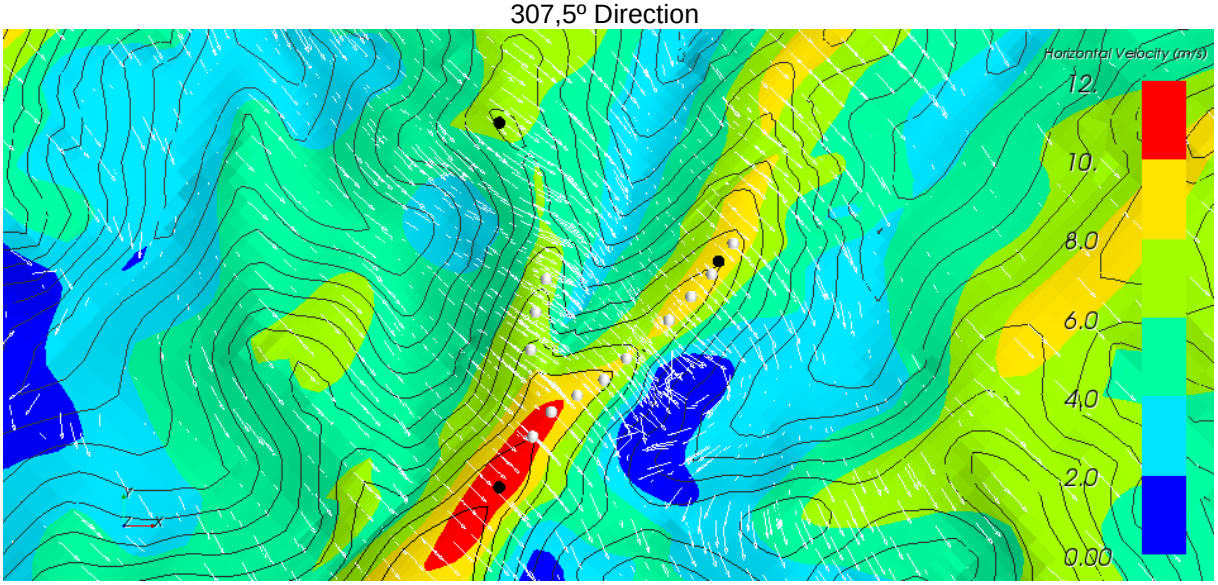

315º Direction

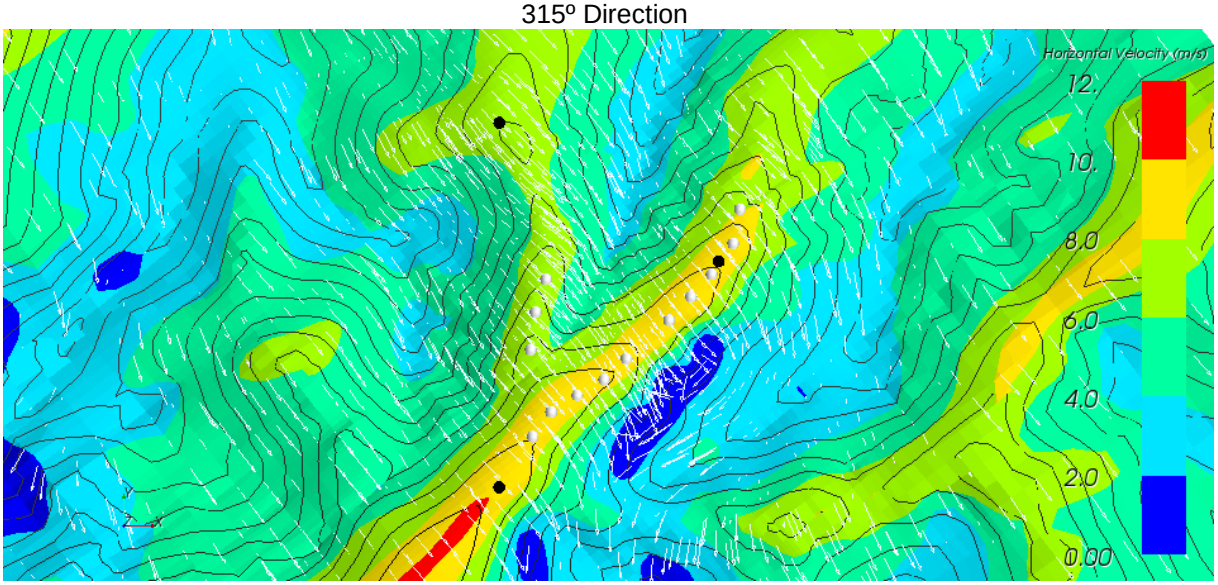

322,5º Direction

Figure 59 - Horizontal velocity contour maps at 44 m a.g.l., for directions 307.5º through 322.5º

Horizontal velocity 2D contours @ 85m a.g.l.

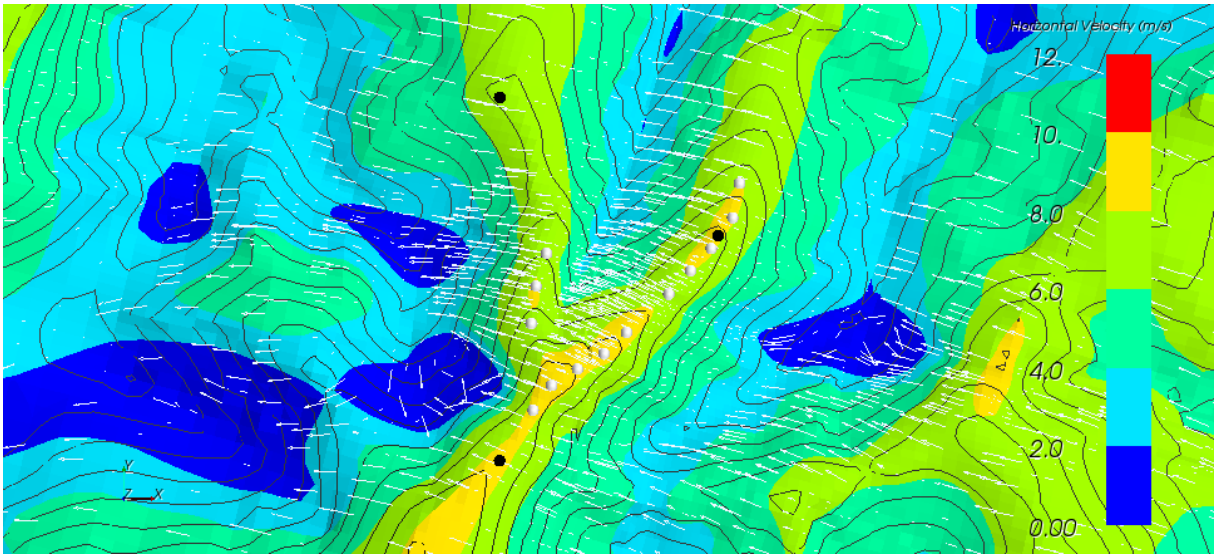

105º Direction

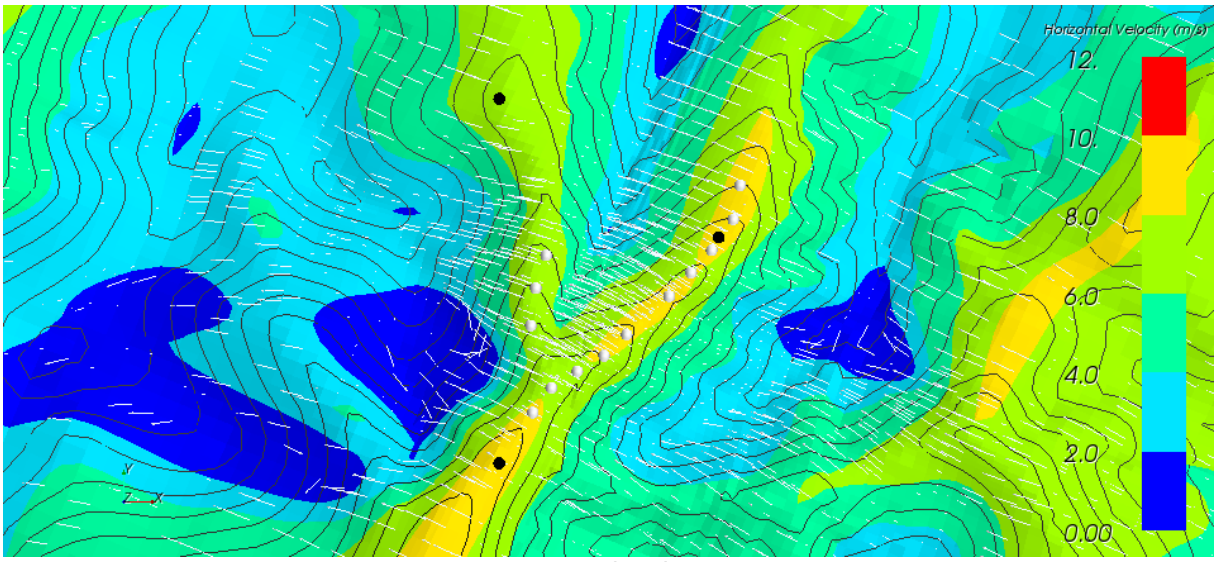

112,5º Direction

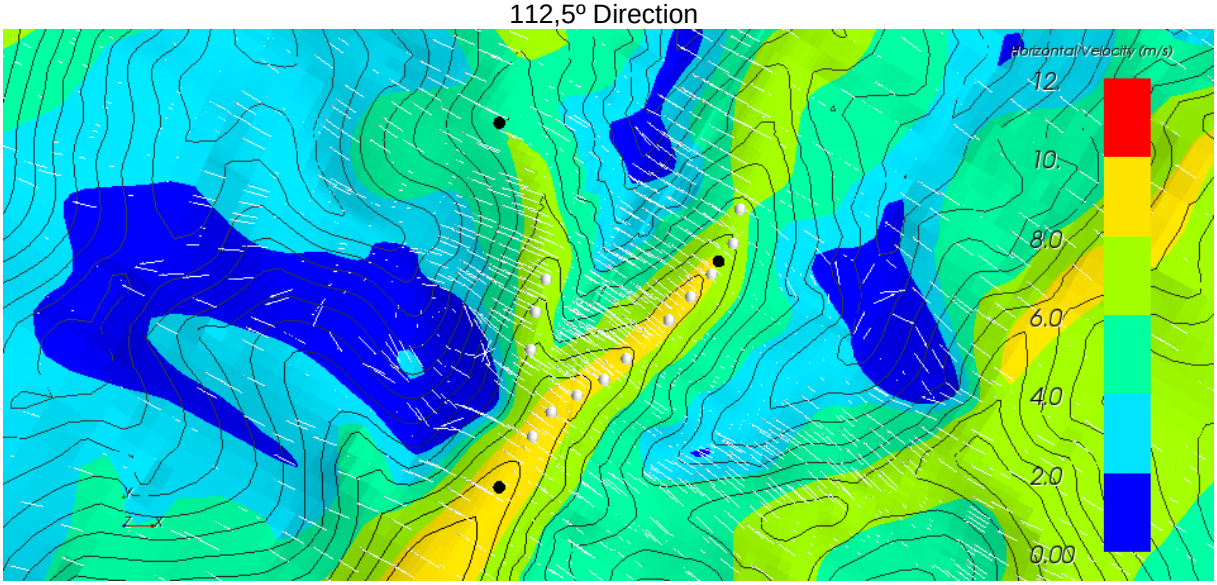

120º Direction

Figure 60 - Horizontal velocity contour maps at 85 m a.g.l., for directions 105º through 120º

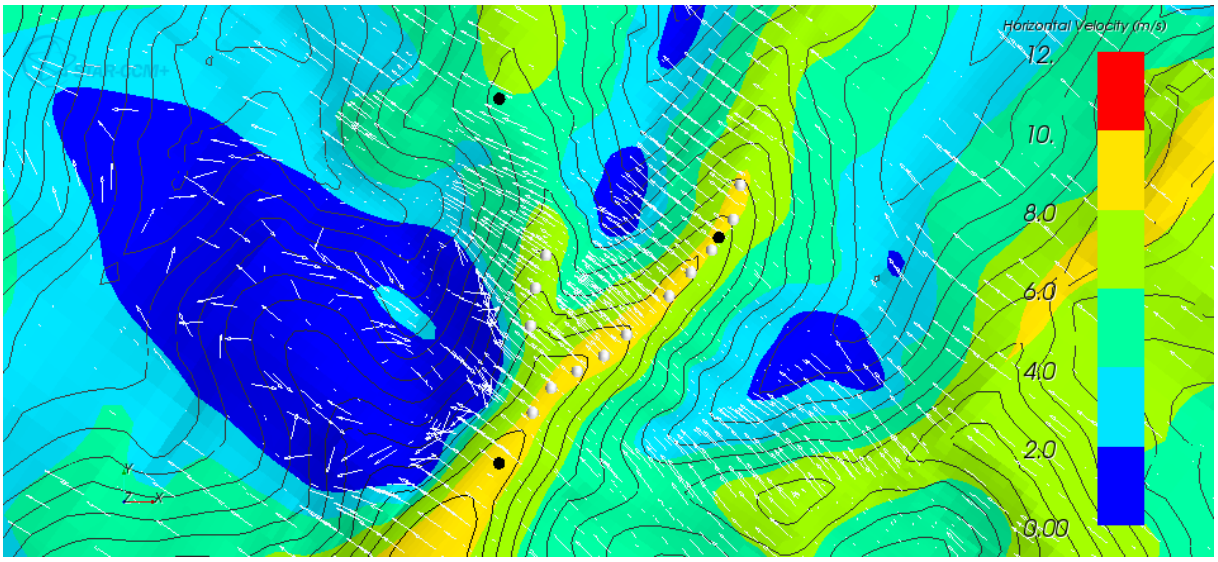

127,5º Direction

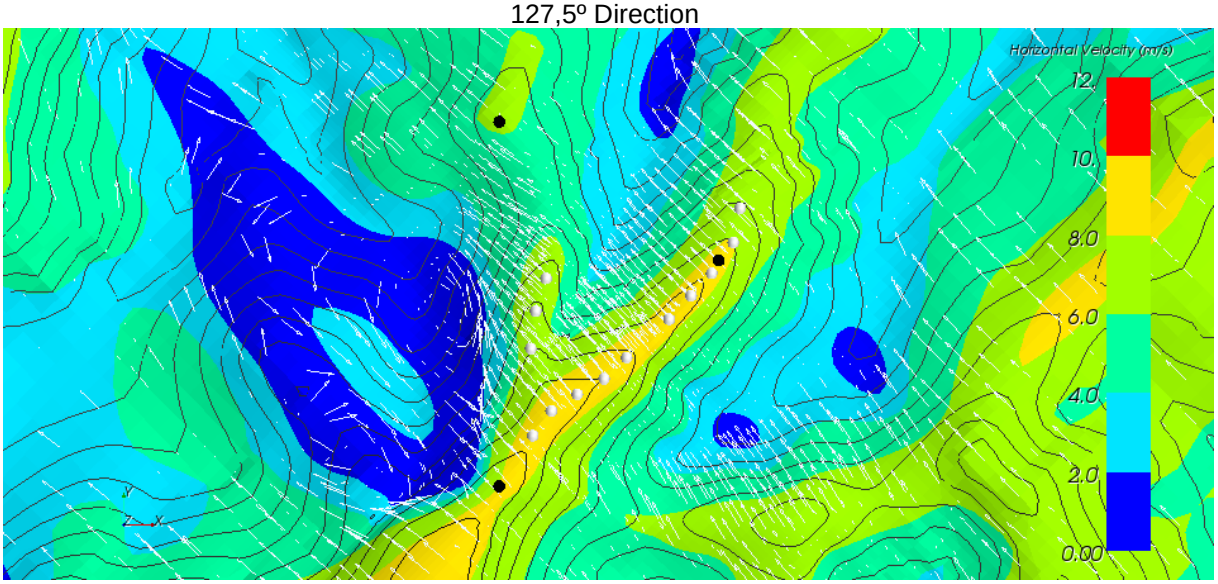

135º Direction

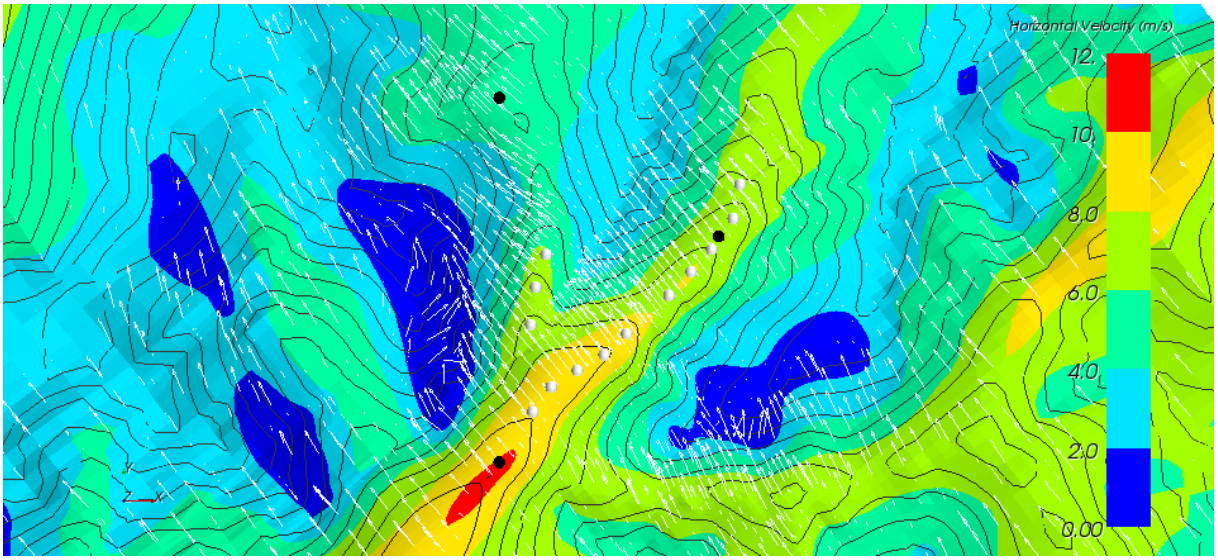

142,5º Direction

Figure 61 - Horizontal velocity contour maps at 85 m a.g.l., for directions 127.5º through 142.5º

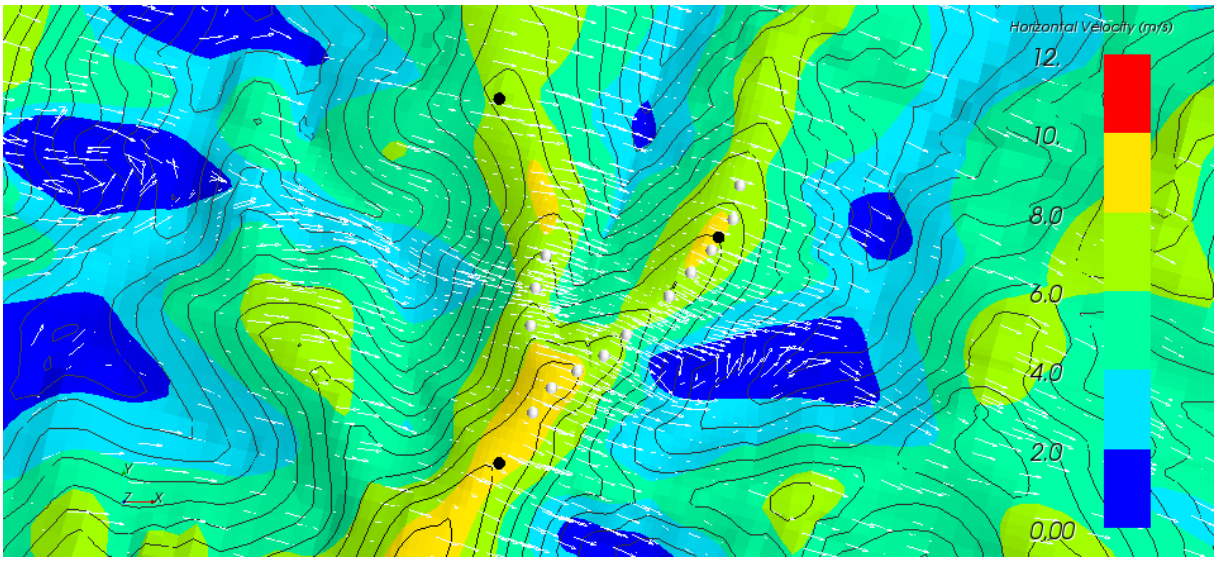

285º Direction

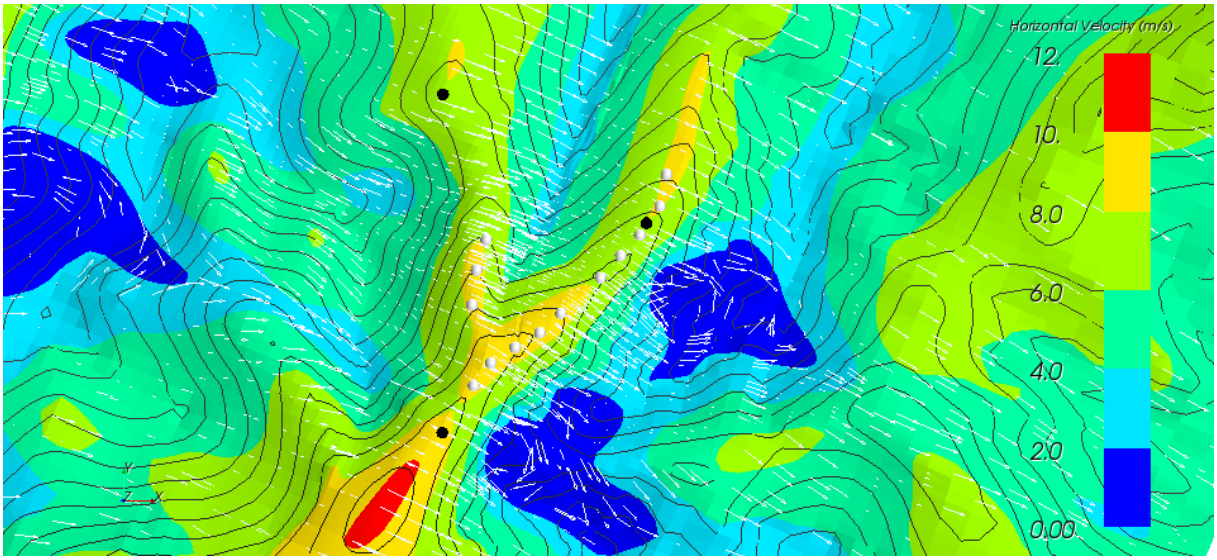

292,5º Direction

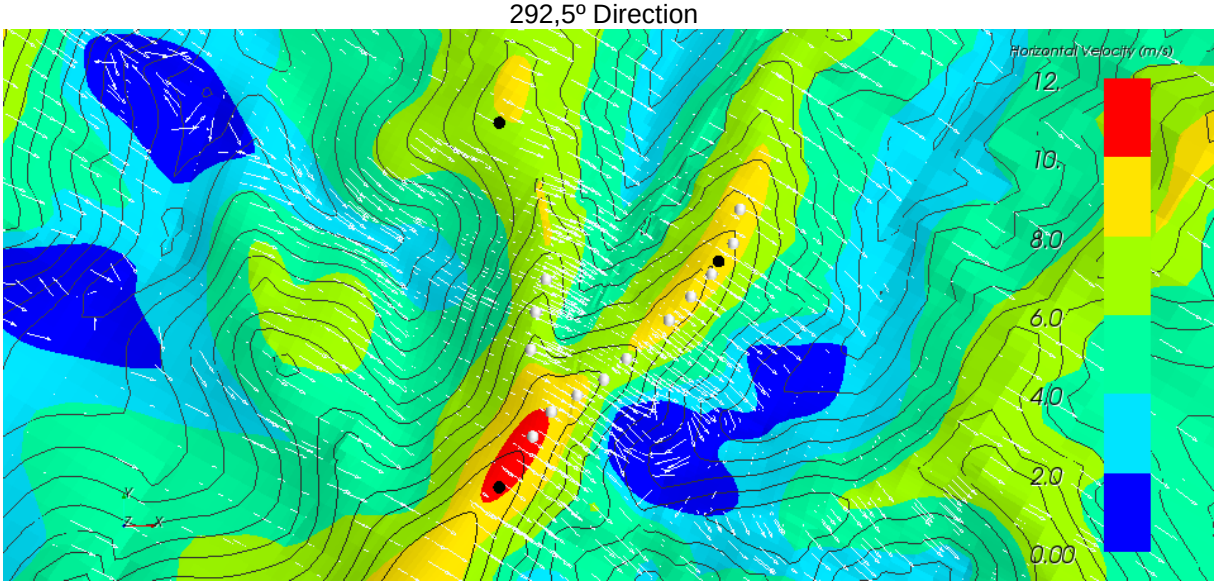

300º Direction

Figure 62 - Horizontal velocity contour maps at 85 m a.g.l., for directions 285º through 300º

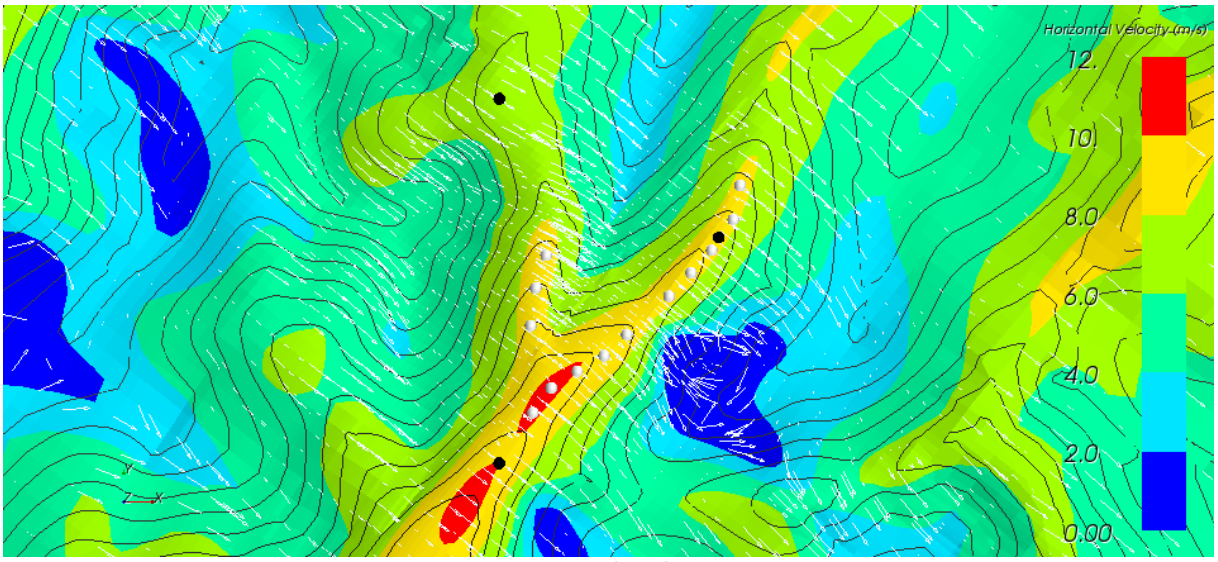

307,5º Direction

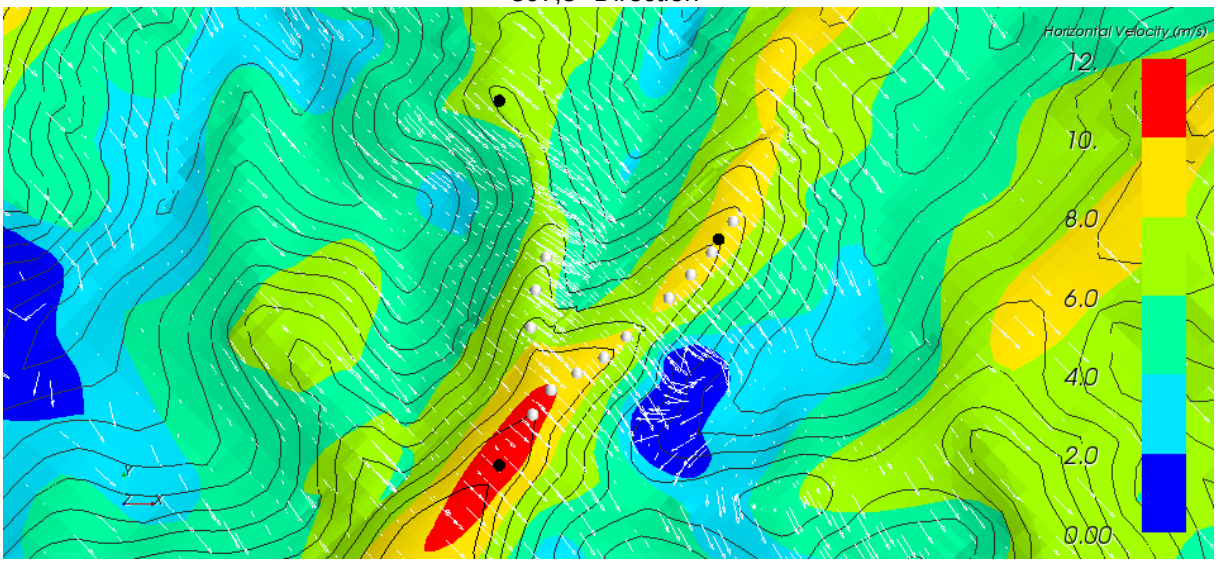

315º Direction

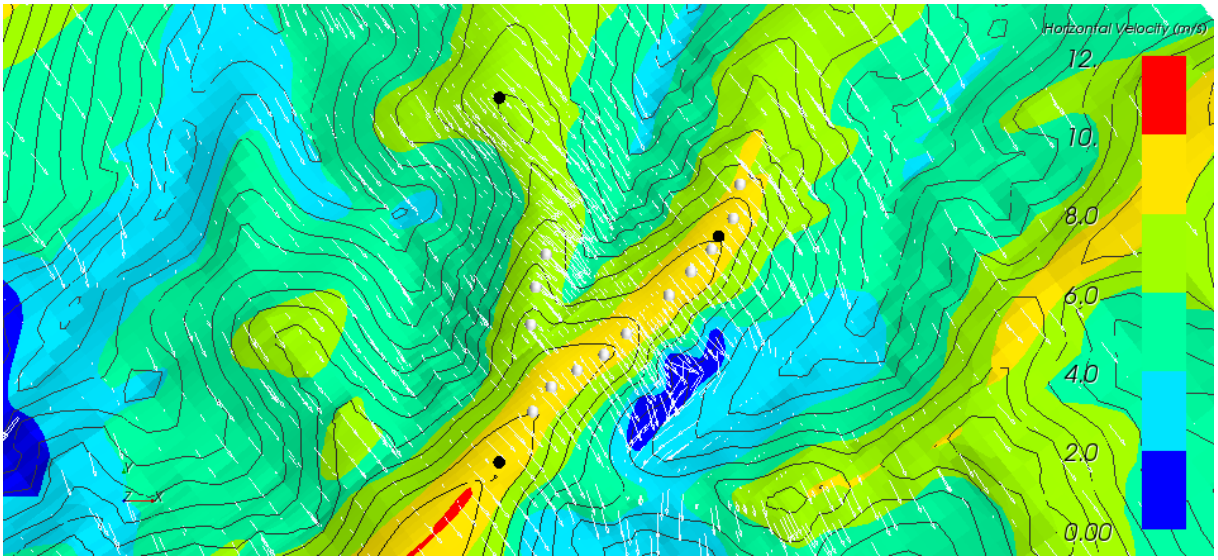

322,5º Direction

Figure 63 - Horizontal velocity contour maps at 85 m a.g.l., for directions 307.5º through 322.5º

Horizontal velocity 2D contours @ 126m a.g.l.

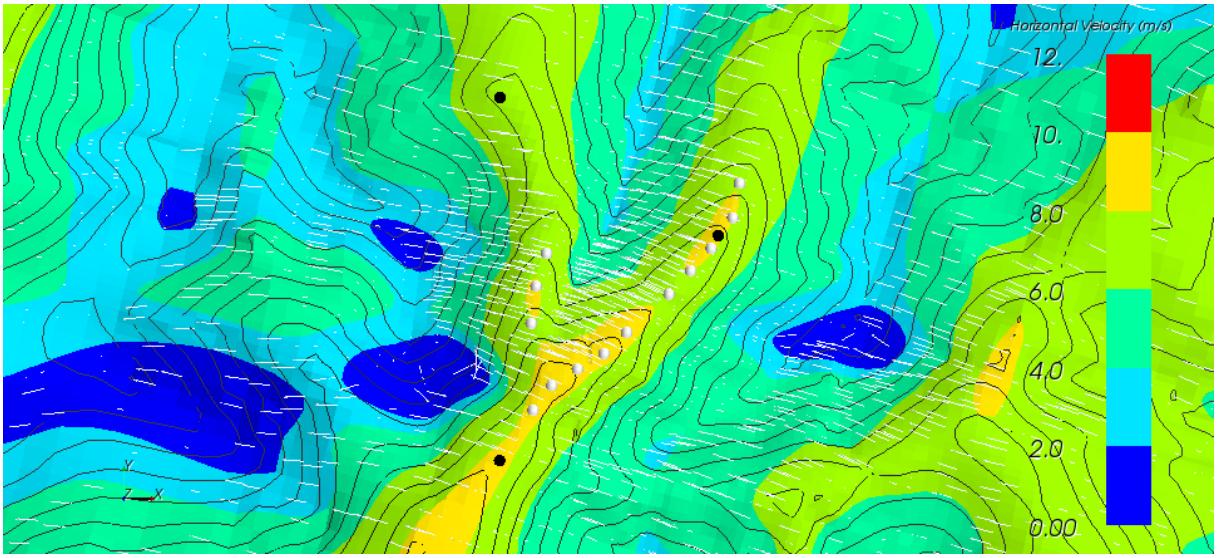

105º Direction

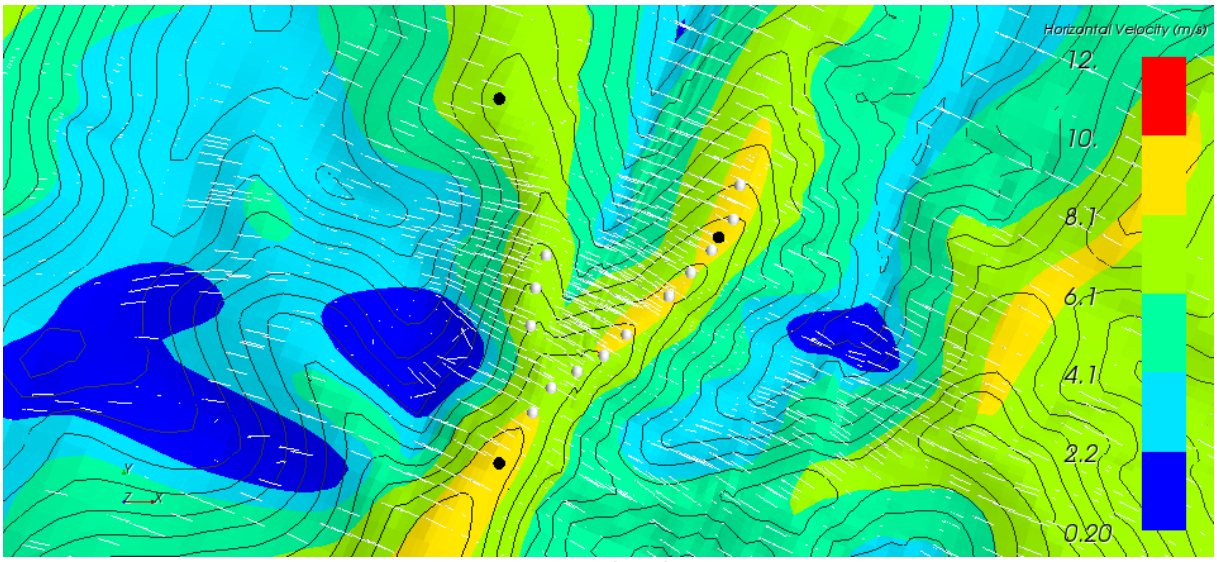

112,5º Direction

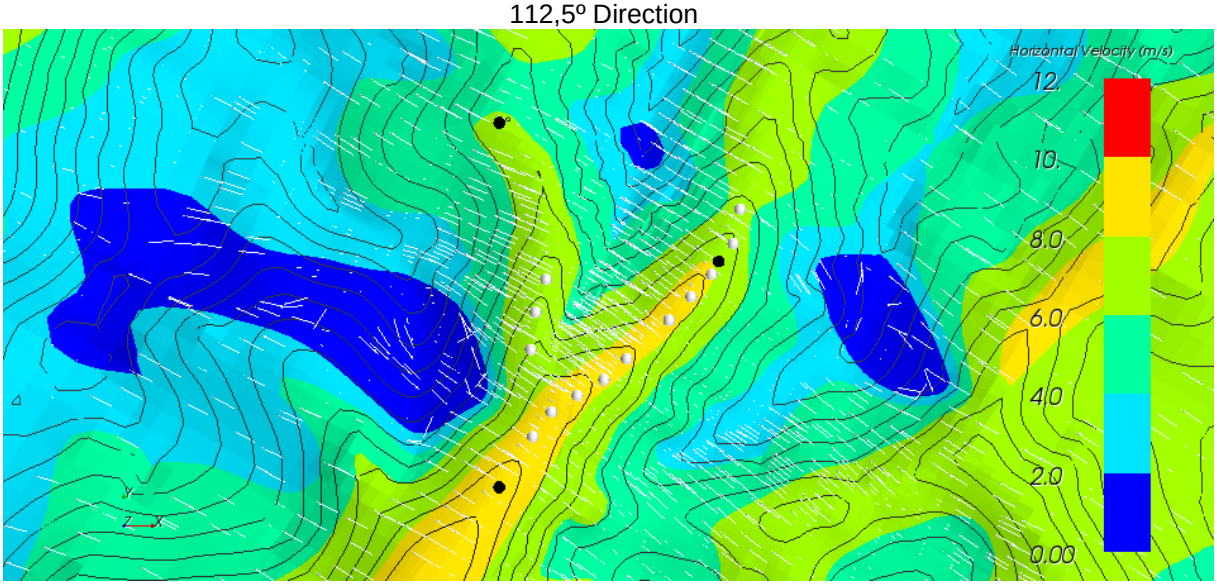

120º Direction

Figure 64 - Horizontal velocity contour maps at 126 m a.g.l., for directions 105º through 120º

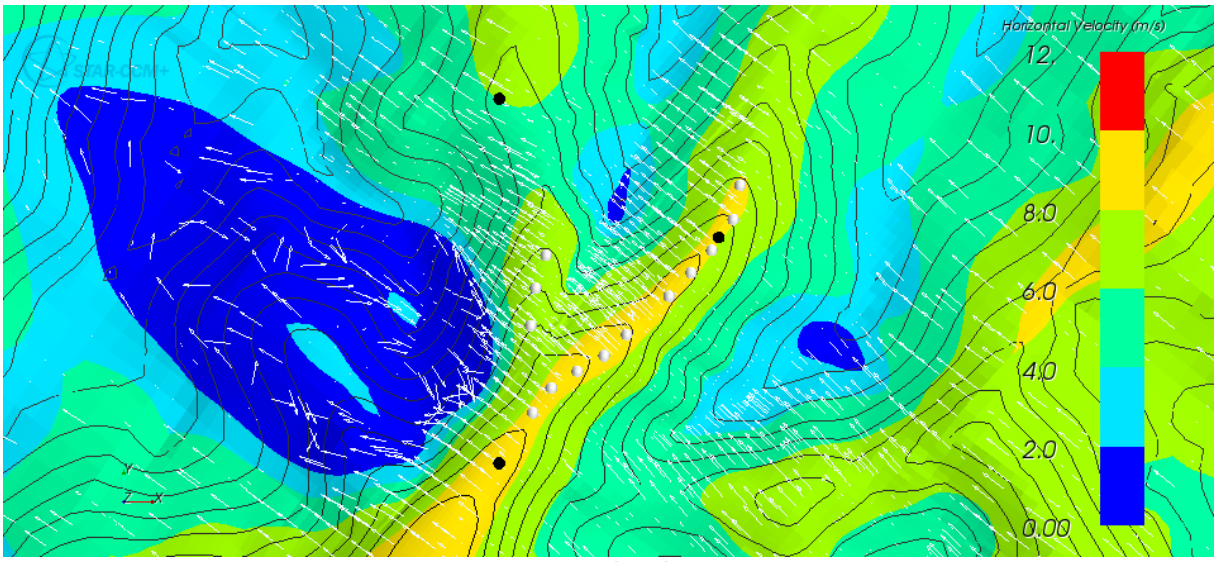

127,5º Direction

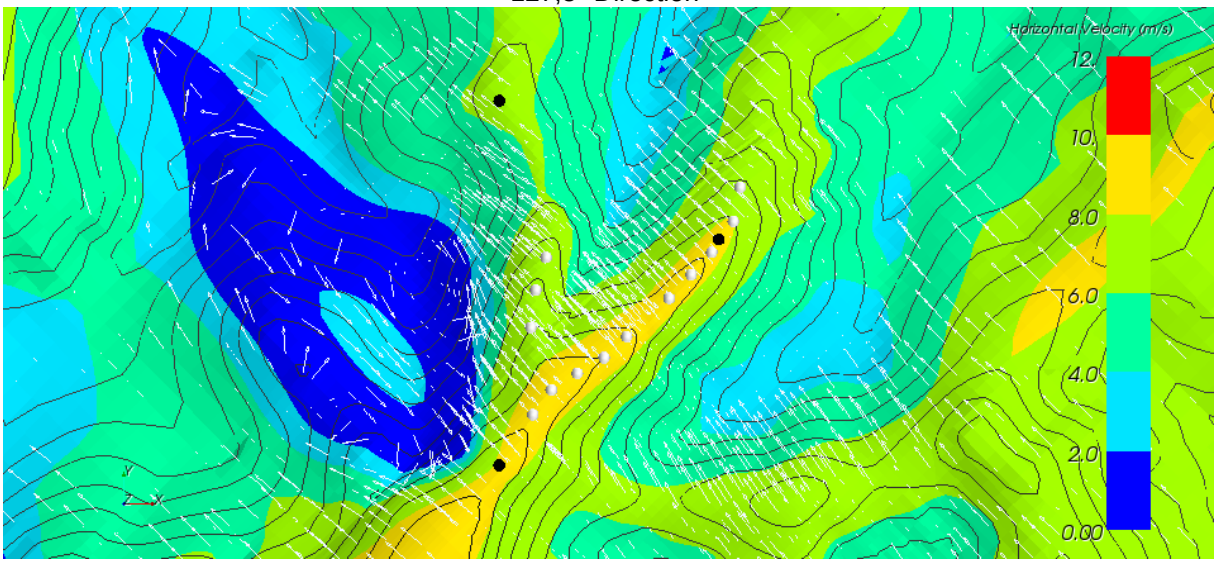

135º Direction

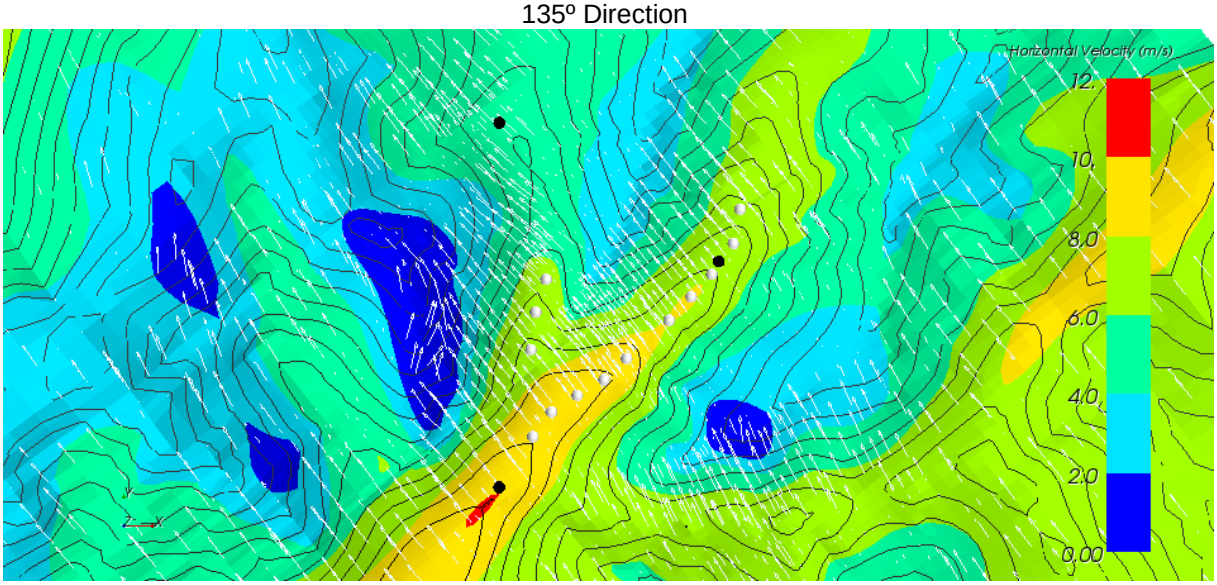

142,5º Direction

Figure 65 - Horizontal velocity contour maps at 126 m a.g.l., for directions 127.5º through 142.5º

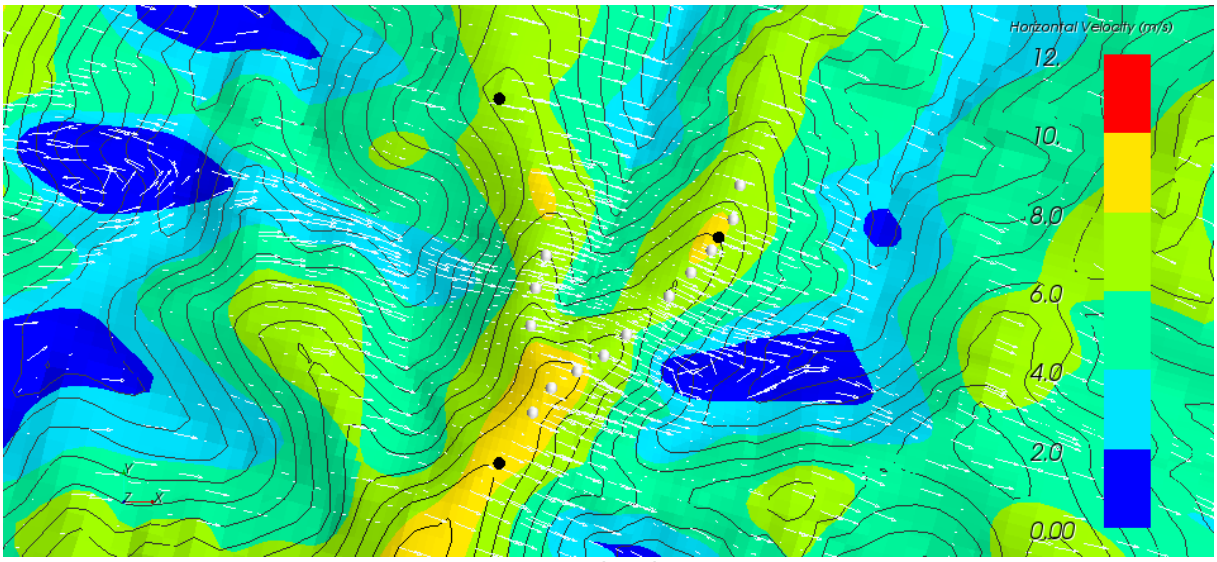

285º Direction

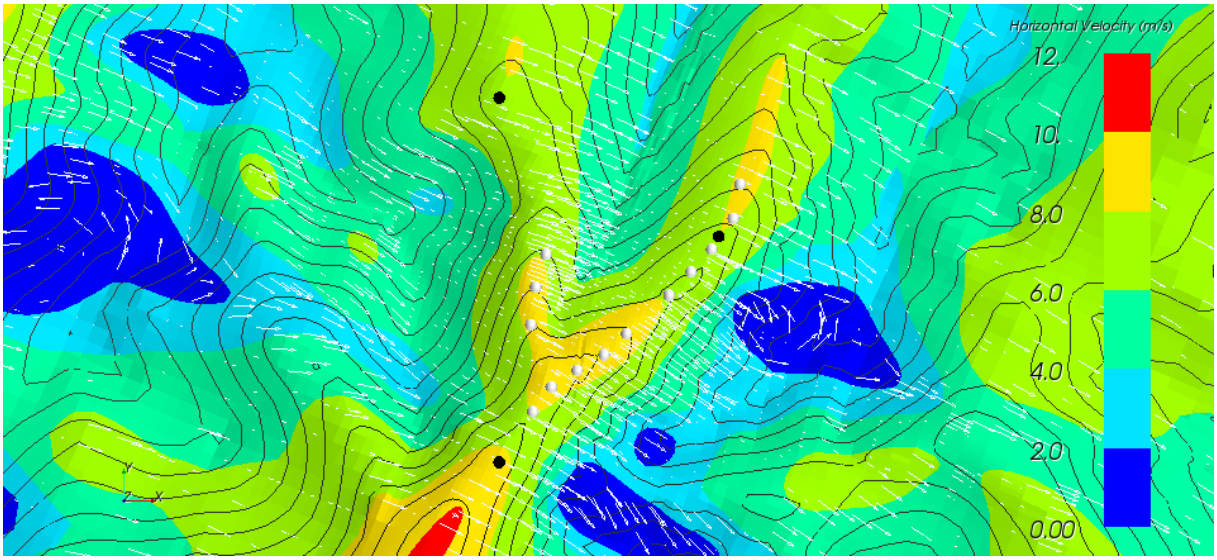

292,5º Direction

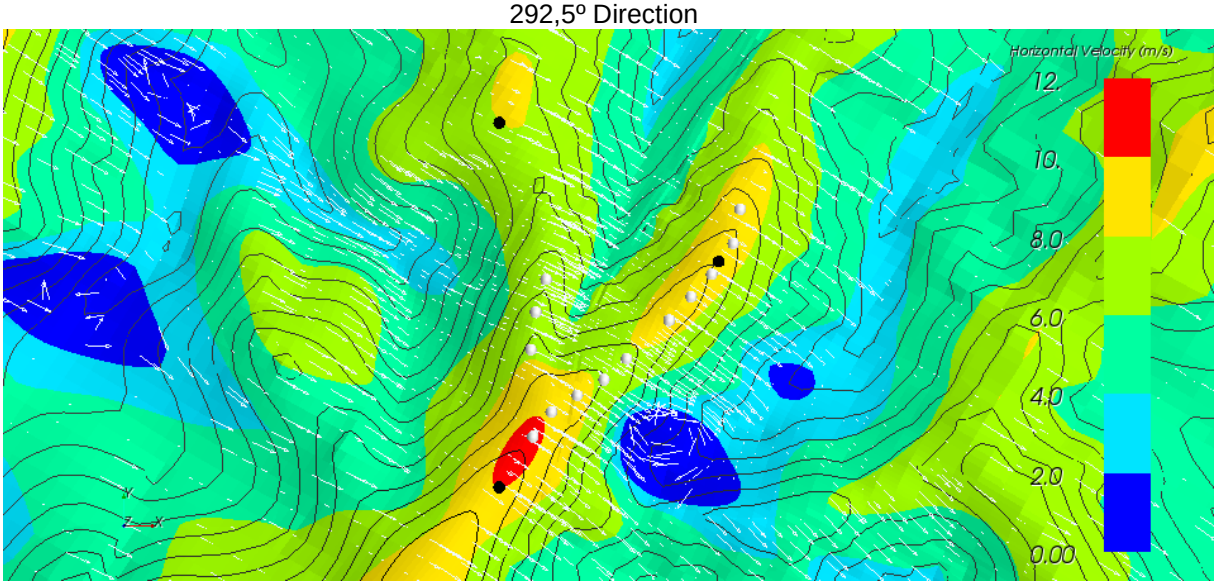

300º Direction

Figure 66 - Horizontal velocity contour maps at 126 m a.g.l., for directions 285º through 300º

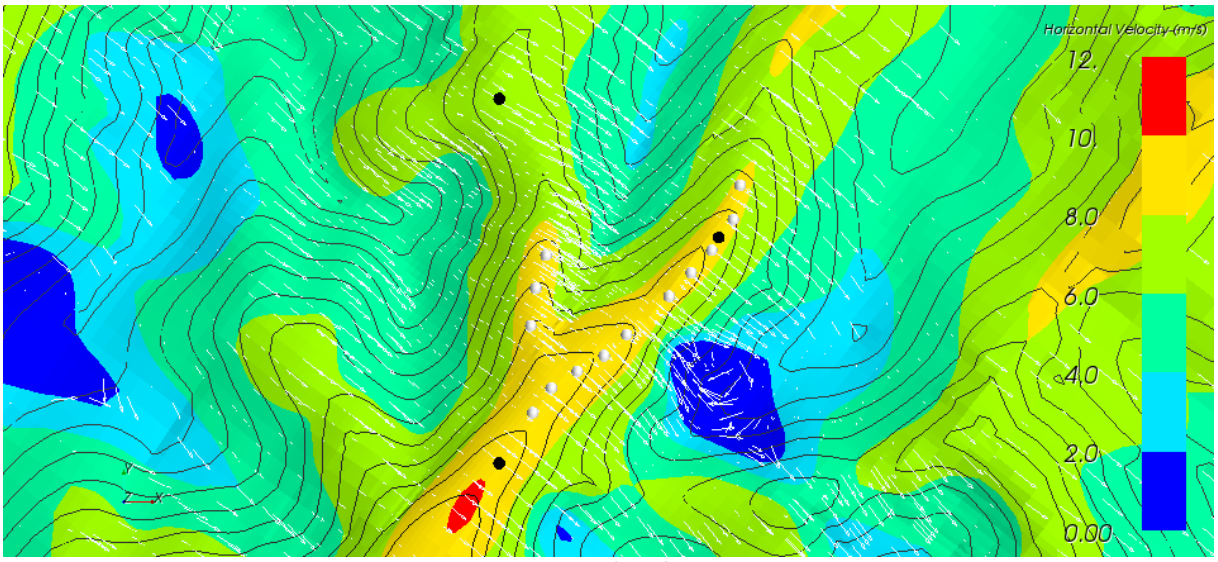

307,5º Direction

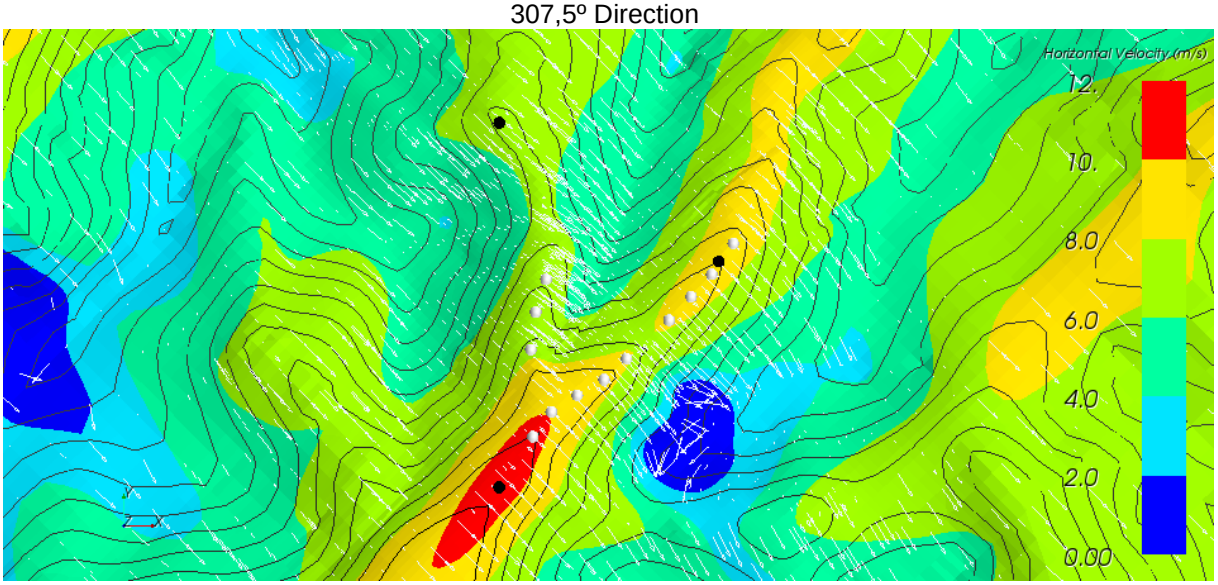

315º Direction

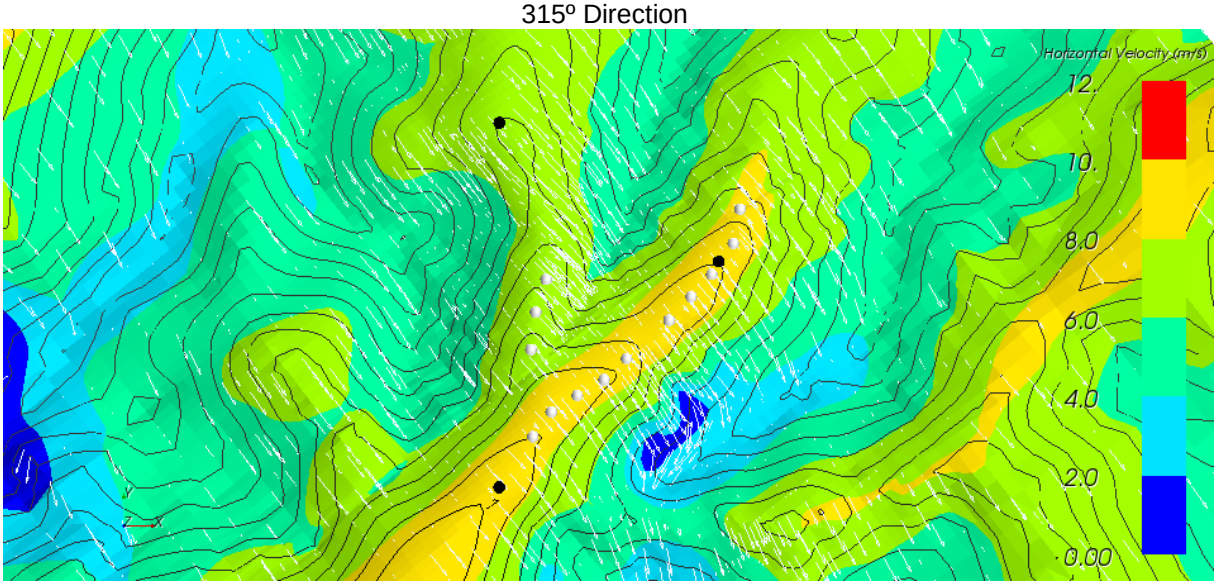

322,5º Direction

Figure 67 - Horizontal velocity contour maps at 126 m a.g.l., for directions 307.5º through 322.5º

Flow pitch 2D contours @ 44m a.g.l.

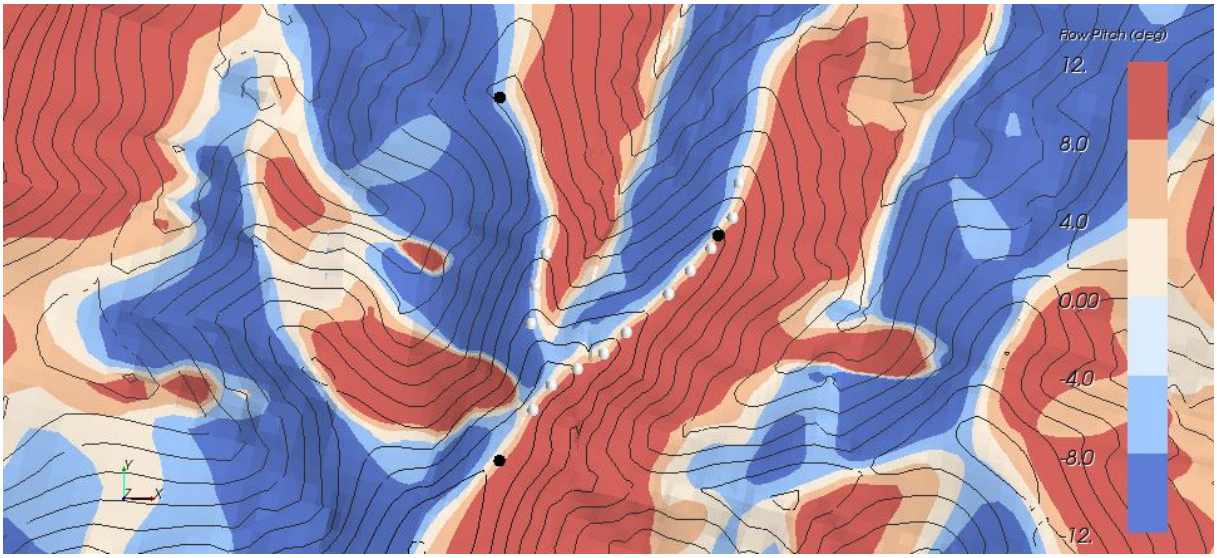

105º Direction

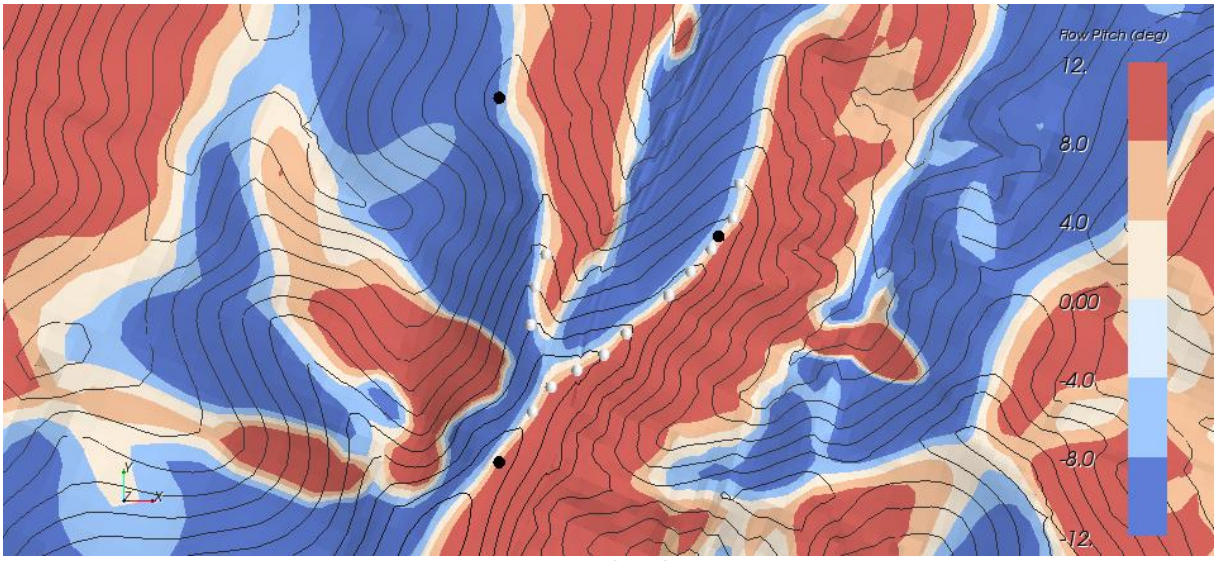

112,5º Direction

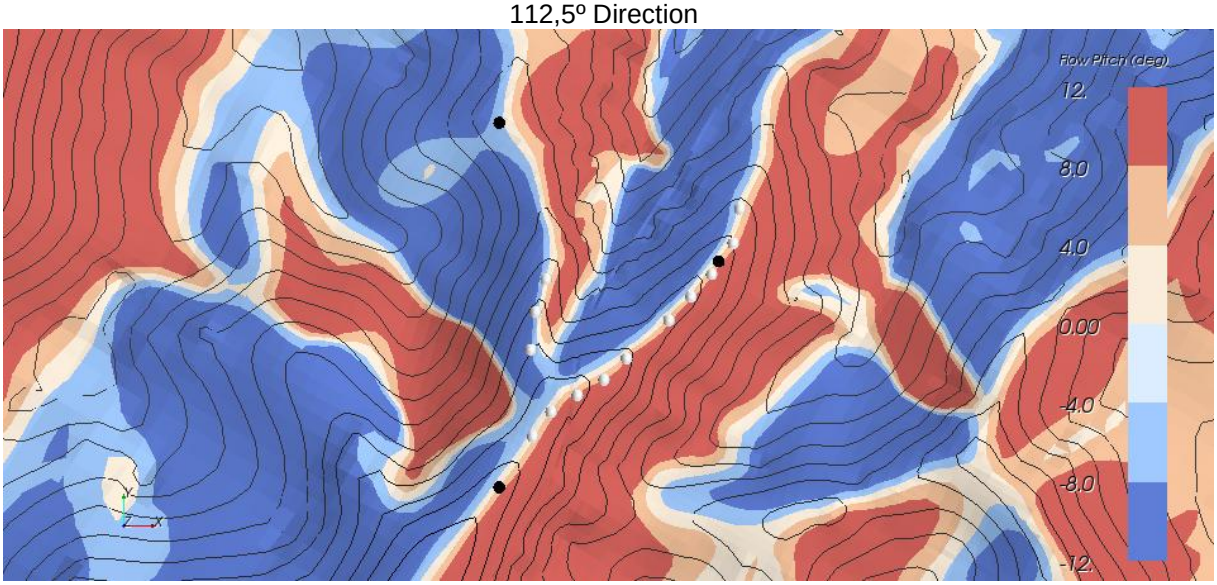

120º Direction

Figure 68 – Flow pitch contour maps at 44 m a.g.l., for directions 105º through 120º

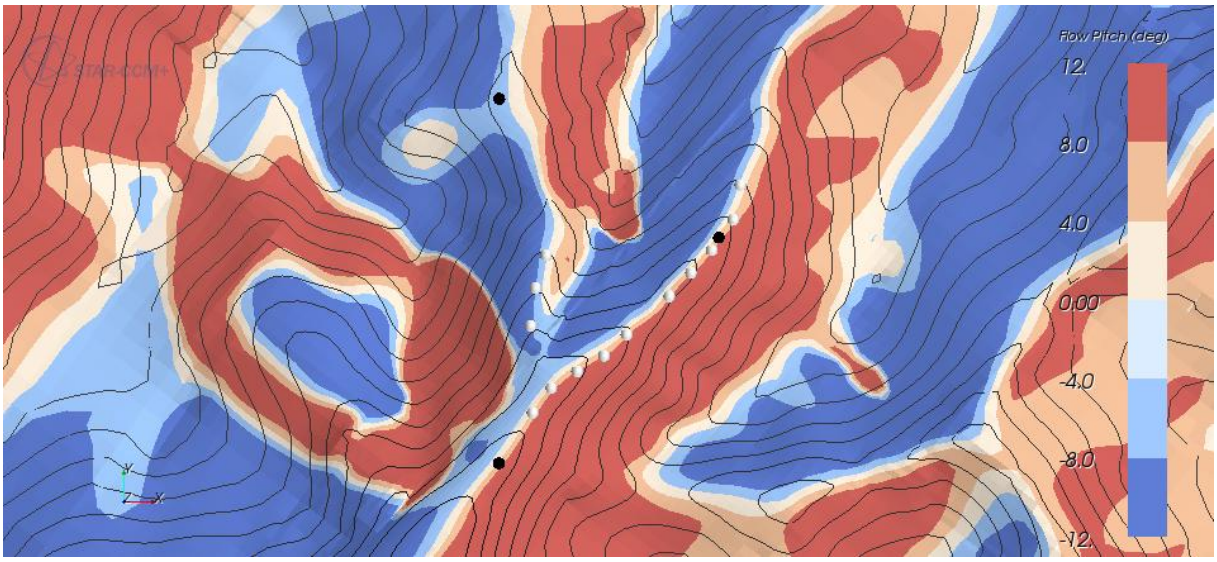

127,5º Direction

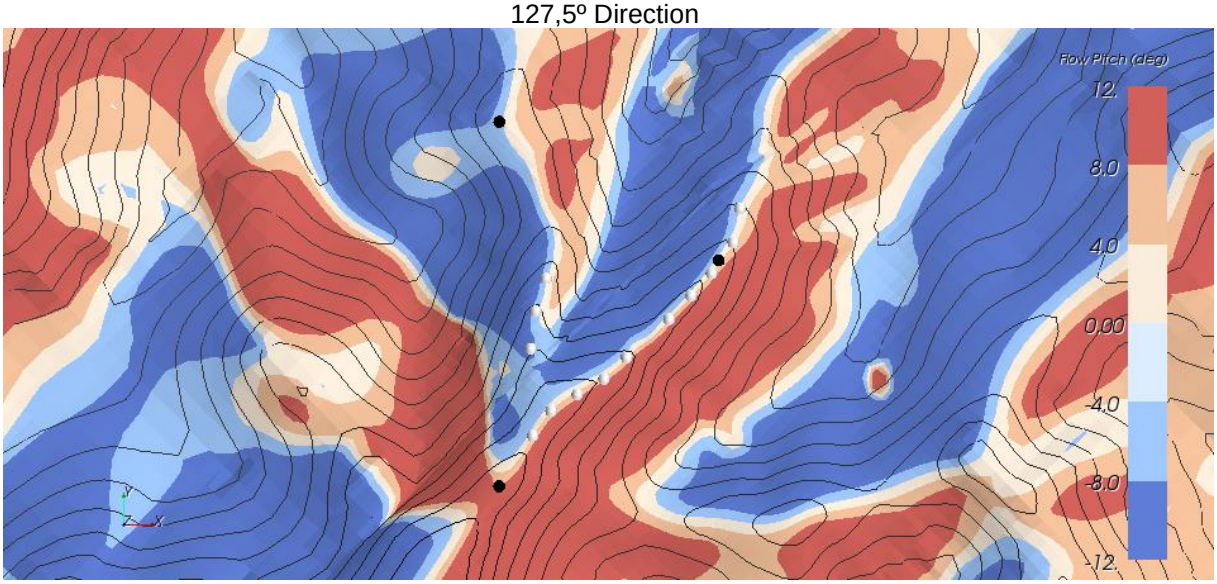

135º Direction

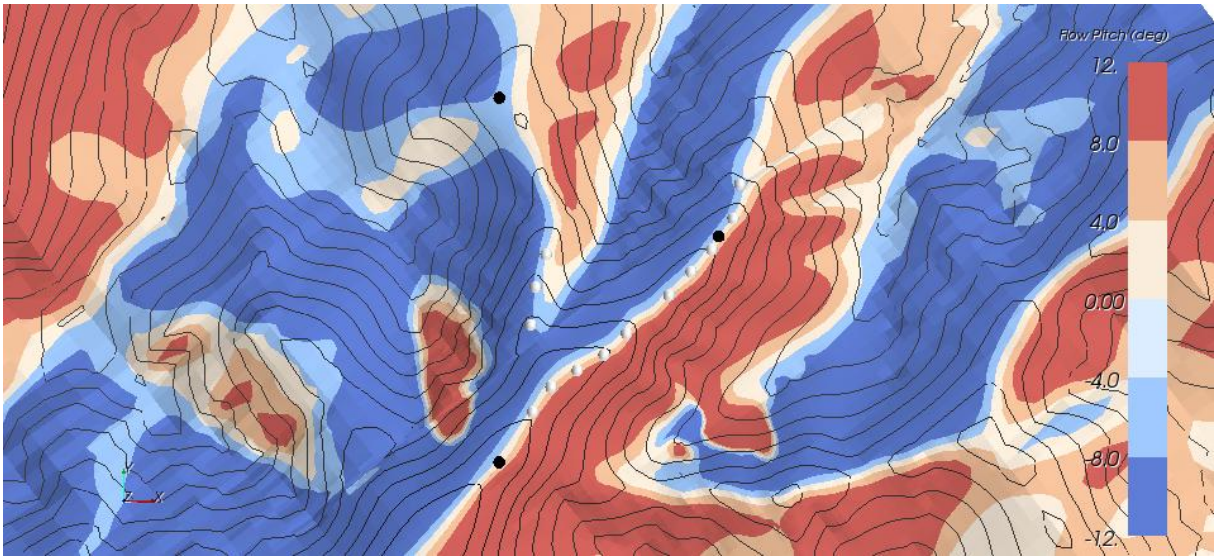

142,5º Direction

Figure 69 - Flow pitch contour maps at 44 m a.g.l., for directions 127.5º through 142.5º

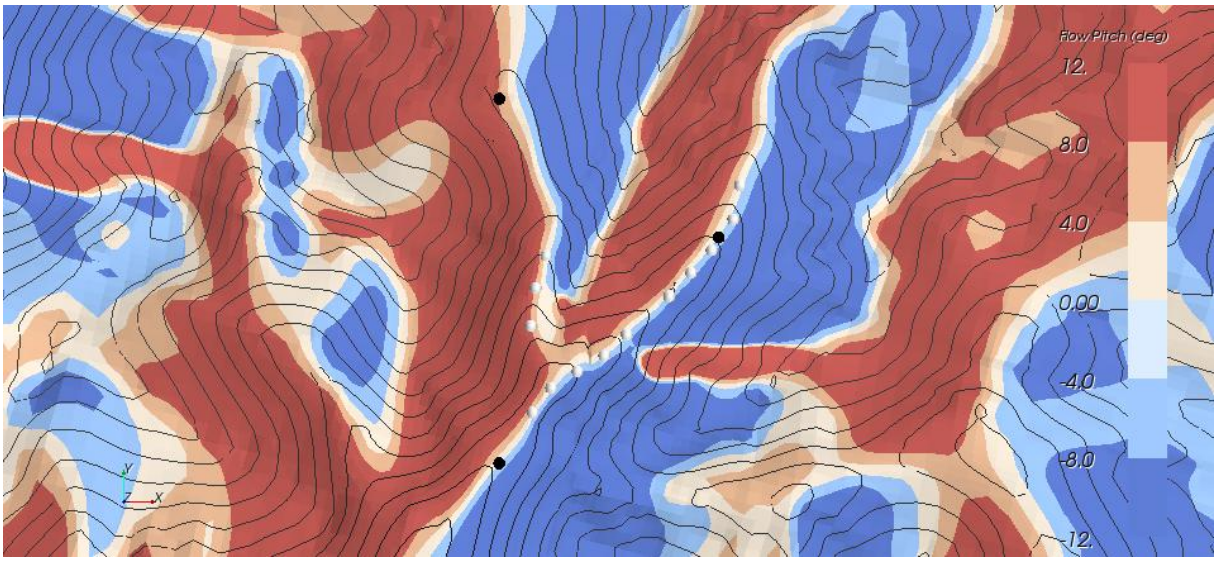

285º Direction

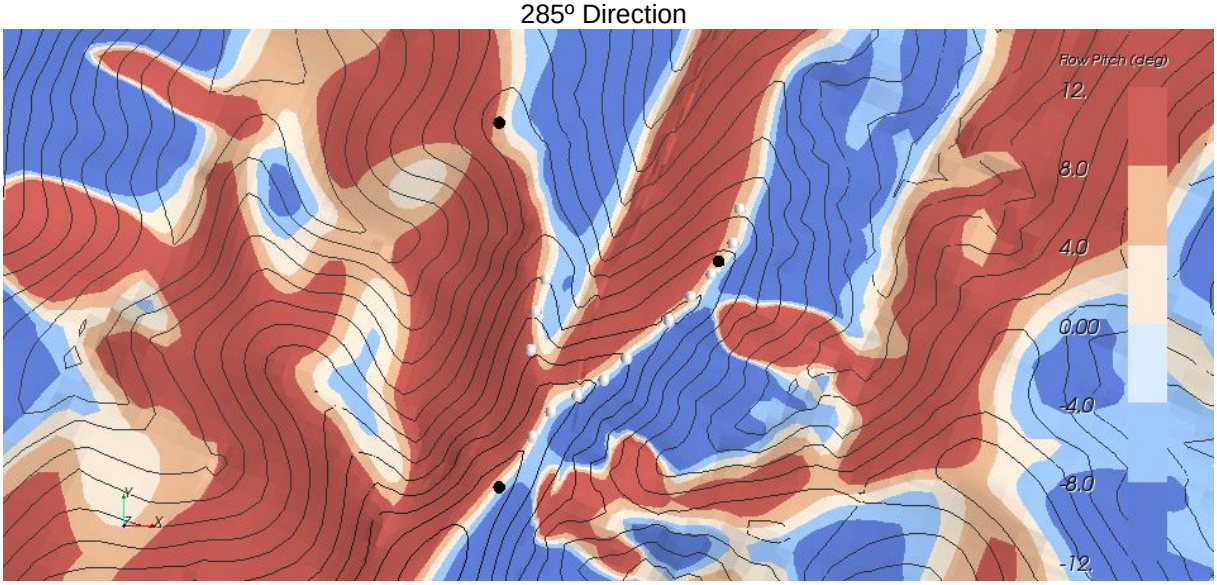

292,5º Direction

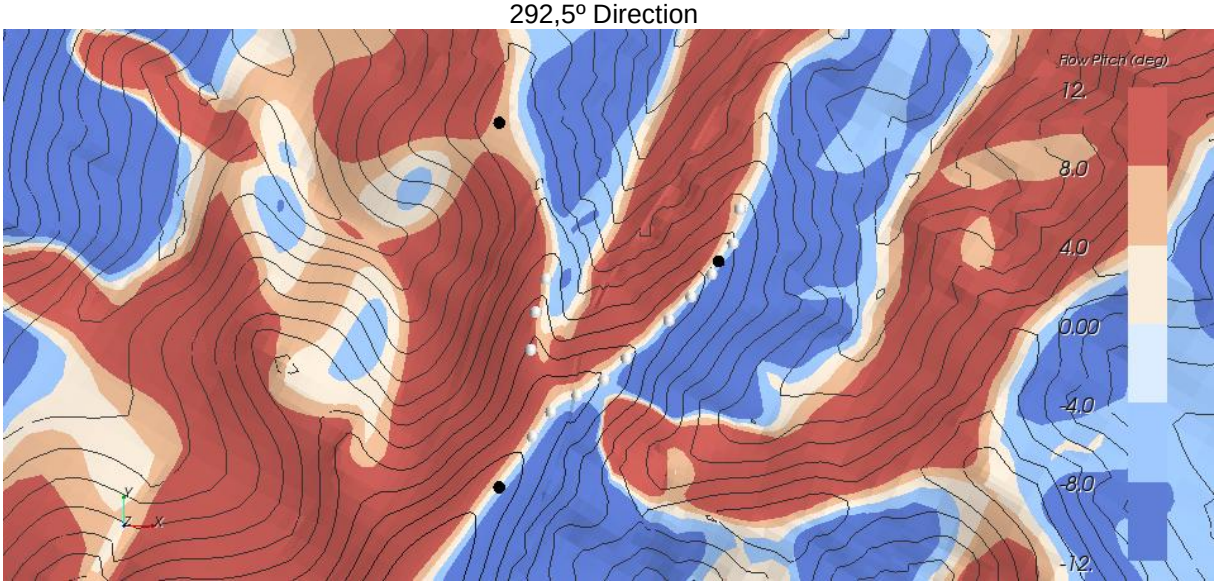

300º Direction

Figure 70 - Flow pitch contour maps at 44 m a.g.l., for directions 285º through 300º

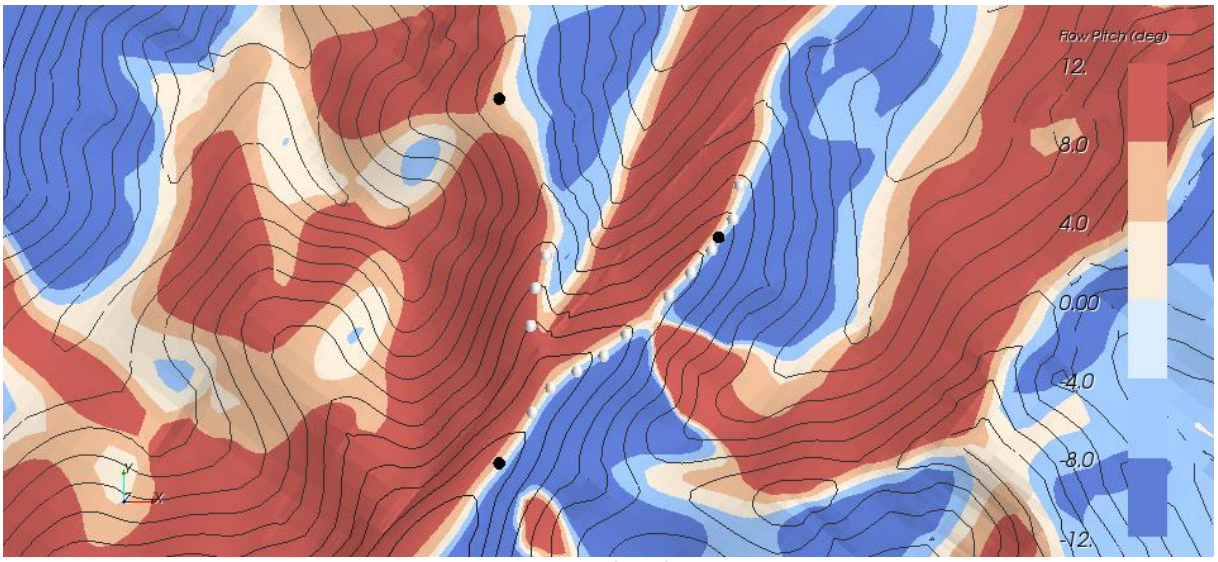

307,5º Direction

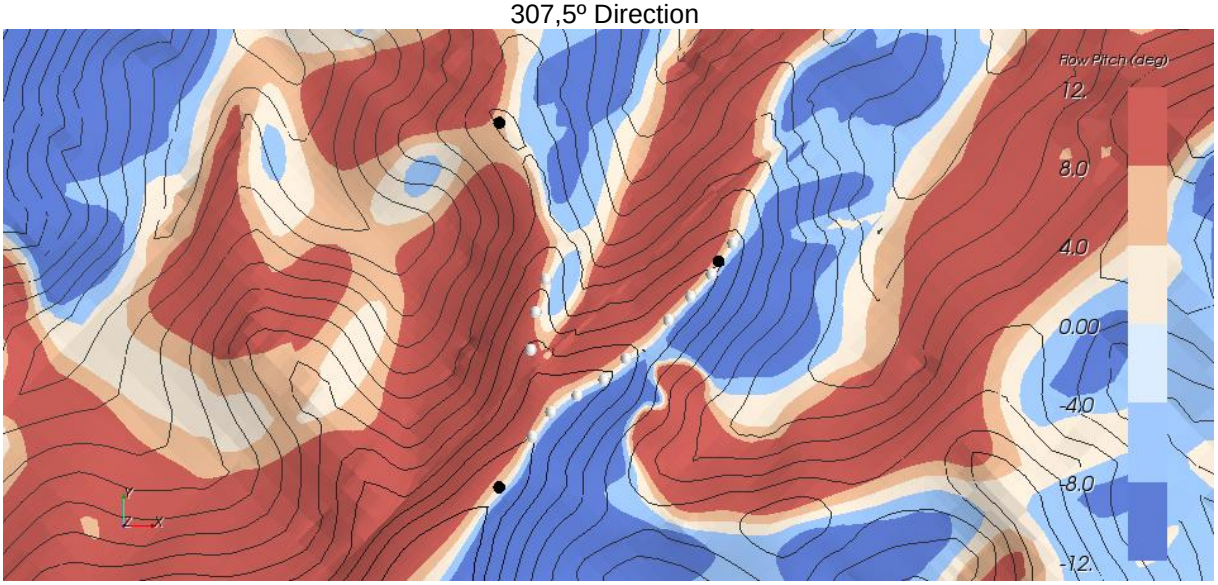

315º Direction

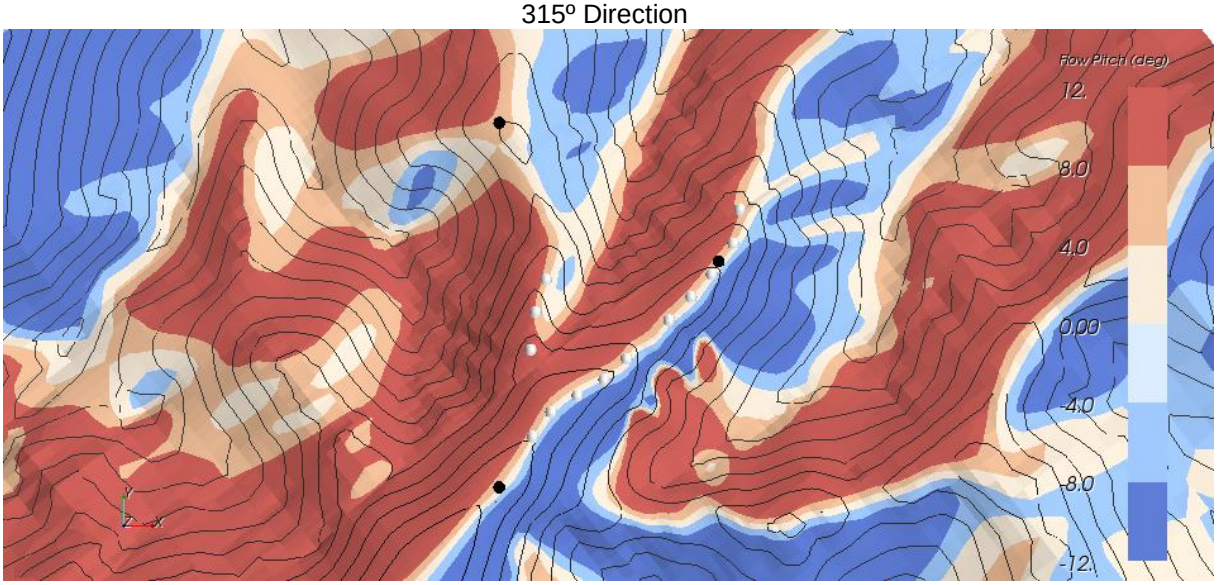

322,5º Direction

Figure 71 - Flow pitch contour maps at 44 m a.g.l., for directions 307.5º through 322.5º

Flow pitch 2D contours @ 85m a.g.l.

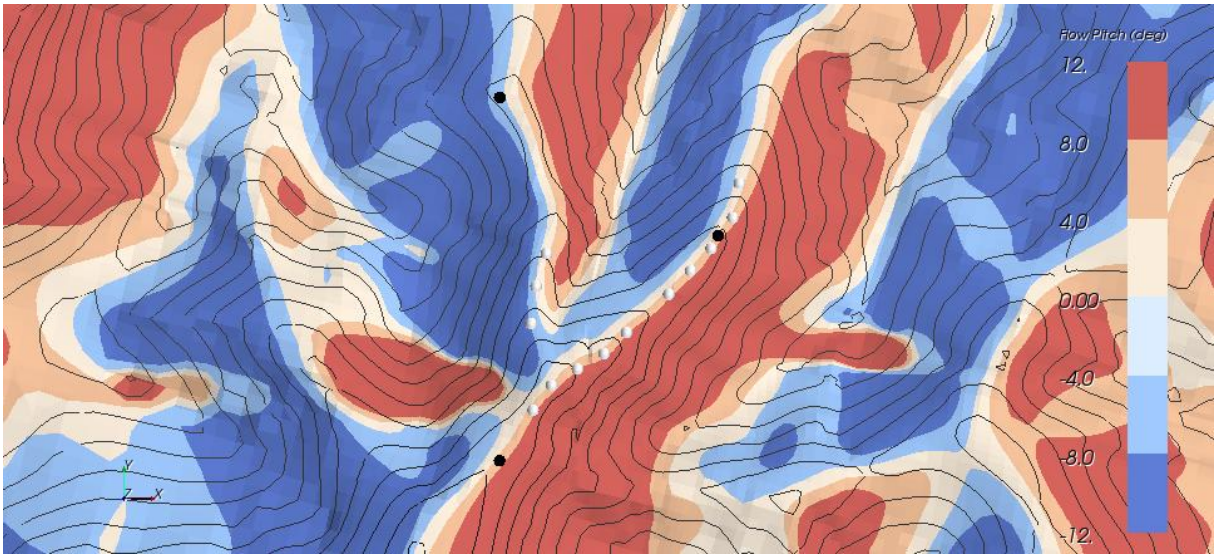

105º Direction

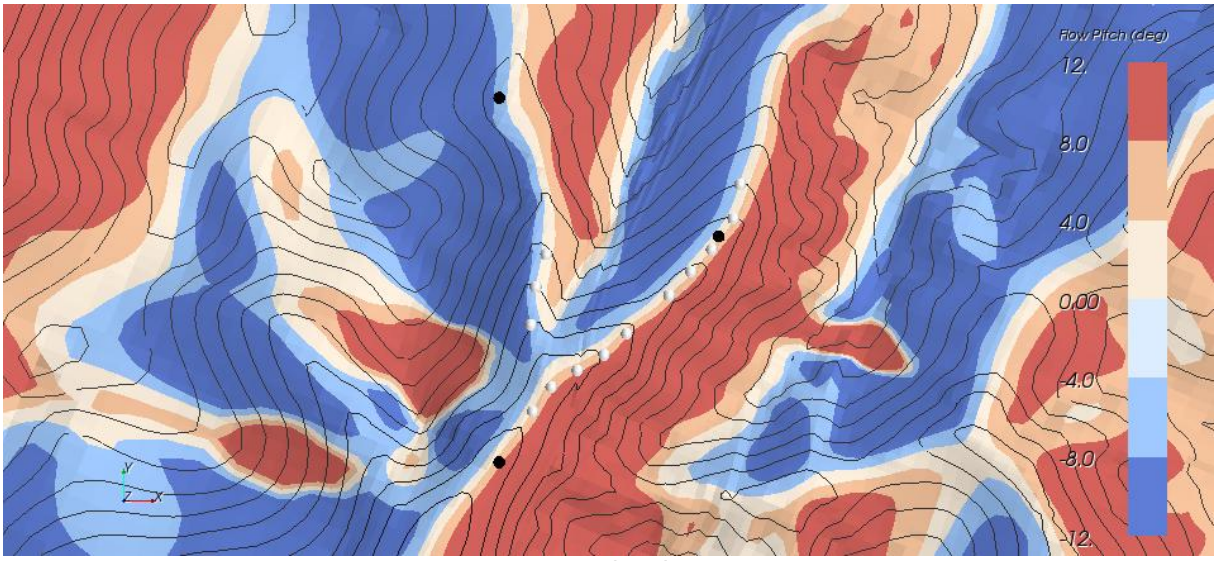

112,5º Direction

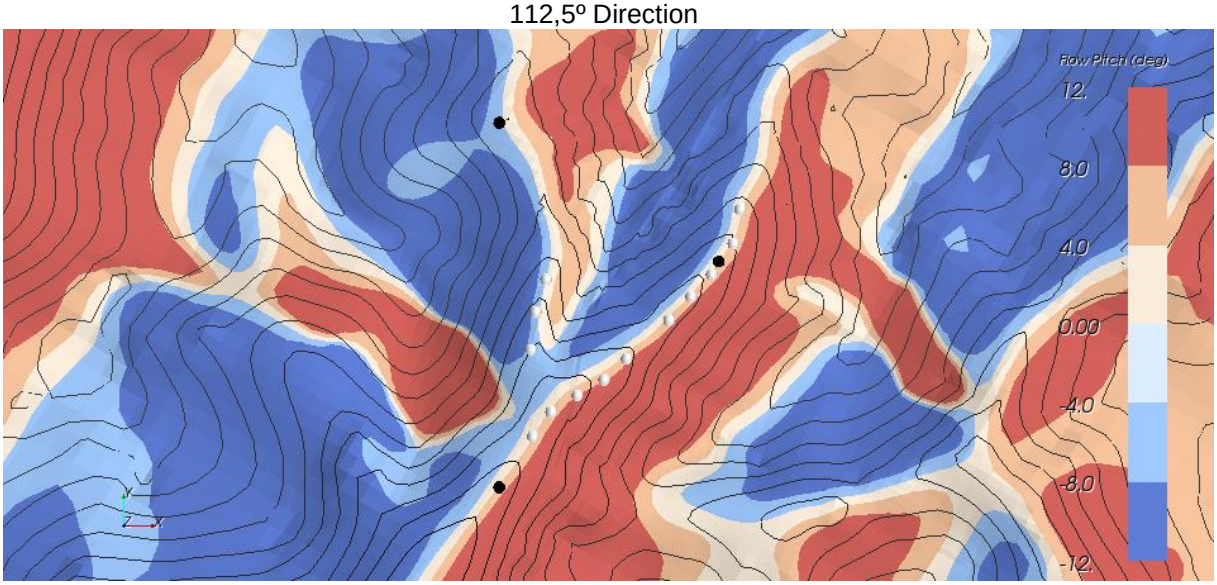

120º Direction

Figure 72 - Flow pitch contour maps at 85 m a.g.l., for directions 105º through 120º

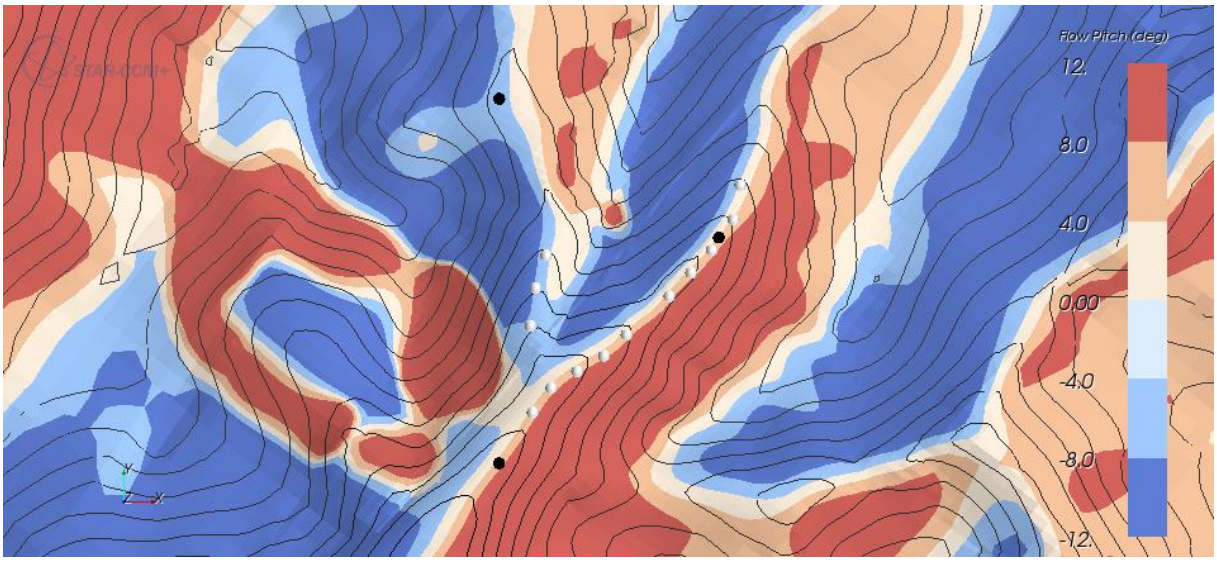

127,5º Direction

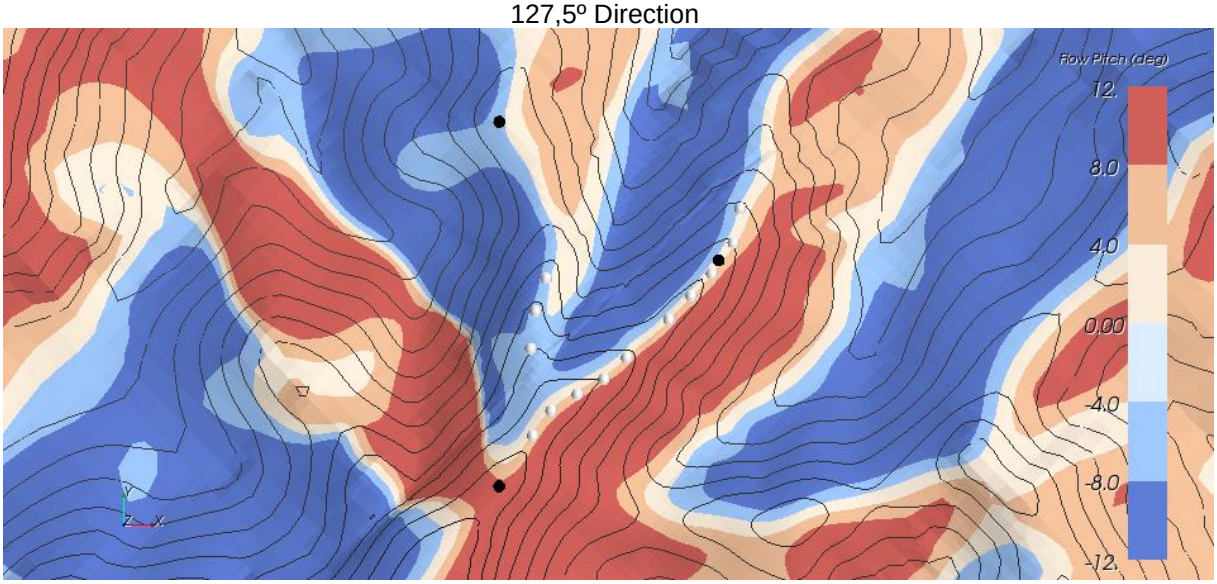

135º Direction

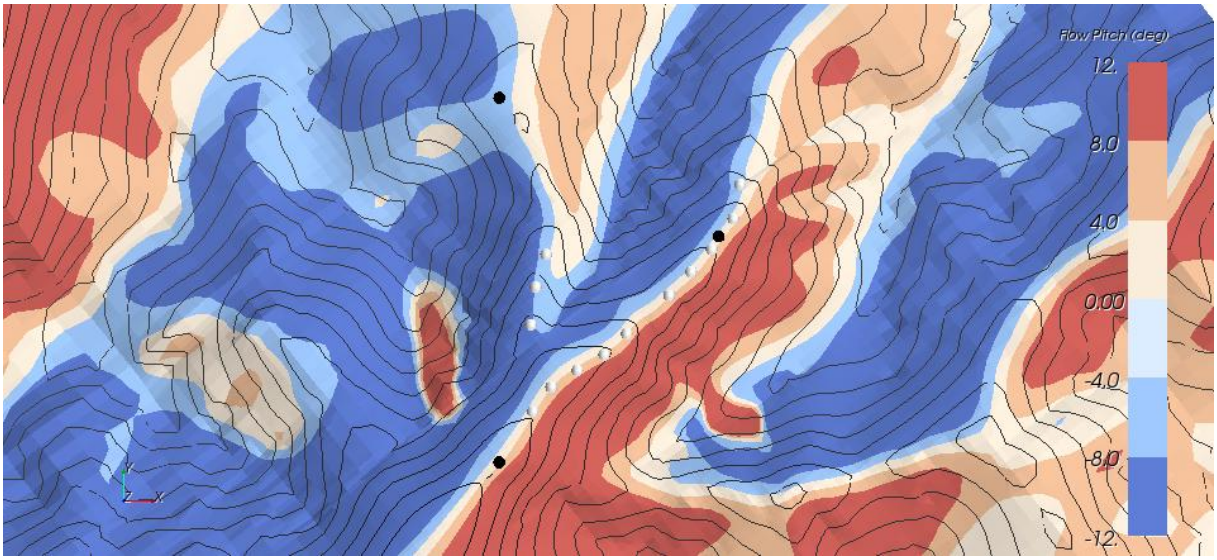

142,5º Direction

Figure 73 - Flow pitch contour maps at 85 m a.g.l., for directions 127.5º through 142.5º

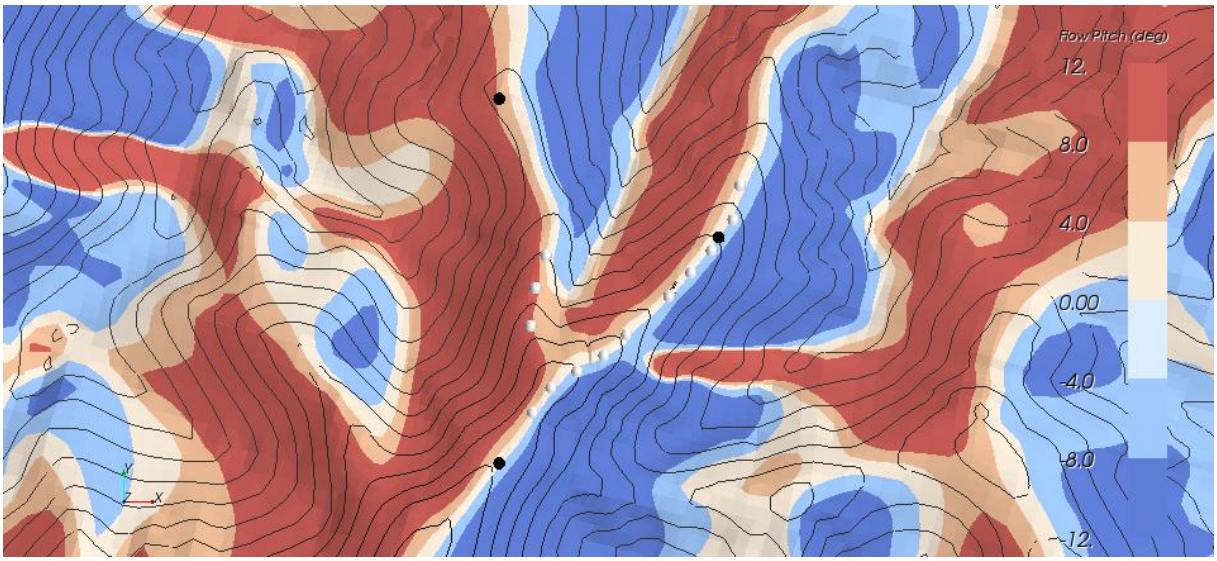

285º Direction

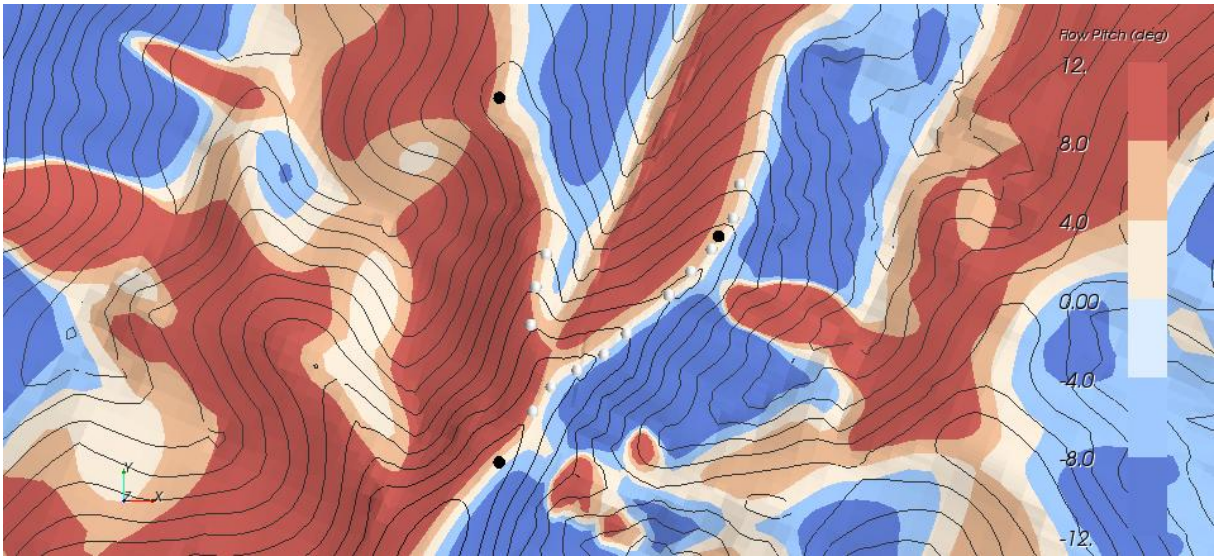

292,5º Direction

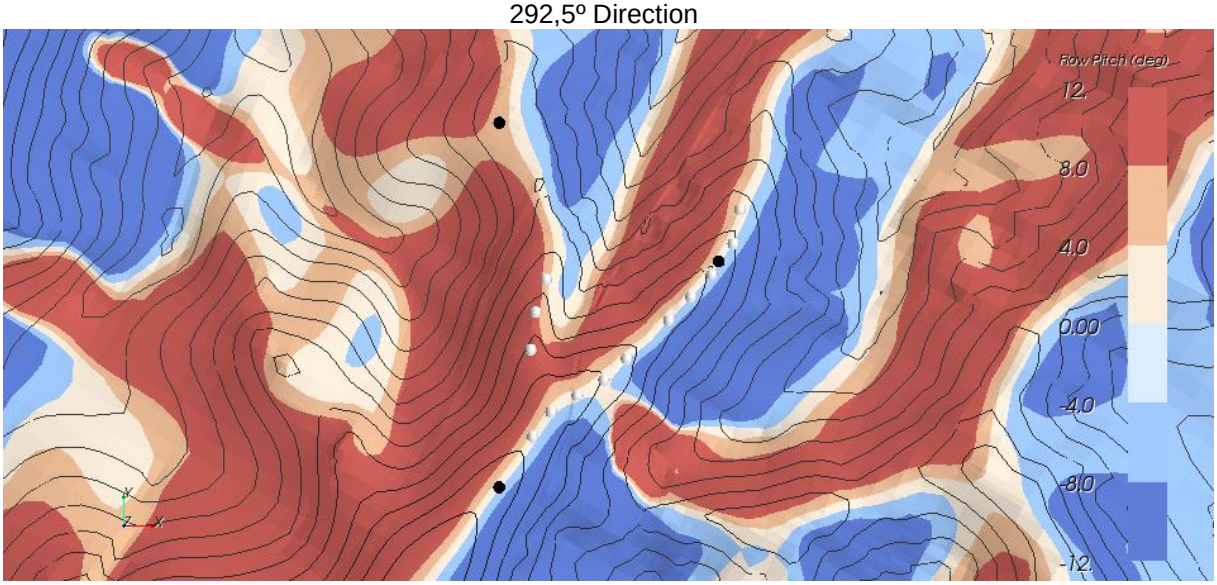

300º Direction

Figure 74 - Flow pitch contour maps at 85 m a.g.l., for directions 285º through 300º

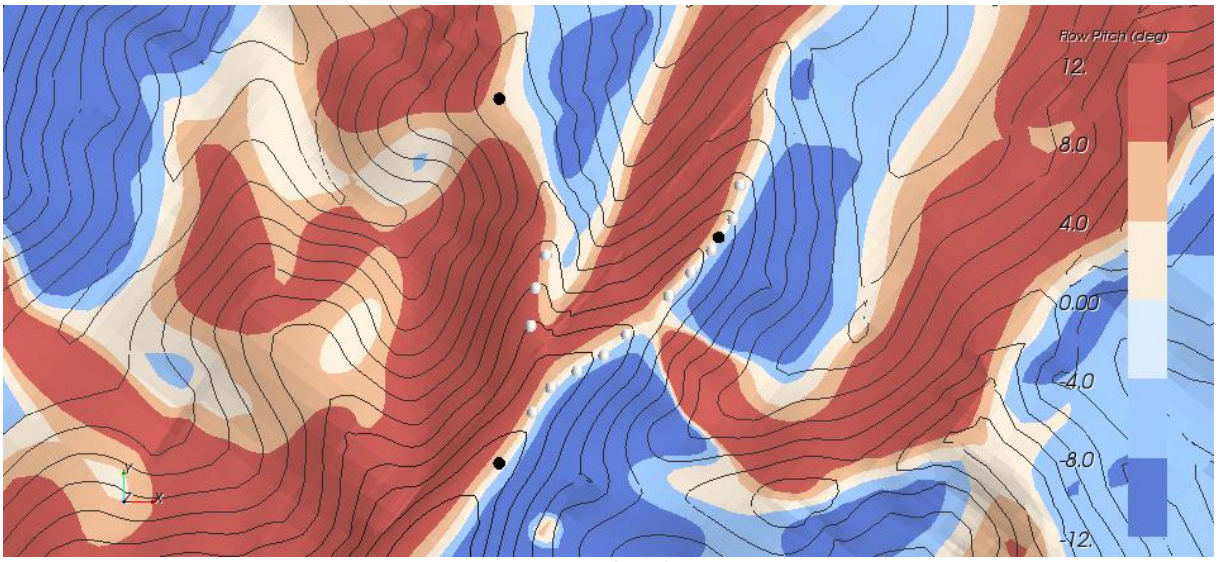

307,5º Direction

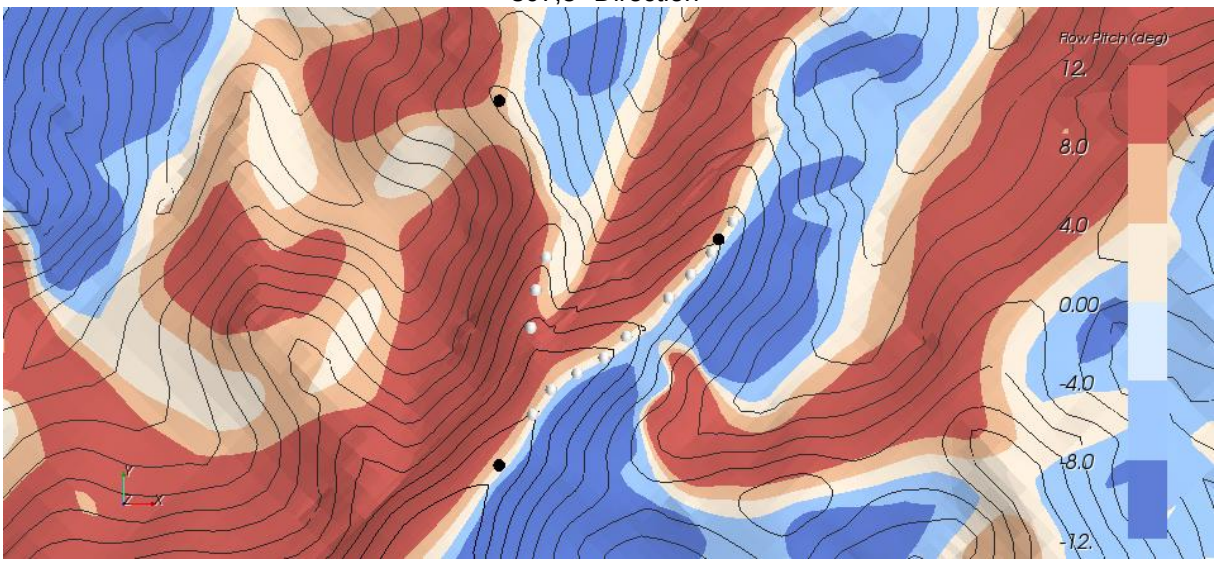

315º Direction

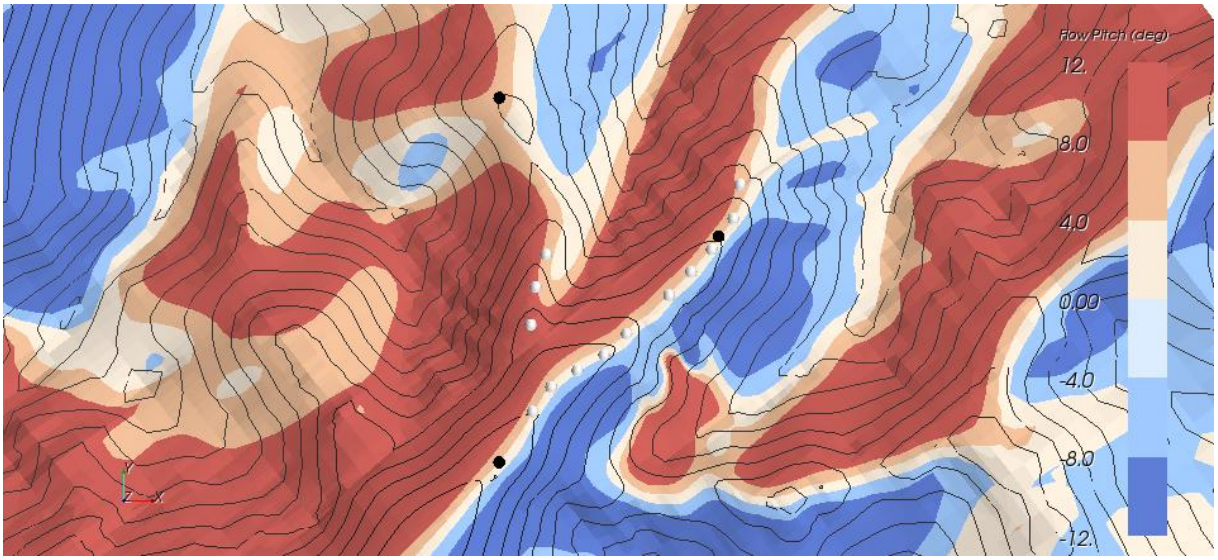

322,5º Direction

Figure 75 - Flow pitch contour maps at 85 m a.g.l., for directions 307.5º through 322.5º

Flow pitch 2D contours @ 126m a.g.l.

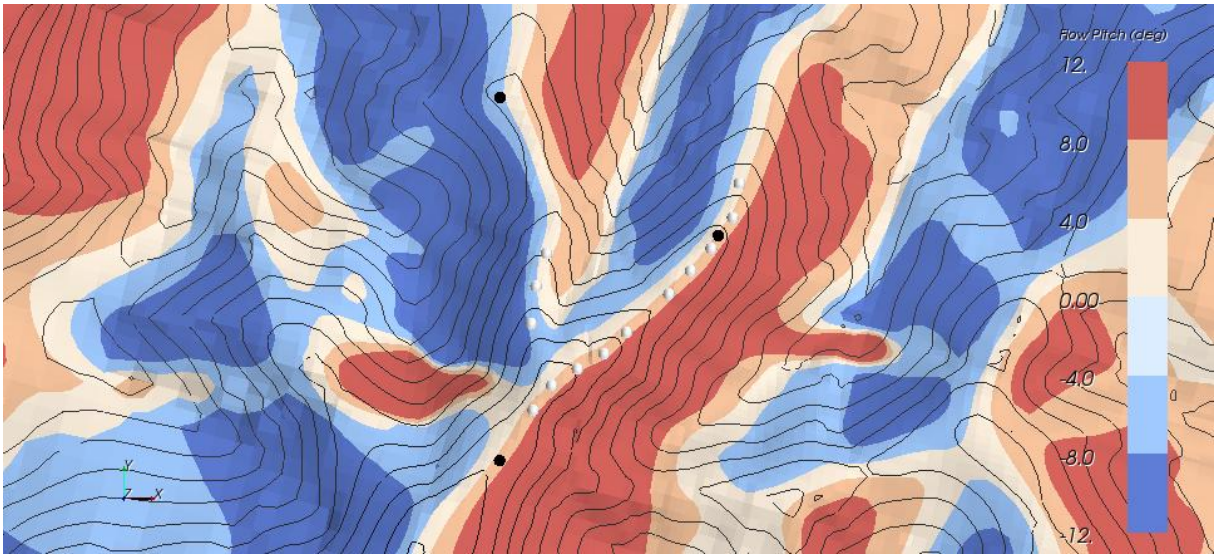

105º Direction

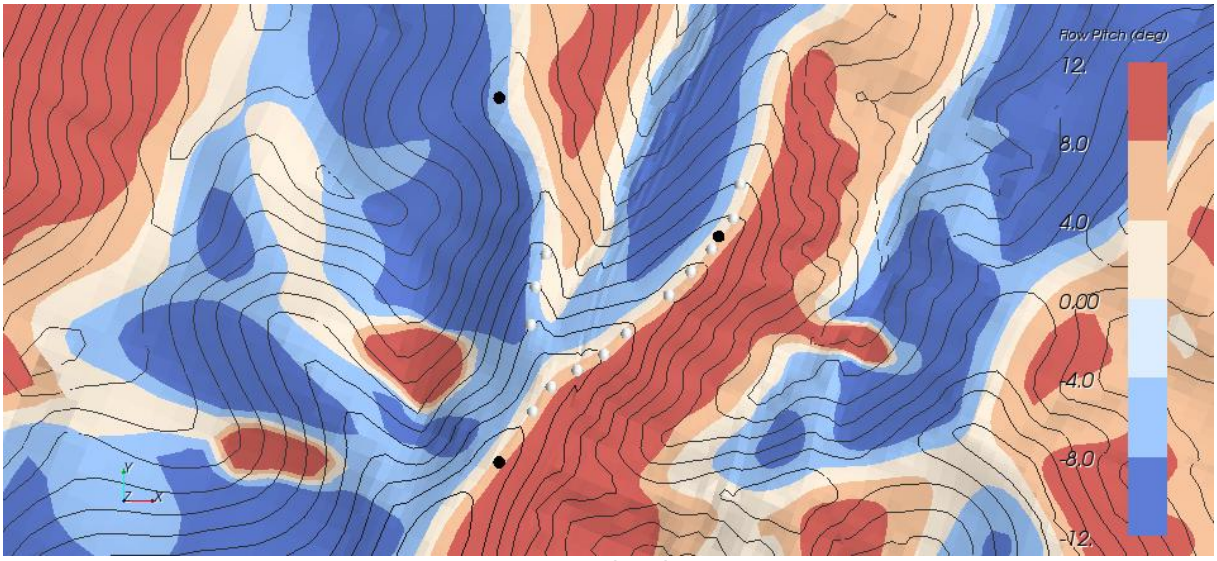

112,5º Direction

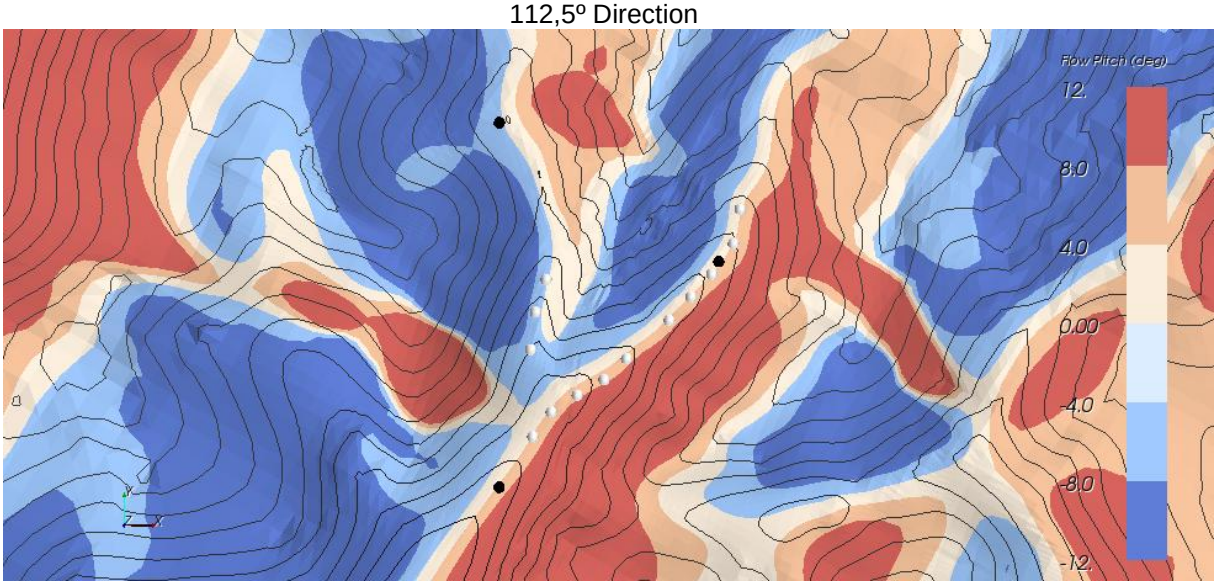

120º Direction

Figure 76 - Flow pitch contour maps at 126 m a.g.l., for directions 105º through 120º

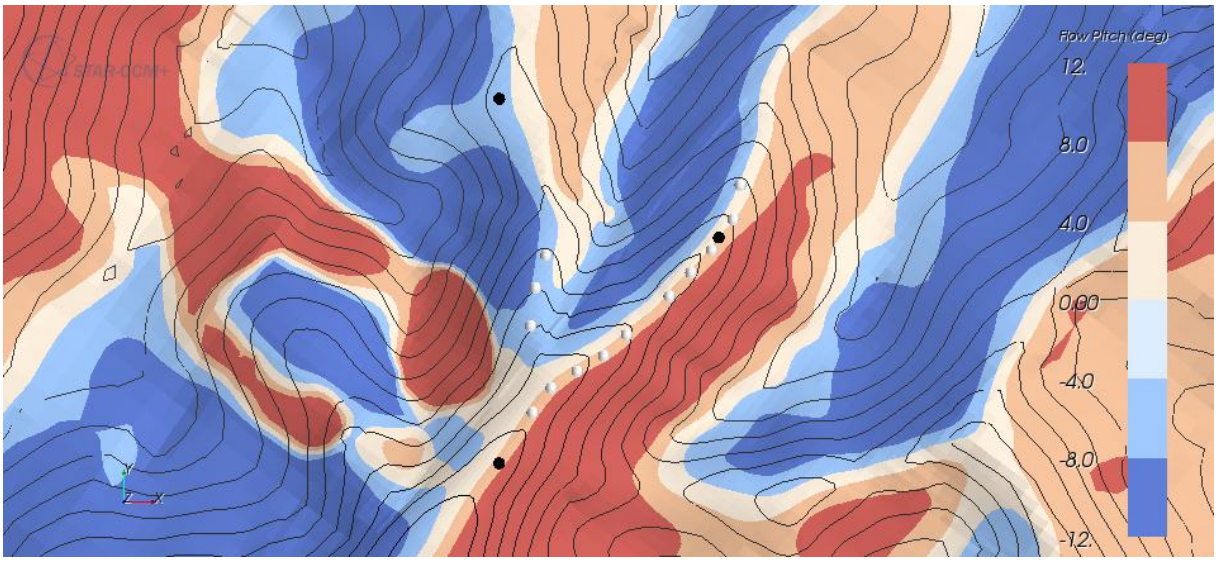

127,5º Direction

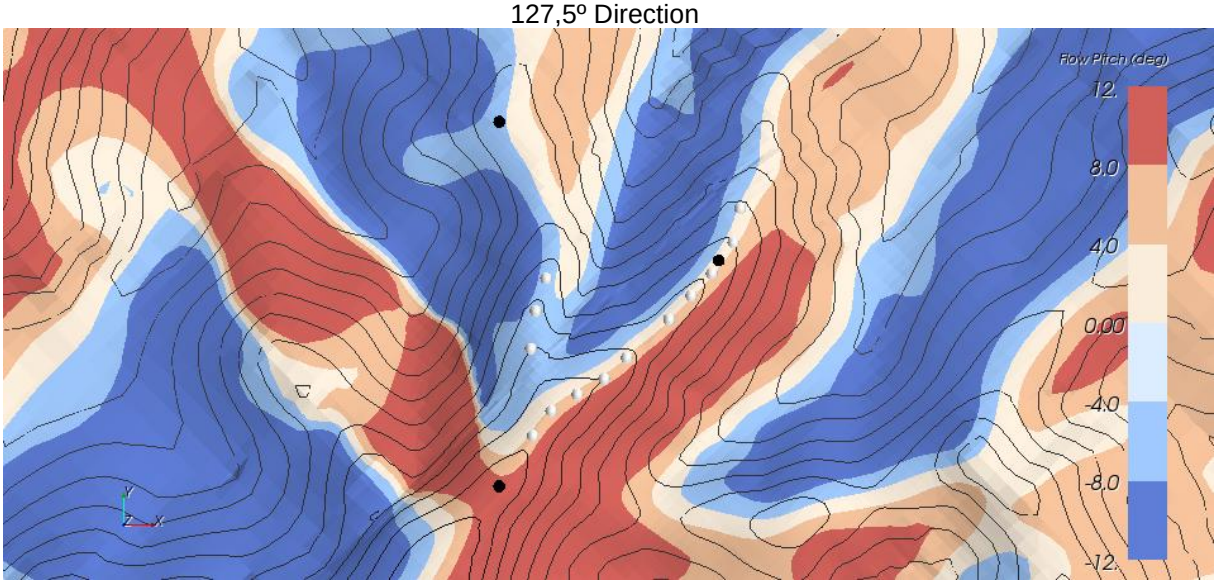

135º Direction

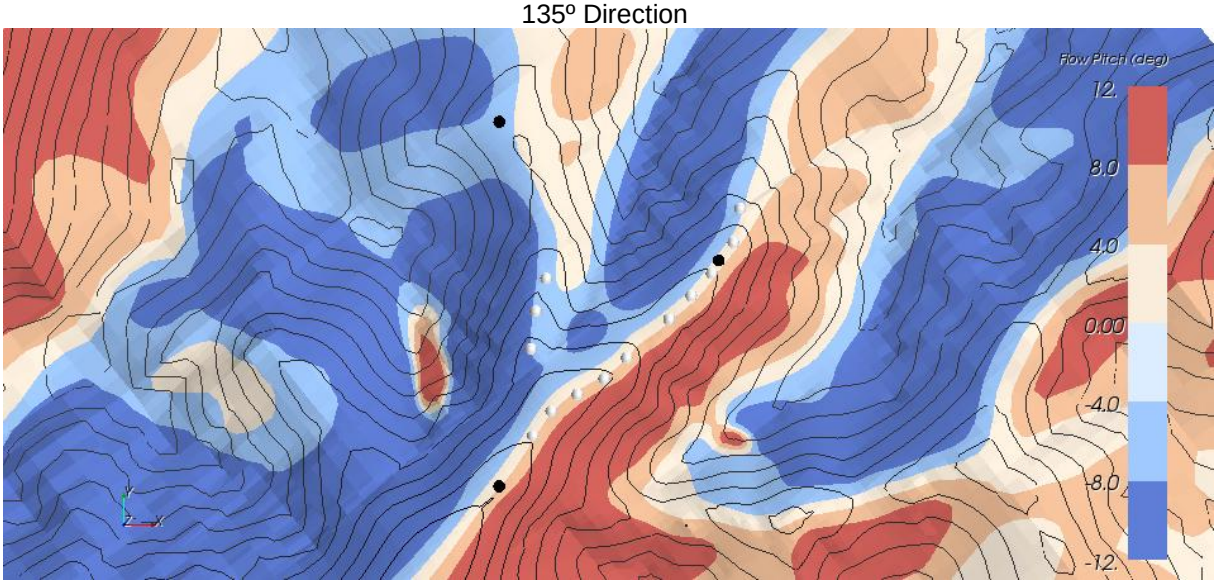

142,5º Direction

Figure 77 - Flow pitch contour maps at 126 m a.g.l., for directions 127.5º through 142.5º

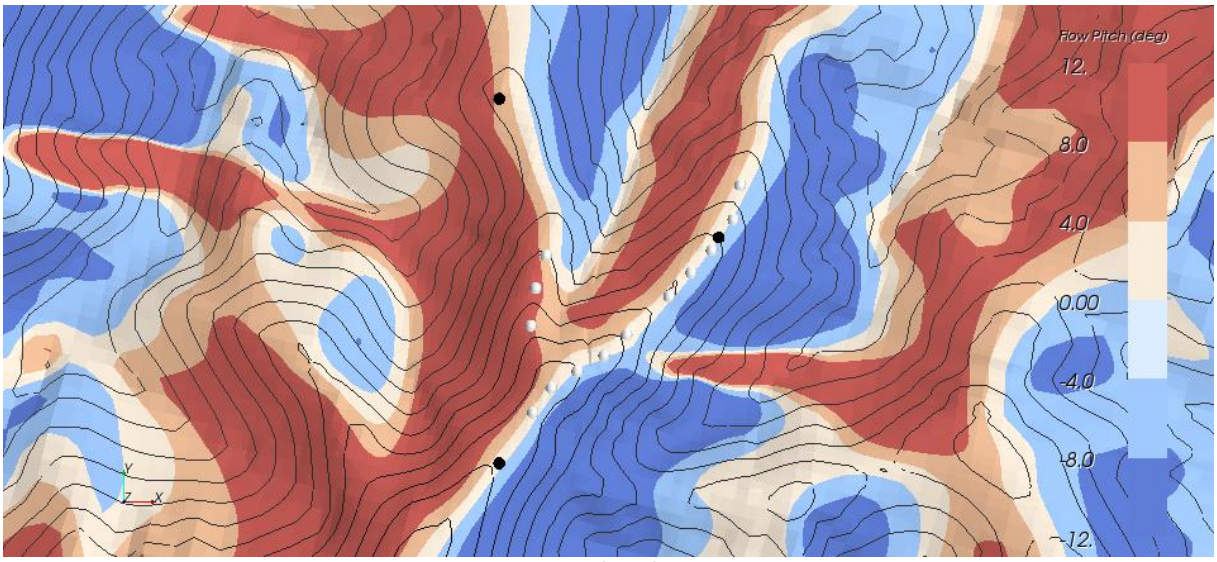

285º Direction

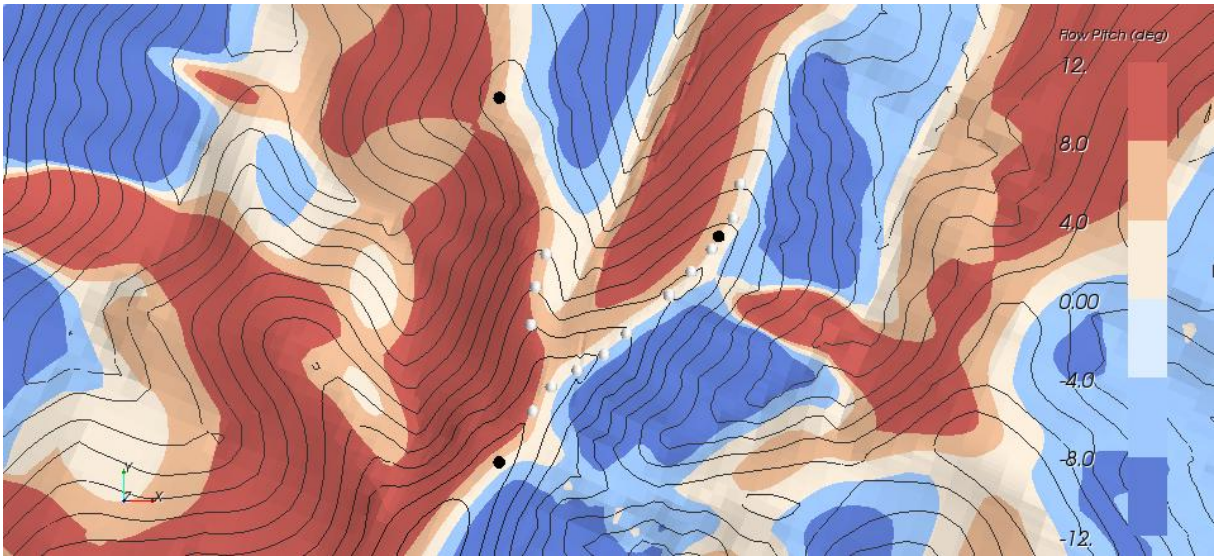

292,5º Direction

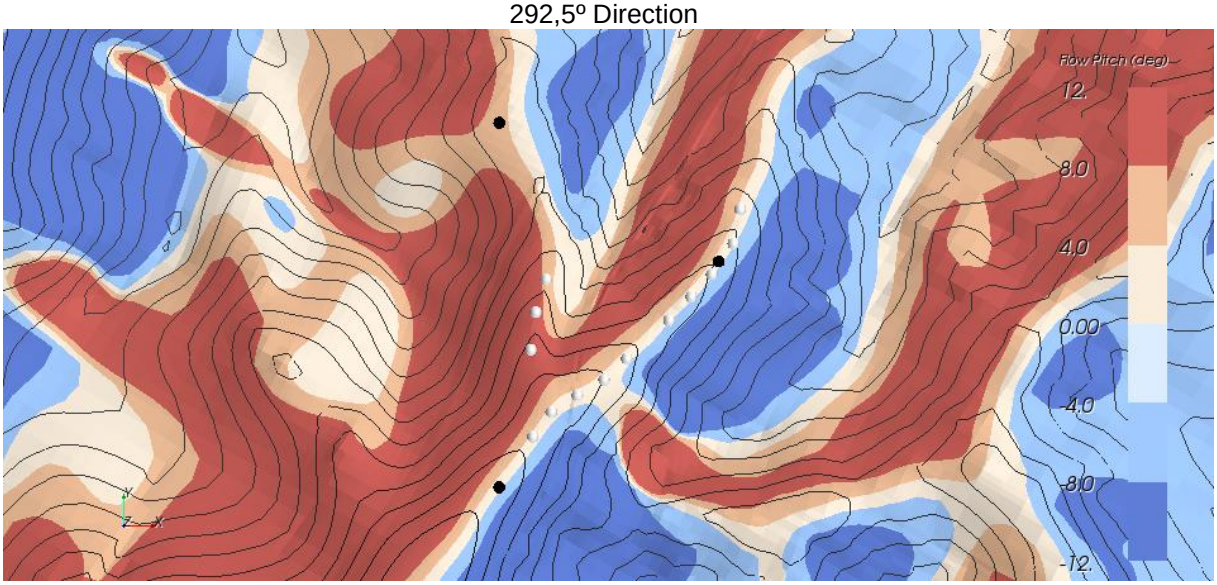

300º Direction

Figure 78 - Flow pitch contour maps at 126 m a.g.l., for directions 285º through 300º

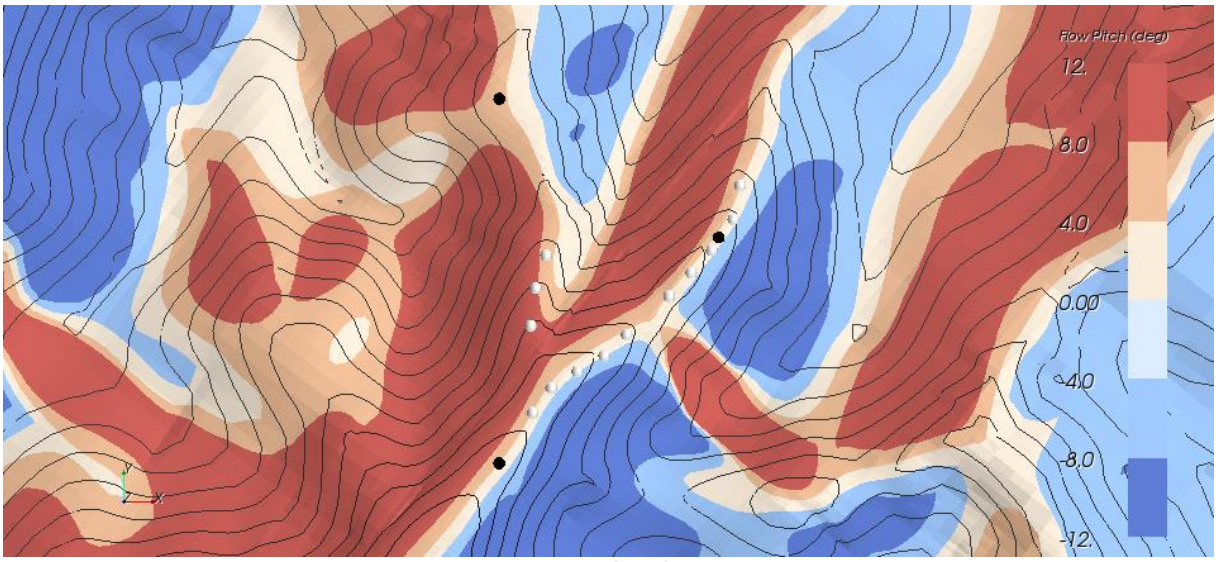

307,5º Direction

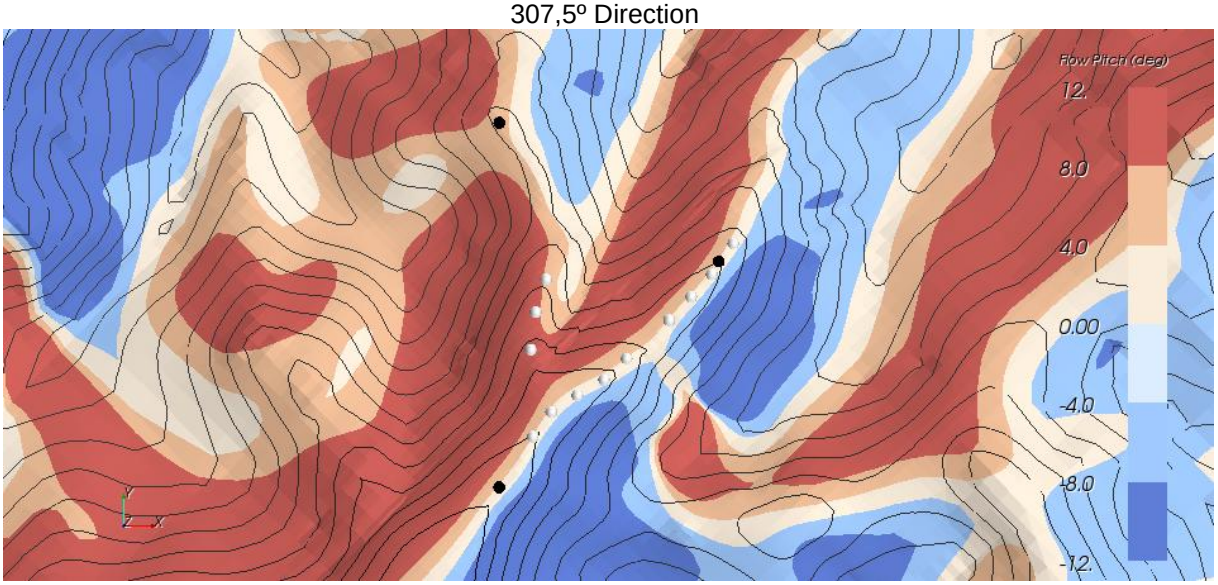

315º Direction

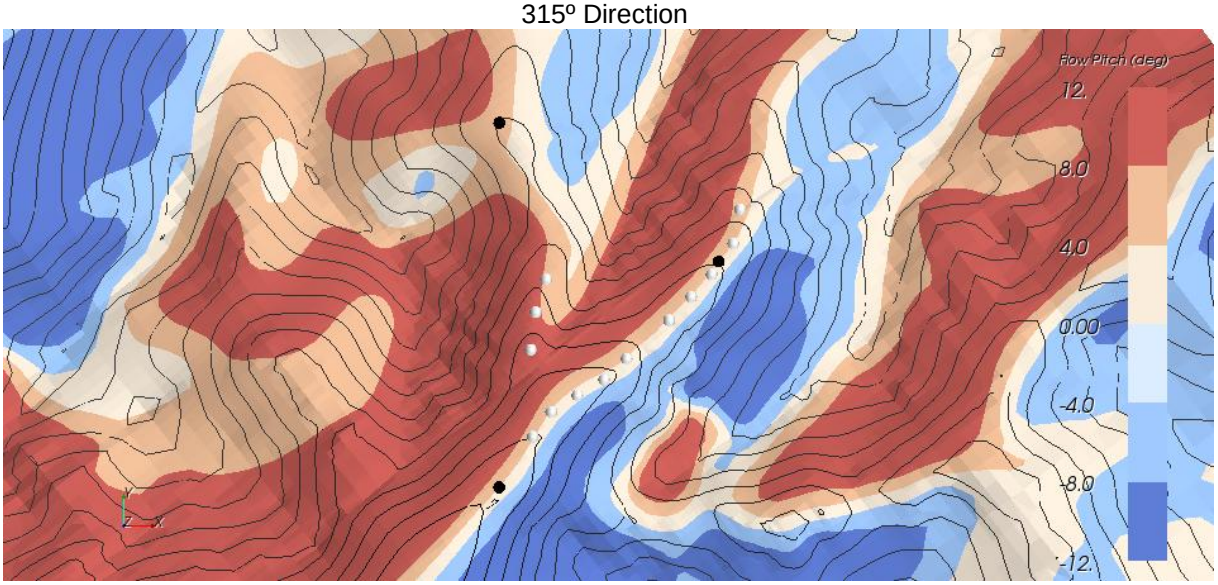

322,5º Direction

Figure 79 - Flow pitch contour maps at 126 m a.g.l., for directions 307.5º through 322.5º

Turbulence Intensity 2D contours @ 44m a.g.l.

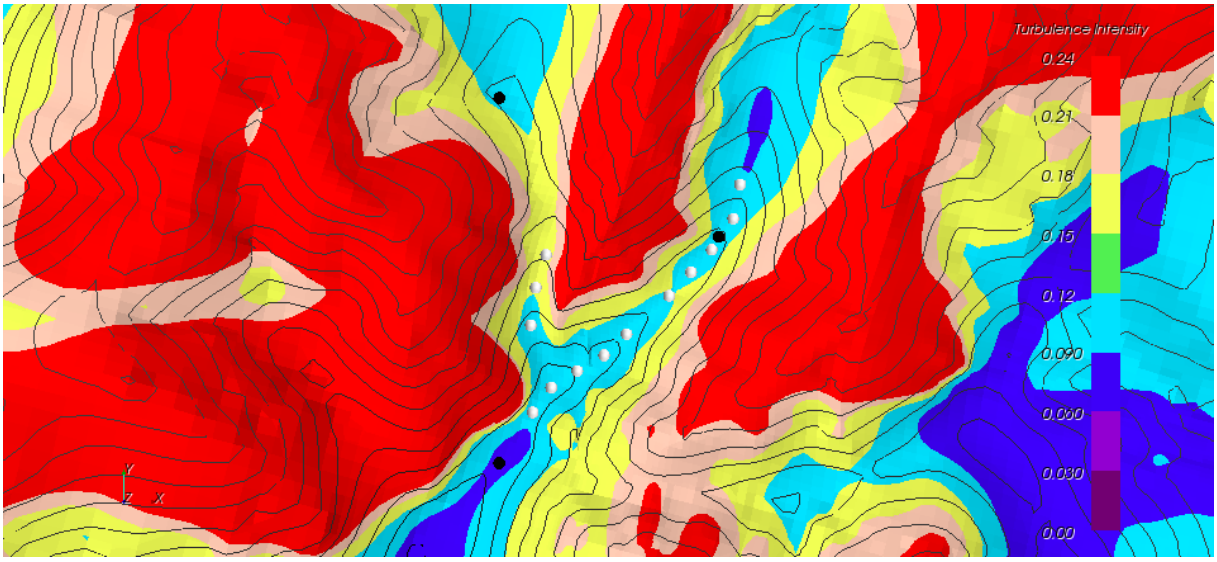

105º Direction

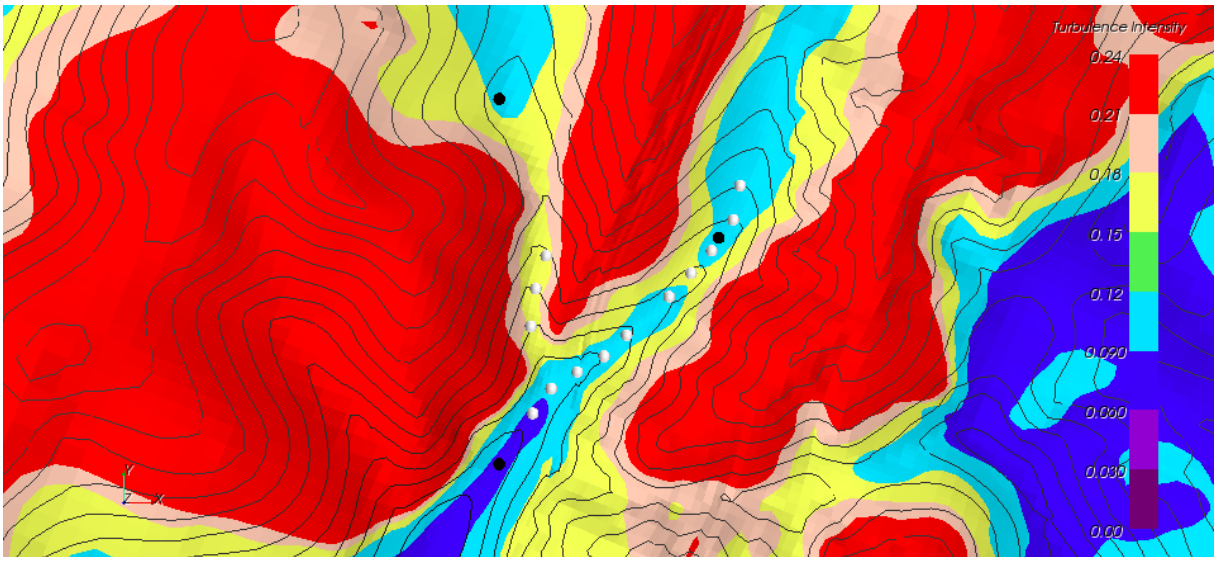

112,5º Direction

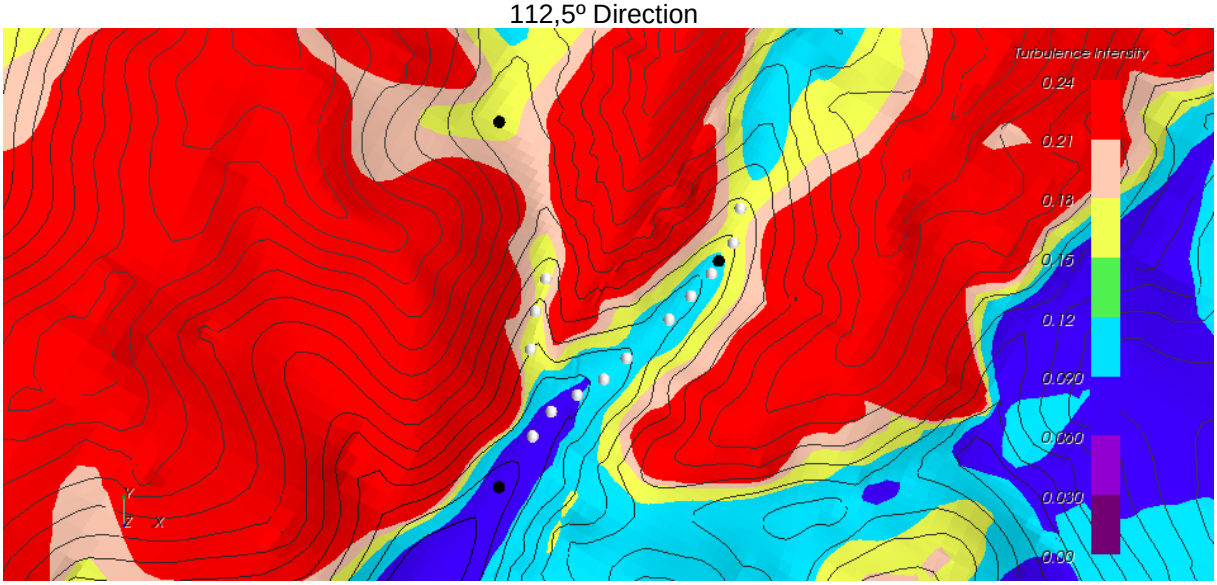

120º Direction

Figure 80 – Turbulent Intensity contour maps at 44 m a.g.l., for directions 105º through 120º

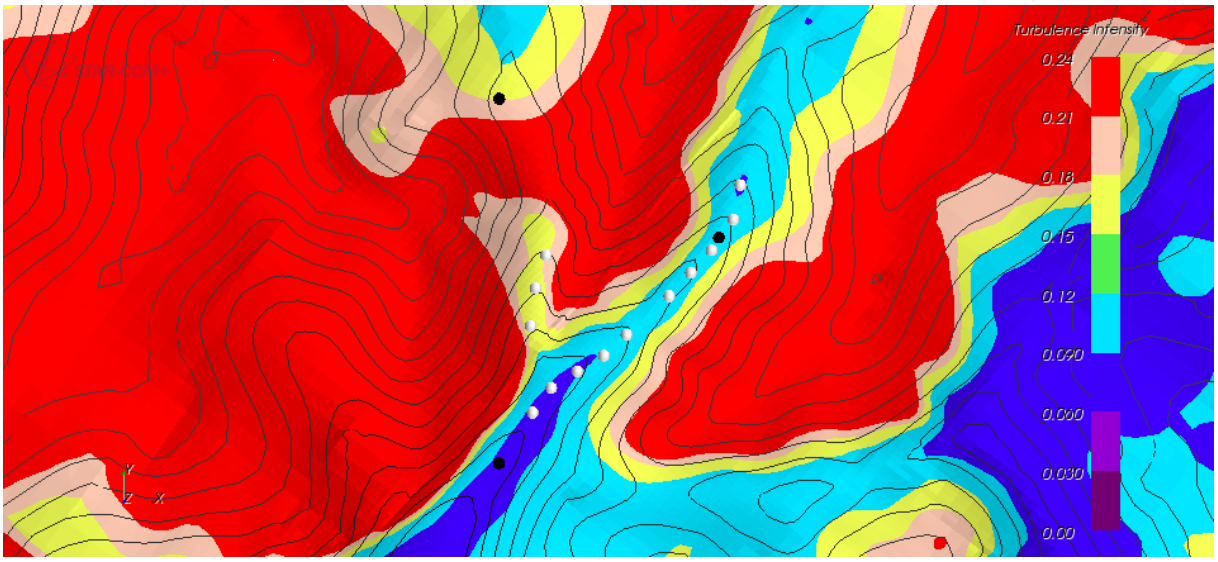

127,5º Direction

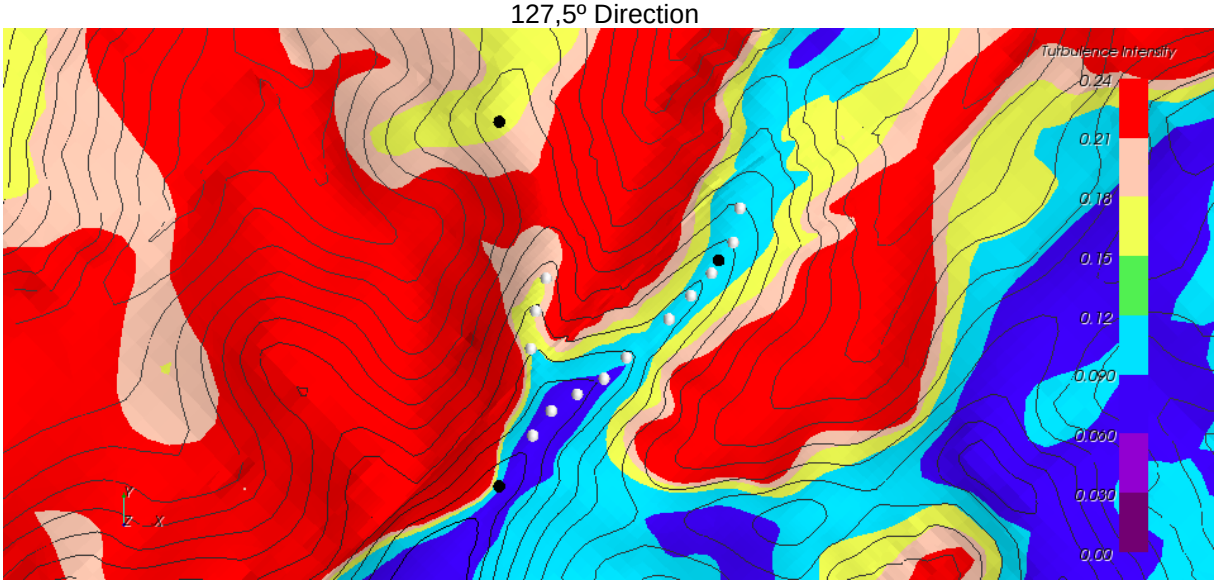

135º Direction

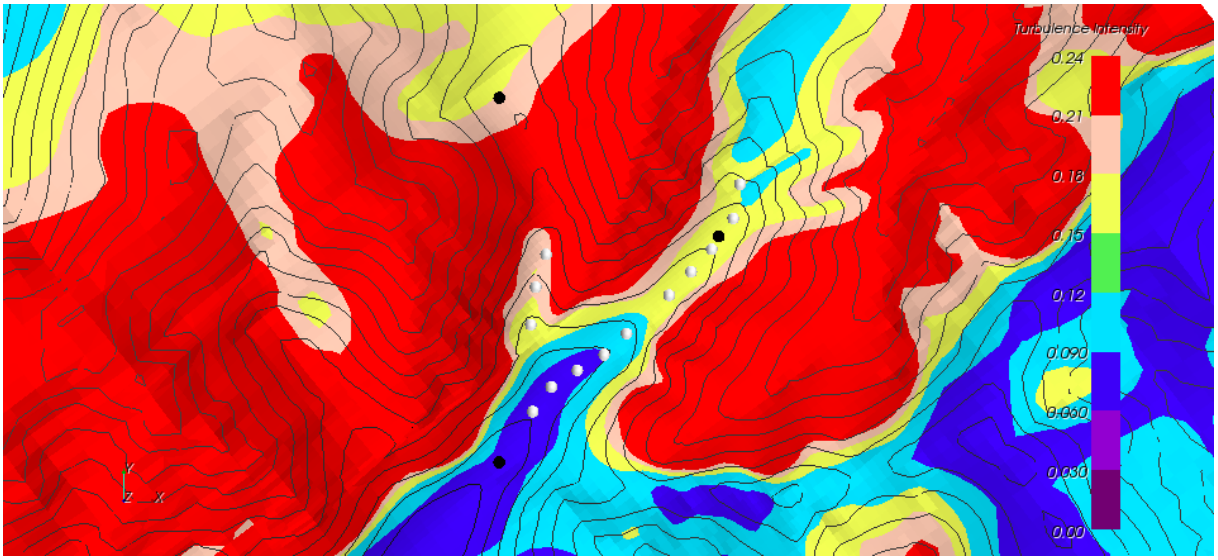

142,5º Direction

Figure 81 - Turbulent Intensity contour maps at 44 m a.g.l., for directions 127.5º through 142.5º

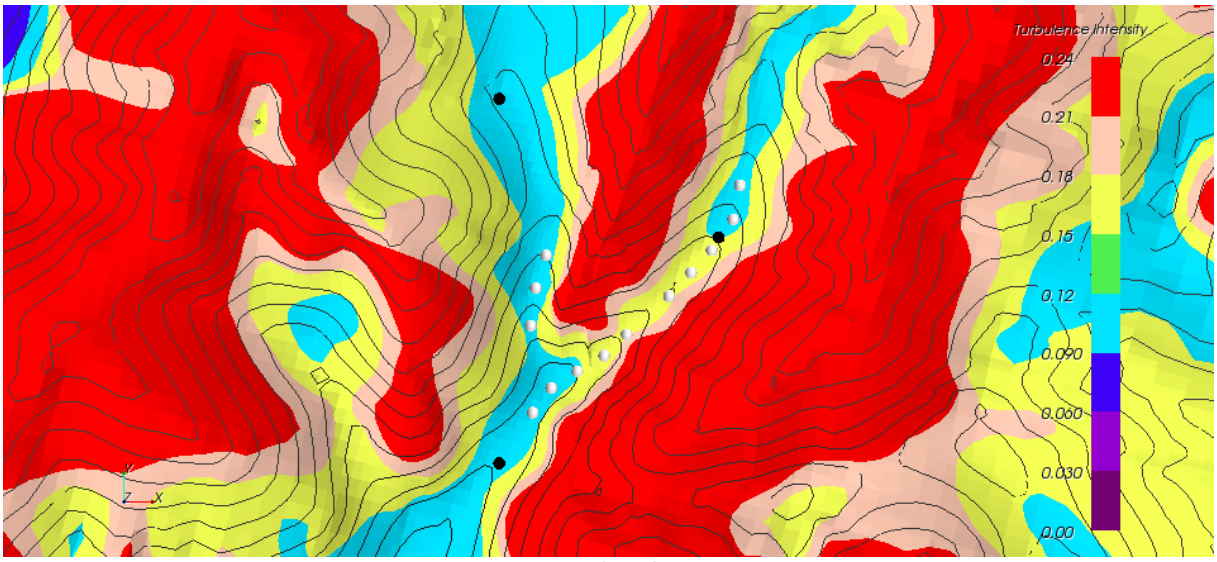

285º Direction

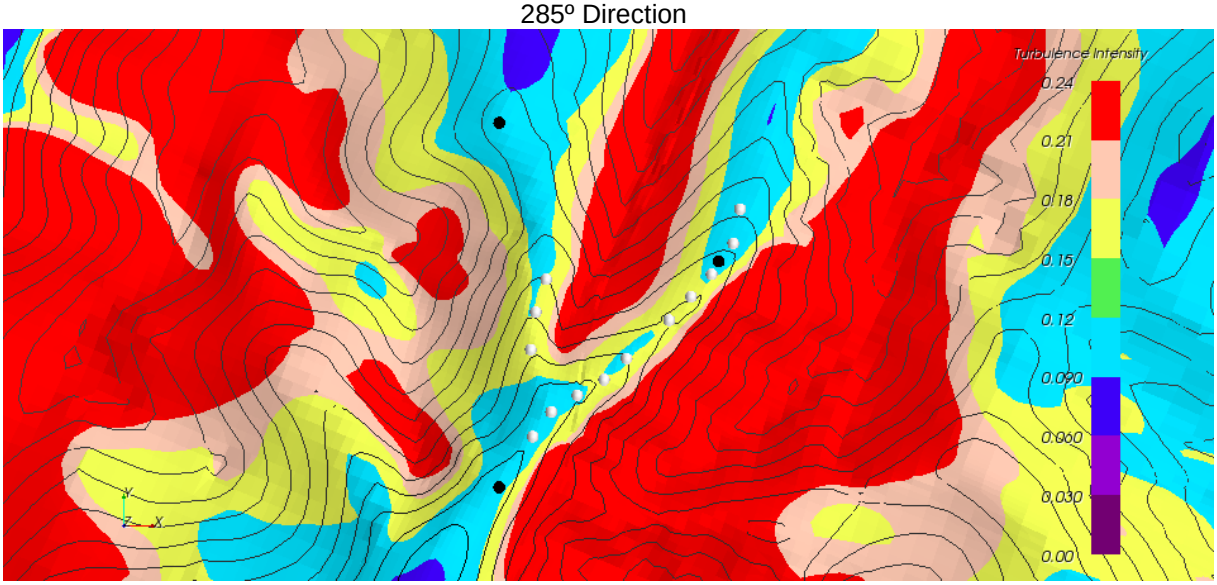

292,5º Direction

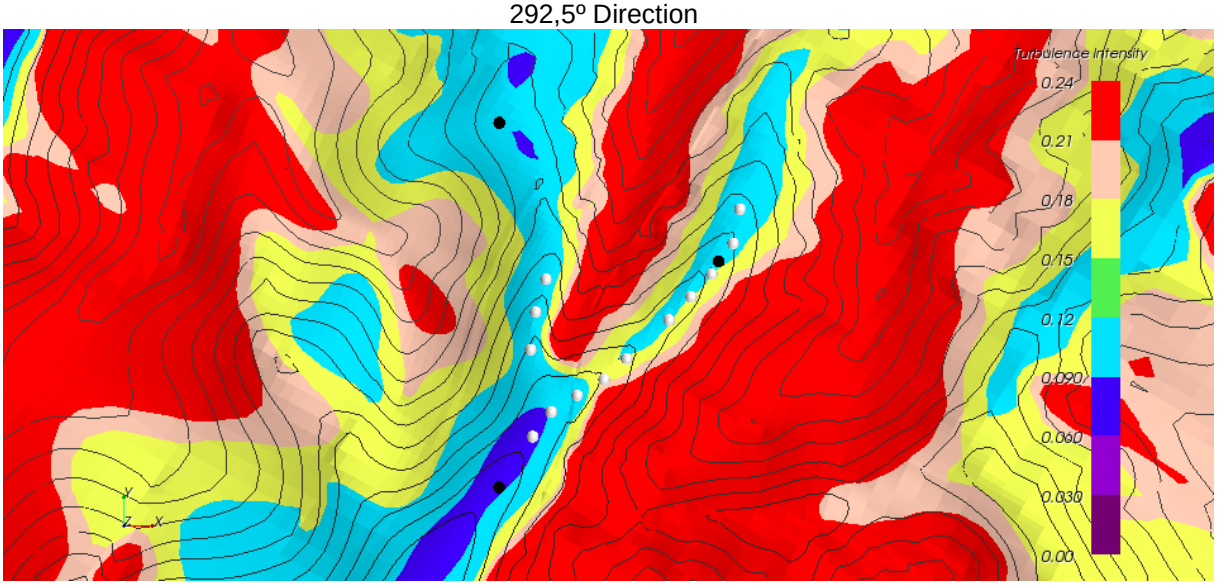

300º Direction

Figure 82 - Turbulent Intensity contour maps at 44 m a.g.l., for directions 285º through 300º

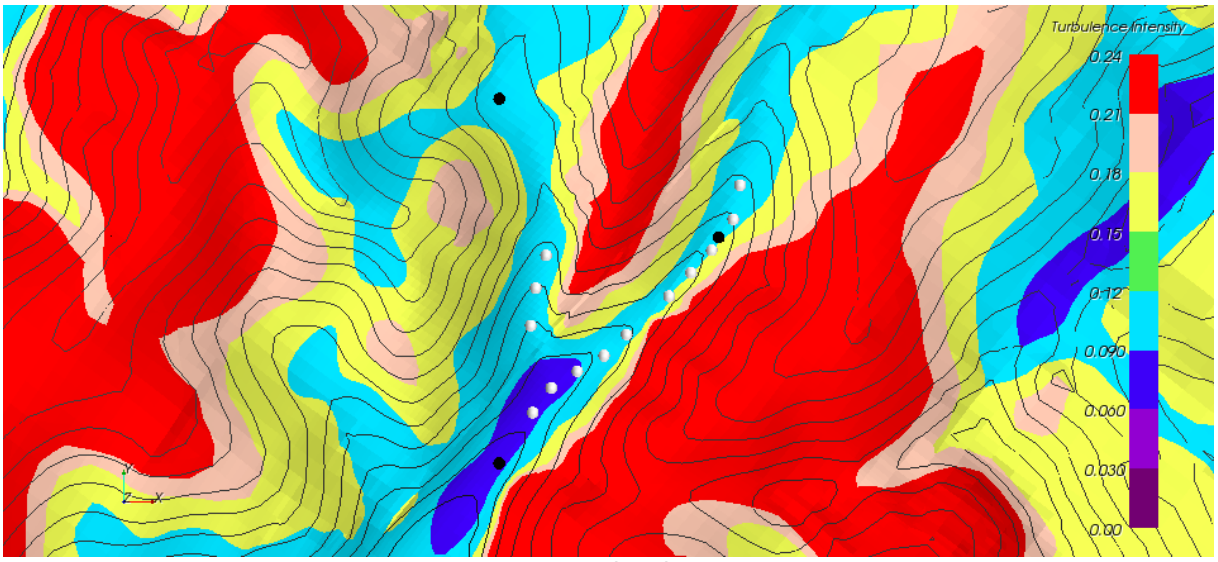

307,5º Direction

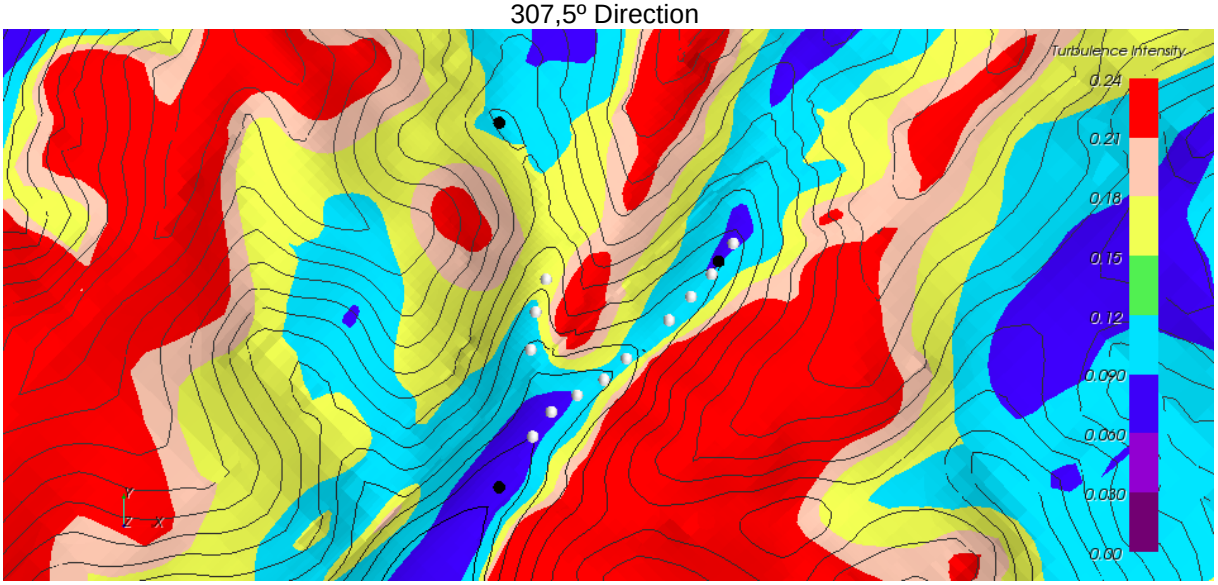

315º Direction

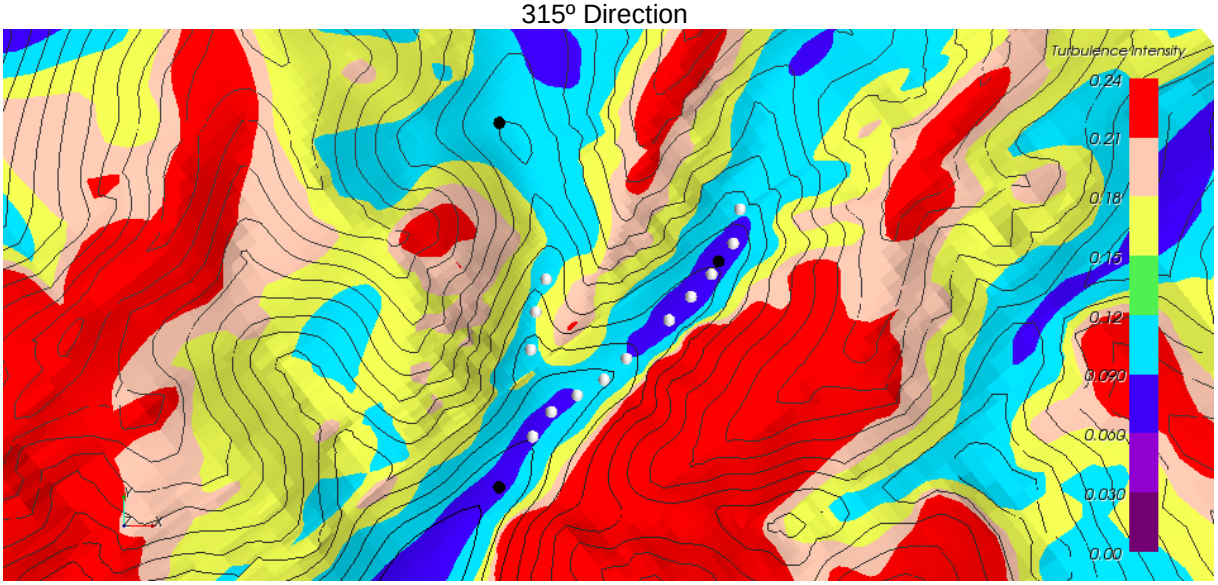

322,5º Direction

Figure 83 - Turbulent Intensity contour maps at 44 m a.g.l., for directions 307.5º through 322.5º

Turbulence Intensity 2D contours @ 85m a.g.l.

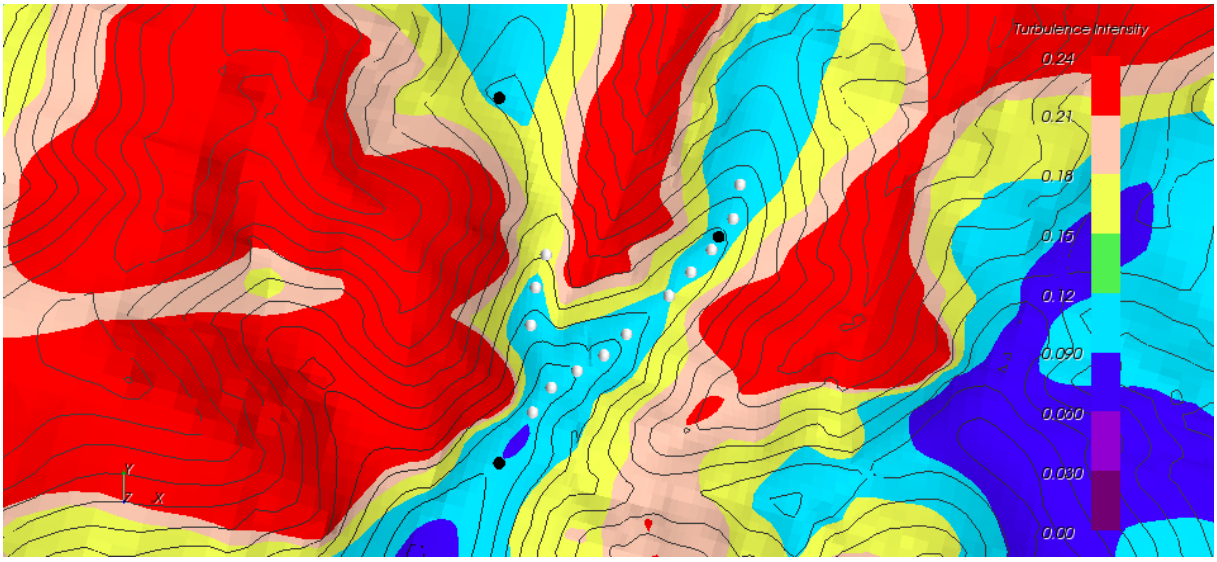

105º Direction

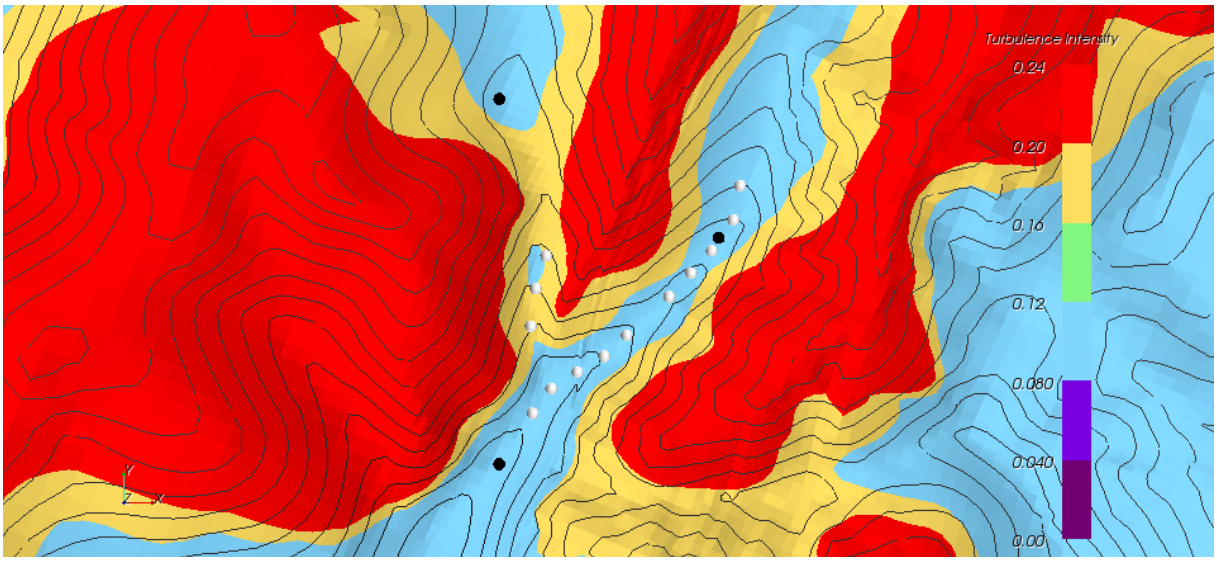

112,5º Direction

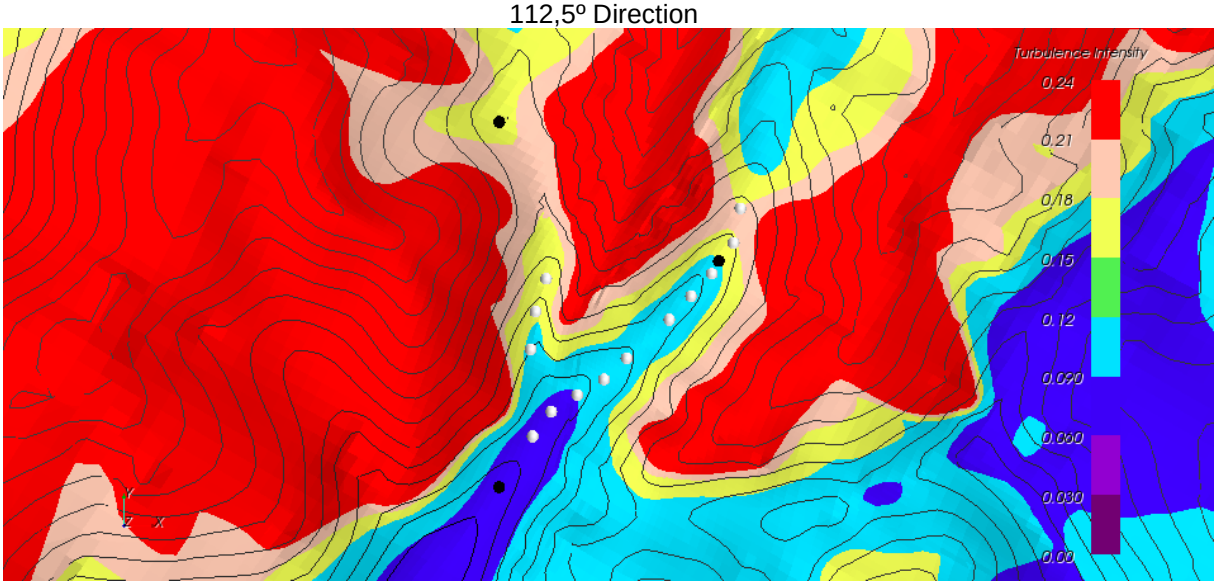

120º Direction

Figure 84 - Turbulent Intensity contour maps at 85 m a.g.l., for directions 105º through 120º

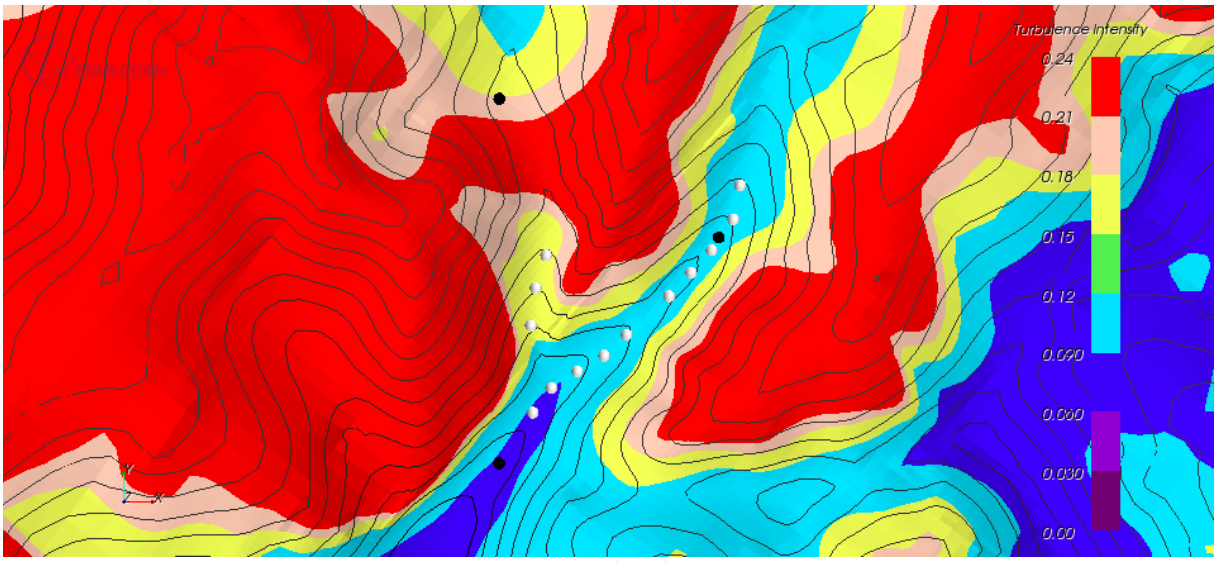

127,5º Direction

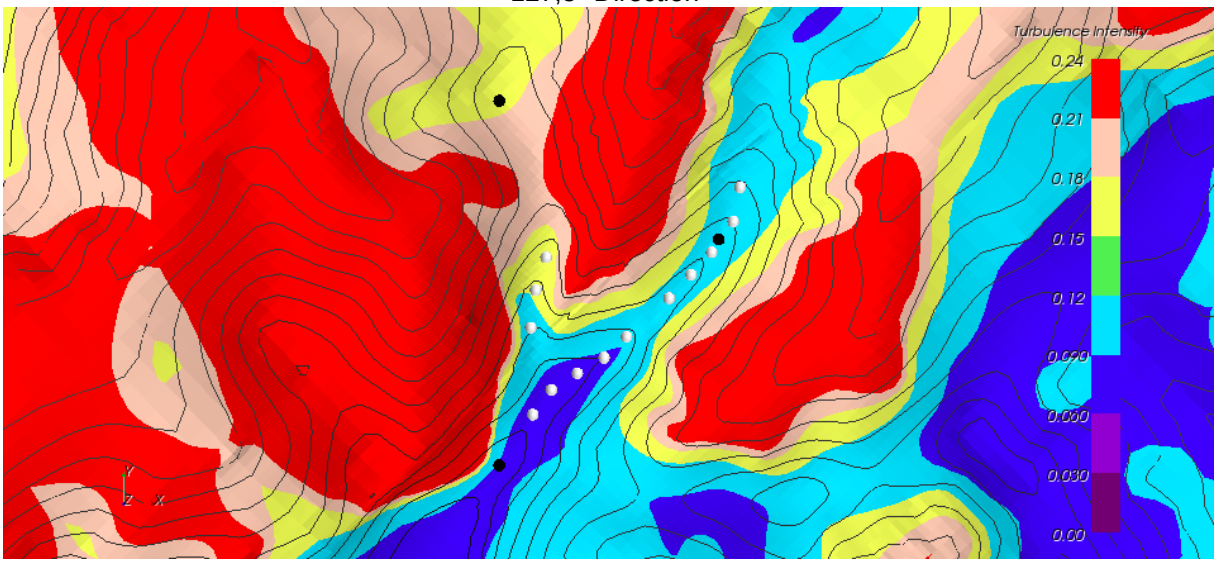

135º Direction

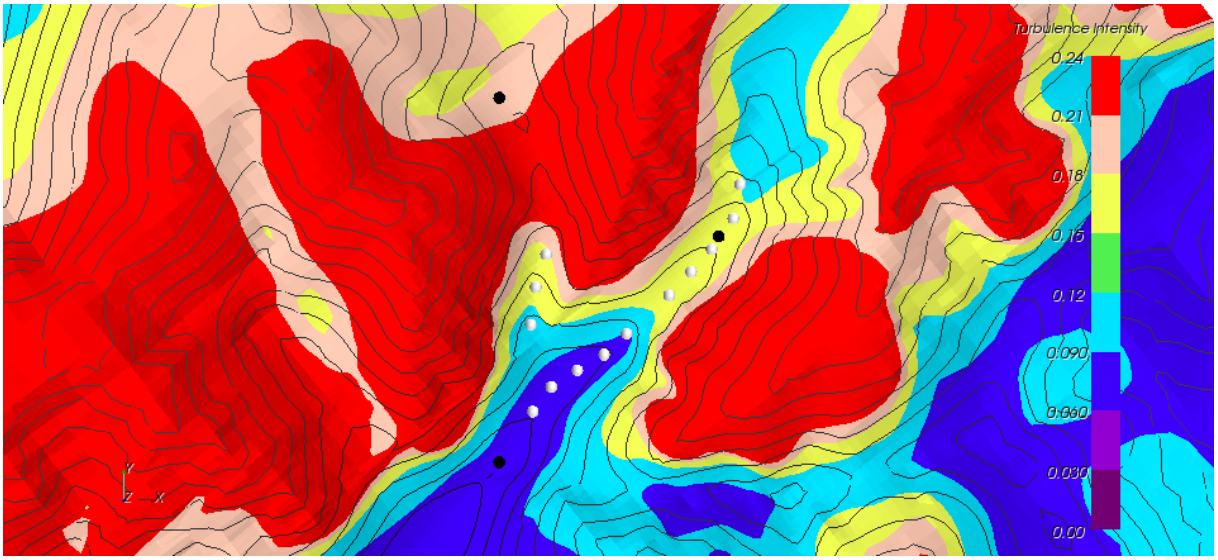

142,5º Direction

Figure 85 - Turbulent Intensity contour maps at 85 m a.g.l., for directions 127.5º through 142.5º

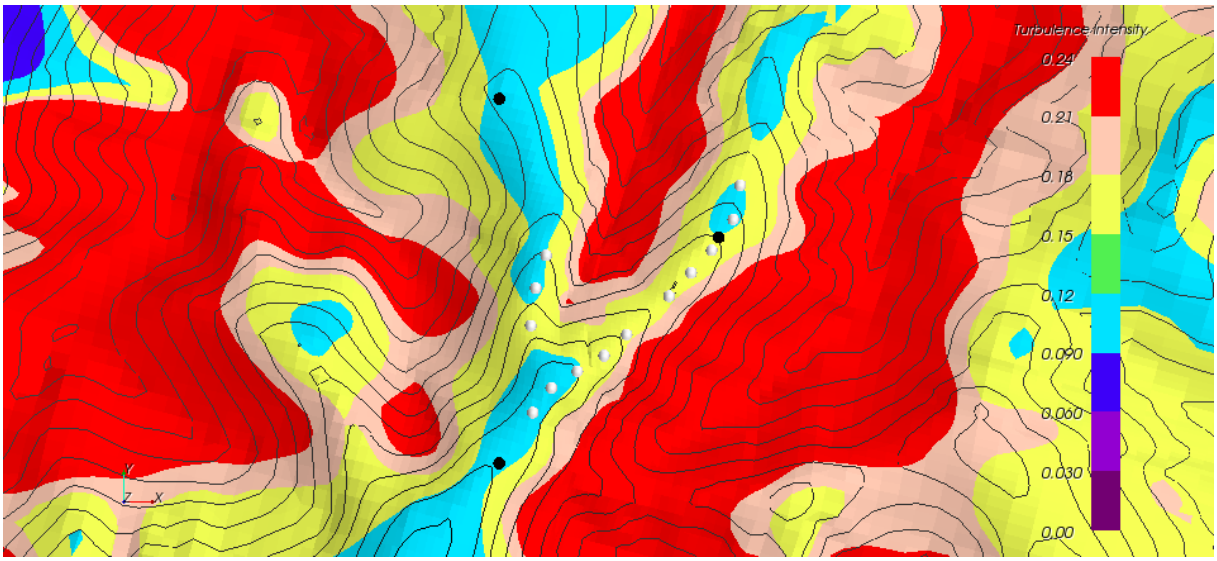

285º Direction

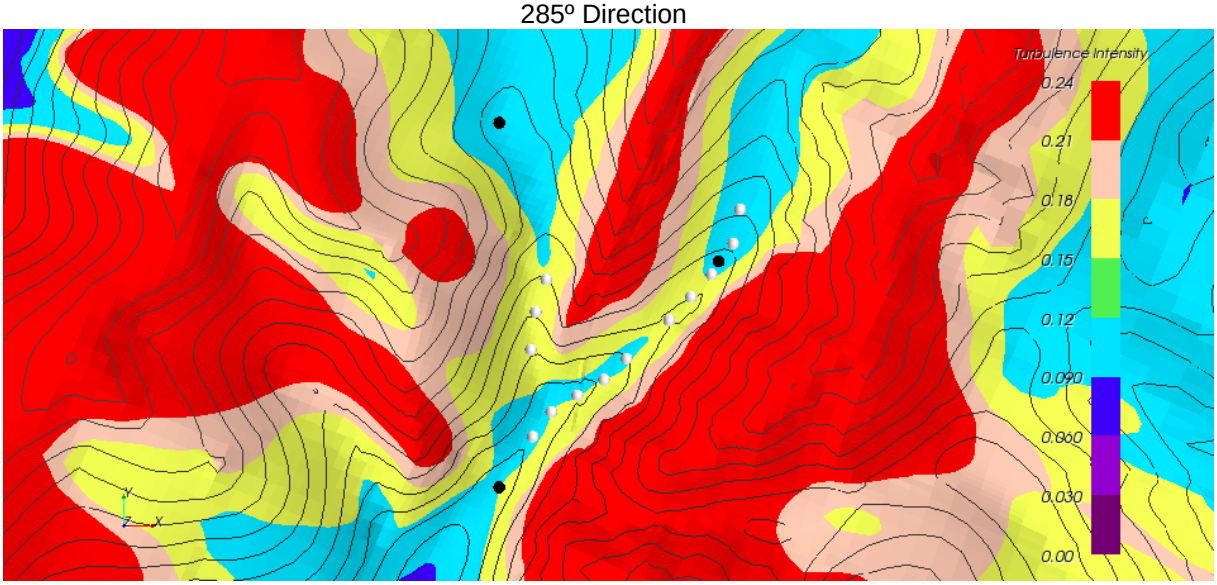

292,5º Direction

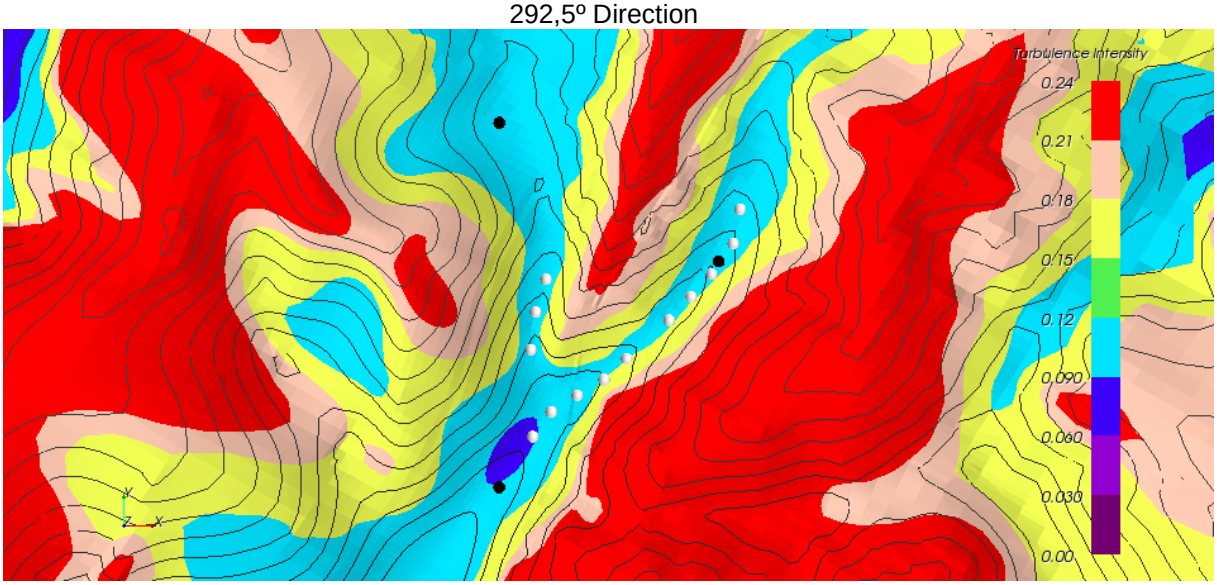

300º Direction

Figure 86 - Turbulent Intensity contour maps at 85 m a.g.l., for directions 285º through 300º

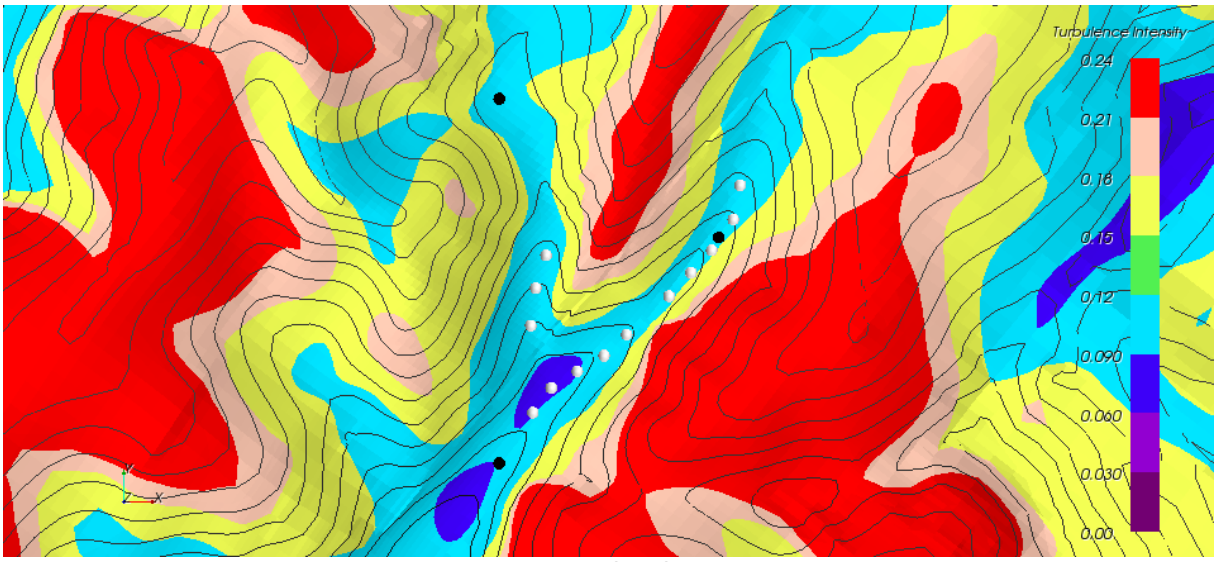

307,5º Direction

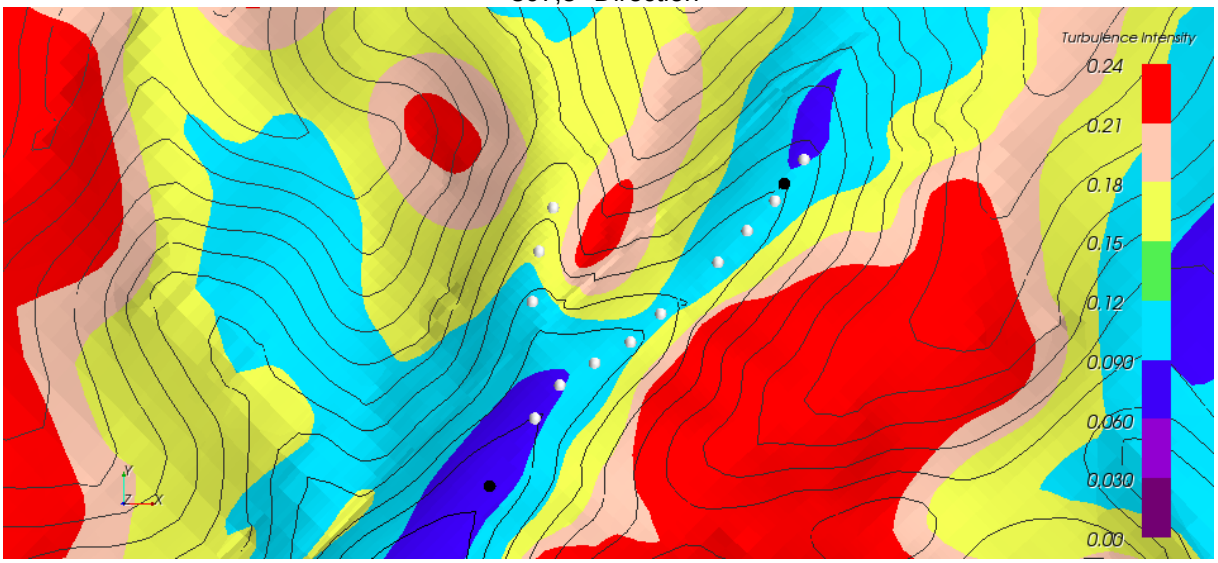

315º Direction

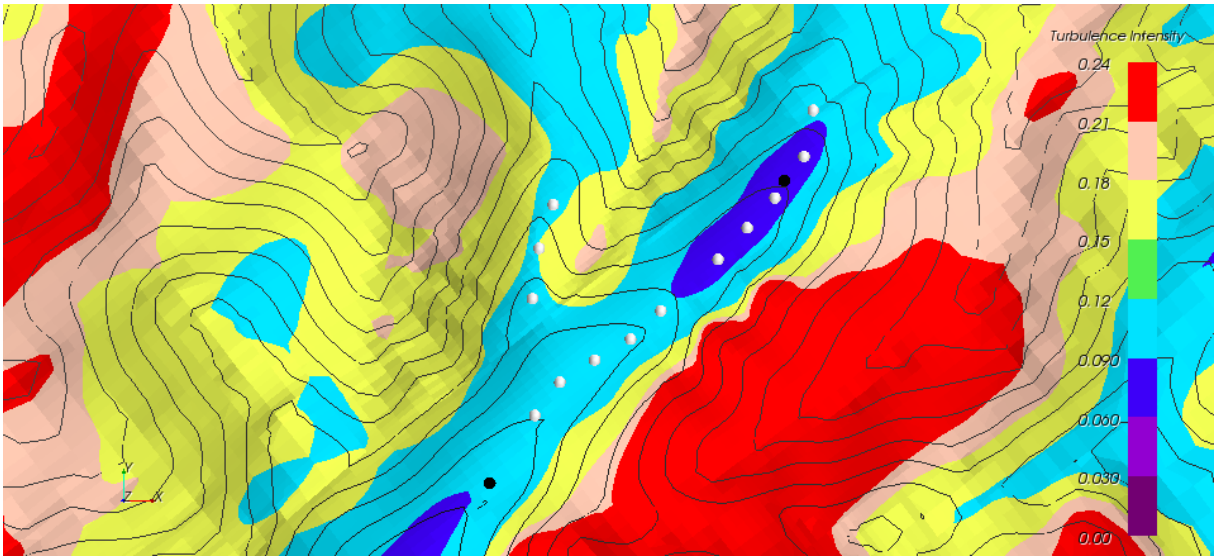

322,5º Direction

Figure 87 - Turbulent Intensity contour maps at 85 m a.g.l., for directions 307.5º through 322.5º

Turbulence Intensity 2D contours @ 126m a.g.l.

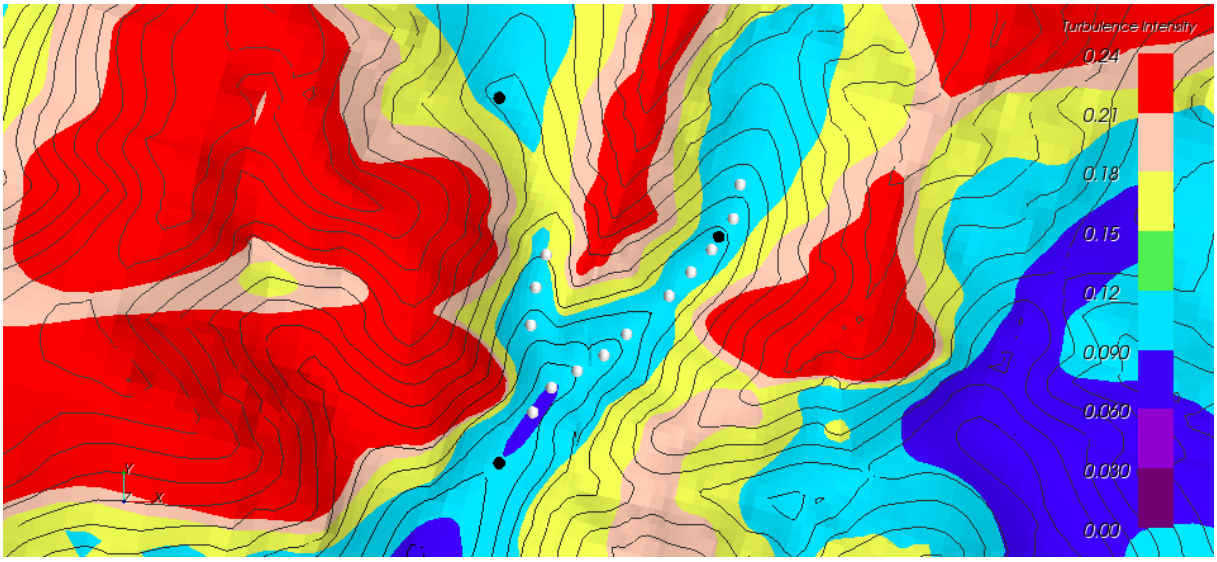

105º Direction

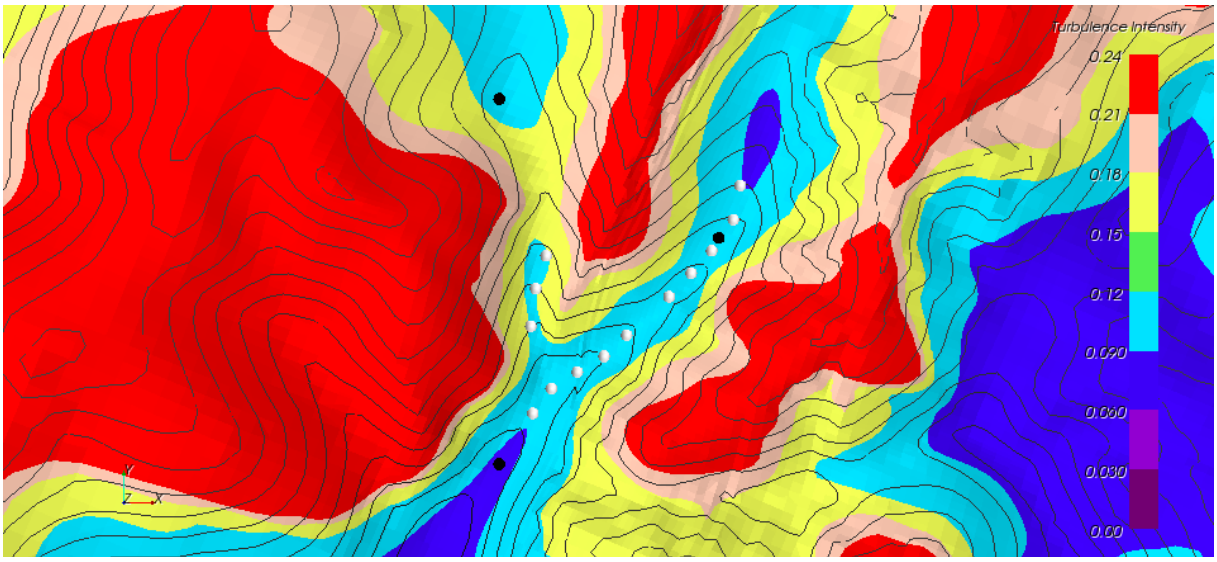

112,5º Direction

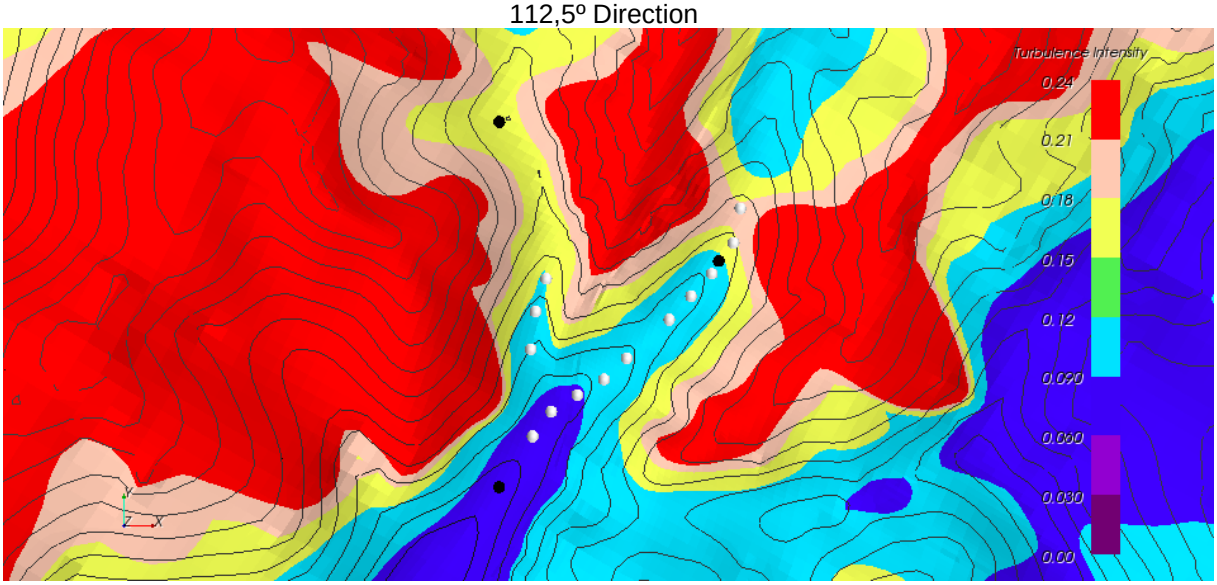

120º Direction

Figure 88 - Turbulent Intensity contour maps at 126 m a.g.l., for directions 105º through 120º

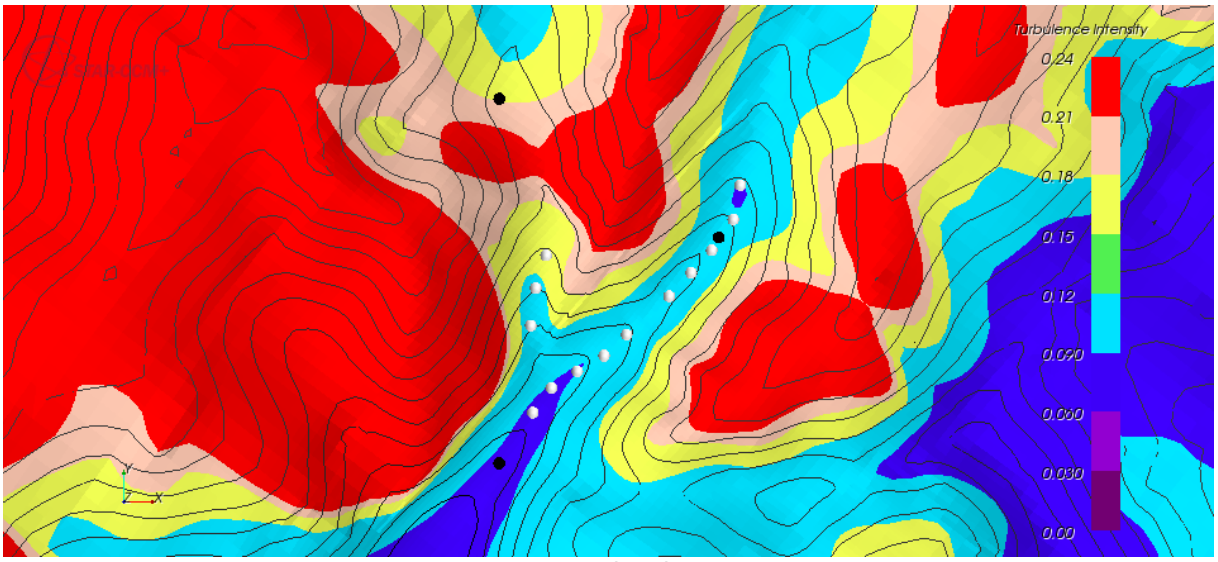

127,5º Direction

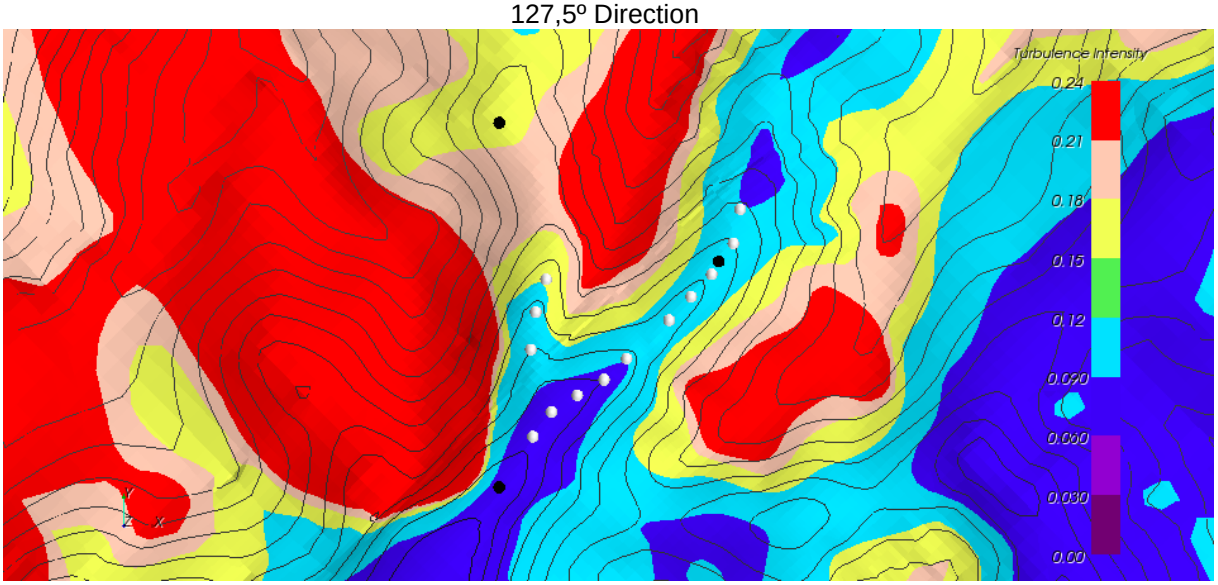

135º Direction

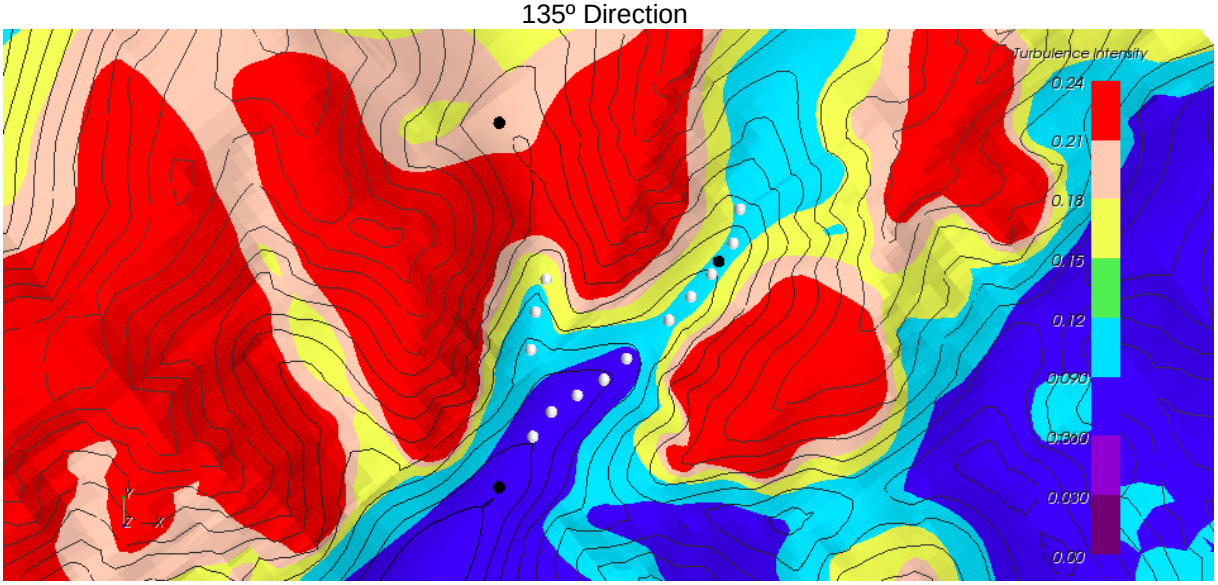

142,5º Direction

Figure 89 - Turbulent Intensity contour maps at 126 m a.g.l., for directions 127.5º through 142.5º

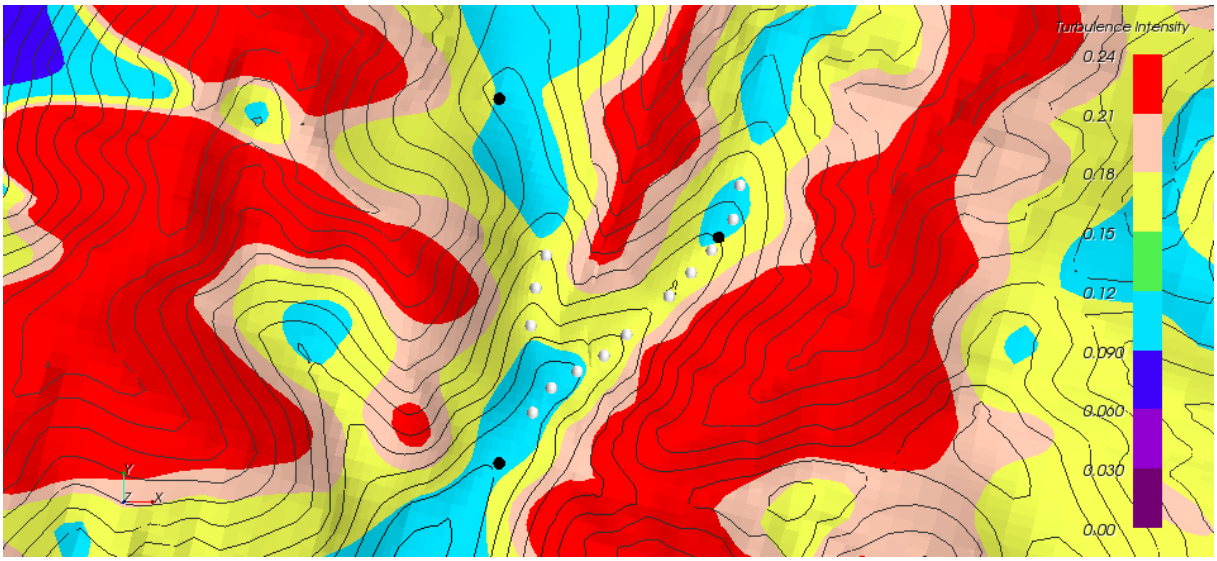

285º Direction

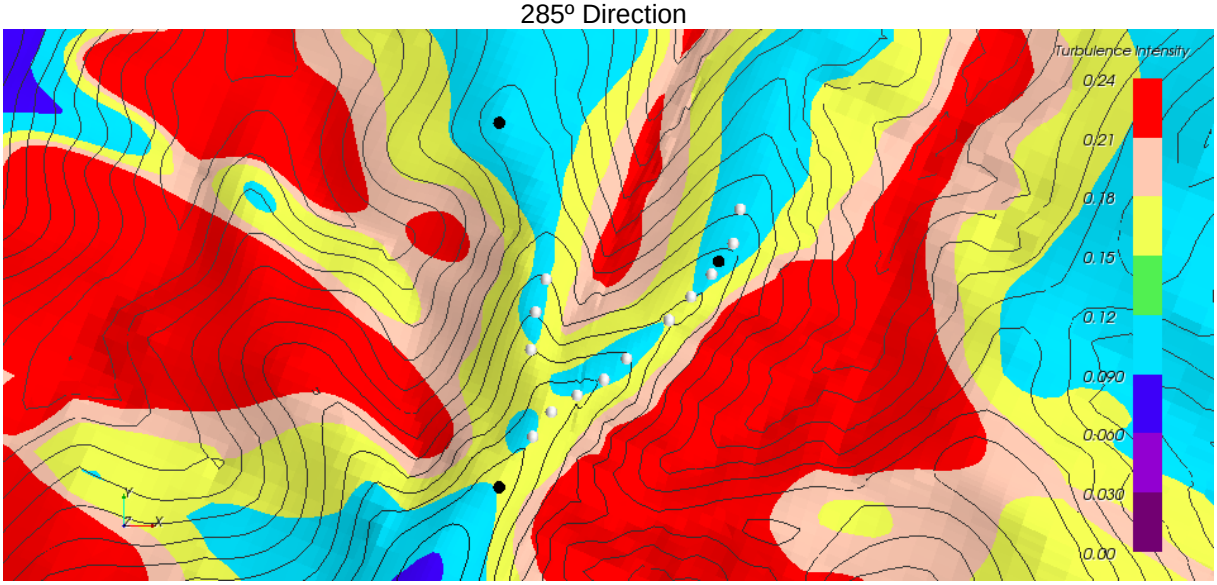

292,5º Direction

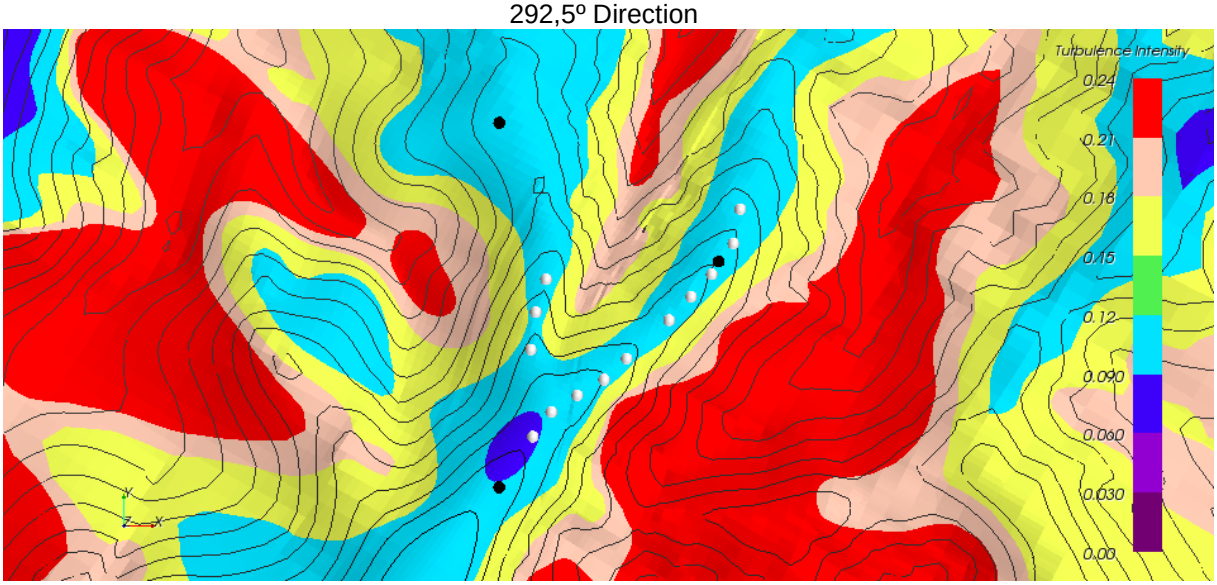

300º Direction

Figure 90 - Turbulent Intensity contour maps at 126 m a.g.l., for directions 285º through 300º

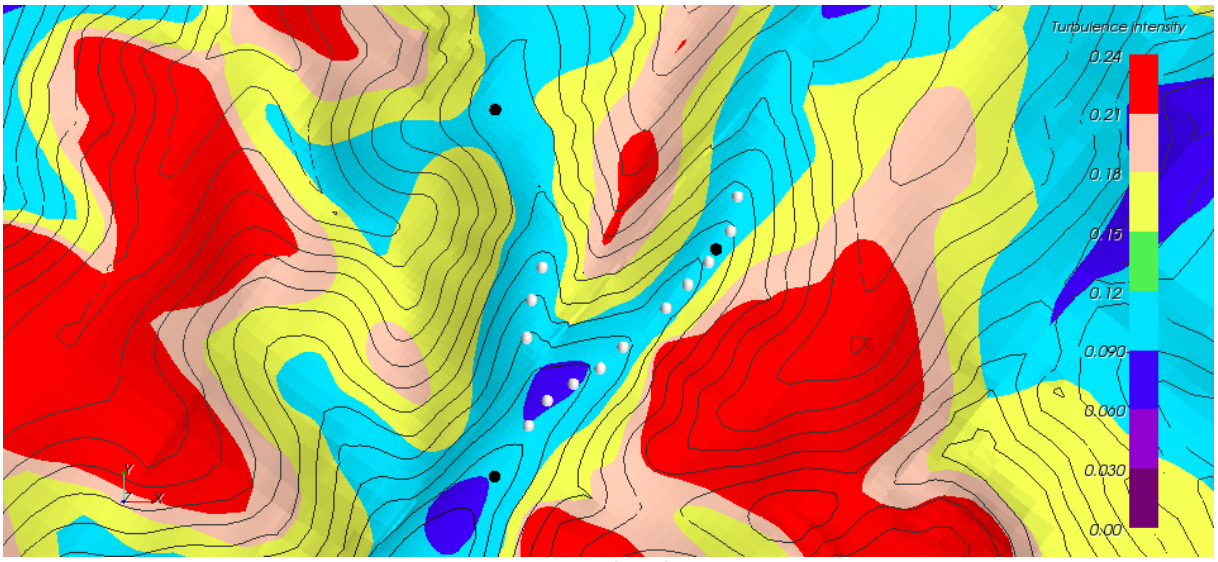

307,5º Direction

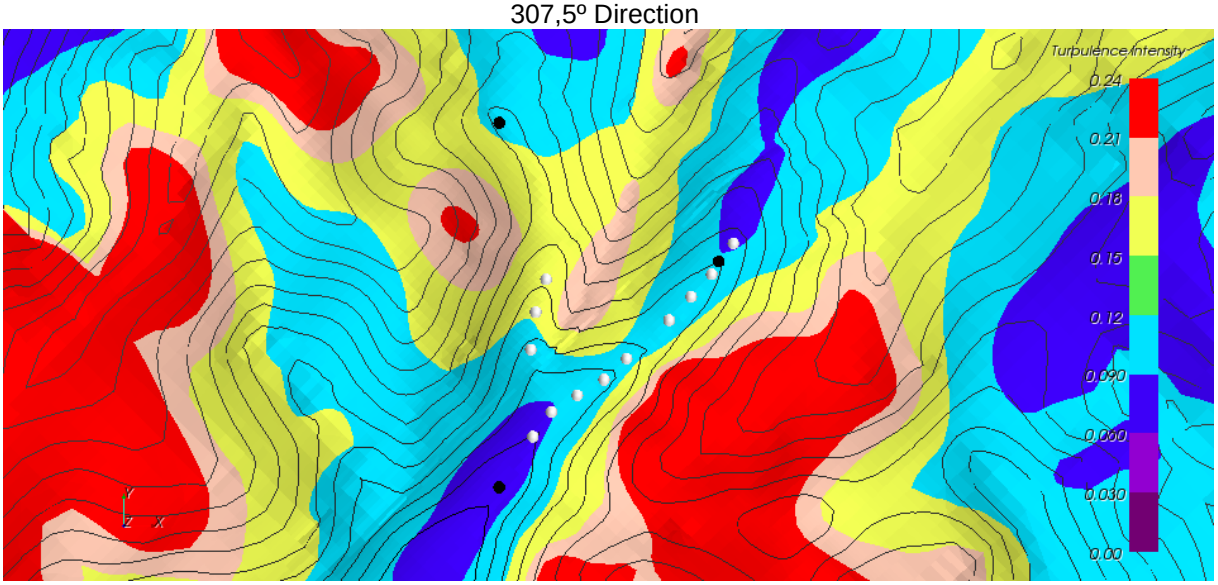

315º Direction

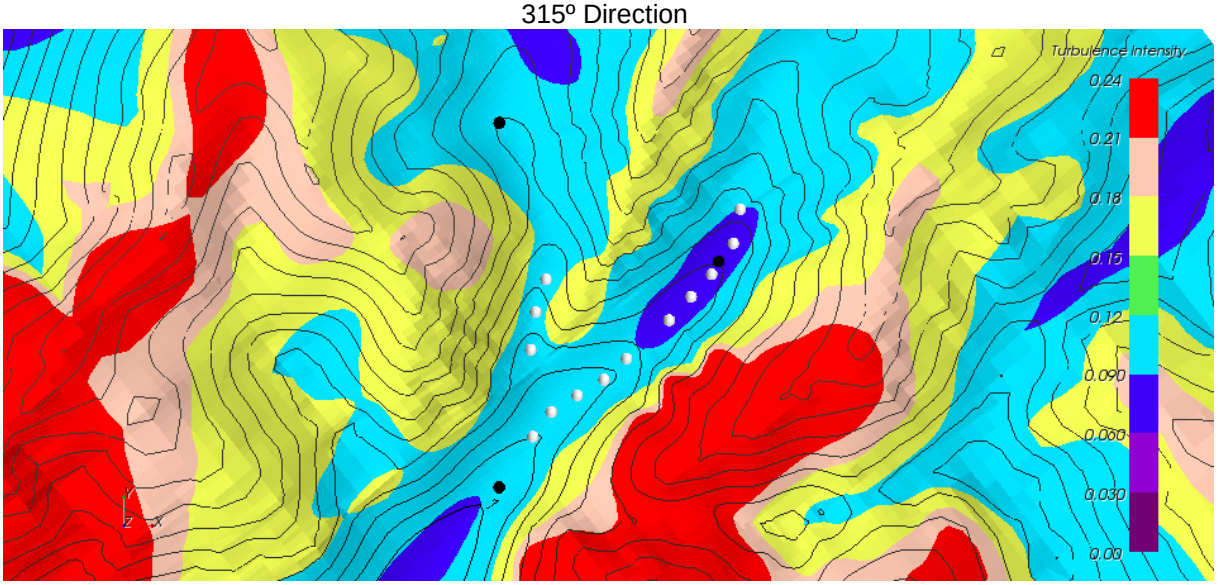

322,5º Direction

Figure 91 - Turbulent Intensity contour maps at 126 m a.g.l., for directions 307.5º through 322.5º

Annex C – Created User Function code

Flow Pitch scalar field function:

```
atan2($$Velocity[2],mag($$Velocity))
```

Flow Yaw scalar field function:

```
3.14159265+acos($Velocity_1/$HorVelocity)
```
, for NW sector winds;

```
3.14159265-acos($Velocity_1/$HorVelocity)
```
, for SE sector winds.

Horizontal velocity scalar field function:

```
sqrt(pow($$Velocity[0],2)+pow($$Velocity[1],2))
```

Turbulence Intensity entry profile:

```
sqrt(2/3*$TurbulentKineticEnergy)/$HorVelocity
```

Logarithmic velocity entry profile:

```
($WallDistance < 1500) ? (0.283/0.4*log((($WallDistance)+0.03)/0.03)) : ($U
/0.4*log(((1500)+0.03)/0.03))
```

Turbulent dissipation rate entry profile:

```
($WallDistance    >     0.95*1500)  ?
(pow(0.033,3/4)*pow($TurbulentKineticEnergy,3/2)/0.4*(1/($WallDistance+0.03
)))   :
(pow(0.033,3/4)*pow($TurbulentKineticEnergy,3/2)/0.4*(1/(0.95*1500+0.03)))
```

Turbulent kinetic energy entry profile:

```
($WallDistance  >  .99*1500)  ?  ((pow($U,2)/sqrt(0.033))*pow((1-0.99),2))  :
((pow($U,2)/sqrt(0.033))*pow((1-$WallDistance/1500),2))
```